Proposal to Continue the Study of Hyperon CP Violation in FY99

The HyperCP Collaboration

December 14, 1997

A. Chan, Y.C. Chen, J. Sheng, P.K. Teng, C. Yu, and Z. Yu
Academia Sinica, Nankang, Taipei 11529, Taiwan, Republic of China

W.S. Choong, G. Gidal, K.B. Luk[1], and P. Zyla
Lawrence Berkeley Laboratory and University of California, Berkeley, CA 94720, USA

M. Crisler, C. James and J. Volk
Fermilab, Batavia, IL 60510, USA

J. Felix, G. Lopez
Universidad de Guanajuato, León, Mexico

R.A. Burnstein, A. Chakravorty, D.M. Kaplan, L.M. Lederman, W. Luebke, D. Rajaram, H.A. Rubin, C.G. White, and S.L. White
Illinois Institute of Technology, Chicago, IL 60616, USA

N. Leros and J.-P. Perroud
Université de Lausanne, Lausanne, Switzerland

H.R. Gustafson, M.J. Longo, and F. Lopez
University of Michigan, Ann Arbor, MI 48109, USA

V. Papavassiliou
New Mexico State University, Las Cruces, NM 88003, USA

M. Jenkins and K. Clark
University of South Alabama, Mobile, AL 36688, USA

M. Carmack, E.C. Dukes[2], C. Durandet, T. Holmstrom, M. Huang, Z. Kou, and K.S. Nelson
University of Virginia, Charlottesville, VA 22901, USA

[1]Spokesperson: LUK@CSA.LBL.GOV, (510)486-7054
[2]Spokesperson: DUKES@UVAHEP.PHYS.VIRGINIA.EDU, (804)982-5364

We pray for the second coming of CP *violation ...*

A. Pais

Summary

In September 1997 the HyperCP (E871) collaboration completed a first run of a study of CP violation in Λ ($\overline{\Lambda}$) and Ξ^- ($\overline{\Xi}^+$) decays. Despite a very aggressive schedule and limited data-taking time, the run was a great success. In two years we built from scratch a hyperon beam and the highest rate spectrometer in the world and used it to accumulate by far the largest sample of hyperon decays. We expect to attain a statistical precision of 2×10^{-4} in the sum of the Λ and Ξ CP asymmetries, two orders of magnitude better than the present limit, and where some theories predict an effect. A non-zero asymmetry would be unambiguous evidence of direct CP violation and the first evidence of CP violation outside of the decay of K^0_L. The collaboration will also make sensitive studies of various rare and forbidden hyperon decays.

The upcoming Tevatron run with the Main Injector will allow us to take advantage of what has been learned from the first run to increase substantially our data sample and improve the quality of the data. Simple improvements to the data acquisition system, modest increases in secondary beam rates, and a new spill structure should permit at least a fourfold increase in statistics and allow us to reach an uncertainty of 1×10^{-4} or better in the hyperon CP asymmetry. Besides increasing our yields, we expect a substantial improvement in the quality of the data due to a number of modest, but significant, improvements in the apparatus and the monitoring software, and a better understanding of our spectrometer.

Contents

1 Introduction

The HyperCP collaboration has undertaken an ambitious effort to observe CP violation in Ξ and Λ hyperon decays at Fermilab. Construction of a new hyperon beam and a fast, new, state-of-the-art detector — to our knowledge, the highest rate spectrometer in the world — was completed in the fall of 1996, and a successful first run of the experiment ended in September 1997. We have accumulated about 75 billion events — the largest data sample ever taken in a HEP experiment — which will enable us to probe CP violation in hyperon decays two orders of magnitude beyond the current limit. *In only 2 hours of running the HyperCP spectrometer accumulated more* Ξ^- *and* $\overline{\Xi}^+$ *events than all previous experiments.*

Observation of CP violation in this experiment would be the first evidence of CP violation outside of the decay of the K_L^0 and unambiguous evidence of direct CP violation. We have also accumulated an enormous sample of charged kaon decays which will allow a sensitive search for CP violation in $K^\pm \to \pi^\pm\pi^\pm\pi^\mp$ decays. And finally, the experiment will perform a high-statistics search for rare and forbidden hyperon decays and charged kaon decays.

A second run of the experiment will allow us to build on the success of the first run, taking advantage of what we have learned about our spectrometer to increase both the quantity and quality of the data. We expect to increase our data sample by at least a factor of four to achieve a precision of 1×10^{-4} or better in the CP asymmetry. Most of the increase in yield will simply come from running at the intensity and efficiency that we attained at the end of the 1997 fixed-target run. The quality of the data will also be significantly improved by modest improvements to the apparatus and by better online monitoring software.

We should emphasize that future runs of the experiment at Main Injector energies would not be fruitful due to the much lower hyperon yields at 120 GeV and intractable systematic errors at lower energies.

In the following sections we first briefly review the physics of CP violation in hyperon decays. (Other physics topics the collaboration will study are described in Appendix A.) We then describe the spectrometer and how well it performed in the 1997 fixed-target run. The 1997 run is summarized and preliminary results are given. Finally we outline our expectations for the FY99 run and how we propose to achieve them.

2 Physics of Hyperon CP Violation

The central idea of our hyperon CP violation experiment is simple. We compare the Λ and $\overline{\Lambda}$ decay distributions in the following reactions:

$$\begin{array}{lll} \Xi^- \to \Lambda^0 \pi^- & \text{and} & \overline{\Xi}^+ \to \overline{\Lambda}^0 \pi^+ \\ \quad \hookrightarrow p \pi^- & & \quad \hookrightarrow \overline{p} \pi^+, \end{array}$$

where the Ξ^- and $\overline{\Xi}^+$ hyperons are produced unpolarized. Any difference in these distributions is unambiguous evidence of direct CP violation.

2.1 Signatures for CP Violation in Hyperon Decays

Because the non-leptonic weak decays of spin-$\frac{1}{2}$ hyperons violate parity, they can decay into admixtures of both S- and P-wave final states. In terms of the S- and P-wave amplitudes, the hyperon nonleptonic decays are conventionally described by the Lee–Yang variables α, β, and γ [1]:

$$\alpha = \frac{2\mathrm{Re}(S^*P)}{|S|^2+|P|^2}, \qquad \beta = \frac{2\mathrm{Im}(S^*P)}{|S|^2+|P|^2}, \qquad \gamma = \frac{|S|^2-|P|^2}{|S|^2+|P|^2}, \tag{1}$$

where $\alpha^2+\beta^2+\gamma^2 = 1$. The decay distribution of the daughter spin-$\frac{1}{2}$ baryon in the rest frame of the parent hyperon (the proton in the decay $\Lambda \to p\pi^-$, for example) is not isotropic, because of parity violation, but is given by:

$$\frac{dP}{d\Omega} = \frac{1}{4\pi}(1+\alpha \vec{P}_p \cdot \hat{p}_d), \tag{2}$$

where $\vec{P}_p$ is the parent hyperon polarization and $\hat{p}_d$ is the daughter baryon momentum direction in the rest frame of the parent. As shown in Fig. 1, protons are predominantly emitted in the direction of the Λ polarization and antiprotons are predominantly emitted in the direction opposite to the $\overline{\Lambda}$ polarization.

If CP is conserved then, as shown in Fig. 1, $\alpha = -\overline{\alpha}$, where the overlined quantity refers to the antihyperon. Hence the observable sensitive to CP violation is[1]:

$$A = \frac{\alpha+\overline{\alpha}}{\alpha-\overline{\alpha}}. \tag{3}$$

Measuring the alpha parameter in a hyperon decay is done by measuring the slope of the daughter $\cos\theta$ distribution in the frame where the parent polarization defines the polar axis. That distribution is given by:

$$\frac{dN}{d\cos\theta} = \frac{1}{2}(1+P_p\alpha_p\cos\theta), \tag{4}$$

[1]There are other observables sensitive to CP violation but none of them is as experimentally accessible as α. See the P-871 proposal for details about these other CP observables.

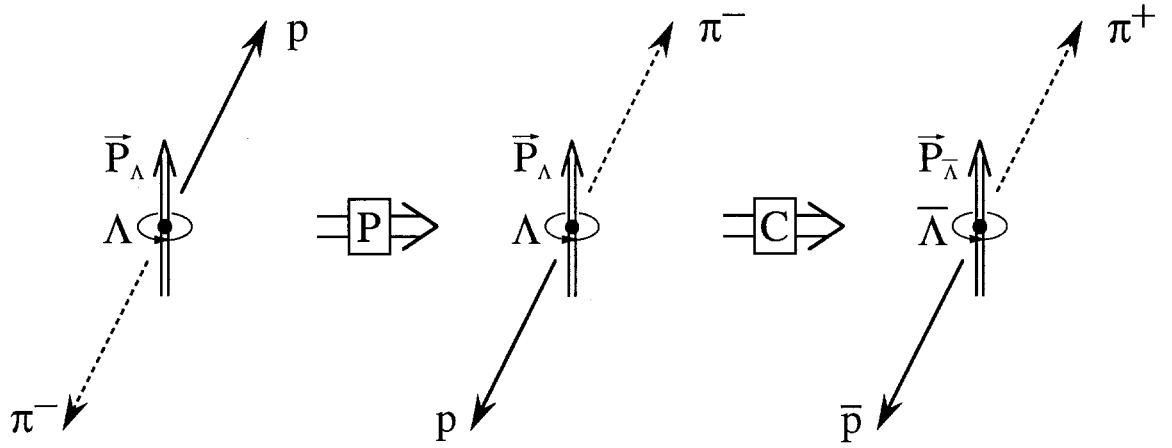

Figure 1: Λ decay under P and C transformations.

where θ is the angle between the parent polarization and the daughter momentum. *Since the slope of the* $\cos\theta$ *distribution is given by the product* $P_p\alpha_p$*, the alpha parameter can only be extracted if the parent polarization is known.*

How HyperCP produces hyperons of a well-known polarization is as follows. In HyperCP we measure the proton and antiproton $\cos\theta$ distributions from Λ and $\overline{\Lambda}$ hyperons that are produced from Ξ^- and $\overline{\Xi}^+$ decays. In general the polarization of the daughter baryon in a non-leptonic spin-$\frac{1}{2}$ hyperon decay is given by:

$$\vec{P}_d = \frac{(\alpha + \vec{P}_p \cdot \hat{p}_d)\hat{p}_d + \beta(\vec{P}_p \times \hat{p}_d) + \gamma[\hat{p}_d \times (\vec{P}_p \times \hat{p}_d)]}{1 + \alpha\vec{P}_p \cdot \hat{p}_d}. \tag{5}$$

If the parent hyperon is unpolarized then this equation simplifies to:

$$\vec{P}_d = \alpha\, \hat{p}_d. \tag{6}$$

We produce Ξ^- and $\overline{\Xi}^+$ hyperons through the reaction $p + \mathrm{Cu} \to \Xi^\pm + X$. Because of parity conservation in strong interactions and because the hyperons are produced with $p_t \cong 0$, the Ξ's must be unpolarized. As a consequence, the daughter Λ is in a helicity state with polarization given by the alpha parameter of Ξ:

$$\vec{P}_\Lambda = \alpha_\Xi \hat{p}_\Lambda. \tag{7}$$

We can now re-write Eq. 4 in the frame in which the Λ polarization defines the polar axis as (Λ helicity frame — see Fig. 2)

$$\frac{dN}{d\cos\theta} = \frac{1}{2}(1 + \alpha_\Xi\alpha_\Lambda \cos\theta), \tag{8}$$

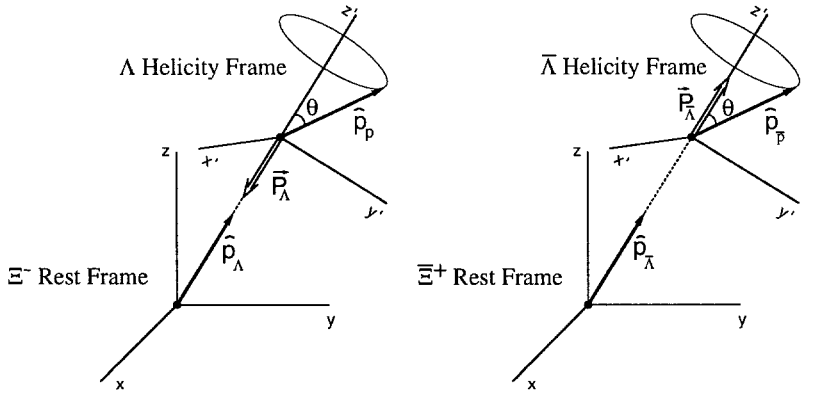

Figure 2: Analysis frames used in the Λ and $\overline{\Lambda}$ polarization analyses. The polar axis in the Λ rest frame (primed frame) is defined by the direction of the Λ momentum in the Ξ rest frame. The Λ and $\overline{\Lambda}$ have helicities of equal magnitude but opposite sign if CP is a good symmetry. However, since the sign of the Λ helicity reverses under CP, the probabilities of the proton and antiproton being emitted with polar angle θ are identical if CP is a good symmetry.

where θ is the angle between the proton momentum and the Λ polarization vector in the Λ rest frame. Hence, what we measure and compare are the products $\alpha_\Xi\alpha_\Lambda$ and $\alpha_{\overline{\Xi}}\alpha_{\overline{\Lambda}}$ which, *if CP is a good symmetry*, should be identical since both α_Ξ and α_Λ flip sign under CP.

We define the asymmetry parameter $A_{\Xi\Lambda}$, which is given by:

$$A_{\Xi\Lambda} = \frac{\alpha_\Xi\alpha_\Lambda - \alpha_{\overline{\Xi}}\alpha_{\overline{\Lambda}}}{\alpha_\Xi\alpha_\Lambda + \alpha_{\overline{\Xi}}\alpha_{\overline{\Lambda}}} \simeq A_\Xi + A_\Lambda, \tag{9}$$

and should be zero if CP is a good symmetry. HyperCP cannot distinguish whether an observed asymmetry originates in Ξ or Λ decay since α_Ξ and α_Λ are not measured separately. However, almost all theories (including the Standard Model) predict like signs for A_Ξ and A_Λ so the probability of any cancellation is remote [2].

2.2 Predictions

Model-independent expressions for the observable A have been explicitly calculated for various hyperon decays [3]. To leading order they are, for $\Lambda \to p\pi^-$ decay:

$$A_\Lambda \cong -\tan(\delta_1^P - \delta_1^S)\sin(\phi_1^P - \phi_1^S), \tag{10}$$

and for $\Xi^- \to \Lambda\pi^-$ decay:

$$A_\Xi \cong -\tan(\delta_3^P - \delta_3^S)\sin(\phi_1^P - \phi_1^S), \tag{11}$$

where ϕ are CP-violating weak phases, and δ are strong phase shifts.

Note that a difference in the S- and P-wave final-state interaction phases is essential in order for A to be non-zero. The $p\pi^-$ phase shifts have been measured, and $\delta_1^P - \delta_1^S = 7^\circ$ with an error of about 1° [4]. The $\Lambda\pi$ phase shifts have not been measured and there is about an order of magnitude variation in the S-wave theoretical predictions (see [5] and [6]).

The magnitudes of the CP asymmetries in hyperon decays depend on the values of ϵ, ϵ', the top quark mass and the hadronic matrix elements. (Note that although limits on the magnitude of ϵ' constrain ϕ_1^S, they do not put any limits on ϕ_1^P, and hence on the asymmetry A [7].) Calculations are notoriously difficult, and *results are not reliable to better than an order of magnitude*, with the largest uncertainty due to the inability in determining the hadronic matrix elements.

The magnitudes of the predicted CP asymmetries are model dependent. In the Standard Model CP-violation effects are due solely to the complex phase in the CKM matrix, and hence hyperon CP asymmetries can only arise from matrix elements which involve transitions to the third quark generation. These are thought to be dominated by the gluon-penguin diagram for both kaon and hyperon decays [8]. (See Fig. 3). Theories with no $|\Delta S| = 1$, CP-odd effects, such as Superweak models and models with a very heavy neutral Higgs, predict no CP asymmetries. Models in which $|\Delta S| = 1$ CP nonconservation is dominant, such as the Weinberg model, predict asymmetries which are on the order of those calculated in the Standard Model. In Table 1 are shown some recent predictions for the CP asymmetries A_Ξ and A_Λ.

Table 1: Predictions of A_Ξ and A_Λ.

Model	A_Ξ $[10^{-4}]$	A_Λ $[10^{-4}]$	
CKM Model	$-(0.1-1)$	$-(0.1-0.5)$	[9]
Weinberg	≈ -3.2	≈ -0.25	[3]
Multi-Higgs (FCNE)	≈ 0	≈ 0	[9]
LR (isoconjugate)	≈ 0.5	≈ -0.11	[3]
LR (with mixing)	< 1	< 7	[7]

HyperCP has generated renewed theoretical interest in CP violation in hyperon decays. Recent papers by Pakvasa *et al.* [7], Wise *et al.* [5], Deshpande *et al.* [10], Valencia *et al.* [11], and Datta *et al.* [6], explicitly refer to HyperCP and anticipate our results. Our analysis technique has also been suggested as a means of looking for CP violation in beauty baryon decays in a paper by Albrecht *et al.* [12].

2.3 Comparison with Direct CP violation in Kaon Decays

A brief word about the difference between CP violation in kaons and hyperons. Although there is a close relationship between direct CP violation in kaon and hyperon decays, the differences are important. The most promising method of looking for direct CP violation in neutral kaons is by measuring ϵ'/ϵ. A non-zero value of ϵ'/ϵ is expressed through the interference of isospin $I = 0$ and $I = 2$ final states, whereas a non-zero value of A in hyperon decays is due to the interference between S-wave and P-wave final states. In Standard Model calculations the value of ϵ'/ϵ is very sensitive to the top quark mass whereas the hyperon CP asymmetry parameter A is not [13]. The reason for this sensitivity is the cancellation of the QCD and electroweak penguin diagrams [14]. Hence ϵ'/ϵ diminishes with increasing top mass and becomes negative at a top mass above around 200 GeV/c^2.

As mentioned above, measurements of ϵ' only set limits on the weak phase ϕ_1^S and not on ϕ_1^P — that is, a small value of ϵ' does not preclude a large value of A. Hence, to quote He and Valencia [11]:

> ...this measurement is complementary to the measurement of ϵ'/ϵ, in that it probes potential sources of CP violation at a level that has not been probed by the kaon experiments.

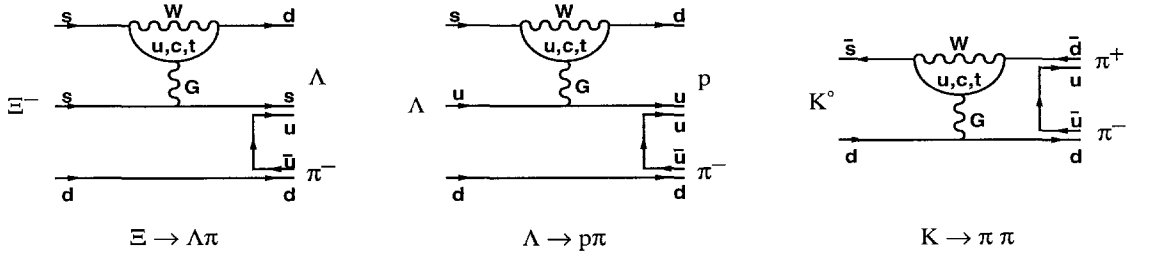

Figure 3: Gluon penguin diagrams responsible for $|\Delta S| = 1$ direct CP violation in $\Xi^- \to \Lambda\pi^-$, $\Lambda \to p\pi^-$, and $K \to \pi^+\pi^-$ decays. The electroweak penguin diagrams are identical except that the gluon is replaced by the γ and Z°.

2.4 Present Experimental Limits

The only data on CP violation in hyperon decays comes from the comparison of the alpha parameters in Λ and $\overline{\Lambda}$ decays. The experimental limits are weak. The three published results are given in Table 2. Each of the three experiments used a different technique, all were limited by statistical, not systematic errors, and none was a dedicated CP-violation experiment.

Table 2: Experimental results on $A_\Lambda = (\alpha_\Lambda + \alpha_{\overline{\Lambda}})/(\alpha_\Lambda - \alpha_{\overline{\Lambda}})$.

Mode	Result	Experiment
$pp \to \Lambda X, \overline{p}p \to \overline{\Lambda} X$	0.02 ± 0.14	R608 [16]
$e^+e^- \to J/\psi \to \Lambda\overline{\Lambda}$	0.01 ± 0.10	DM2 [17]
$p\overline{p} \to \Lambda\overline{\Lambda}$	0.010 ± 0.022	PS185 [18]

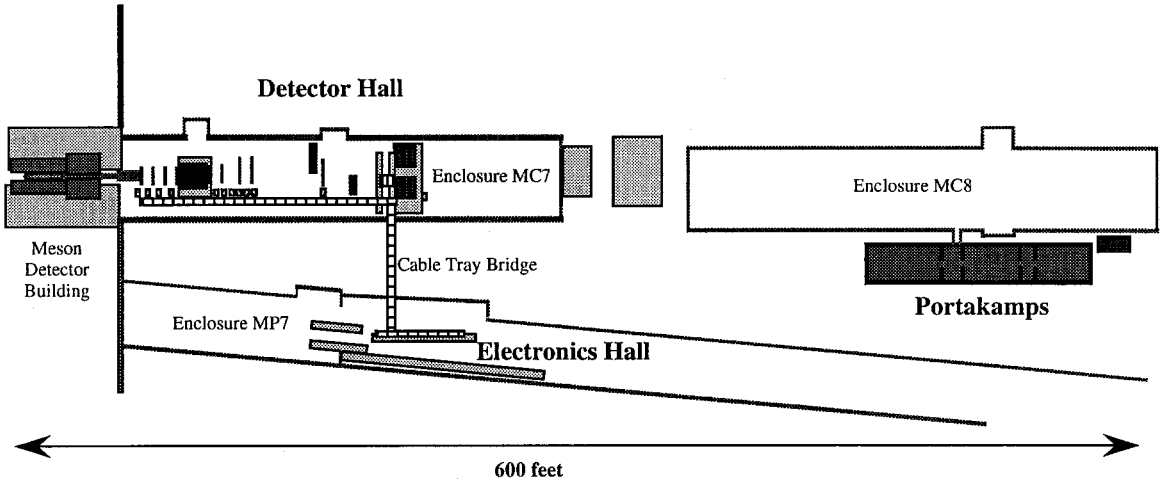

Figure 4: HyperCP experimental layout. The spectrometer rests in MC7, the front-end electronics are in MP7, and the data acquisition system and on-line computers are in the Portakamps.

3 Description and Performance of the Spectrometer in 1997

The layout of the experimental area is given in Fig. 4, and the plan and elevation views of the spectrometer are shown in Fig. 5. The spectrometer is in the Meson Center beam line at Fermilab. For reasons related to radiation safety and economics, the front-end and trigger electronics are in the neighboring beam line (MP), and the data acquisition system is in a Portakamp 100 m away.

CP violation in hyperon decays is best studied using a simple, high-rate spectrometer. High rate is required to achieve the necessary statistics, while simplicity is demanded to keep systematic effects small and controllable.

Ξ hyperons are produced by steering an 800 GeV proton beam into a 2 mm by 2 mm copper target, either 2 cm or 6 cm in length. Different target lengths are used to

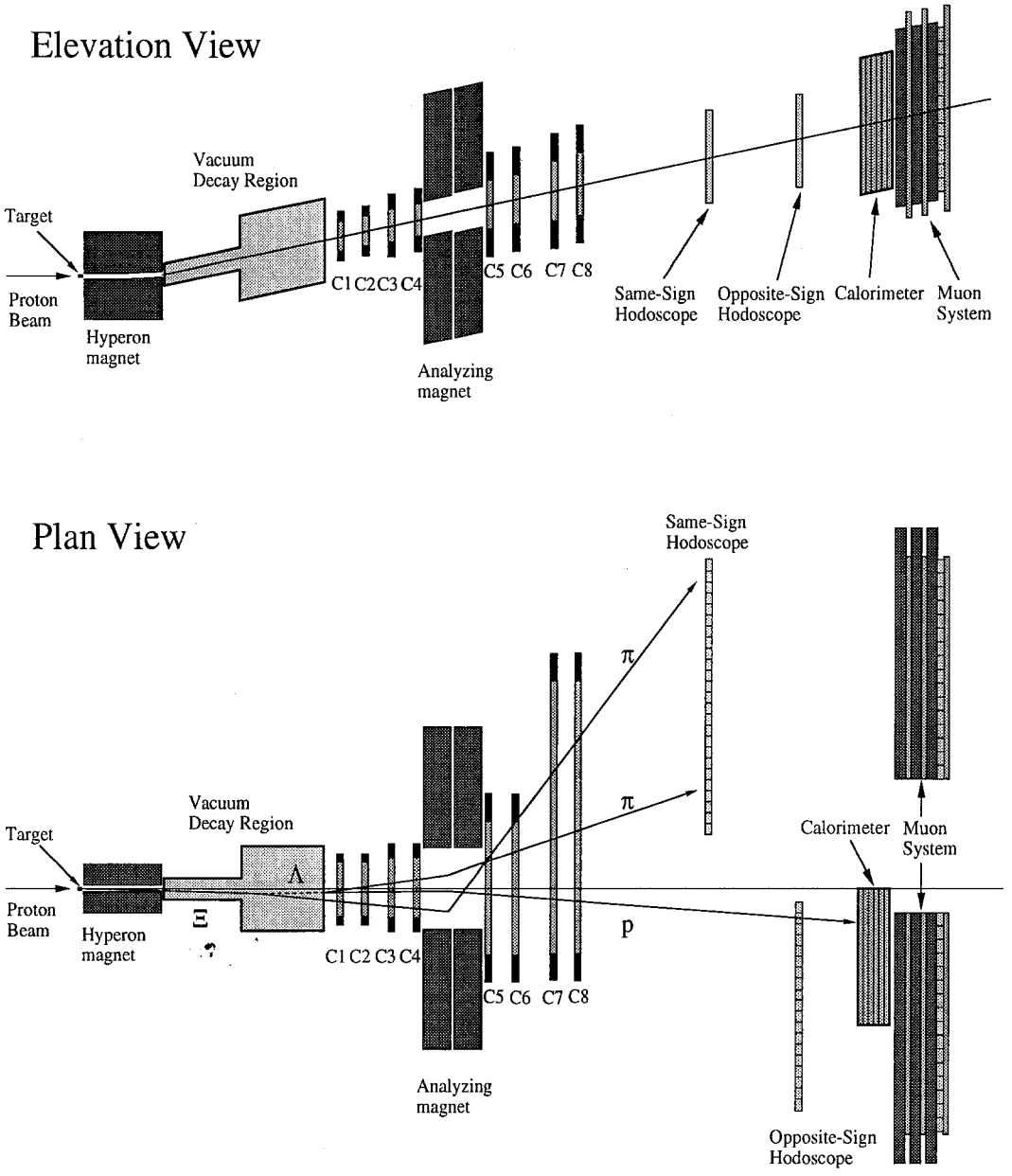

Figure 5: Plan and elevation views of the HyperCP apparatus.

equalize the secondary beam rate in the spectrometer between Ξ^- and $\overline{\Xi}^+$ runs. A 4.88 μsr collimator centered with the incoming proton beam and embedded within a 6 m long 1.67-T dipole magnet selects charged particles having an average momentum of about 170 GeV/c. To go from Ξ^- to $\overline{\Xi}^+$ running, the polarities of both the selection magnet and the spectrometer analysis magnet are reversed. A typical primary beam intensity of 1.5×10^{11} protons per spill gives a secondary beam rate of 20 MHz at the exit of the collimator. Upon exiting the collimator, the secondary beam traverses a 13 m long evacuated decay pipe after which it enters the spectrometer proper.

Immediately downstream of the decay region are four high-rate proportional wire chambers, followed by an analyzing magnet composed of two BM109 dipoles having a combined p_t kick of 1.43 GeV/c, followed by another four high-rate proportional wire chambers. The analysis magnet has sufficient strength to ensure that the protons and pions from the Ξ, Λ and K decays are always well separated from each other as well as from the charged beam in the downstream portion of the spectrometer. This allows a simple, yet selective, trigger to be formed by requiring the coincidence of charged particles in the hodoscopes at the rear of the spectrometer, on either side of the channeled beam. A hadronic calorimeter on the proton side is used to make the trigger "blind" to muons and to reduce the trigger rate from interactions of the channeled beam in the spectrometer. A simple muon system at the rear of the spectrometer allows access to rare and forbidden decays. To reduce multiple scattering and secondary interactions, helium bags are positioned between the detector components and within the analyzing magnet apertures.

The data are recorded with two data acquisition (DAQ) systems: a fast DAQ to read out events to tape and a slow DAQ used to read out the scalers and other beam-line information to disk. The fast DAQ reads data from two front-end latch systems: one for the spectrometer chambers and the other for the muon chambers. The data are transferred into a large (960 Mbyte) fast buffer via five parallel optical paths. The events are then built in parallel in five VME crates by 15 MVME167 single-board computers and written by 45 Exabyte 8505 tape drives. At the 20 MHz secondary-beam rate, the data acquisition system has a rate to tape of 13 Mbytes/s or approximately 75,000 events per second of beam.

3.1 Wire Chambers

The heart of the HyperCP spectrometer is eight high-rate, narrow-pitch multiwire proportional chambers (MWPC)[2]. All MWPCs have a similar construction; four anode wire planes are sandwiched by cathode foils and two outer grounded foils terminate the field region. The anode planes comprise two bend-view windings (X & X', shifted by half a wire spacing) and two windings inclined at $\pm 26.6°$ (U & V). All together the MWPC

[2]A ninth chamber, intended to provide an additional measurement of the high momentum daughter baryon position, had an insignificant effect on the mass resolution and was eventually used as a replacement chamber.

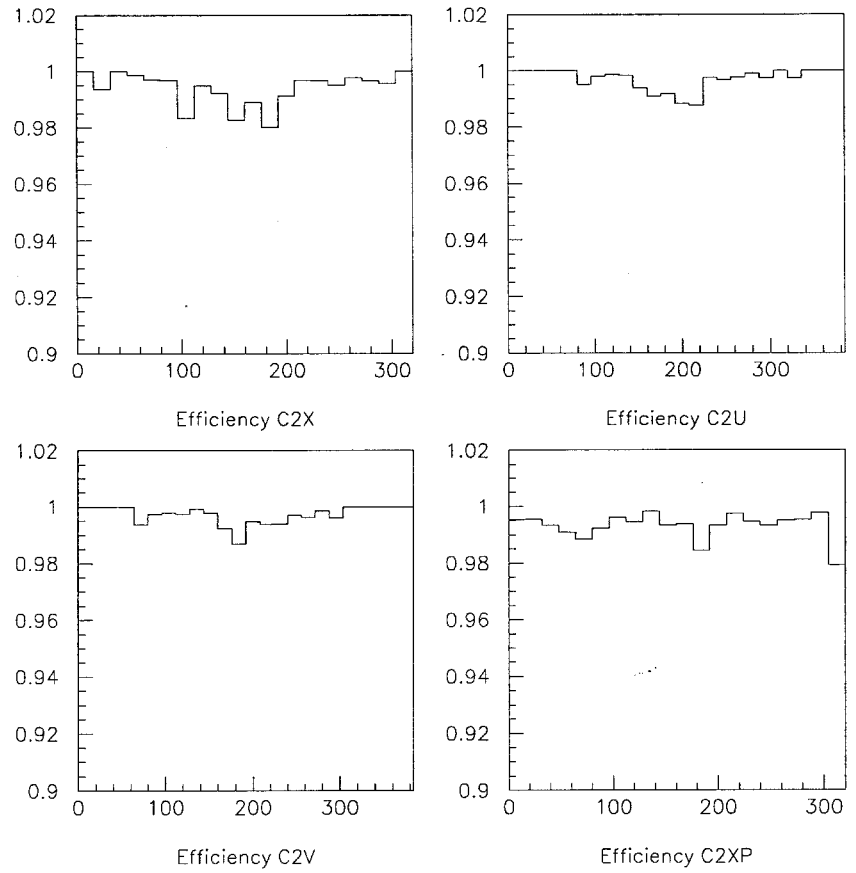

Figure 6: Localized chamber 2 efficiencies in groups of 16 wires at a channeled beam intensity of 20 MHz.

system comprises 18,752 instrumented wires.

The wire chambers all have small anode-cathode gaps (3 mm) and narrow wire spacings in order to perform efficiently and to have good aging properties in the intense secondary beam emanating from the collimator. For the majority of the 1997 run the total secondary beam rate through the chambers was about 20 MHz, corresponding to a typical individual wire rate of 0.4 MHz and a local flux of 0.5 MHz/cm^2 at the center of the most upstream chamber. The hyperon decay products inhabit the same region of the upstream wire chambers as the channeled beam while in the downstream chambers they inhabit somewhat disjoint regions. For this reason chambers C1–C4 were filled with a "fast-gas" mixture of CF_4-isobutane to reduce their sensitivity to out-of-time hits. The downstream chambers C5–C8 were filled with an Argon-Ethane-isopropyl mixture, since less time resolution was needed. To accommodate the higher intensity planned for the 1999 run we intend to use the fast gas mixture in all chambers.

At the nominal intensity of $\sim$ 20 MHz the efficiencies across the chambers were high and relatively uniform, dipping only slightly in the beam region, as shown in Fig. 6.

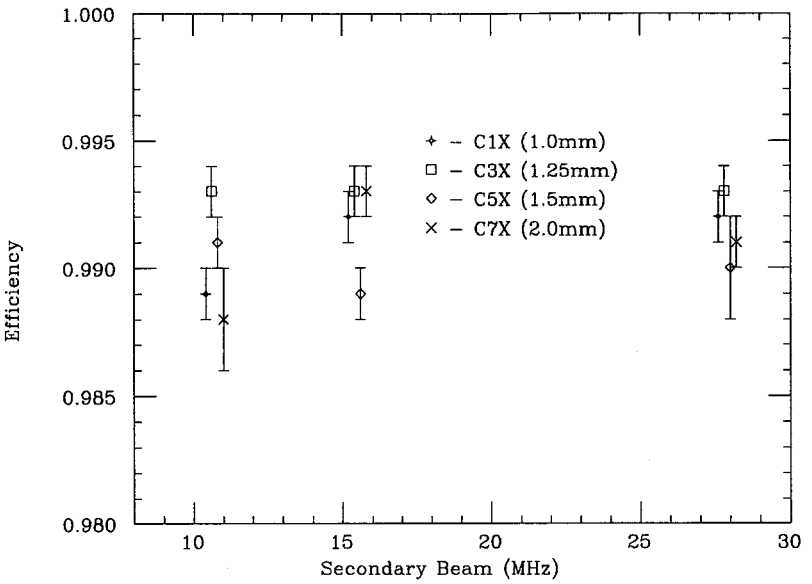

Figure 7: Chamber efficiency versus secondary beam intensities. Most of the running was at 20 MHz.

Furthermore, as seen in Fig. 7, the efficiencies were insensitive to intensity over the running range of the experiment.

In addition to its good timing properties, the CF_4-isobutane mixture is also known to mitigate the effects of aging. Over the course of the 1997 run a moderate amount of charge ($\sim$ 0.02C/cm) was accumulated along the wires in the beam region of the upstream chambers. Periodic monitoring of ^{55}Fe pulse amplitude in the beam region (see Fig. 8) has shown no indication of gain degradation of the anode wires due to aging. Another defense against aging is to operate the chambers at a low avalanche gain. Due to the low noise of the front-end system, the chambers achieve the efficiencies shown at an avalanche gain of only $\sim 4 \times 10^4$.

3.2 Trigger

A total of 24 triggers was used in the experiment, most for diagnostic and monitoring purposes. The triggers were fast, with single-bucket resolution (19 ns), simple, and provided high yields to tape. Only first-level triggers were employed. Common to all the physics triggers was a left-right coincidence of charged particles in the Same-Sign (as the channeled beam) and Opposite-Sign hodoscopes at the rear of the spectrometer. The addition of the hadronic calorimeter to the Cascade[3] and Kaon triggers reduced their rates by about a factor of six, with a very conservative minimum energy threshold. The typical Ξ-trigger rate was 30 kHz and the overall trigger rate including the Kaon,

[3]Calling it a Cascade trigger is a bit of a misnomer as it only requires two charged particles of opposite sign, and hence is really a Lambda trigger.

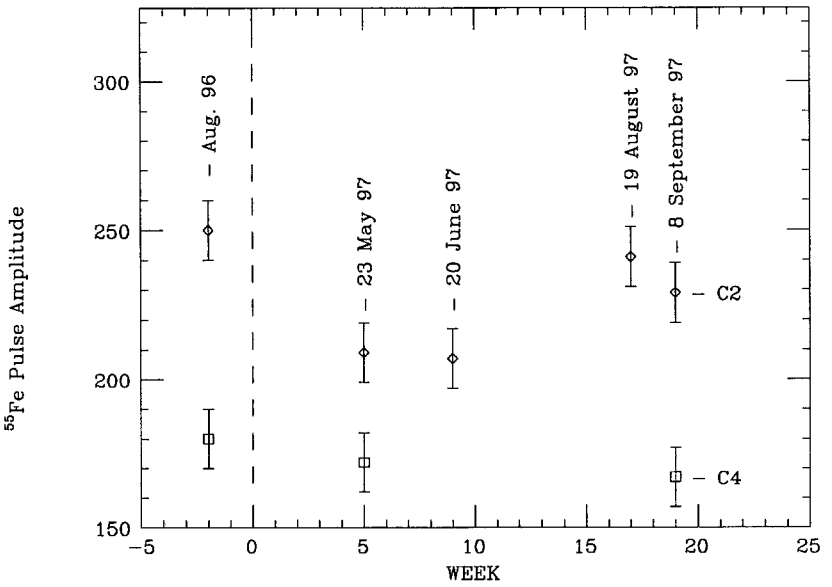

Figure 8: Gain vs time for chambers C2 and C4, measured with an ^{55}Fe source.

muon, and monitoring triggers was 75 kHz.

The trigger worked well and provided a high yield to tape. For example, typical Λ ($\overline{\Lambda}$) yields were 20% (5%) for the Cascade trigger. The trigger rate was about a factor of two higher than our Monte Carlo predictions, which is not surprising since the simulations did not include gamma conversions and particle production at the collimator exit. Every hodoscope element, sub-trigger, and trigger was scaled and written to disk by the slow DAQ, as well as being latched and written to tape by the fast DAQ.

3.3 Hadronic Calorimeter

The calorimeter is employed to provide a "muon blind" component to the standard left-right trigger and to reduce the trigger rate due to interactions in the spectrometer material. The calorimeter: 1) is fast, to avoid pile-up due to the high rate of interactions in the spectrometer, 2) has a sharp energy threshold, and 3) has the ability to detect muons. The calorimeter is 1 m^2 in area and 9.6 interaction lengths long. All of the protons from Λ's decaying in the evacuated decay volume lie within a fiducial area of about half the calorimeter area.

The left hand plot in Fig. 9 shows the trigger efficiency as a function of energy of charged particles entering the calorimeter for a trigger threshold of about 50 GeV [4]. Note the sharp turn-on in acceptance. The right hand plot shows the total energy entering the calorimeter for charged particles of momentum between 100 and 120 GeV/c. Our preliminary (uncalibrated) estimate of the calorimeter resolution is: $\sigma/E = 80\%/\sqrt{E} + 2.5\%$.

[4]The minimum energy from a Λ decay proton is about 70 GeV.

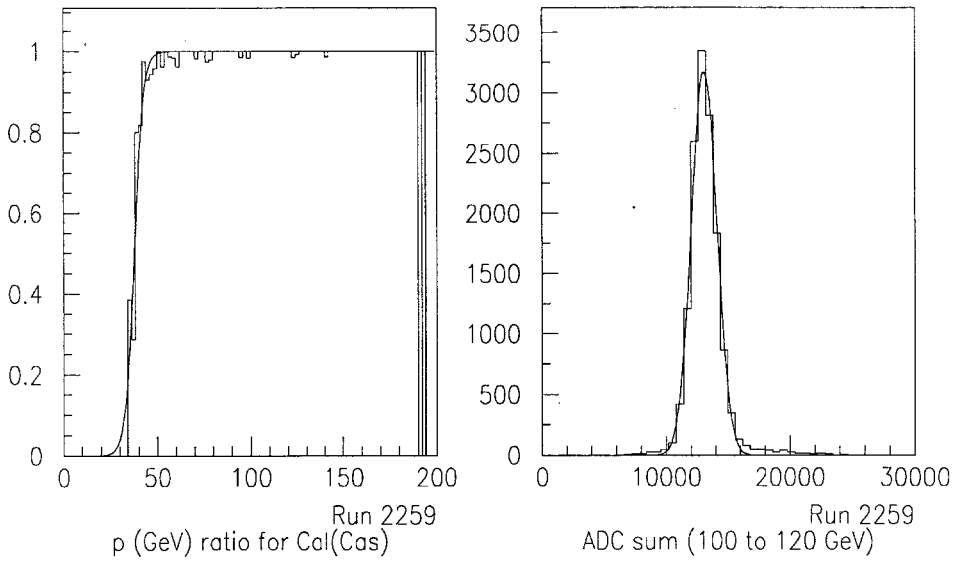

Figure 9: The left-hand plot shows the calorimeter trigger efficiency as a function of energy. The right hand plot shows the sum of the raw photomultiplier signals for all charged particles of momentum between 100 and 120 GeV/c.

3.4 Muon System

A muon station at the rear of the spectrometer was employed to allow rare and forbidden Hyperon decays to be accessed. (See Appendix A for more details on these physics topics.) The muon system is made up of two identical detectors, one on each side of the beam. Each consists of three stations (front, mid and rear) of proportional tubes separated by 0.81 m of steel. Each station contains an x and y readout plane. Two crossed scintillator hodoscopes following the rear proportional tube station provided triggering capability and helped to identify in-time proportional tube hits[5].

The proportional tubes use an Argon $-$ CO_2 (90/10) gas mixture. The efficiencies of the various muon detector elements, measured with beam, are shown in Fig. 10. Due to the wall thickness separating prop-tube cells, their efficiency is limited to $\sim$ 94%.

3.5 Data Acquisition System

The HyperCP data acquisition system is the fastest in the world, with a trigger rate of up to 80 kHz and a throughput to tape of 13 MB/s. Simplicity and parallelism are its hallmarks. The average dead time per event was 3 μs, and the average event size during standard running was 550 bytes. With the trigger rate listed above, HyperCP produced data at 44 MB/s during the spill for a continuous rate to tape of 13 MB/s. Tests with

[5]The proportional tube time resolution is limited to the total drift time since a simple latch read-out is used.

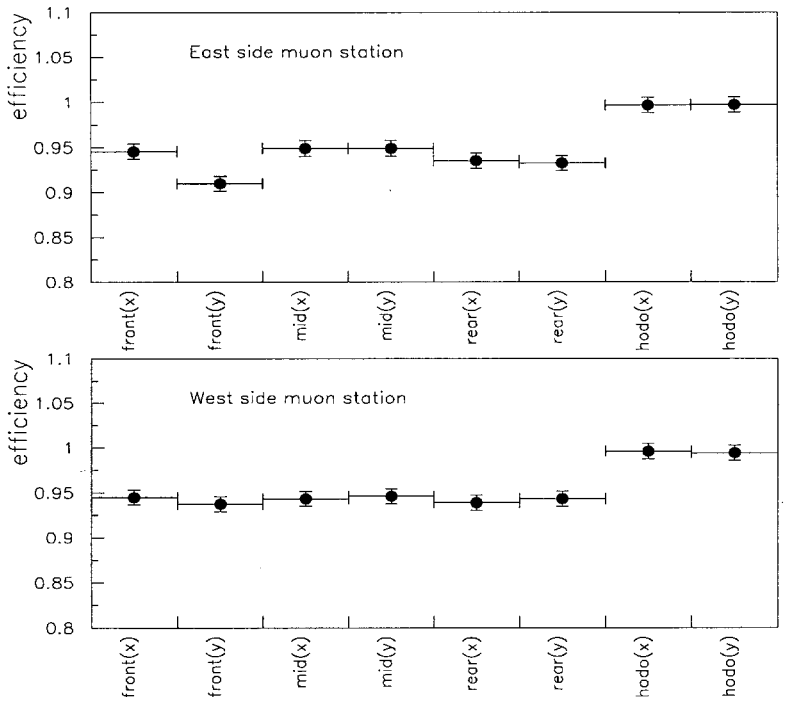

Figure 10: Average individual detector efficiencies of the muon system. The two rightmost points are the muon scintillator efficiencies whereas the other points are proportional tube efficiencies. Note that the maximum theoretical efficiency of the proportional tubes is 94% due to dead space between cells.

improved DAQ software made towards the end of the run gave a maximum sustainable data rate to tape of 17 MB/s.

Figure 11 shows the structure of the data-acquisition system. Information from the detectors was digitized and sparsified by two front-end systems: one based on the Nevis protocol and used to read out the wire chambers, latches and calorimeter ADC's, the other custom system designed by the Taiwan group and used to read out the muon chambers. The data were then transmitted via optical fibers to the VDAS (video data-acquisition system) spill buffers [19] in the control room. Five event-building systems operating in parallel accessed the VDAS to assemble events and record them on tape. Each event-building system was housed in a single VME crate and was composed of three MVME167 processors, five Event Buffer Interfaces (to provide access to the VDAS), and three Ciprico RF3573 SCSI host adapters [20] which each control three Exabyte 8505 tape drives [21]. Control of the system was provided via Ethernet links to each "Boss" MVME167 processor and to two booting and monitoring processors (not shown in the diagram) located in the Electronics Hall.

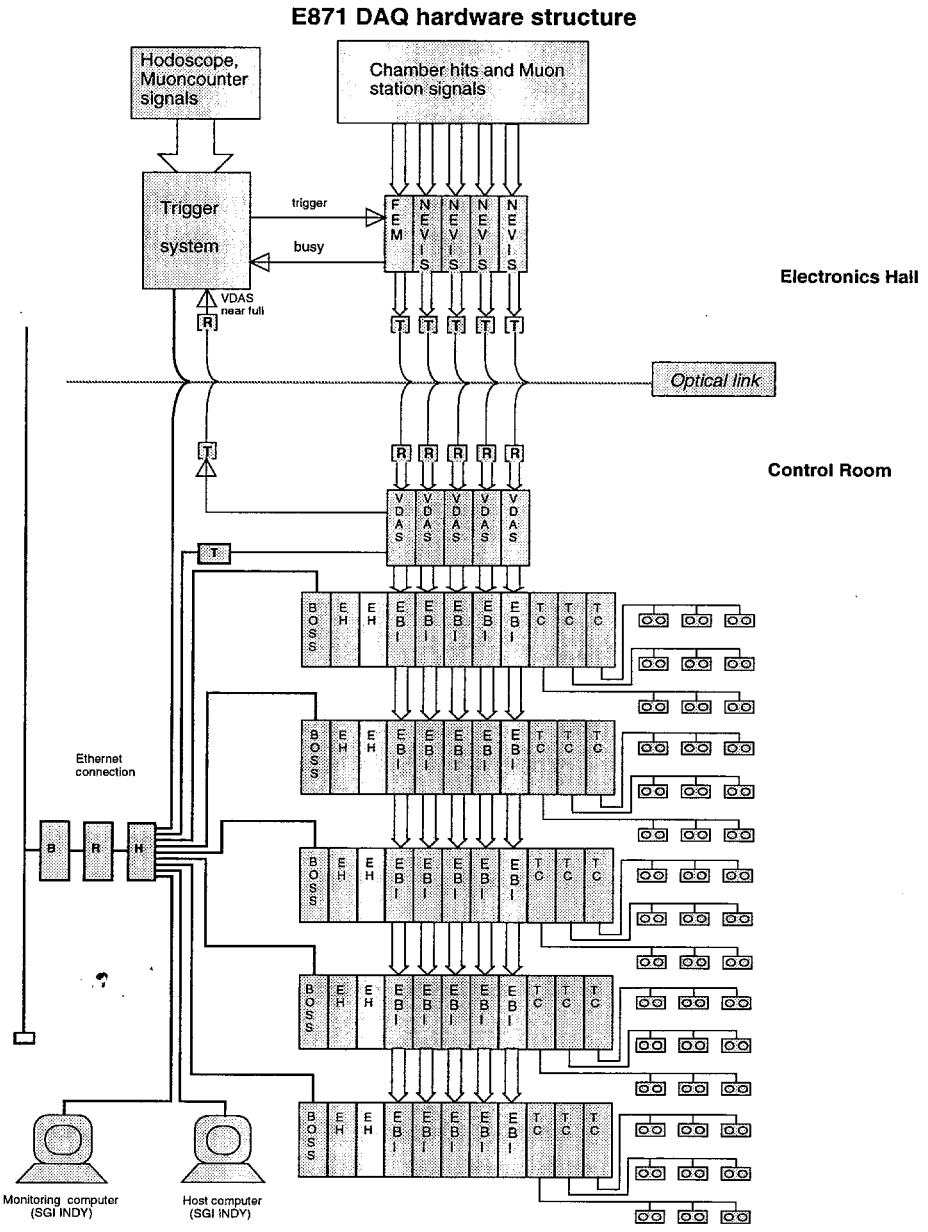

Figure 11: Block diagram of the HyperCP data acquisition system.

4 Synopsis of the 1997 Run

Although the fixed target run began in June 1996, because of our low priority, HyperCP did not receive beam until October 1996. After four months of beamline and spectrometer commissioning, the run officially began for HyperCP on April 4, 1997. Normal data-taking was completed after 16 weeks of running at the end of July[6] and was followed by systematic studies and special runs, which ended on September 5. The performance of the spectrometer improved continually throughout the run, and by the end of the run HyperCP was running at a high efficiency and consistently at our nominal beam intensity. The spectrometer worked as proposed. The only real surprise that we encountered is the fact that the $\overline{\Xi}^+$ production cross section is apparently about a factor of two lower than anticipated, which is part of the reason we did not accumulate as many $\overline{\Xi}^+$'s as expected.

A total of 75 billion events on 11,266 data tapes was accumulated during the run, with 63 billion events on 9,376 data tapes from the 16 weeks of normal data-taking. About twice as much time was spent running on positives than negatives because of the smaller $\overline{\Xi}^+$ yields.

The number of events written to tape and the yields are given in Table 3. We expect to reconstruct 1.6 billion $\Xi \to \Lambda\pi$ decays and 280 million $K^\pm \to 3\pi$ decays, as well as a large number of $\Omega \to \Lambda K$, and $K_s \to \pi^+\pi^-$ decays[7]. Since the statistical error in $A_{\Xi\Lambda}$ is given by:

$$\delta A_{\Xi\Lambda} = \frac{1}{2\alpha_\Xi \alpha_\Lambda}\sqrt{\frac{3}{N} + \frac{3}{\overline{N}}}, \tag{12}$$

where N and $\overline{N}$ are the numbers of Ξ^- and $\overline{\Xi}^+$ events respectively, this sample of 2.84×10^8 $\overline{\Xi}^+$ and 1.31×10^9 Ξ^- events translates into an overall sensitivity of $\delta A_{\Xi\Lambda} \simeq 2 \times 10^{-4}$.

Further efforts at enhancing the Ξ yield by improving the reconstruction software and "rescuing" events in which one track has only its direction measured are underway.

5 Status of the Analysis of the 1997 Data

Since the end of the run we have concentrated our efforts on: 1) careful studies of the track reconstruction codes, 2) improving the event yield, 3) bringing up the farm code, and 4) making preliminary physics studies. Three different tracking codes using different algorithms were written and very carefully compared. Many other studies, such as measuring chamber efficiencies, magnetic field maps, alignment constants, etc., have been undertaken and are still in progress.

[6]However, three weeks were lost due to accelerator down time.

[7]The K_s's are produced by secondary beam interactions near the exit of the collimator.

Table 3: Total number of events written to tape and expected number of reconstructed events.

Events on tape			
	Channeled beam polarity		
Trigger	+	−	Total
Cascade	24.5×10^9	14.9×10^9	39.4×10^9
Kaon	40.8×10^9	21.3×10^9	62.1×10^9
All	48.8×10^9	25.6×10^9	74.4×10^9
Expected Number of Reconstructed Events			
	Channeled beam polarity		
	+	−	Total
$\Xi \rightarrow \Lambda\pi$	284×10^6	1310×10^6	1.59×10^9
$K \rightarrow 3\pi$	204×10^6	75×10^6	279×10^6

5.1 Status of the Farm Data Processing

As Table 4 shows, the amount of computing power needed to reconstruct the events is quite large. Hence all of the primary data analysis will take place on the Fermilab farms. This analysis is underway and we expect that by the end of 1998, *and well before the beginning of the FY99 run*, all of the data will have been reconstructed.

The farm analysis began November 15 with one older, low-performance farm, `fnsfh` of two production systems utilizing 31 and 32 30-MIPS SGI Indy worker nodes. The efficiency for getting complete jobs through the original SGI systems has been very low due to a combination of hardware and software problems (not related to our code) which are not resolved as of this writing, despite the hard work of personnel in the Fermilab Computing Division.

On November 21 we were allocated two additional higher-performance farms: `fnsfo`, an SGI system with ten 114-MIPS workers, and `fnckm`, an IBM system with ten 115-MIPS workers. Our experience with these farms has been much better, and outside of a few startup problems we have run continuously on these systems.

With the current farm systems we have processed about 1% of the data. By February we hope to be ramped up to 10,000 MIPS. Our experience with the two higher-performance farms indicates that we can reconstruct about 45 million events per day on each farm. Hence with a 10,000 MIPS system we expect to be able to reconstruct about 375 million events per day, which corresponds to 200 days to reconstruct the entire 75 billion event data sample. Taking overhead into account, all the raw data should be processed in one calendar year.

We expect that the Monte Carlo analysis will take a further several months of time on the farms. Physics analysis will be conducted on machines at the home institutions,

Table 4: HyperCP 1997 run computing requirements.

Process	Events	Analysis time (MIPS-sec) Per event	Total
Raw data processing	75×10^9	2.0	150×10^9
Physics analysis	5×10^9	0.2	1×10^9
Monte Carlo studies	5×10^9	4.0	20×10^9
Total:			170×10^9

where there are about 4,000 MIPS of computing power available.

5.2 Preliminary Results

In what follows we show some plots that give an indication of the quality of the data. All of these results are preliminary, as we continue to work on the code and constants, and come from a tiny fraction of the data.

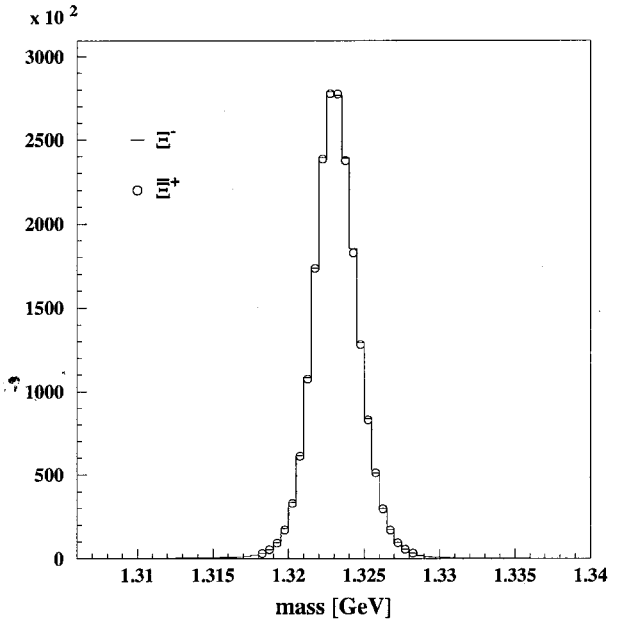

Figure 12: $\Lambda\pi$ invariant mass for negative and positive Ξ-trigger events. The mass resolution is 1.5 MeV/c^2.

A normalized comparison of the $\Lambda\pi^-$ and $\overline{\Lambda}\pi^+$ masses, based on some 2 million reconstructed Ξ^- and 0.5 million $\overline{\Xi}^+$ events, processed by the farms, is shown in Fig. 12.

The excellent mass resolution of $\sigma = 1.5\,\mathrm{MeV/c^2}$ is already at the level expected from the Monte Carlo. The level of the background is considerably less than 10^{-3}. As the background is thought to be mainly poorly measured Ξ's, improvements in the magnetic field parametrization and alignment constants will reduce it further.

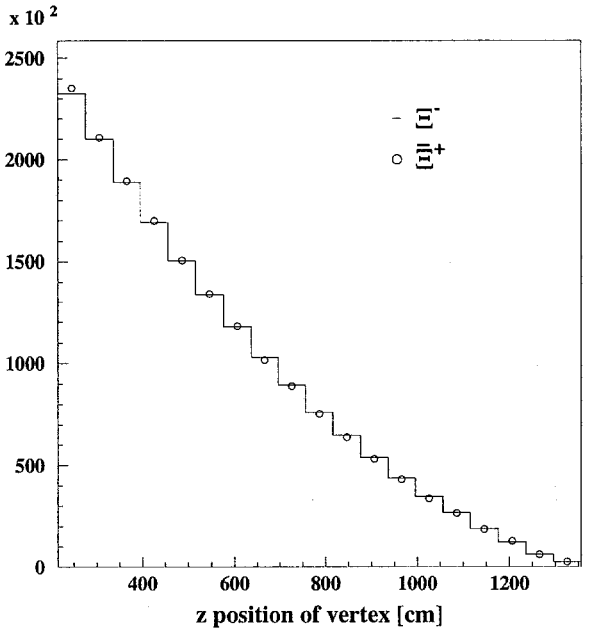

Figure 13: Decay vertex distribution for Ξ^- and $\overline{\Xi}^+$ events.

Figure 13 shows the distributions of the Ξ^- and $\overline{\Xi}^+$ decay vertices. The agreement is excellent. No acceptance corrections have been made in this or any other plot. Figure 14 shows the $\pi^\pm\pi^\pm\pi^\mp$ invariant mass in the region of the $K^\pm$ mass. The mass resolution of 2.7 $\mathrm{MeV/c^2}$ is again consistent with Monte Carlo estimates. Figure 15 shows a comparison of Ω^- and $\overline{\Omega}^+$ masses as measured through their ΛK decay products. The agreement in mass *and background level* is again striking. Finally, we note that approximately 1% of our triggers is from the $\pi^+\pi^-$ decays of K_s's produced near the exit of the collimator, which provides us with a running calibration of the spectrometer magnetic field. The resultant $\pi^+\pi^-$ invariant mass distribution is shown in Fig. 16.

In Fig. 17 we show the preliminary *uncorrected* distributions of the cosine of the polar angle that the proton (anti-proton) makes with respect to the Λ ($\overline{\Lambda}$) polarization in the Λ ($\overline{\Lambda}$) helicity frame — the key comparison in finding a CP-violating effect in our experiment. The errors are negligible compared to the size of the symbols used. *Again, we emphasize that no acceptance corrections have been made.* The approximate linearity shows illustrates the excellent acceptance over the full polar angle range. The two distributions are clearly comparable. A detailed analysis of these events, which represents less than one day of running, would already establish CP invariance at a statistical level about an order of magnitude better than the best published result.

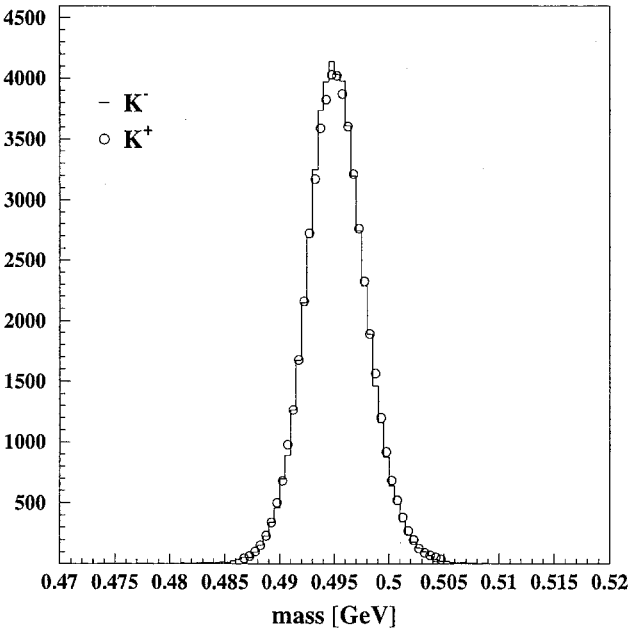

Figure 14: The $\pi^{\pm}\pi^{\pm}\pi^{\mp}$ invariant mass for positive and negative K-trigger events. The mass resolution is 2.7 MeV/c^2.

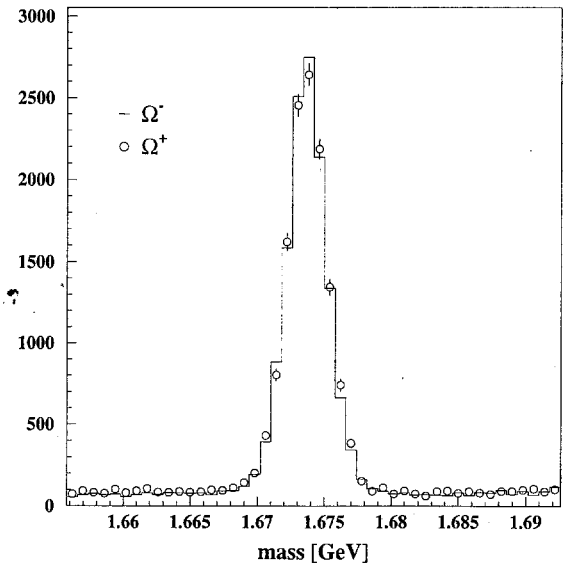

Figure 15: ΛK mass distributions for events after kinematic and geometric fit. The mass resolution is 1.5 MeV/c^2.

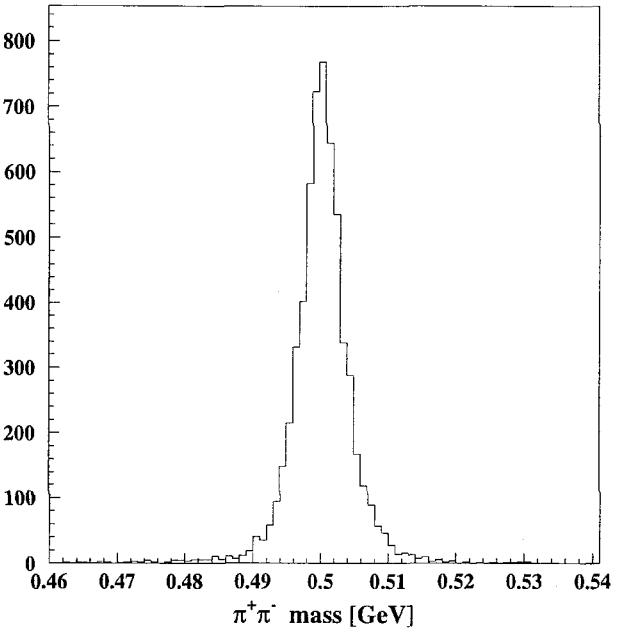

Figure 16: Distribution of $\pi^+\pi^-$ mass. The mass resolution is 4.6 MeV/c^2.

We have started studying the systematic effects that were addressed in the original proposal, and which are summarized in Appendix B. Although the previous results are quite promising, and show no indication of biaes, these studies are still quite immature.

In addition to searching for CP violation in Ξ and Λ decay, there are several analysis efforts going in parallel that address other physics topics. These are briefly discussed in Appendix A.

6 FY99 Run

The Fermilab draft long-range schedule of November 1997 has the Tevatron fixed-target run beginning April 1, 1999, with 8 weeks of startup and 20 weeks of fixed-target beam. In what follows, we assume a 16 week run with normal data-taking followed by a 4 week series of systematic studies.

6.1 Sensitivity in CP violation for the FY99 Run

With the commissioning of the Main Injector, the upcoming 800 GeV fixed target program in FY99 will allow us to meet and exceed the original goals of HyperCP. Most of the improvement will come from accruing more data by running more efficiently and at a higher intensity. In the 1997 run we started with a rather low intensity and efficiency. Merely running at the intensity and efficiencies that we routinely achieved during the last month of the run will increase our yield by about a factor of three. A better duty

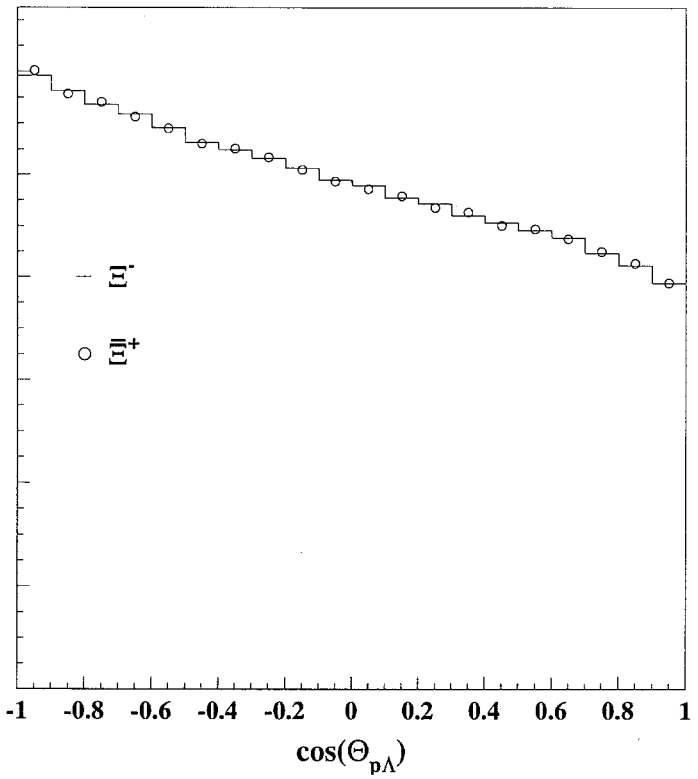

Figure 17: Distribution of cosine of the angle $\theta_{p\Lambda}$ between the momentum of p($\overline{\text{p}}$) and the $\Lambda(\overline{\Lambda})$ polarization in the $\Lambda(\overline{\Lambda})$ rest frame.

factor and a slight increase in intensity will increase that to at least a factor of four. If offline studies show no degradation in the quality of the special high-intensity data we took in 1997, then we could increase that factor to about six before DAQ bandwidth and radiation safety become limiting factors. Note that the length of the FY99 run should be almost the same as our official 1997 run, which lasted from the beginning of April until the end of July, but which had three weeks of accelerator down time. However, it is imperative that we hit the ground running, which given the modest changes we will make to the apparatus, should be feasible.

Combining the samples of 1997 and FY99 runs, the projected statistical uncertainty in $A_{\Xi\Lambda}$ is 9×10^{-5} or better. In addition to increasing the data volume, the data quality will be improved with minor, but significant, improvements in the apparatus, monitoring software, and better understanding of our spectrometer.

Table 5 is a comparison of the running conditions between the 1997 run and the FY99 run. We intend to increase the nominal proton intensity by a factor of 1.33 from what it was at the end of the 1997 run, corresponding to a secondary beam rate of 25 MHz for the upcoming run. As shown in Fig. 7, this conservative increase in intensity will have very little effect in the performance of the spectrometer. Indeed, we have run at

	1997 run	FY99 run
Nominal intensity (protons/s)	7.5×10^9	1.0×10^{10}
Channeled beam rate (MHz)	20	25
Spill duty factor	18s/60s	40s/80s
Calendar time (Weeks)	16	16
Mean 'efficiency' (%)	28	50
Effective total number of spills	44,440	60,480
Total number of protons	6×10^{15}	2.4×10^{16}

Table 5: Comparison of protons on target for the 1997 and FY99 runs, excluding special data-taking runs.

even higher intensities. Increased backgrounds are holding us back from running at even higher intensities.

It is proposed that the Tevatron will have a 40 second spill followed by a 40 second interspill period in the FY99 run, for a 50% duty factor. The duty factor in the 1997 run was 30%, which means that, for a given intensity, a gain of 1.66 in yield is achieved.

The 'efficiency' given in Table 5 is the product of two factors: 1) the fraction of total spills that we wrote good data to tape, and 2) the fraction of the nominal beam intensity at which we ran. For the 1997 run it is calculated by dividing the total amount of protons incident on target during normal data-taking by the number of protons we would have taken had we run at the nominal beam intensity 24 hours a day for the entire period. Hence the 'efficiency' includes accelerator down-time, which was about three weeks in the 1997 run, our own inefficiencies, and the less than nominal intensities at which we ran at the beginning of the official run. We expect to have an overall 'efficiency' in FY99 of 50% — what we routinely achieved at the end of the 1997 run — for a gain of 1.78 in yield.

With these gains we will accumulate a factor of four more data in FY99 than in our first run. And as we continue to explore the intensity-and-yield limit of our experiment based on data on tape, it is quite feasible that we can do better than a factor of four.

6.2 Improvements for the FY99 Run

Although the apparatus worked remarkably well, particularly given the tight fabrication schedule and minimum commissioning time, a number of areas of improvement has been identified. The major area of improvement is an increase in the speed of the fast data acquisition system, where our intention is to double the throughput to tape.

The modifications are itemized below. Not listed is a host of minor, but significant improvements that require a minimum of funding and effort. Nevertheless, these improvements taken in aggregate, will substantially improve the quality of the data.

- **Data acquisition modifications.**

  Some of the improvements to the data acquisition system have already been designed and tested. These include reducing the event size, tape-writing via the SCSI bus on the single-board computers, and switching to the new Exabyte 8705 tape drives.

  The maximum rate we could write to tape in the 1997 run, 13 MB/s, was limited by software inefficiencies. Improved software was tested towards the end of the run which will allow a rate of 17 MB/s, close to the theoretical maximum throughput of the tape drives. The effective rate can also be improved by a data compression scheme for the wire chamber data. Such a scheme exists in software and reduces the event size by about 30%. Implementation of this scheme in the hardware (before the VDAS buffers) is straightforward.

  With data compression in place, the average event size for the FY99 run will be 385 Bytes, as shown in Table 6. Since the trigger rate will be about 100,000 Hz, we will acquire 1.54 GB of data in every 80-s spill. This translates to a minimum DAQ throughput of 19 MB/s for writing all events to tape in 80 s. This requirement is beyond the capability of the 45 Exabyte 8505 tape drives in the 1997 DAQ system. This, coupled with the fact that the Exabyte 8505 tape drives we used in the 1997 run have been heavily used and are worn out, dictates replacing them with the new Exabyte 8705 drives that use the same tape medium but have a throughput of 1 MB/s.

  By upgrading the real-time operating system to VxWorks 5.3, the tape drives can be connected directly to the SCSI bus on the MVME167 single-board computers, reducing the traffic congestion on the VME back plane. This is an option not available with VxWorks 5.1. Figure 18 shows the results of a test driving three Exabyte-8705 tape drives from one SCSI port of a MVME167. It is clear that we can achieve a throughput of about 40 MB/s with three Exabyte 8705 drives on each of the fifteen MVME167 computers that we have in our existing DAQ.

  We also intend to reduce the dead-time of the front-end readout electronics. This will be done by increasing the speed of the readout clock, reducing the event size by limiting the maximum number of latched words per crate, and re-routing the gating system.

  The upgraded DAQ system for the FY99 run should have enough headroom to allow for beam intensities beyond what we stated in Sec. 6.1.

- **Collimator modifications.**

  There are indications that the collimator was misaligned resulting in the loss of some fraction of the secondary beam. We are currently using data to understand the misalignment and to correct the problem for the 1999 run. We will also take the opportunity to modify parts of the collimator to eliminate a hot spot producing

	1997 run	FY99 run
Trigger rate (Hz)	75,000	100,000
Event size (Bytes)	550	385
Data volume per spill (MB)	825	1540
DAQ throughput (MB/s)	13	19
Total number of spills	44,440	60,480
Total number of events (billion)	63	242
Total data volume (TB)	33	93
Number of 5-GB tapes	9,376	20,000

Table 6: Specifications of the DAQ for the 1997 and FY99 runs, excluding special data-taking runs.

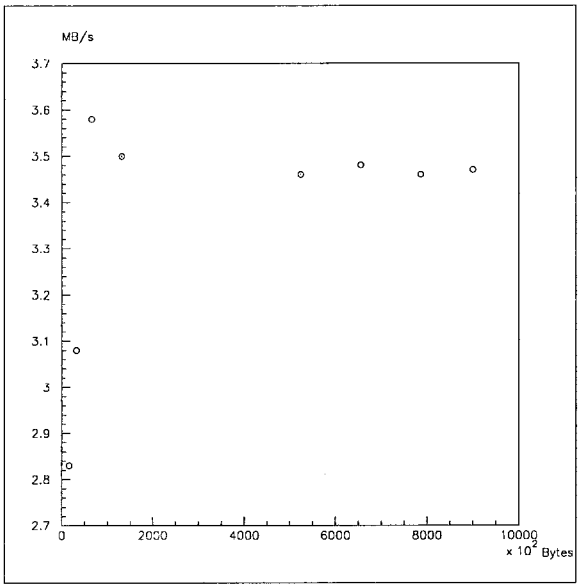

Figure 18: Throughput of Exabyte 8705 tape drive as a function of the data-block size. Three Exabyte 8705 drives in compressed mode were used with one MVME 167 single-board computer.

tertiary particles and to minimize the thermal stress in the two high-precision Hall probes located near the exit of the channel (which knocked out their temperature sensors).

- **Preamplifier modifications.**

  The preamps on one of the large chambers downstream of the analysis magnet would occasionally break into oscillation during bursts of high instantaneous beam intensity. A simple retrofit by back-terminating the preamplifier outputs will alle-

viate this problem.

- **Minimum bias trigger modifications.**

  Our minimum bias events were collected with a simple secondary beam counter that could only handle low intensity. We plan to replace it with a coarsely segmented scintillating fiber hodoscope.

- **Target SWIC modifications.**

  During the run, the two 0.5 mm-pitch target SWICs developed a few dead or inefficient channels in the critical region for monitoring the incident angle of the proton beam. They should be replaced for the 1999 run.

- **Air conditioning modifications.**

  There are two air conditioning units in MC7 for cooling the preamplifiers and discriminators of the wire chambers. These units did not have enough capacity. With improved air conditioning in this area the rate of electronic failure will drop significantly. This, in turn, will increase our run time efficiency by reducing the number of accesses to MC7 for replacing bad cards.

6.3 Analysis of the FY99 Data

The amount of data we will need to analyze is estimated in Table 7. We expect to take 240 billion events of normal data and about 35 billion events for special studies. Because of improved data compaction and more efficient utilization of tape, we expect to write about 20,000 tapes, or only about a factor of two more than we wrote in the 1997 run. The total number of events will be increased by a factor of four, *if we keep the trigger fractions the same.* The Cascade trigger faction, which was about 50% in the 1997 run, could be increased to about 75% by prescaling some of the other triggers (and sacrificing some of the other physics). This would reduce the number of events written to tape by 25%. However, we assume throughout this proposal that the trigger fractions remain the same as in the 1997 run.

To analyze this data we request 20,000 MIPS of Fermilab farm nodes beginning in January, 2000. Assuming that our reconstruction program runs at its current speed, it should take 400 days to reconstruct all of the data.

6.4 Cost Estimate and Schedule

Institutional responsibilities will be the same as in the 1997 run. The responsibilities for the apparatus modifications and cost estimates are given in Table 8. Most of the funding for the upgrades will come through the DOE via the collaborating institutions. Fermilab will be responsible for the modifications to the collimator, and associated rigging.

Table 7: HyperCP FY99 run computing requirements.

Process	Events	Analysis time (MIPS-sec) Per event	Total
Raw data processing	275×10^9	2.0	550×10^9
Physics analysis	20×10^9	0.2	4×10^9
Monte Carlo studies	20×10^9	4.0	80×10^9
Total:			634×10^9

Table 8: HyperCP FY99 cost estimate.

Cost Estimate for the FY99 Run				
Project	Institution	Number	Cost	Total
Preamp retrofit	UVa	500	\$20	\$10,000
Replacement:MQS104 preamp chips	UVa	60	\$50	\$3,000
Replacement:MVL107 disc. chips	LBNL	100	\$20	\$2,000
Replacement:ADC chips	UVa	2	\$500	\$1,000
Calorimeter trigger module	UVa	1	\$2,000	\$2,000
Secondary beam counter	USA	1	\$8,000	\$8,000
DAQ upgrade (including tape drives)	IIT, LBNL, Taiwan	1	\$100,000	\$100,000
Collimator modifications	FNAL, LBNL	1	\$10,000	\$10,000
Hall probe replacement	FNAL	2	\$3,000	\$ 6,000
Subtotal:				\$132,000

APPENDIX

A Other Physics

We have built a world-class charged hyperon beam and spectrometer which allows other physics topics to be addressed besides the CP violation in hyperon decays. Most of these will be studied with unprecedented sensitivity. These are briefly described below.

- **CP violation in $K^{\pm} \to 3\pi$ decays.**
  We have accumulated 280 million $K^{\pm} \to \pi^{\pm}\pi^{\pm}\pi^{\mp}$ decays which will allow CP to be tested through the asymmetry in the slope parameter of the Dalitz plot. We expect a statistical precision of about 6×10^{-4}, an order of magnitude better than the current limit [22]. Theoretical predictions range from 1.4×10^{-3} to about 10^{-6} [23, 24, 25, 26].

- **Flavor changing neutral currents in hyperon decays.**
  No experiment has ever observed strangeness-changing neutral currents in hyperon decays such as $\Sigma^+ \to p\mu^+\mu^-$. Our single event sensitivity will be about 10^{-9}.

- **Flavor changing neutral currents in charged kaon decays.**
  The decay $K^+ \to \pi^+\mu^+\mu^-$ has recently been observed by E787 at BNL at a branching ratio of about 5×10^{-8}. HyperCP should see a few tens of these decays and confirm their result.

- **Lepton number nonconservation in kaon and hyperon decays.**
  Why total lepton number seems conserved is not understood and remains a question of fundamental importance. HyperCP addresses this problem through the $|\Delta L| = 2$ decays: $\Sigma^- \to p\mu^-\mu^-$ and $\Xi^- \to p\mu^-\mu^-$, as well as through the associated kaon decay: $K^+ \to \pi^-\mu^+\mu^+$. We will improve the current limits by four orders of magnitude to about 10^{-8}.

- **Measurement of the β parameter in Ξ decays.**
  The experiment accumulated a large amount of polarized Ξ^- and $\overline{\Xi}^+$'s by running at non-zero production angles. Measurement of the β term in equation (5) allows a determination of the strong phase shifts in Ξ decay through the relationship:

$$\frac{\beta}{\alpha} = -\tan(\delta_3^S - \delta_3^P),$$

where δ_3^S and δ_3^P are respectively the S- and P-wave strong phase shifts. This will allow the recent theoretical predictions of the phase shift, which differ significantly from earlier calculations, to be tested. Note that a small value for the phase shifts would imply that the asymmetry $A_{\Xi\Lambda}$ is dominated by CP violation in Λ decays.

- **Measurement of the polarizations of the Ξ^-, $\overline{\Xi}^+$, Ω^-, and $\overline{\Omega}^+$, and magnetic moments of Ξ^- and $\overline{\Xi}^+$hyperons.**
  Why hyperons are produced polarized in high energy interactions remains a mystery. HyperCP will study Ξ^- and $\overline{\Xi}^+$polarization at low x_F and p_T where there are little data, as well as the Ω^- and $\overline{\Omega}^+$ polarizations. Previous experiments concluded that if Ω^- is polarized, its magnitude must be small, and no experiment has measured the $\overline{\Omega}^+$ polarization. A byproduct of this will be precision measurements of the Ξ^- and $\overline{\Xi}^+$magnetic moments.

- **Production cross sections for π^-, K^-, Ξ^-, and Ω^- and antiparticles.**
  It is important that HyperCP address this topic. It is already apparent that the $\overline{\Xi}^+$cross section is significantly smaller than anticipated. We have data with different targets and production angles which will allow cross sections at low x_F and p_T to be measured.

- **Tests of CPT.**
  The excellent mass resolution and large data sample will allow precise tests of CPT through comparison of the masses and lifetimes of the Ω^-, Ξ^-, Λ^0, K^+, and their associated antiparticles.

B Systematic Errors

A precision measurement can only be successful if systematic effects can be controlled and understood. In general, we have identified four categories of potential sources of bias: (1) acceptance differences between Ξ^- and $\overline{\Xi}^+$ decays, (2) non-zero polarization of the parent Ξ, (3) differences in the particle anti-particle interaction rate within the spectrometer (*i.e.*, p versus $\overline{p}$, and π^- versus π^+ interaction cross sections), and (4) different backgrounds under the Λ and $\overline{\Lambda}$ and the Ξ^- and $\overline{\Xi}^+$ mass peaks.

Because the α parameters for the Ξ and Λ both change sign under CP, the proton decay distribution in the Λ rest frame should be identical to the anti-proton decay distribution in the $\overline{\Lambda}$ rest frame (assuming the parent Ξ's are unpolarized and CP is conserved). In principle, since both magnet polarities are flipped, no acceptance corrections are required! Implicit is that the magnetic fields, detector components, and reconstruction efficiencies remain stable between positive and negative running. To facilitate this stability, the magnetic polarity is changed frequently (about every four hours at full beam intensity), the magnetic fields are monitored with high-precision Hall probes, and an approximately uniform secondary beam flux is maintained by using different length targets. Given that real experiments are never ideal, acceptance variations will be tracked and corrected.

It should be emphasized that absolute normalizations are not important: for example, a *uniform* difference in chamber efficiency from Ξ^- to $\overline{\Xi}^+$ running would produce no bias. Crucial to the elimination of biases is the analysis method. Because the Λ direction in the Ξ rest frame changes from event to event, so too does the direction of the Λ polarization and hence the analysis frame in which the proton polar angle is measured (see Fig. 19).

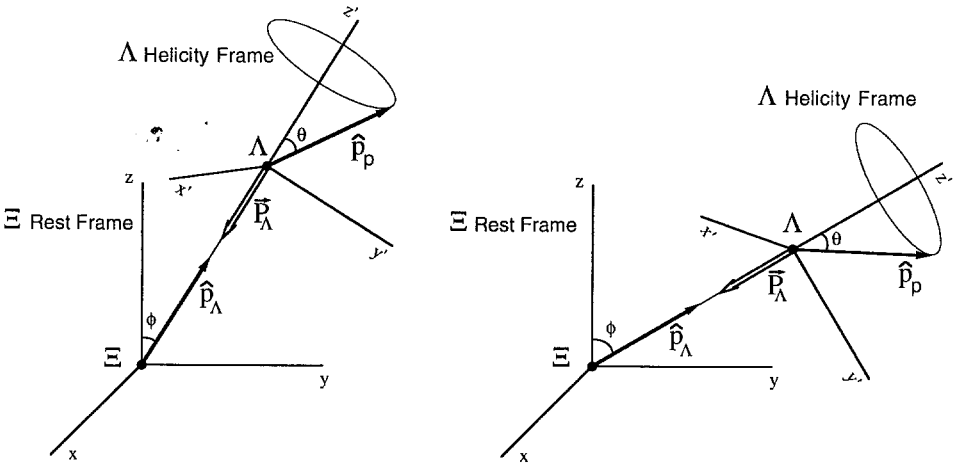

Figure 19: Two Ξ decays with identical proton polar angles θ in the Λ helicity frame, but different directions in the laboratory.

As a consequence, acceptance differences localized to a particular part of the apparatus only weakly map to a particular part of the proton or antiproton angular distribution, from which $\alpha_\Lambda \alpha_\Xi$ is extracted. Indeed, in the limit of uniform Λ acceptance, any correlation at all would vanish.

Because of mistargeting and the finite size of the hyperon channel, some parent Ξ's may be produced with non-zero polarization. The magnitude of this polarization, although expected to be quite small, if not zero, will be measured and any bias can, in principle, be removed (if required). For these events, the parent Ξ will have a small, fixed polarization in the lab frame; however, in the Λ helicity frame, the effects of this polarization will be diluted as discussed above. Special runs with measurable Ξ polarizations were taken to calibrate this effect.

Finally, differences in particle and anti-particle interaction cross sections are currently being studied. Small corrections may be required but we expect to understand this bias to better than $\sim 1 \times 10^{-4}$.

C MicroMegas Chambers

We are investigating the possibility of replacing the upstream wire chambers with a new system with better rate capability and resolution. Charpak, Giomataris, *et al.,* [27] are developing a new kind of high-rate asymmetric wire chamber, dubbed "MicroMegas" due to its use of a nickel micromesh as one electrode in a parallel-plate gas-amplification structure. The asymmetric structure provides sufficient gas thickness (3 mm) for efficient detection of minimum-ionizing tracks while keeping the amplification gap small (100 μm) to allow fast ($\approx$100 ns) clearing of the positive ions. Rate capability in excess of 10^5 particles/mm^2/s has been demonstrated with no evident aging effects. MicroMegas chambers can be constructed out of very little material: there are no wires, the $\approx$50%-transparent micromesh is only 3 μm thick, and the remaining elements are kapton foils and a sparse array of small plastic spacers.

MicroMegas chambers of 25×25 cm^2 active area are now available from the Eurisys company, and one will soon be delivered to Berkeley for testing and evaluation. Eurisys has also quoted on production of 40×40 cm^2 detectors, which would be suitable for replacing some of the MWPCs upstream of the analyzing magnets. Such replacement would both lessen the confusion due to track overlap and improve rate capability in that critical region of the spectrometer where hyperon-decay tracks can overlap with each other and with secondary-beam tracks. If after evaluation these chambers are found to be a workable solution, we will consider whether such an apparatus upgrade is appropriate given the time available for shakedown prior to the beginning of the 1999 run.

References

[1] T.D. Lee and C.N. Yang, Phys. Rev. **108** (1957) 1645.

[2] G. Valencia, private communication.

[3] J.F. Donoghue, X.-G. He and S. Pakvasa, Phys. Rev. D**34** (1986) 833.

[4] L.D. Roper, R.M. Wright, and B.T. Feld, Phys. Rev. **138** (1965) 190.

[5] M. Lu, M.B. Wise, and M.J. Savage, Phys. Lett. **B337** (1994) 133.

[6] A. Datta and S. Pakvasa, Phys. Lett. **B344** (1995) 430.

[7] D. Chang, X.-G. He, and S. Pakvasa, Phys. Rev. Lett. **20** (1995) 3927.

[8] M. Shifman, A. Vainshtein, and V. Zakharov, Nucl. Phys. **B120** (1977) 316.
F. Gilman and M. Wise, Phys. Lett. **B93** (1980) 129.

[9] X.-G. He and S. Pakvasa, in Proceedings of the 8the Meeting Division of Particles and Fields of the American Physical Society, edited by S. Seidel (World Scientific, Singapore, 1995), pp. 984–990.

[10] N.G. Deshpande, X.-G. He, and S. Pakvasa, Phys. Lett. **B326** (1994) 307.

[11] X.-G. He and G. Valencia, *CP Violation in* $\Lambda \to p\pi^-$ *Beyond the Standard Model*, Phys. Rev. D**52** (1995) 5257.

[12] H. Albrecht, *et al.*, "The Interest in Studying Beauty Baryon in pN Interactions at HERA", DESY 93–156.

[13] X.-G. He, H. Steger and G. Valencia. Phys. Lett. **B272** (1991) 411.

[14] J.M. Flynn and L. Randall, Phys. Lett. **B224** (1989) 221.

[15] E.A. Paschos and Y.L. Wu, Mod. Phys. Lett. **A6** (1991) 93.

[16] P. Chauvat et al., Phys. Lett. **163B** (1985) 273.

[17] M.H. Tixier et al., Phys. Lett. **B212** (1988) 523.

[18] P.D. Barnes et al., Phys. Rev. C**54** (1996) 1877.

[19] A. E. Baumbaugh *et al.*, IEEE Trans. Nucl. Sci. **NS-33**, 903 (1985); K. L. Knickerbocker *et al.*, IEEE Trans. Nucl. Sci. **NS-34**, 245 (1986).

[20] Ciprico, 1161 Homestead Ln., Chanhassen, MN 55317.

[21] Exabyte Corp., 1685 38th Street, Boulder CO 80301.

[22] W.T. Ford et al., Phys. Rev. Lett. **25** (1970) 1370.

[23] B. Grinstein, S.J. Reg, and M.B. Wise, Phys. Rev. D**33** (1986) 1495.

[24] A.A. Bel'kov et al., Phys. Lett. **B300** (1993) 283.

[25] G. D'Ambrosio, G. Isidori, and N. Puver, Phys. Lett. **B273** (1991) 497.

[26] H.-Y. Cheng Phys. Rev. D**44** (1991) 919.

[27] Y. Giomataris et al., NIM A 376,29 (1996).

Fermilab Proposal P-871
Revised Version

Search for CP Violation in the Decays of $\Xi^-/\overline{\Xi}^+$ and $\Lambda/\overline{\Lambda}$ Hyperons

J. Antos, Y.C. Chen, C.N. Chiou, C. Ho, A. Sumarokov, and P.K. Teng
Academia Sinica, Nankang, Taipei 11529, Taiwan, Republic of China

M. Botlo
Brookhaven National Laboratory, Upton, NY 11973, USA

G. Abrams, C. Ballagh, H. Bingham, D. Chapman, G. Gidal, P.M. Ho, K.B. Luk[1], and J. Lys
Lawrence Berkeley Laboratory and University of California, Berkeley, CA 94720, USA

L. Pinsky
University of Houston, Houston, TX 77204, USA

L. Lederman
Illinois Institute of Technology, Chicago, IL 60616, USA

M. Jenkins and K. Clark
University of South Alabama, Mobile, AL 36688, USA

E.C. Dukes[2], K. Nelson, D. Pocanic
University of Virginia, Charlottesville, VA 22901, USA

T. Alexopoulos, A. Erwin, and M. Thompson
University of Wisconsin, Madison, WI 53706, USA

March 26, 1994

[1]Spokesperson: LUK@CSA.LBL.GOV, (510)486-7054
[2]Spokesperson: DUKES@UVAHEP.PHYS.VIRGINIA.EDU, (804)982-5376

We pray for the second coming of CP *violation ...*

A. Pais

Abstract

We propose to perform a sensitive search for *CP* violation in Ξ^- ($\overline{\Xi}^+$) and Λ ($\overline{\Lambda}$) decays. Unpolarized Ξ^- ($\overline{\Xi}^+$) hyperons are produced by protons and momentum selected with a magnetic channel. The decay sequences $\Xi^- \to \Lambda\pi^-$ ($\overline{\Xi}^+ \to \overline{\Lambda}\pi^+$) and $\Lambda \to p\pi^-$ ($\overline{\Lambda} \to \bar{p}\pi^+$) are detected with a simple wire chamber spectrometer with high-rate capability. By studying the angular distribution of the proton (antiproton) with respect to the helicity axis in the Λ ($\overline{\Lambda}$) rest frame, the product of the decay parameters $\alpha_\Lambda\alpha_\Xi$ ($\alpha_{\overline{\Lambda}}\alpha_{\overline{\Xi}}$) can be extracted. Any difference between $\alpha_\Lambda\alpha_\Xi$ and $\alpha_{\overline{\Lambda}}\alpha_{\overline{\Xi}}$ is evidence that *CP* symmetry is violated. In a typical Fermilab fixed target run, 4×10^9 Ξ^- and $\overline{\Xi}^+$ decays can be collected, enabling a measurement of the relevant asymmetry to 10^{-4} sensitivity, comparable to the level of standard model predictions for the asymmetry and well over two orders of magnitude better than the present limit. A non-zero asymmetry would be the first evidence of *CP* violation outside of the neutral kaon system and would be unambiguous evidence of direct *CP* violation.

Contents

List of Tables

[1] Assuming a 21% λ_I Be target.

1 Introduction

In the 30 years since the discovery of *CP* violation [1], our understanding of the phenomenon has improved little despite a long series of beautiful experiments. It still remains a small peculiarity unique to the neutral kaon system. Although *CP* violation can be accommodated nicely within the framework of the standard model, its origin and magnitude remain a profound mystery and many questions need to be answered before we can claim to have an understanding of it. Perhaps foremost among these is whether *CP* violation is a phenomenon unique to the neutral kaon system or a property shared by other particles. The standard model tells us that it should be evident elsewhere — in the decays of hyperons and neutral B mesons for example — but no experiment has been able to achieve the necessary sensitivity to see *CP* violation outside of the neutral kaon system. Another outstanding question is whether *CP* violation occurs only in $|\Delta S| = 2$ weak transitions — as is predicted by the superweak model of Wolfenstein [2] — or is also evident in direct $|\Delta S| = 1$ decays, as is predicted by the standard model. Despite an impressive experimental effort, both at Fermilab [3] and CERN [4], the question remains open.

For some time it has been known that *CP* violation should manifest itself in the decays of hyperons: in differences in the angular distribution of the daughter baryons between particle and antiparticle [5]. The asymmetries are expected to be small and were presumed to be difficult if not impossible to measure experimentally. In the past decade, however, considerable advances have been made in the development and operation of very high-rate spectrometers. It is no longer inconceivable for an experiment to acquire in a year's time the order of a billion events needed to measure such asymmetries. Recently E756 at Fermilab — an experiment measuring both the $\overline{\Xi}^+$ magnetic moment and polarization [6] — has shown that copious numbers of $\overline{\Xi}^+$ hyperons can be acquired with a simple trigger and with very little background. Analysis of the difference between the daughter decay distributions in the Ξ^- and the $\overline{\Xi}^+$ samples — the signature for *CP* asymmetry — shows no evidence of false asymmetries. This is extremely encouraging considering the fact that the experiment was by no means optimized to measure small asymmetries between Ξ^- and $\overline{\Xi}^+$ decays. The E756 collaboration expects to report a result with a sensitivity of about 10^{-2} which is better than any previous measurement.

In light of these facts, we have examined the possibility of measuring *CP* violation in a dedicated experiment analyzing the non-leptonic decays of charged Ξ and Λ hyperons. We find that in a standard Fermilab fixed target run a sensitivity of 10^{-4} can be achieved in the comparison of the α decay parameters of the Ξ^- ($\overline{\Xi}^+$) and Λ ($\overline{\Lambda}$). This is a

sensitivity on the order of the theoretical predictions of the standard model (as well as other models of *CP* violation), and over two orders of magnitude better than the world average experimental limit of -0.03 ± 0.06 [7] in $\Lambda(\overline{\Lambda})$ decays. Observation of an asymmetry would provide the first evidence of *CP* violation outside of the neutral kaon system as well as evidence of direct *CP* violation. Because of the importance of *CP* violation to our understanding of the standard model we feel that this experiment should be pursued vigorously at Fermilab. We emphasize that the experiment can be done with relatively modest effort and expenditure.

2 Physics of CP Violation in Hyperon Decays

2.1 Signatures for CP Violation in Hyperon Decays

The phenomenology of *CP* violation in hyperon decays has been discussed in several excellent references (see Ref. [9] for example). We briefly review it here. Because the nonleptonic weak decays of spin 1/2 hyperons violate parity they can decay into admixtures of both *S*- and *P*-wave final states:

$$\begin{aligned} S &= +S_1 e^{i(\delta_1^S+\phi_1^S)} + S_3 e^{i(\delta_3^S+\phi_3^S)}, \\ \overline{S} &= -S_1 e^{i(\delta_1^S-\phi_1^S)} - S_3 e^{i(\delta_3^S-\phi_3^S)}, \\ P &= +P_1 e^{i(\delta_1^P+\phi_1^P)} + P_3 e^{i(\delta_3^P+\phi_3^P)}, \\ \overline{P} &= +P_1 e^{i(\delta_1^P-\phi_1^P)} + P_3 e^{i(\delta_3^P-\phi_3^P)}. \end{aligned}$$

Here δ and ϕ are the strong and weak phases, and the subscripts 1 and 3 refer to the $\Delta I = 1/2$ and $\Delta I = 3/2$ isospin transitions. Note that under the combined operation of *CP* the *S*-wave amplitudes and the weak phases change sign.

In terms of the *S*- and *P*-wave amplitudes, the hyperon non–leptonic decays are conventionally described by the Lee–Yang variables: α, β, and γ [8]:

$$\begin{aligned} \alpha &= \frac{2\mathrm{Re}(S^*P)}{|S|^2+|P|^2}, \\ \beta &= \frac{2\mathrm{Im}(S^*P)}{|S|^2+|P|^2}, \\ \gamma &= \frac{|S|^2-|P|^2}{|S|^2+|P|^2}, \end{aligned}$$

where $\alpha^2+\beta^2+\gamma^2 = 1$. Often one sees (in the Particle Data Booklet, for example) the parameterization given in terms of α and ϕ where:

$$\begin{aligned} \beta &= \sqrt{1-\alpha^2}\sin\phi, \\ \gamma &= \sqrt{1-\alpha^2}\cos\phi. \end{aligned}$$

Note that ϕ given above is not the same as the weak phase defined previously. Measured values of α, β, γ, and ϕ are given in the Table 1 for the Ξ^- and Λ hyperons.

The decay distribution of the daughter spin 1/2 baryon in the rest frame of the parent hyperon (the Λ in the decay $\Xi^- \to \Lambda\pi^-$, for example) is given by:

$$\frac{dP}{d\Omega} = \frac{1}{4\pi}(1+\alpha\vec{P}_p\cdot\hat{p}_d), \tag{1}$$

where $\vec{P}_p$ is the parent hyperon polarization and $\hat{p}_d$ is the daughter baryon momentum direction in the rest frame of the parent. The daughter itself is polarized with a

Table 1: Ξ^- and Λ hyperon decay parameters [7].

Mode	α	β	γ	ϕ
$\Xi^- \to \Lambda\pi^-$	-0.456 ± 0.014	0.062 ± 0.062	0.888 ± 0.008	$(4 \pm 4)^\circ$
$\Lambda \to p\pi^-$	0.642 ± 0.013	-0.087 ± 0.047	0.762 ± 0.012	$(-6.5 \pm 3.5)^\circ$

polarization given by:

$$\vec{P}_d = \frac{(\alpha + \vec{P}_p \cdot \hat{p}_d)\hat{p}_d + \beta(\vec{P}_p \times \hat{p}_d) + \gamma(\hat{p}_d \times (\vec{P}_p \times \hat{p}_d))}{(1 + \alpha\vec{P}_p \cdot \hat{p}_d)}. \tag{2}$$

Note that in the case of an unpolarized parent the daughter is in a helicity state with a polarization given by the parent α.

Under the operation of CP both α and β reverse sign whereas γ is unchanged. If CP is conserved, the magnitudes of α and β remain the same under the transformation. Hence to search for CP violation in hyperon decays one looks for a difference in either the α or β parameters, or in the partial decay rate ($\Gamma \propto |S|^2 + |P|^2$) between the particle and antiparticle. Observables that are sensitive to CP asymmetries include:

$$\Delta = \frac{\Gamma - \overline{\Gamma}}{\Gamma + \overline{\Gamma}}, \tag{3}$$

$$A = \frac{\alpha + \overline{\alpha}}{\alpha - \overline{\alpha}}, \tag{4}$$

$$B = \frac{\beta + \overline{\beta}}{\beta - \overline{\beta}}, \tag{5}$$

$$B' = \frac{\beta + \overline{\beta}}{\alpha - \overline{\alpha}}, \tag{6}$$

where overlined quantities refer to the antihyperon.

2.2 Experimental Strategy

The four observables for hyperon decays that are sensitive to CP asymmetries are given in Eqs. (3)–(6). The small theoretical predictions for Δ (see the next section) and the difficulty in measuring small differences in rates makes the possibility of finding CP violation through Δ very unlikely. To search for CP violations through measurements of either B or B' requires hyperons and antihyperons with identical or precisely determined polarizations because the β decay parameter can only be determined by measuring the daughter polarization from a polarized parent. Both Ξ^- and $\overline{\Xi}^+$ hyperons have been shown to be polarized when produced with finite transverse momentum by protons in

inclusive production [6]. However, the magnitude of the polarizations is only 10% at a p_t of about 1 GeV/c and an x_F of 0.4, requiring a prohibitive number of Ξ^- and $\overline{\Xi}^+$ hyperons to measure the *CP* asymmetry in β. Furthermore, the polarizations of the Ξ^- and $\overline{\Xi}^+$ are almost certainly different at the required sensitivity level, making measurements of the differences in β extremely difficult. Hence we propose to search for *CP*-odd asymmetries in the parameter A of Eq. (4).

Determining A requires measuring the α parameters of the hyperon and antihyperon. The α parameter is determined by either: 1) measuring the decay asymmetry of a hyperon of known polarization, or 2) measuring the daughter polarization from either a polarized or unpolarized hyperon. Measurement of the α parameter is much easier with unpolarized hyperons if the daughter decay analyzes its own polarization. The Ξ^- and $\overline{\Xi}^+$ hyperons are ideal candidates because they decay with large branching ratios (100%) into Λ and $\overline{\Lambda}$ whose polarizations can be measured through their parity violating weak decay. Unpolarized Ξ^- and $\overline{\Xi}^+$ hyperons are produced by targeting at 0° incident angle.

The daughter Λ polarization from an unpolarized Ξ decay is simply:

$$\vec{P}_\Lambda = \alpha_\Xi \hat{p}_\Lambda, \tag{7}$$

where $\hat{p}_\Lambda$ is the direction of the Λ momentum in the rest frame of the Ξ^-. The Λ is found in a helicity state with polarization given by the Ξ^- alpha parameter: $|\vec{P}_\Lambda| = 0.456$. A difference between the Λ and $\overline{\Lambda}$ polarizations is direct evidence of *CP* violation.

The Λ ($\overline{\Lambda}$) polarization is measured through the decay asymmetry given by:

$$\frac{dP}{d\Omega} = \frac{1}{4\pi}(1 + \alpha_\Lambda \vec{P}_\Lambda \cdot \hat{p}_p), \tag{8}$$

where $\hat{p}_p$ is the direction of the proton (antiproton) momentum in the Λ ($\overline{\Lambda}$) rest frame. Since $\vec{P}_\Lambda = \alpha_\Xi \hat{p}_\Lambda$, the asymmetry in the decay proton (antiproton) direction in the Λ ($\overline{\Lambda}$) rest frame is given by the product of the Λ ($\overline{\Lambda}$) and Ξ^- ($\overline{\Xi}^+$) alpha parameters:

$$\frac{dP}{d\cos\theta} = \frac{1}{2}(1 + \alpha_\Lambda \alpha_\Xi \cos\theta), \tag{9}$$

where θ is the polar angle the proton (antiproton) makes with respect to the Λ ($\overline{\Lambda}$) polarization direction. It should be emphasized that ***in the absence of CP violation the proton and antiproton distributions should be identical***, as should be every other kinematic variable from the Ξ^- and $\overline{\Xi}^+$ decays.

Because we measure the product of the Λ and Ξ alpha parameters, the *CP* asymmetry extracted is the sum of the Λ and Ξ asymmetries given in Eq. (4) (see Appendix 1):

$$\mathcal{A} = \frac{\alpha_\Lambda \alpha_\Xi - \alpha_{\overline{\Lambda}} \alpha_{\overline{\Xi}}}{\alpha_\Lambda \alpha_\Xi + \alpha_{\overline{\Lambda}} \alpha_{\overline{\Xi}}} = A_\Lambda + A_\Xi, \tag{10}$$

where A_Λ and A_Ξ are defined by:

$$A_\Lambda = \frac{\alpha_\Lambda + \alpha_{\overline{\Lambda}}}{\alpha_\Lambda - \alpha_{\overline{\Lambda}}}, \tag{11}$$

$$A_\Xi = \frac{\alpha_\Xi + \alpha_{\overline{\Xi}}}{\alpha_\Xi - \alpha_{\overline{\Xi}}}. \tag{12}$$

Hence the measured asymmetry is sensitive to *CP* violation in both Λ and Ξ^- alpha parameters. Theoretical predictions indicate that any cancellation is highly unlikely.

2.3 Theoretical Predictions

Model independent expressions for the observables given in Eqs. (3)-(6) have been explicitly calculated [9]. To leading order they are, for $\Lambda \to p\pi^-$ decay:

$$\Delta \cong \sqrt{2}\frac{S_3}{S_1}\sin(\delta_3^S - \delta_1^S)\sin(\phi_3^S - \phi_1^S) \tag{13}$$

$$A \cong -\tan(\delta_1^P - \delta_1^S)\sin(\phi_1^P - \phi_1^S), \tag{14}$$

$$B \cong \cot(\delta_1^P - \delta_1^S)\sin(\phi_1^P - \phi_1^S), \tag{15}$$

$$B' \cong -\sin(\phi_1^P - \phi_1^S), \tag{16}$$

and for $\Xi^- \to \Lambda\pi^-$ decay:

$$\Delta = 0, \tag{17}$$

$$A \cong -\tan(\delta_3^P - \delta_3^S)\sin(\phi_1^P - \phi_1^S), \tag{18}$$

$$B \cong \cot(\delta_3^P - \delta_3^S)\sin(\phi_1^P - \phi_1^S). \tag{19}$$

The *CP* asymmetry Δ results from the interference between the $|\Delta I| = 1/2$ and $|\Delta I| = 3/2$ amplitudes whereas the other asymmetries are due to the interference of *S*- and *P*-waves. Δ vanishes in Ξ decays because there is only one isospin channel. Note that *CPT* invariance only guarantees the total decay width or lifetime be the same for the particle and the anti-particle.

Calculations of *CP* asymmetries in hyperon decays are difficult and the predicted asymmetries vary (see Ref. [9,10,11,12,13,14,15,16,17]). For example, predictions of the asymmetry *A* given by Eq. (4) range from 10^{-3} to 10^{-5}. To calculate the magnitude of the asymmetries requires the values of ϵ, ϵ', the top quark mass and the hadronic matrix elements. Results are not reliable to better than an order of magnitude [16].

The hierarchy of the observables given above can be reliably estimated. Because the $|\Delta I| = 1/2$ amplitudes are about 20 times larger than the $|\Delta I| = 3/2$ amplitudes and because $\sin(\delta_i) \approx 1/10$, Donoghue *et al.* find that $\Delta \approx A/10 \approx B'/100$ [9]. In only B' do the strong interaction final state phases cancel out, and the predicted magnitude is the largest of all the asymmetries. *A* is suppressed by the small value of the final state

phase shifts whereas Δ is further suppressed by the $|\Delta I| = 1/2$ rule. Unfortunately, as mentioned in the previous section, measuring B or B' is prohibitively difficult because a hyperon parent with precisely known polarization is needed.

The magnitudes of the predicted *CP* asymmetries are model dependent. Theories with no $|\Delta S| = 1$ *CP*-odd effects, such as the superweak model and models with a very heavy neutral Higgs, predict no *CP* asymmetries [9]. Models in which $|\Delta S| = 1$ *CP* nonconservation is dominant, such as the Weinberg model [18], predict asymmetries which are on the order of those calculated in the standard model.

In the standard model *CP* violation effects are due solely to the complex phase in the Cabbibo–Kobayashi–Maskawa matrix [19] and hence *CP* asymmetries can only arise from matrix elements which involve transitions to the third quark generation. These are thought to be dominated by the gluon penguin diagram [20] shown in Fig. 1 for both kaon and hyperon decays. The standard model predictions vary quite a bit. For example, Donoghue [14] predicts asymmetries in A which range from $-(0.3 \rightarrow 4.0)\times 10^{-4}$ for Λ ($\overline{\Lambda}$) hyperons and $-(0.4 \rightarrow 4.8)\times 10^{-4}$ for Ξ^- ($\overline{\Xi}^+$) hyperons, where much of the uncertainty is due to the incomplete knowledge of the hadronic matrix elements. To illustrate the range of expected values in the standard model, Valencia [21] has compiled predictions based on the method of Xe, Steger, and Valencia [16] with the matrix elements calculated using several different models. These are shown in Fig. 2. Non standard models further widen the range.

2.3.1 Differences Between Direct *CP* Violation in Kaons and Hyperons

Although there is a close relationship between direct *CP* violation in kaon and hyperon decays, the differences are important. The most promising method of looking for direct *CP* violation in neutral kaons is by measuring ϵ'/ϵ where:

$$1 - 6Re(\frac{\epsilon'}{\epsilon}) \approx \left| \frac{\frac{A(K_l \rightarrow \pi^0\pi^0)}{A(K_s \rightarrow \pi^0\pi^0)}}{\frac{A(K_l \rightarrow \pi^+\pi^-)}{A(K_s \rightarrow \pi^+\pi^-)}} \right| . \tag{20}$$

The ratio ϵ'/ϵ can be written in the form [23]:

$$\frac{\epsilon'}{\epsilon} = -\frac{1}{\sqrt{2}|\epsilon|}\frac{1}{ReA_0}\frac{ReA_2}{ReA_0}\left[ImA_0 - \frac{ReA_0}{ReA_2}ImA_2\right], \tag{21}$$

where A_0 and A_2 are the amplitudes leading to isospin-zero and isospin-two final states. Direct *CP* violation in kaon decays arises from the interference of isospin $I = 0$ and $I = 2$ final states whereas the direct *CP* violation which is responsible for the difference in alpha parameters between hyperon and antihyperon is due to the interference between *S*-wave and *P*-wave final states.

Another difference between the two different examples of direct *CP* violation is that in standard model calculations the value of ϵ'/ϵ is very sensitive to the top quark mass

whereas $A = (\alpha + \overline{\alpha})/(\alpha - \overline{\alpha})$ is not. The reason for this sensitivity in kaon decays is that the two terms in Eq. 21 with opposite sign have been shown to have the same phase [22] and hence tend to cancel. The amplitude A_0 is due to the *QCD* penguin diagram whereas amplitude A_2 is due to the electroweak penguin diagram, which involves exchanges of Z° and γ. Although the latter amplitude is expected to be much smaller than the former, its importance in Eq. 21 is amplified by the fact that the factor ReA_0/ReA_2 is quite large due to the small size of ReA_2 relative to ReA_0. The electroweak penguin also has a contribution that increases as m_t^2. Hence ϵ'/ϵ diminishes with increasing top mass, vanishing at a top quark mass of about 220 GeV/c^2 and becoming negative thereafter [23]. The dependence on the top quark mass is shown in Fig. 3 for both ϵ'/ϵ and $A_\Lambda = (\alpha_\Lambda + \alpha_{\overline{\Lambda}})/(\alpha_\Lambda - \alpha_{\overline{\Lambda}})$. Should the top quark mass be very heavy — and the CDF and D0 limits are getting ever higher — then we have the unfortunate situation where, even if the standard model explanation of direct *CP* violation is correct, the theory mimics the superweak theory for ϵ'/ϵ.

3 Comparison with Other Past and Proposed Hyperon CP Violation Experiments

The only data on *CP* violation in hyperon decays comes from the comparison of the alpha parameters in Λ and $\overline{\Lambda}$ decays. The experimental limits are weak: the world average compiled by the Particle Data Group is $A = (\alpha_\Lambda + \alpha_{\overline{\Lambda}})/(\alpha_\Lambda - \alpha_{\overline{\Lambda}}) = -0.03 \pm 0.06$ [7]. The three published results are given in Table 2 below. Each of the three experiments used a different technique — and none used the technique we propose here. Their bounds are all limited by statistical, not systematic errors. The first result in Table 2 is from an ISR experiment (R608) which produced Λ and $\overline{\Lambda}$ in $pp \rightarrow \Lambda X$ and $p\overline{p} \rightarrow \overline{\Lambda} X$ reactions. They quote $\alpha P(\overline{\Lambda})/\alpha P(\Lambda) = -1.04 \pm 0.29$. We have converted their result to a limit on A assuming the polarization is the same for Λ and $\overline{\Lambda}$. The data sample consisted of 10,000 $\overline{\Lambda}$'s and 17,000 Λ's. The large error is due to the small polarization of the Λ and $\overline{\Lambda}$.

The second result is from the DM2 detector in the Orsay e^+e^- colliding ring DCI. They ran on the J/ψ resonance and used the decays $J/\psi \rightarrow \Lambda\overline{\Lambda}$. The branching ratio is small — 1.4×10^{-3} [7] — which is why with a total of 8.6×10^6 J/ψ decays only 770 events were used in the analysis. Nevertheless, because of the large Λ polarization, their sensitivity is comparable to the R608 measurement. The third result is from a LEAR experiment (PS185) producing Λ hyperons in the threshold reaction $p\overline{p} \rightarrow \Lambda\overline{\Lambda}$. The polarization of the two Λ's is assumed to be equal by C-parity conservation in strong interactions. A total of 4,063 $\Lambda\overline{\Lambda}$ pairs was used in the analysis.

Table 2: Experimental limits on $A = (\alpha_\Lambda + \alpha_{\overline{\Lambda}})/(\alpha_\Lambda - \alpha_{\overline{\Lambda}})$.

Mode	Limit	Experiment
$p\overline{p} \rightarrow \Lambda X$, $p\overline{p} \rightarrow \overline{\Lambda} X$	0.02 ± 0.14	R608 [24]
$e^+e^- \rightarrow J/\psi \rightarrow \Lambda\overline{\Lambda}$	0.01 ± 0.10	DM2 [25]
$p\overline{p} \rightarrow \Lambda\overline{\Lambda}$	-0.07 ± 0.09	PS185 [26]

There has been considerable interest at CERN in pursuing these measurements to better precision with an improved higher luminosity LEAR (SuperLEAR) [27]. CERN has decided not to pursue this, largely due to budget constraints, and it appears that the LEAR program will end in 1995. A proposal has also been submitted to Fermilab to construct a similar facility dedicated to searching for *CP* violation in Λ ($\overline{\Lambda}$) decays [28]. This experiment requires the main ring injector upgrade to produce the necessary amount of antiprotons as well as the construction of a dedicated storage ring. Hence it entails a large financial commitment on the part of the lab. Both the LEAR and Fermilab storage ring proposals claim a sensitivity on the order of this proposal.

There has also been interest in pursuing hyperon *CP* violation at a tau-charm factory through the decay process $J/\psi \to \Lambda\overline{\Lambda}$. Even with optimistic assumptions on the luminosity and monochromaticity, the expected asymmetry reach is only 5×10^{-4} [29] and hence is not competitive with this proposal.

Only in fixed target experiments at either Fermilab or CERN can sufficient statistics be collected to provide a sensitivity at the 1×10^{-4} level.

4 Yields

4.1 Required Yields

The goal of this experiment is to search for direct *CP* violation in Λ and Ξ^- decays by determining the observable $\mathcal{A} = (\alpha_\Lambda\alpha_\Xi - \alpha_{\overline{\Lambda}}\alpha_{\overline{\Xi}})/(\alpha_\Lambda\alpha_\Xi + \alpha_{\overline{\Lambda}}\alpha_{\overline{\Xi}})$ with a sensitivity at the 10^{-4} level. The number of events needed to measure the asymmetry to this precision is 2×10^9 each for Ξ^- and $\overline{\Xi}^+$ (see Appendix 2). For a nominal Fermilab fixed target run of 200 days; 2×10^7 events per day, 14,000 events per spill, or 700 events per spill second are required. Assuming a 50% duty factor 1,400 *reconstructed* Ξ events per spill second are needed.

4.2 Ξ^- and $\overline{\Xi}^+$ Yields

A magnetic channel with a solid angle of 4.88 μsr selects Ξ^- and $\overline{\Xi}^+$ hyperons with small x_F and a mean p_t of 0 GeV/c, ensuring that the average production polarization is very small if not zero. The $\overline{\Xi}^+$ to π^+ ratio has been measured in p + Cu collisions at 400 GeV [30]. The ratio is about 1×10^{-3} at an x_F of 0.27 and a p_t between 0.0 GeV/c and 0.8 GeV/c which is approximately the kinematic acceptance of the magnetic channel. The π, K, and p yields can be estimated fairly reliably using the parameterization of Malensek [31] which has been used extensively at Fermilab in the design of beam lines. They have been cross-checked with a Pythia simulation which agrees to about 20%. Table 3 is a summary of the yields entering and exiting the magnetic channel for a production angle of 0 mrad and for 1×10^{10} 800 GeV protons incident on a 8.84 cm long (0.21 λ_I) Be target. The acceptance of the magnetic channel is shown in Fig. 8. The estimated number of $\overline{\Xi}^+$'s, with momentum between 110 GeV and 215 GeV, entering the collimator is 65,000 per 1×10^{10} protons. This yields 8,500 $\overline{\Xi}^+$'s at the exit of the collimator where the loss due to decay in the channel has been taken into account.

We have cross-checked the $\overline{\Xi}^+$ yield in several different ways, all of which agree to within a factor of two. The most straightforward estimate is based on E756 measurements. In four full days of running E756 collected 8×10^4 $\overline{\Xi}^+$'s. An increase in yield of about 25,000 over E756 is needed. How that increase is attained is given in Table 4. Note that only a factor of 20 increase in proton intensity is needed. Much of the increase in yield comes from running the experiment for 100 full days rather than 4. Decreasing both the p_T (necessary to produce unpolarized Ξ's) and x_F also provides substantial increases in the yield.

The Ξ^- cross section at low x_F and small transverse momentum has not been measured at high energies. However, the invariant cross section of Ξ^- hyperons produced by 800 GeV protons on Be at 2.5 mrad has been measured by E756. The result is similar to the E495 measurement of the Ξ° cross section at 5 mrad with 400 GeV protons [32]. (In the CERN hyperon experiment the Ξ^- and Ξ° production cross sections were found

Table 3: Ξ, π, K, and p yields per 10^{10} protons[a].

Particle	Yields at Collimator Entrance[b]	Exit[c]
Negative Beam		
Ξ^-	1.1×10^5	1.5×10^4
π^-	3.6×10^7	1.5×10^7
K^-	2.9×10^6	1.2×10^6
Total:	3.9×10^7	1.6×10^7
Positive Beam		
$\bar{\Xi}^+$	6.5×10^4	8.5×10^3
π^+	6.5×10^7	2.7×10^7
K^+	6.5×10^6	2.7×10^6
p	3.2×10^7	1.3×10^7
Total:	1.0×10^8	4.3×10^7

[a] Assuming a 21% λ_I Be target.
[b] Inside a cone with a solid angle of 4.88 μsr centered along the incident beam direction.
[c] Decay loss and channel acceptance have been taken into account.

to be identical [33].) Hence we use the parameterization given by E495 for Ξ° production to estimate the Ξ^- yield at 0 mrad. The number of Ξ^-'s at the collimator exit is approximately 15,000.

After correcting for the probability that the Ξ^- ($\bar{\Xi}^+$) and Λ ($\bar{\Lambda}$) decay in the vacuum region, the spectrometer acceptance, and the branching fraction of $\Lambda \to p\pi^-$ (64%), approximately 4,100 (2,300) events remain. Taking the trigger efficiency, reconstruction efficiency and event selection cuts into account, the final number of Ξ^- ($\bar{\Xi}^+$) is about 2,500 (1,400) per 1×10^{10} protons (see Table 5). The thoroughly tested E756 Monte Carlo and reconstruction programs have been used to estimate the efficiencies.

4.3 Muon Background

Muon background has not been a serious problem for any of the hyperon experiments done at Fermilab the past 15 years. For example, E555 [34], E756, and E800 have all run at much higher target interaction rates than contemplated in P871 with no untoward effects. Nevertheless, we have taken care in the design of the P871 spectrometer to minimize effects due to muon halo.

To estimate the actual muon flux we again rely on data from E756. In that experi-

Table 4: Comparison of P871 and E756 $\bar{\Xi}^+$ yields.

	E756	P871	Gain
Run time	4 days	50 days	12.5
Channel solid angle	2.36 μsr	4.88 μsr	2
$< x_F >$	0.4	0.2	7
$< p_T >$	0.75 GeV/c	0.0 GeV/c	7
Proton intensity (s^{-1})	5×10^8	1×10^{10}	20
Lifetime	0.5	0.6	1.2
Total:			29,400

ment ungated scalers recorded: 1) the singles rate in an upstream wire chamber (a 2 mm pitch MWPC (*C4*) with an active area of 10"×20" and located at 26 m from the exit of the hyperon magnet), 2) the singles rate in a downstream wire chamber (a 2 mm pitch MWPC (*C12*) with an active area of 15"×47" and positioned behind the analysis magnet at 49 m from the exit of the hyperon magnet), and 3) a single track trigger ("*pion*") defined by a small aperture scintillator telescope. Approximately 90% of the "*pion*" triggers were fully reconstructed in the offline analysis and were successfully traced back to the target. In Fig. 4 is shown the muon fluence in the upstream and downstream wire chambers as a function of number of protons for three different hyperon magnetic field settings. The targeting angle in all cases was 0 degrees. The muon fluence is defined as the difference between the singles rate of the MWPC and the "*pion*" trigger rate. The muon fluence has little dependence on the hyperon magnetic field integral: it increases slightly as the hyperon magnet field integral decreases. An independent measurement of the muon fluence using a lead-scintillator telescope agrees with these results [35]. We also cross-checked the rates with those measured by E800 in similar conditions [36] and find comparable rates.

From these measurements we estimate a muon rate in P871 of approximately 7×10^6 Hz in the upstream chambers and 2×10^6 Hz in the downstream chambers. The reduction in rate in the downstream chambers is due to the shielding and sweeping of the analysis magnet since the solid angles subtended by the upstream and downstream chambers are approximately the same. This rate will not be a problem for the wire chambers. Nor is it a problem for the trigger elements: the pion hodoscope is subdivided such that the muon rate in any individual counter is small, and the calorimeter used for the proton (antiproton) trigger is essentially muon blind.

Table 5: Ξ^- and $\overline{\Xi}^+$/ acceptance and yields per 10^{10} protons.

	Ξ^-	$\overline{\Xi}^+$
Total entering collimator:	110,000	65,000
Total exiting collimator:	15,000	8,500
Spectrometer Acceptance		
BR ($\Xi^- \to \Lambda\pi^-$)	1.00	
BR ($\Lambda \to p\pi^-$)	0.641	
Ξ^- & Λ decay in vacuum region	0.50	
Geometric acceptance	0.87	
Trigger acceptance	0.99	
Reconstruction efficiency	0.73	
Software selection cuts	0.84	
Overall acceptance (and BR):	0.17	
Total events passing all cuts:	2,540	1,440

5 Experimental Design

The design of the apparatus is based on 15 years of experience in doing hyperon physics at Fermilab, and in particular, the experience gathered in E756 [6]. The spectrometer is relatively simple. The emphasis is on good acceptance, high efficiency, and high-rate capability. The Ξ^- and $\overline{\Xi}^+$ events will be produced, trigger selected and analyzed under almost identical conditions.

Although the spectrometer described in this section is similar to E756, it is vastly superior in rate capability. The wire chambers and readout used in E756 were built 20 years ago and are not suitable for high-rate experiments. The maximum trigger rate in E756 was about 500 Hz. We intend to increase this rate by over two orders of magnitude.

Figures 5 and 6 show the plan and elevation views of the apparatus. The spectrometer, approximately 60 m long and 2 m wide, consists of a hyperon magnet (M1), 8 wire chamber stations (C1–C8), a pair of momentum analyzing magnets (M2), a hodoscope for triggering on the pions from Ξ and Λ decay, and a small hadronic calorimeter for triggering on the proton (antiproton) from Λ ($\overline{\Lambda}$) decay. To change from Ξ^- to $\overline{\Xi}^+$ running will require that the polarity of all the magnets be changed and that the target be changed.

5.1 Beam

The hyperons will be produced by an 800 or 900 GeV primary proton beam with an intensity of 2×10^{11} per 20 second spill. The beam should have a Gaussian profile with a full width at half maximum of about 1 mm when it is focussed on the target. The beam divergence should be kept as small as possible. The beam position immediately upstream of the target will be monitored with two 0.5 mm wire pitch SWIC's separated by 2 m. This arrangement determines the targeting angle to better than 0.5 mrad. For particles produced with a momentum of 150 GeV/c, the resolution in the transverse momentum due to the uncertainty in the targeting angle is only 75 MeV/c. Although we plan to take most of the data at 0 mrad production angle, it is important that the primary proton beam can be targeted at a production angle up to approximately ± 5 mrad in the vertical and horizontal planes for systematic studies as well as Ξ^- and $\overline{\Xi}^+$ yield measurements.

5.2 Target

Two targets, one for Ξ^- and the other for $\overline{\Xi}^+$ production, will be mounted on a target holder that can be moved remotely in the vertical as well as the horizontal direction. This allows fine tuning of the target position with respect to the spectrometer so that the secondary beam is symmetrically produced with respect to the nominal production direction. The targets, identical in size, will be short to minimize potential target size

effects, and will have different interaction lengths in order to produce the same charged particle flux in the spectrometer. A high-A target will be used because: 1) the physical length of the target can be made shorter, 2) fewer primary protons are needed to produce the required number of Ξ's, and 3) the relative yield of hyperons at low x_F is higher with heavy target material [32].

5.3 Hyperon Channel

After the primary protons interact in the target, a secondary charged beam is defined by a curved channel embedded in a dipole magnet with a uniform vertical field. The channel consists of brass and tungsten blocks as shown in Fig. 7. The 90 cm-long upstream tungsten block serves as a dump for the beam protons which strike the upstream face of the defining collimator at 7.5 mm to the left of the central orbit. The defining aperture is 5 mm wide in the bend view and 1 cm high in the vertical direction, giving a solid angle acceptance of 4.88 μsr.

The design of the magnetic channel has been optimized to maximize the Ξ to charged particle ratio and to select a narrow momentum bite. The central orbit of the channel has a radius of 270.27 m and a bend angle, defined by the tangents to the central orbit at the entrance and exit of the channel, of 22.56 mrad. With a field of 1.85 T, the central orbit corresponds to the trajectory of a 150 GeV/c charged particle. The channel acceptance — defined as the fraction of particles within the solid angle that emerge from the exit of the channel — is shown in Fig. 8 as a function of the secondary beam momentum.

At 0 mrad production angle, positively charged secondaries are mainly protons with momenta greater than 200 GeV/c. Because of the narrow and lower momentum bite of the channel, these high energy protons are not transported to the spectrometer, effectively increasing the fraction of $\overline{\Xi}^+$'s in the beam.

When the magnetic field of the sweeping magnet is reversed, a negatively charged beam is selected. With an NMR probe permanently installed in the collimator, it is possible to reproduce the field to high precision. In E756, even without an NMR, the momentum acceptance of the channel between the two charge modes agreed to 0.25 GeV/c, or better than one part in 10^3.

5.3.1 Decay Region

To minimize the number of interactions in the spectrometer, the 25 m long decay region will be evacuated using a 60 cm diameter vacuum pipe with thin windows at the ends. Space between the chambers will be filled with helium bags.

5.4 Spectrometer

Measuring the asymmetry to the 10^{-4} level requires a large flux of Ξ's which are accompanied by a much larger flux of charged pions (and protons). The limiting factor in

the number of Ξ's that can be accumulated is not the production cross section of the Ξ, which is quite large, but the maximum charged fluence the wire chambers can tolerate. In order to collect 1,400 reconstructed $\bar{\Xi}^+$ decays per second the spectrometer must be able to tolerate the passage of 4.3×10^7 Hz of protons and pions when a positively charged beam is selected (the fraction of Ξ^-'s in the negative beam is larger with the same fluence).

5.4.1 Wire Chambers

The wire chambers must have low mass and high-rate capability. There will be four wire chambers upstream of the analysis magnet and four behind. Table 6 is a summary of the geometry of the wire chambers that has been used in the Monte Carlo studies. Each chamber will contain three views, one having vertically strung wires and the other two having wires inclined at a stereo angle. The stereo angle will be chosen so that the resolutions in the bend and non-bend views are comparable. Since there are multiple planes in each view, there is sufficient redundancy to allow the chamber efficiencies to be measured accurately and the tracking efficiency is thus a weak function of the individual plane efficiency.

Table 6: Geometry of the wire chambers.

Z (m)[a]	Width (cm)	Height (cm)	Pitch (cm)	No. of Channels
26.0	76.8	45	0.1	3 × 768
30.0	76.8	45	0.1	3 × 768
34.0	76.8	45	0.1	3 × 768
38.0	76.8	45	0.1	3 × 768
44.0	76.8	45	0.1	3 × 768
46.0	198.4	60	0.2	3 × 992
49.0	198.4	60	0.2	3 × 992
52.0	198.4	60	0.2	3 × 992
Total channels:				20,448

[a]From the exit of the collimator

The chambers upstream of the analysis magnet will have small diameter ($12-15\,\mu$m) anode wires spaced at 1 mm and an anode-cathode gap of 3 mm or less. Since the particle density after the analysis magnet is reduced, it is possible to use chambers having a more conventional wire spacing of 2 mm at that location. All chambers will use either a fast gas such as $CF_4(80\%)/i-C_4H_{10}(20\%)$ or a traditional magic gas $Ar/i-C_4H_{10}/CF_3Br+$ Methylal at a gain of less than 10^5. The latter mixture may

be preferred in the higher flux chambers since only ionization within ~1 mm of the anode would undergo avalanche multiplication.

The rate limitation is given by the flux in the most upstream chamber which is 26 m downstream of the exit of the collimator. From the Monte Carlo simulation, the beam size at the first chamber is about 10 cm high and 25 cm wide. The rate is approximately 4×10^5 $s^{-1}cm^{-2}$ in the busiest region. If a 1 mm wire spacing MWPC is used, the highest rate per wire will be about 0.4 MHz. This is a high intensity, but not above that encountered in other high-rate experiments. Wire chambers operating at rates of several times 10^7 $s^{-1}cm^{-2}$ have successfully been built [37].

Another concern is radiation damage over the course of a 10^7 second run. Assuming that all of the ionization in a 6 mm path length is amplified at a maximal gain of 10^5, we estimate a deposited charge of ~ 0.08 C/cm on the hottest wires. This is within the accepted limit of $\sim$ 1C/cm for 25 μm wires in traditional chamber gases.

Chamber Electronics

A low input impedance preamplifier will be mounted close to the wire followed by an Amplifier/Discriminator incorporating shaping circuitry to reduce the ion tail. Experience in E771 has shown that separating these two stages with approximately 30 feet of cable suppresses parasitic feedback sufficiently well to have stable operation at an anode threshold of $\sim 12,000e$. The discriminators will have a delayed output going to the data aquisition system as well as an optional prompt output for trigger purposes.

5.4.2 Analysis Magnet

The momentum analyzing magnet will be made up of two standard BM109 dipoles, each with an aperture of 61 cm wide by 30 cm high and an effective length of 2 m. The total transverse momentum kick is 1.8 GeV/c. The field is known to be uniform and can be easily mapped with the Fermilab ziptrack. From the experience gained in E756, the relative field values can be determined to better than 1×10^{-3}. As shown in Figs. 9 and 10, the agreement in the Ξ^- and $\overline{\Xi}^+$ as well as the Λ and $\overline{\Lambda}$ masses measured in E756 is excellent.

5.4.3 Hadronic Calorimeter

A simple hadronic calorimeter, used only to distinguish protons (antiprotons) (from Ξ decays) from background muons, is situated 70 meters downstream of the exit of the collimator, far enough downstream that the charged beam exiting the collimator is well separated from it. A schematic of the calorimeter is shown in Fig. 11. Its lateral size is 105×90 cm^2, and it is $6\lambda_I$ deep. It is a sampling calorimeter with scintillator as the active medium and lead as the absorber. There are a total of 50 layers of 0.5 cm scintillator and 2.0 cm lead, giving an interaction length of 20.3 cm and a radiation

length of 0.70 cm. Lead was chosen rather than iron as the absorber material because it gives a better energy resolution [38] and has a shorter radiation length, which confines electromagnetic showers from muon radiative processes to a smaller volume, allowing them to be discriminated against in the trigger rather easily.

The calorimeter is segmented laterally into seven horizontal and two vertical sections, and longitudinally into two sections, for a total of 28 channels. Each module is 62.5 × 45 × 15 cm^3. Essentially all of the protons from Λ decay which clear the spectrometer magnet enter a fiducial region which is at least one interaction length from the edge of the calorimeter. Protons entering at the edge of the calorimeter fiducial region have over 90% of their energy contained within the lateral extent of the calorimeter [39]. The longitudinal containment is better: only 2.5% of the shower energy will leak out the back [40].

The light is read out using photomultipliers coupled to wavelength shifter light guides on the top and the bottom of the calorimeter. We anticipate using Bicron BC-408 scintillator and Bicron BC-482A wavelength shifter (WLS) [41], which has a long attenuation length, good light output, and shows little degradation in light output when exposed to air for long periods of time. The wavelength shifter absorption spectrum is well matched to the emission spectrum of the BC-408, and the emission spectrum is well matched to the sensitivity of bialkali photomultipliers. Photomultipliers with a transistor base design [42] will be used to provide good gain stability with rate. We currently favor using the R-580 photomultiplier manufactured by Hamamatsu because of its excellent high rate characteristics [43]. The calorimeter response will be fast, with a FWHM of approximately 25 ns.

In the design shown in Fig. 11 the light is only read out on one end of the module in order that the calorimeter be hermetic. Because the light output at the WLS side of the scintillator tiles depends on the distance of the shower from the WLS, a special wrapping will be used to recover lateral uniformity of response. This will be done using Tyvek (Q173D) wrapping paper, from Du Pont [44], with a uniformity correction pattern, applied using a silk screen printing technique as has been done with the Zeus calorimeter [45]. A test rig will be constructed to determine the required pattern and test scintillator uniformity.

Calorimeter Energy Resolution

The hadronic energy resolution will be approximately $\sigma/\mathrm{E} = 60\%/\sqrt{E}$ [46], independent of energy as the calorimeter is compensating [47]. (If an iron absorber is used, with the same ratio of scintillator to absorber, the energy resolution would be worse: $\sigma/\mathrm{E} = 80\%/\sqrt{E}$ at 100 GeV. [38]) The electromagnetic resolution should be approximately $\sigma/\mathrm{E} = 30\%/\sqrt{E}$ [48]. The uncertainty in the muon energy loss is dominated by sampling fluctuations and hence should be similar to the electromagnetic energy resolution.

Calorimeter Muon Discrimination

The minimum proton (antiproton) momentum from Λ ($\overline{\Lambda}$) decay is 70 GeV (see Fig. 12). The resolution of the calorimeter at that energy is $\sigma = 5$ GeV. We wish to have very good efficiency for these protons, so the energy threshold will be set at approximately 20 GeV or 20σ away. (Note that the real-time energy resolution of the calorimeter will be worse than $60\%/\sqrt{E}$ and there will be some uncertainty in the trigger energy threshold due to drifts in the phototube gains.)

Muons deposit an energy of 1.9 GeV in the calorimeter due to ionization (assuming an *e/mip* ratio of 0.70, which is true for low momentum muons [49]). The uncertainty in the measurement of this energy is approximately $\sigma = 0.5$ GeV, assuming a Gaussian distribution. The distribution is better described by a Landau distribution, particularly at higher energies, where radiative processes are no longer rare. Note that the critical energy for muons in lead is approximately 250 GeV, well above our Monte Carlo estimate of 25 GeV for the mean muon momentum. Hence the tail of the Landau should not be pronounced. Experimental data taken with a similar calorimeter show that less than one out of a thousand muons of 20 GeV momentum deposit more than 8 GeV energy in the calorimeter [49].

To further discriminate against radiating high energy muons, the calorimeter trigger can be set to require a minimum energy in either adjacent calorimeter modules or in both the front and the back of the calorimeter. Electromagnetic showers induced by muon radiative processes are well localized, as is the ionization itself, whereas hadronic showers have a much longer and wider shower.

Calorimeter Radiation Damage

Radiation damage is not a problem. A hadron flux of approximately 10^5 per second over the period of a year gives a total flux of 6×10^{11} over an area of approximately 40×40 cm^2, or a dose of 10 Gy [50]. BC-408 scintillator has been measured to suffer little light reduction after a dose of 10 kGy [51].

Calorimeter Calibration

The calibration of the calorimeter will be easy. Every spill second over a thousand protons (or antiprotons) from Λ decays will be incident on the calorimeter. These have a momentum which is very well measured and will be used to calibrate the calorimeter and track its time dependence. An elaborate calibration system is not needed.

5.4.4 Hodoscope

A simple hodoscope, situated on the beam side of the spectrometer 60 meters from the exit of the collimator is used to trigger on pions from Ξ and Λ decay (see Fig 14). It

consists of 21 scintillation counters, each of 14×60 cm^2 area and 2 cm thickness. Each counter overlaps its neighbor by 2 cm giving a total width of 252 cm. The light is read out with phototubes placed at both ends. With these short, thick counters we expect a very high efficiency. We anticipate using Bicron BC-404 for the scintillator because of its fast response, and fast phototubes, such as the EMI 9814B [52] which has a FWHM of 3 ns. The hodoscope provides the timing for the experiment.

5.5 Trigger

The trigger has been kept simple in order to minimize potential biases. It relies on the fact that the decay of a Ξ^- ($\overline{\Xi}^+$) produces two pions with the same sign charge, but less momentum, than the beam exiting the hyperon channel, and a proton (antiproton) with the *opposite* sign charge. Because the polarity of the analysis magnet will be set equal to that of the hyperon magnet, the pions from the Ξ decay will be bent in the same direction (beam side) as the charged beam exiting the collimator, and the proton (antiproton) will be bent in the opposite direction to the charged beam. At the rear of the spectrometer both of the pions from the Ξ decay are well separated from the proton (antiproton), and both the pions and the proton (antiproton) are well separated from the charged beam exiting the collimator (see Fig. 13).

The trigger requires: 1) the presence, at the rear of the spectrometer, of a charged hadron in a hadronic calorimeter on the side opposite to the beam side of the spectrometer; and 2) the presence, again at the rear of the spectrometer, of at least one charged particle in a scintillator hodoscope on the beam side of the spectrometer. These two requirements — respectively called the proton and pion triggers — together are called the left-right trigger.

Because of the possibility of a large muon flux at the rear of the spectrometer — up to 2 MHz at the last MWPC (based on E756 studies) — either the proton trigger or the pion trigger must be made "muon blind". This is best done using a hadronic calorimeter. Because the protons have a higher momentum and are more tightly bunched together, the proton trigger rather than the pion trigger is implemented with the calorimeter. The pion trigger uses a simple scintillation counter hodoscope. Both of these trigger elements are placed outside of the intense charged particle beam exiting the collimator which has a flux of: 1.6×10^7 (4.3×10^7) per second in Ξ^- ($\overline{\Xi}^+$) mode with a nominal 10^{10} protons per second on target (see Table 3). This beam corresponds to an average bucket occupancy of 0.30 and 0.81, respectively for Ξ^- and $\overline{\Xi}^+$ running, of charged particles exiting the collimator. (The bucket spacing at Fermilab is 18.9 ns).

5.5.1 Trigger Rate

The trigger rate is summarized in Table 7. The trigger rate will be dominated by interactions of the charged beam exiting the collimator with material in the spectrometer,

as has been found in E756 using a similar trigger. The trigger rate must be kept below 100 kHz, the bandwidth to tape of the data acquisition system, a factor of 160 (430) less than the charged particle flux exiting the collimator in the Ξ^- ($\overline{\Xi}^+$) mode.

With 1.4% of an interaction length of material in the spectrometer, a rate of approximately 220 kHz (600 kHz) interactions per 10^{10} protons/s is expected for Ξ^- ($\overline{\Xi}^+$) running. Less than 5% of these interactions satisfy the left-right trigger, giving a trigger rate of 8 kHz (22 kHz) for Ξ^- ($\overline{\Xi}^+$) running. This is based on a sophisticated Monte Carlo simulation that reproduces the E756 trigger rate to better than 50%.

The spectrometer acceptance for Ξ's is given in Table 5. The trigger acceptance for Ξ's is well matched to the geometric acceptance: 99% of all the Ξ's that have both Ξ and Λ decay vertices in the vacuum decay region and whose decay products make it through the spectrometer magnet are accepted by the trigger. A total of 4,100 (2,300) Ξ^- ($\overline{\Xi}^+$) events are triggered on per 10^{10} protons/s on target. Of these 2,540 and 1,440 respectively for the Ξ^- and $\overline{\Xi}^+$ modes pass all software selection cuts.

Table 7: Trigger rate (per 10^{10} protons/s on target).

	Negative Running	Positive Running
Background trigger rate	8,300 Hz	22,200 Hz
$\Xi^\pm \rightarrow \Lambda\pi^\pm$ trigger rate	4,100 Hz	2,300 Hz
$K^\pm \rightarrow \pi^\pm\pi^\pm\pi^\mp$ trigger rate	900 Hz	2,000 Hz
Total:	13,300 Hz	26,500 Hz

5.5.2 Proton Trigger

Because of the large muon rate, a hadronic calorimeter is used, rather than a hodoscope (as was used in E756), to detect the presence of a proton (antiproton) from the Λ ($\overline{\Lambda}$) decay. The muon rejection of the calorimeter has to be approximately two orders of magnitude in order that the data acquisition system not saturate. To be safe, an order of magnitude more rejection is desirable because of the large uncertainty in the estimate of the muon rates.

The calorimeter must be fast, have good energy resolution, and be large enough to insure a good efficiency over its entire fiducial area. It does not have to be particularly radiation hard, or well segmented, and calibration is easy due to the large flux of well-measured protons incident on it.

Although the muon rejection factor seems easy to attain, measuring an asymmetry to 1×10^{-4} makes a high trigger efficiency for both protons and antiprotons extremely desirable. Hence the energy threshold on the proton trigger must be set low enough

for good efficiency. Although the amount of energy a muon deposits in dense matter is small, at large enough energies, radiative processes become important [53]. These processes, unlike ionization, are characterized by large energy fluctuations, and produce electromagnetic showers.

We estimate that the average muon momentum at the calorimeter will be about 25 GeV. (The exact value depends somewhat on the details of the siting of the experiment.) As discussed in the section describing the hadronic calorimeter, this is well below the critical energy of lead and experimental data taken with a similar calorimeter indicates that a rejection factor of one in 10^3 should be easy to obtain which retaining a very high proton (antiproton) efficiency.

5.5.3 Pion Trigger

The pion trigger is implemented with a simple scintillator hodoscope situated on the beam side of the spectrometer, 60 meters from the exit of the collimator (see Fig. 5). The hodoscope intercepts all but the unwanted low momentum pions clearing the magnet aperture. It does not intercept any of the charged particle beam exiting the collimator.

5.5.4 Trigger Electronics

The trigger electronics will be simple. The hodoscope trigger will employ standard NIM electronics. Fast phototubes are used to provide good single bucket timing.

Signals from the calorimeter phototubes will be split in two, with part going to flash ADC's (or perhaps the fast ADC's being developed for the KTeV experiment [54]) and then to the data acquisition system. The digitization of the signals should take less than 5 microseconds. The dynamic range of the ADC's should be sufficient to allow the muon energy to be well measured. The other part of the phototube output will be used to form the trigger, which will be done with the analog sum of the total energy in the calorimeter, and perhaps, front and rear sums, or separate lateral sums as well. This needs to be done in about half a microsecond.

5.6 Data Acquisition

The design goal of the DAQ system is to read 20,000 channels with a maximum trigger rate of 100,000 per spill second, build events, and write them to tape. We assume a maximum event size of 416 bytes (a factor of 2 larger than that of E756), resulting in a sustained data logging requirement of about 14 Mbyte/s — a high rate, but no larger than has been previously logged at Fermilab. The overall system deadtime should not exceed 10%, meaning that we should be able to log comfortably at least 90,000 triggers per second, *a factor of three greater than the estimated $\bar{\Xi}^+$ trigger rate and a factor of seven greater than the estimated Ξ^- trigger rate.*

The maximum event size is calculated as follows. There are 8 chambers, each with 3 wire planes (X, U and V plane). The ideal hit multiplicity for an event of interest is 3 per plane. If we take double hits and noise hits into account, a maximum of 8 hits per plane is a reasonable estimate. To be even more conservative, we always consider this worst case in our throughput calculations. Since each wire channel needs 2 bytes for encoding, a maximum of 384 bytes will be read out from all the chambers. Furthermore, we assume that a total of 20 bytes are generated by scintillators and calorimeter. The run and event number, event length and end of event marker will take up another 12 bytes. Therefore a maximum event size of 416 Bytes presents a very conservative estimate.

The design of the acquisition system is driven by the requirements of modularity (new technologies should be implementable as they become available without affecting the overall system), and scalability (it should be possible to accommodate an increase in performance).

The layout of the acquisition system is given in Fig. 15. The centerpiece is a standard 6U VME crate (DAQ-crate) that holds one or more Front-End Interfaces (FEI) that communicate with Front-End Crates (FEC), Event Builders (EB), Interfaces to Tape units (TI), and a State Machine (StM) which controls and monitors the activities of the readout sequences. A group of FEC's form a read-out branch. Several such branches can be accessed in parallel. Auxiliary readout of scalars, magnetic field monitors and other slow control devices will be done separately but will be embedded into the standard data stream.

The FEC contains the Front-End Modules (FEM) that read and latch the signals from the MWPC's and counters. The FEI communicates with the DAQ-crate and a Front-End Processor (FEP) which executes a real time kernel (e.g. VxWorks) for time-critical operations. The main functions of the FEP are data collection from all FEM's in the FEC, data reduction through reformatting of the event fragment, and temporary storage of data until the EB pulls a new block of events into its local memory.

There are six system components:

1. Front-End Module: In Fig. 16 the 256 differential ECL detector signals are received by the FEM and converted to TTL logic. The data are latched into a FIFO array. The FIFO's are deep enough to derandomize the intensity fluctuations of the incoming beam. The hit is then encoded as absolute wire address by an address encoder such as a digital signal processor and stored in one of two VME accessible on-board buffers. At the end of encoding, the address encoder will put out a word to signal the End of Event (EOE), e.g. FFFF, and append it to the event fragment. Data are written into the same buffer until the FEP decides to read out the FEM. The FEP broadcasts a SWITCH_BUFFER signal on the VME bus to all FEM's in the FEC and subsequently performs a block-read of the full buffer. In summary, the FEM's act as VME slaves to the FEP and have a double buffer scheme implemented. A "busy" signal will be generated to disable the trigger when the readout sequence cannot keep up with the trigger rate. Also a minimum

deadtime will be imposed once a trigger is accepted. In the current design we set the deadtime to 100 ns, limiting the FIFO speed to 10 MHz.

2. Front-End Processor (FEP): The FEP retrieves data with chained VME block-reads from all FEM's. After the FEP has fetched all these packets it assembles the data belonging to the same trigger and forms a new event fragment containing event number and fragment length. The FEP has large on-board memory (maximum 128 MByte) to hold event fragments over one full spill. This enables the FEI to transfer data during the spill and in between spills.

3. Event Builder (EB): The EB fetches all the event fragments from all FEC's to the local memory. Then it builds the final event from the event fragments belonging to the same trigger before writing it out to the permanent storage.

4. State Machine (StM): This module will synchronize and arbitrate the related DAQ processes. For example, it coordinates the trigger signals and the data transport through the DAQ.

5. Front-End-Interface (FEI): One FEC has to communicate with the DAQ-crate at a sustained rate of almost 2 MByte/s. The total throughput from all FEC's to the EB is expected to be around 18 MByte/s. Thus we will employ a fast link that enables us to daisy-chain several or all FEC's with the DAQ-crate. In case the setup latency for transfers is substantial we will use the State Machine to control the data flow.

6. Data Logging: We expect to log up to 14 MByte of data per second to the permanent storage. An array of five Exabyte Mammoth tape drives [55], which will be available at the end of 1994, and which write (in non-compressed mode) 3 MByte/s and pack 20 GByte per tape will be used.

5.7 Total Ξ Yields

The total Ξ^- and $\overline{\Xi}^+$ yield is limited by the bandwidth of the data acquisition system and by the requirement that we run on positives and negatives with the same fluence through the wire chambers. In order to saturate the bandwidth of the DAQ (10% dead time) a trigger rate per spill second of 90,000 is needed. In Ξ^- running this corresponds to a total flux of 108 MHz exiting the collimator and a *reconstructed* Ξ^- yield of 17,100 per spill second. To keep the charged particle fluence through the wire chambers the same in $\overline{\Xi}^+$ running, a corresponding trigger rate is 67,000 per spill second is needed giving a *reconstructed* $\overline{\Xi}^+$ yield of 3,600 per spill second.

At these rates the total Ξ^- and $\overline{\Xi}^+$ yield in a 200 day run with 50% duty factor is 9×10^9 each (assuming 80% of the running is on $\overline{\Xi}^+$). This corresponds to an error in the asymmetry $\mathcal{A} = (\alpha_\Lambda \alpha_\Xi - \alpha_{\overline{\Lambda}} \alpha_{\overline{\Xi}})/(\alpha_\Lambda \alpha_\Xi + \alpha_{\overline{\Lambda}} \alpha_{\overline{\Xi}})$ of 0.5×10^{-4}.

Because of uncertainties in our yield estimates, and because of the uneven spill structure in fixed target running, we are being more conservative and claim a maximum trigger rate of only 30 kHz per spill second. In Ξ^- running this corresponds to 36 MHz of charged particles exiting the collimator and a *reconstructed* Ξ^- yield of 5,700 per spill second. The corresponding reconstructed $\overline{\Xi}^+$ yield per spill second is 1,200. The total yield at this trigger rate, again assuming that 80% of the running is on $\overline{\Xi}^+$, is 2.9×10^9 for both Ξ^- and $\overline{\Xi}^+$. This corresponds to an error in the asymmetry $\mathcal{A} = (\alpha_\Lambda \alpha_\Xi - \alpha_{\overline{\Lambda}} \alpha_{\overline{\Xi}})/(\alpha_\Lambda \alpha_\Xi + \alpha_{\overline{\Lambda}} \alpha_{\overline{\Xi}})$ of 0.8×10^{-4}.

Table 7: HyperCP FY99 run computing requirements.

Process	Events	Analysis time (MIPS-sec) Per event	Total
Raw data processing	275×10^9	2.0	550×10^9
Physics analysis	20×10^9	0.2	4×10^9
Monte Carlo studies	20×10^9	4.0	80×10^9
Total:			634×10^9

Table 8: HyperCP FY99 cost estimate.

Cost Estimate for the FY99 Run				
Project	Institution	Number	Cost	Total
Preamp retrofit	UVa	500	\$20	\$10,000
Replacement:MQS104 preamp chips	UVa	60	\$50	\$3,000
Replacement:MVL107 disc. chips	LBNL	100	\$20	\$2,000
Replacement:ADC chips	UVa	2	\$500	\$1,000
Calorimeter trigger module	UVa	1	\$2,000	\$2,000
Secondary beam counter	USA	1	\$8,000	\$8,000
DAQ upgrade (including tape drives)	IIT, LBNL, Taiwan	1	\$100,000	\$100,000
Collimator modifications	FNAL, LBNL	1	\$10,000	\$10,000
Hall probe replacement	FNAL	2	\$3,000	\$ 6,000
Subtotal:				\$132,000

APPENDIX

A Other Physics

We have built a world-class charged hyperon beam and spectrometer which allows other physics topics to be addressed besides the CP violation in hyperon decays. Most of these will be studied with unprecedented sensitivity. These are briefly described below.

- **CP violation in $K^{\pm} \to 3\pi$ decays.**
  We have accumulated 280 million $K^{\pm} \to \pi^{\pm}\pi^{\pm}\pi^{\mp}$ decays which will allow CP to be tested through the asymmetry in the slope parameter of the Dalitz plot. We expect a statistical precision of about 6×10^{-4}, an order of magnitude better than the current limit [22]. Theoretical predictions range from 1.4×10^{-3} to about 10^{-6} [23, 24, 25, 26].

- **Flavor changing neutral currents in hyperon decays.**
  No experiment has ever observed strangeness-changing neutral currents in hyperon decays such as $\Sigma^+ \to p\mu^+\mu^-$. Our single event sensitivity will be about 10^{-9}.

- **Flavor changing neutral currents in charged kaon decays.**
  The decay $K^+ \to \pi^+\mu^+\mu^-$ has recently been observed by E787 at BNL at a branching ratio of about 5×10^{-8}. HyperCP should see a few tens of these decays and confirm their result.

- **Lepton number nonconservation in kaon and hyperon decays.**
  Why total lepton number seems conserved is not understood and remains a question of fundamental importance. HyperCP addresses this problem through the $|\Delta L| = 2$ decays: $\Sigma^- \to p\mu^-\mu^-$ and $\Xi^- \to p\mu^-\mu^-$, as well as through the associated kaon decay: $K^+ \to \pi^-\mu^+\mu^+$. We will improve the current limits by four orders of magnitude to about 10^{-8}.

- **Measurement of the β parameter in Ξ decays.**
  The experiment accumulated a large amount of polarized Ξ^- and $\overline{\Xi}^+$'s by running at non-zero production angles. Measurement of the β term in equation (5) allows a determination of the strong phase shifts in Ξ decay through the relationship:

$$\frac{\beta}{\alpha} = -\tan(\delta_3^S - \delta_3^P),$$

where δ_3^S and δ_3^P are respectively the S- and P-wave strong phase shifts. This will allow the recent theoretical predictions of the phase shift, which differ significantly from earlier calculations, to be tested. Note that a small value for the phase shifts would imply that the asymmetry $A_{\Xi\Lambda}$ is dominated by CP violation in Λ decays.

- **Measurement of the polarizations of the Ξ^-, $\overline{\Xi}^+$, Ω^-, and $\overline{\Omega}^+$, and magnetic moments of Ξ^- and $\overline{\Xi}^+$hyperons.**
  Why hyperons are produced polarized in high energy interactions remains a mystery. HyperCP will study Ξ^- and $\overline{\Xi}^+$polarization at low x_F and p_T where there are little data, as well as the Ω^- and $\overline{\Omega}^+$ polarizations. Previous experiments concluded that if Ω^- is polarized, its magnitude must be small, and no experiment has measured the $\overline{\Omega}^+$ polarization. A byproduct of this will be precision measurements of the Ξ^- and $\overline{\Xi}^+$magnetic moments.

- **Production cross sections for π^-, K^-, Ξ^-, and Ω^- and antiparticles.**
  It is important that HyperCP address this topic. It is already apparent that the $\overline{\Xi}^+$cross section is significantly smaller than anticipated. We have data with different targets and production angles which will allow cross sections at low x_F and p_T to be measured.

- **Tests of CPT.**
  The excellent mass resolution and large data sample will allow precise tests of CPT through comparison of the masses and lifetimes of the Ω^-, Ξ^-, Λ^0, K^+, and their associated antiparticles.

B Systematic Errors

A precision measurement can only be successful if systematic effects can be controlled and understood. In general, we have identified four categories of potential sources of bias: (1) acceptance differences between Ξ^- and $\overline{\Xi}^+$ decays, (2) non-zero polarization of the parent Ξ, (3) differences in the particle anti-particle interaction rate within the spectrometer (*i.e.*, p versus $\overline{p}$, and π^- versus π^+ interaction cross sections), and (4) different backgrounds under the Λ and $\overline{\Lambda}$ and the Ξ^- and $\overline{\Xi}^+$ mass peaks.

Because the α parameters for the Ξ and Λ both change sign under CP, the proton decay distribution in the Λ rest frame should be identical to the anti-proton decay distribution in the $\overline{\Lambda}$ rest frame (assuming the parent Ξ's are unpolarized and CP is conserved). In principle, since both magnet polarities are flipped, no acceptance corrections are required! Implicit is that the magnetic fields, detector components, and reconstruction efficiencies remain stable between positive and negative running. To facilitate this stability, the magnetic polarity is changed frequently (about every four hours at full beam intensity), the magnetic fields are monitored with high-precision Hall probes, and an approximately uniform secondary beam flux is maintained by using different length targets. Given that real experiments are never ideal, acceptance variations will be tracked and corrected.

It should be emphasized that absolute normalizations are not important: for example, a *uniform* difference in chamber efficiency from Ξ^- to $\overline{\Xi}^+$ running would produce no bias. Crucial to the elimination of biases is the analysis method. Because the Λ direction in the Ξ rest frame changes from event to event, so too does the direction of the Λ polarization and hence the analysis frame in which the proton polar angle is measured (see Fig. 19).

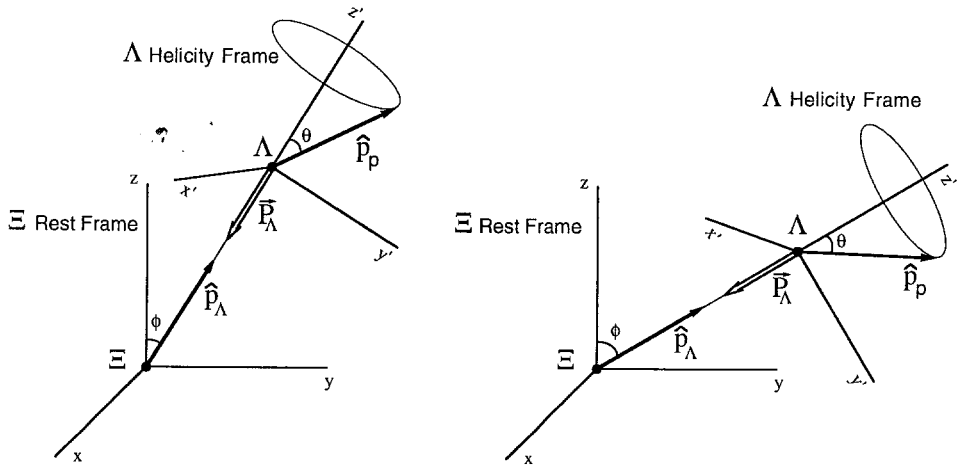

Figure 19: Two Ξ decays with identical proton polar angles θ in the Λ helicity frame, but different directions in the laboratory.

As a consequence, acceptance differences localized to a particular part of the apparatus only weakly map to a particular part of the proton or antiproton angular distribution, from which $\alpha_\Lambda \alpha_\Xi$ is extracted. Indeed, in the limit of uniform Λ acceptance, any correlation at all would vanish.

Because of mistargeting and the finite size of the hyperon channel, some parent Ξ's may be produced with non-zero polarization. The magnitude of this polarization, although expected to be quite small, if not zero, will be measured and any bias can, in principle, be removed (if required). For these events, the parent Ξ will have a small, fixed polarization in the lab frame; however, in the Λ helicity frame, the effects of this polarization will be diluted as discussed above. Special runs with measurable Ξ polarizations were taken to calibrate this effect.

Finally, differences in particle and anti-particle interaction cross sections are currently being studied. Small corrections may be required but we expect to understand this bias to better than $\sim 1 \times 10^{-4}$.

C MicroMegas Chambers

We are investigating the possibility of replacing the upstream wire chambers with a new system with better rate capability and resolution. Charpak, Giomataris, *et al.,* [27] are developing a new kind of high-rate asymmetric wire chamber, dubbed "MicroMegas" due to its use of a nickel micromesh as one electrode in a parallel-plate gas-amplification structure. The asymmetric structure provides sufficient gas thickness (3 mm) for efficient detection of minimum-ionizing tracks while keeping the amplification gap small (100 μm) to allow fast ($\approx$100 ns) clearing of the positive ions. Rate capability in excess of 10^5 particles/mm^2/s has been demonstrated with no evident aging effects. MicroMegas chambers can be constructed out of very little material: there are no wires, the $\approx$50%-transparent micromesh is only 3 μm thick, and the remaining elements are kapton foils and a sparse array of small plastic spacers.

MicroMegas chambers of 25×25 cm^2 active area are now available from the Eurisys company, and one will soon be delivered to Berkeley for testing and evaluation. Eurisys has also quoted on production of 40×40 cm^2 detectors, which would be suitable for replacing some of the MWPCs upstream of the analyzing magnets. Such replacement would both lessen the confusion due to track overlap and improve rate capability in that critical region of the spectrometer where hyperon-decay tracks can overlap with each other and with secondary-beam tracks. If after evaluation these chambers are found to be a workable solution, we will consider whether such an apparatus upgrade is appropriate given the time available for shakedown prior to the beginning of the 1999 run.

References

[1] T.D. Lee and C.N. Yang, Phys. Rev. **108** (1957) 1645.

[2] G. Valencia, private communication.

[3] J.F. Donoghue, X.-G. He and S. Pakvasa, Phys. Rev. D**34** (1986) 833.

[4] L.D. Roper, R.M. Wright, and B.T. Feld, Phys. Rev. **138** (1965) 190.

[5] M. Lu, M.B. Wise, and M.J. Savage, Phys. Lett. **B337** (1994) 133.

[6] A. Datta and S. Pakvasa, Phys. Lett. **B344** (1995) 430.

[7] D. Chang, X.-G. He, and S. Pakvasa, Phys. Rev. Lett. **20** (1995) 3927.

[8] M. Shifman, A. Vainshtein, and V. Zakharov, Nucl. Phys. **B120** (1977) 316.
F. Gilman and M. Wise, Phys. Lett. **B93** (1980) 129.

[9] X.-G. He and S. Pakvasa, in Proceedings of the 8the Meeting Division of Particles and Fields of the American Physical Society, edited by S. Seidel (World Scientific, Singapore, 1995), pp. 984–990.

[10] N.G. Deshpande, X.-G. He, and S. Pakvasa, Phys. Lett. **B326** (1994) 307.

[11] X.-G. He and G. Valencia, *CP Violation in* $\Lambda \to p\pi^-$ *Beyond the Standard Model*, Phys. Rev. D**52** (1995) 5257.

[12] H. Albrecht, *et al.*, "The Interest in Studying Beauty Baryon in pN Interactions at HERA", DESY 93–156.

[13] X.-G. He, H. Steger and G. Valencia. Phys. Lett. **B272** (1991) 411.

[14] J.M. Flynn and L. Randall, Phys. Lett. **B224** (1989) 221.

[15] E.A. Paschos and Y.L. Wu, Mod. Phys. Lett. **A6** (1991) 93.

[16] P. Chauvat et al., Phys. Lett. **163B** (1985) 273.

[17] M.H. Tixier et al., Phys. Lett. **B212** (1988) 523.

[18] P.D. Barnes et al., Phys. Rev. C**54** (1996) 1877.

[19] A. E. Baumbaugh *et al.*, IEEE Trans. Nucl. Sci. **NS-33**, 903 (1985); K. L. Knickerbocker *et al.*, IEEE Trans. Nucl. Sci. **NS-34**, 245 (1986).

[20] Ciprico, 1161 Homestead Ln., Chanhassen, MN 55317.

[21] Exabyte Corp., 1685 38th Street, Boulder CO 80301.

[22] W.T. Ford et al., Phys. Rev. Lett. **25** (1970) 1370.

[23] B. Grinstein, S.J. Reg, and M.B. Wise, Phys. Rev. D**33** (1986) 1495.

[24] A.A. Bel'kov et al., Phys. Lett. **B300** (1993) 283.

[25] G. D'Ambrosio, G. Isidori, and N. Puver, Phys. Lett. **B273** (1991) 497.

[26] H.-Y. Cheng Phys. Rev. D**44** (1991) 919.

[27] Y. Giomataris et al., NIM A 376,29 (1996).

Fermilab Proposal P-871
Revised Version

Search for CP Violation in the Decays of $\Xi^-/\overline{\Xi}^+$ and $\Lambda/\overline{\Lambda}$ Hyperons

J. Antos, Y.C. Chen, C.N. Chiou, C. Ho, A. Sumarokov, and P.K. Teng
Academia Sinica, Nankang, Taipei 11529, Taiwan, Republic of China

M. Botlo
Brookhaven National Laboratory, Upton, NY 11973, USA

G. Abrams, C. Ballagh, H. Bingham, D. Chapman, G. Gidal, P.M. Ho, K.B. Luk[1], and J. Lys
Lawrence Berkeley Laboratory and University of California, Berkeley, CA 94720, USA

L. Pinsky
University of Houston, Houston, TX 77204, USA

L. Lederman
Illinois Institute of Technology, Chicago, IL 60616, USA

M. Jenkins and K. Clark
University of South Alabama, Mobile, AL 36688, USA

E.C. Dukes[2], K. Nelson, D. Pocanic
University of Virginia, Charlottesville, VA 22901, USA

T. Alexopoulos, A. Erwin, and M. Thompson
University of Wisconsin, Madison, WI 53706, USA

March 26, 1994

[1]Spokesperson: LUK@CSA.LBL.GOV, (510)486-7054
[2]Spokesperson: DUKES@UVAHEP.PHYS.VIRGINIA.EDU, (804)982-5376

We pray for the second coming of CP *violation ...*

A. Pais

Abstract

We propose to perform a sensitive search for *CP* violation in Ξ^- ($\overline{\Xi}^+$) and Λ ($\overline{\Lambda}$) decays. Unpolarized Ξ^- ($\overline{\Xi}^+$) hyperons are produced by protons and momentum selected with a magnetic channel. The decay sequences $\Xi^- \to \Lambda\pi^-$ ($\overline{\Xi}^+ \to \overline{\Lambda}\pi^+$) and $\Lambda \to p\pi^-$ ($\overline{\Lambda} \to \overline{p}\pi^+$) are detected with a simple wire chamber spectrometer with high-rate capability. By studying the angular distribution of the proton (antiproton) with respect to the helicity axis in the Λ ($\overline{\Lambda}$) rest frame, the product of the decay parameters $\alpha_\Lambda\alpha_\Xi$ ($\alpha_{\overline{\Lambda}}\alpha_{\overline{\Xi}}$) can be extracted. Any difference between $\alpha_\Lambda\alpha_\Xi$ and $\alpha_{\overline{\Lambda}}\alpha_{\overline{\Xi}}$ is evidence that *CP* symmetry is violated. In a typical Fermilab fixed target run, 4×10^9 Ξ^- and $\overline{\Xi}^+$ decays can be collected, enabling a measurement of the relevant asymmetry to 10^{-4} sensitivity, comparable to the level of standard model predictions for the asymmetry and well over two orders of magnitude better than the present limit. A non-zero asymmetry would be the first evidence of *CP* violation outside of the neutral kaon system and would be unambiguous evidence of direct *CP* violation.

Contents

List of Tables

[1]Assuming a 21% λ_I Be target.

1 Introduction

In the 30 years since the discovery of *CP* violation [1], our understanding of the phenomenon has improved little despite a long series of beautiful experiments. It still remains a small peculiarity unique to the neutral kaon system. Although *CP* violation can be accommodated nicely within the framework of the standard model, its origin and magnitude remain a profound mystery and many questions need to be answered before we can claim to have an understanding of it. Perhaps foremost among these is whether *CP* violation is a phenomenon unique to the neutral kaon system or a property shared by other particles. The standard model tells us that it should be evident elsewhere — in the decays of hyperons and neutral B mesons for example — but no experiment has been able to achieve the necessary sensitivity to see *CP* violation outside of the neutral kaon system. Another outstanding question is whether *CP* violation occurs only in $|\Delta S| = 2$ weak transitions — as is predicted by the superweak model of Wolfenstein [2] — or is also evident in direct $|\Delta S| = 1$ decays, as is predicted by the standard model. Despite an impressive experimental effort, both at Fermilab [3] and CERN [4], the question remains open.

For some time it has been known that *CP* violation should manifest itself in the decays of hyperons: in differences in the angular distribution of the daughter baryons between particle and antiparticle [5]. The asymmetries are expected to be small and were presumed to be difficult if not impossible to measure experimentally. In the past decade, however, considerable advances have been made in the development and operation of very high-rate spectrometers. It is no longer inconceivable for an experiment to acquire in a year's time the order of a billion events needed to measure such asymmetries. Recently E756 at Fermilab — an experiment measuring both the $\overline{\Xi}^+$ magnetic moment and polarization [6] — has shown that copious numbers of $\overline{\Xi}^+$ hyperons can be acquired with a simple trigger and with very little background. Analysis of the difference between the daughter decay distributions in the Ξ^- and the $\overline{\Xi}^+$ samples — the signature for *CP* asymmetry — shows no evidence of false asymmetries. This is extremely encouraging considering the fact that the experiment was by no means optimized to measure small asymmetries between Ξ^- and $\overline{\Xi}^+$ decays. The E756 collaboration expects to report a result with a sensitivity of about 10^{-2} which is better than any previous measurement.

In light of these facts, we have examined the possibility of measuring *CP* violation in a dedicated experiment analyzing the non-leptonic decays of charged Ξ and Λ hyperons. We find that in a standard Fermilab fixed target run a sensitivity of 10^{-4} can be achieved in the comparison of the α decay parameters of the Ξ^- ($\overline{\Xi}^+$) and Λ ($\overline{\Lambda}$). This is a

sensitivity on the order of the theoretical predictions of the standard model (as well as other models of *CP* violation), and over two orders of magnitude better than the world average experimental limit of -0.03 ± 0.06 [7] in $\Lambda(\overline{\Lambda})$ decays. Observation of an asymmetry would provide the first evidence of *CP* violation outside of the neutral kaon system as well as evidence of direct *CP* violation. Because of the importance of *CP* violation to our understanding of the standard model we feel that this experiment should be pursued vigorously at Fermilab. We emphasize that the experiment can be done with relatively modest effort and expenditure.

2 Physics of CP Violation in Hyperon Decays

2.1 Signatures for CP Violation in Hyperon Decays

The phenomenology of *CP* violation in hyperon decays has been discussed in several excellent references (see Ref. [9] for example). We briefly review it here. Because the nonleptonic weak decays of spin 1/2 hyperons violate parity they can decay into admixtures of both *S*- and *P*-wave final states:

$$\begin{aligned} S &= +S_1 e^{i(\delta_1^S+\phi_1^S)} + S_3 e^{i(\delta_3^S+\phi_3^S)}, \\ \overline{S} &= -S_1 e^{i(\delta_1^S-\phi_1^S)} - S_3 e^{i(\delta_3^S-\phi_3^S)}, \\ P &= +P_1 e^{i(\delta_1^P+\phi_1^P)} + P_3 e^{i(\delta_3^P+\phi_3^P)}, \\ \overline{P} &= +P_1 e^{i(\delta_1^P-\phi_1^P)} + P_3 e^{i(\delta_3^P-\phi_3^P)}. \end{aligned}$$

Here δ and ϕ are the strong and weak phases, and the subscripts 1 and 3 refer to the $\Delta I = 1/2$ and $\Delta I = 3/2$ isospin transitions. Note that under the combined operation of *CP* the *S*-wave amplitudes and the weak phases change sign.

In terms of the *S*- and *P*-wave amplitudes, the hyperon non–leptonic decays are conventionally described by the Lee–Yang variables: α, β, and γ [8]:

$$\begin{aligned} \alpha &= \frac{2\mathrm{Re}(S^*P)}{|S|^2+|P|^2}, \\ \beta &= \frac{2\mathrm{Im}(S^*P)}{|S|^2+|P|^2}, \\ \gamma &= \frac{|S|^2-|P|^2}{|S|^2+|P|^2}, \end{aligned}$$

where $\alpha^2+\beta^2+\gamma^2 = 1$. Often one sees (in the Particle Data Booklet, for example) the parameterization given in terms of α and ϕ where:

$$\begin{aligned} \beta &= \sqrt{1-\alpha^2}\sin\phi, \\ \gamma &= \sqrt{1-\alpha^2}\cos\phi. \end{aligned}$$

Note that ϕ given above is not the same as the weak phase defined previously. Measured values of α, β, γ, and ϕ are given in the Table 1 for the Ξ^- and Λ hyperons.

The decay distribution of the daughter spin 1/2 baryon in the rest frame of the parent hyperon (the Λ in the decay $\Xi^- \to \Lambda\pi^-$, for example) is given by:

$$\frac{dP}{d\Omega} = \frac{1}{4\pi}(1+\alpha\vec{P}_p\cdot\hat{p}_d), \tag{1}$$

where $\vec{P}_p$ is the parent hyperon polarization and $\hat{p}_d$ is the daughter baryon momentum direction in the rest frame of the parent. The daughter itself is polarized with a

Table 1: Ξ^- and Λ hyperon decay parameters [7].

Mode	α	β	γ	ϕ
$\Xi^- \to \Lambda\pi^-$	-0.456 ± 0.014	0.062 ± 0.062	0.888 ± 0.008	$(4 \pm 4)^\circ$
$\Lambda \to p\pi^-$	0.642 ± 0.013	-0.087 ± 0.047	0.762 ± 0.012	$(-6.5 \pm 3.5)^\circ$

polarization given by:

$$\vec{P}_d = \frac{(\alpha + \vec{P}_p \cdot \hat{p}_d)\hat{p}_d + \beta(\vec{P}_p \times \hat{p}_d) + \gamma(\hat{p}_d \times (\vec{P}_p \times \hat{p}_d))}{(1 + \alpha \vec{P}_p \cdot \hat{p}_d)}. \tag{2}$$

Note that in the case of an unpolarized parent the daughter is in a helicity state with a polarization given by the parent α.

Under the operation of CP both α and β reverse sign whereas γ is unchanged. If CP is conserved, the magnitudes of α and β remain the same under the transformation. Hence to search for CP violation in hyperon decays one looks for a difference in either the α or β parameters, or in the partial decay rate ($\Gamma \propto |S|^2 + |P|^2$) between the particle and antiparticle. Observables that are sensitive to CP asymmetries include:

$$\Delta = \frac{\Gamma - \overline{\Gamma}}{\Gamma + \overline{\Gamma}}, \tag{3}$$

$$A = \frac{\alpha + \overline{\alpha}}{\alpha - \overline{\alpha}}, \tag{4}$$

$$B = \frac{\beta + \overline{\beta}}{\beta - \overline{\beta}}, \tag{5}$$

$$B' = \frac{\beta + \overline{\beta}}{\alpha - \overline{\alpha}}, \tag{6}$$

where overlined quantities refer to the antihyperon.

2.2 Experimental Strategy

The four observables for hyperon decays that are sensitive to CP asymmetries are given in Eqs. (3)–(6). The small theoretical predictions for Δ (see the next section) and the difficulty in measuring small differences in rates makes the possibility of finding CP violation through Δ very unlikely. To search for CP violations through measurements of either B or B' requires hyperons and antihyperons with identical or precisely determined polarizations because the β decay parameter can only be determined by measuring the daughter polarization from a polarized parent. Both Ξ^- and $\overline{\Xi}^+$ hyperons have been shown to be polarized when produced with finite transverse momentum by protons in

inclusive production [6]. However, the magnitude of the polarizations is only 10% at a p_t of about 1 GeV/c and an x_F of 0.4, requiring a prohibitive number of Ξ^- and $\overline{\Xi}^+$ hyperons to measure the *CP* asymmetry in β. Furthermore, the polarizations of the Ξ^- and $\overline{\Xi}^+$ are almost certainly different at the required sensitivity level, making measurements of the differences in β extremely difficult. Hence we propose to search for *CP*-odd asymmetries in the parameter A of Eq. (4).

Determining A requires measuring the α parameters of the hyperon and antihyperon. The α parameter is determined by either: 1) measuring the decay asymmetry of a hyperon of known polarization, or 2) measuring the daughter polarization from either a polarized or unpolarized hyperon. Measurement of the α parameter is much easier with unpolarized hyperons if the daughter decay analyzes its own polarization. The Ξ^- and $\overline{\Xi}^+$ hyperons are ideal candidates because they decay with large branching ratios (100%) into Λ and $\overline{\Lambda}$ whose polarizations can be measured through their parity violating weak decay. Unpolarized Ξ^- and $\overline{\Xi}^+$ hyperons are produced by targeting at 0° incident angle.

The daughter Λ polarization from an unpolarized Ξ decay is simply:

$$\vec{P}_\Lambda = \alpha_\Xi \hat{p}_\Lambda, \tag{7}$$

where $\hat{p}_\Lambda$ is the direction of the Λ momentum in the rest frame of the Ξ^-. The Λ is found in a helicity state with polarization given by the Ξ^- alpha parameter: $|\vec{P}_\Lambda| = 0.456$. A difference between the Λ and $\overline{\Lambda}$ polarizations is direct evidence of *CP* violation.

The Λ ($\overline{\Lambda}$) polarization is measured through the decay asymmetry given by:

$$\frac{dP}{d\Omega} = \frac{1}{4\pi}(1 + \alpha_\Lambda \vec{P}_\Lambda \cdot \hat{p}_p), \tag{8}$$

where $\hat{p}_p$ is the direction of the proton (antiproton) momentum in the Λ ($\overline{\Lambda}$) rest frame. Since $\vec{P}_\Lambda = \alpha_\Xi \hat{p}_\Lambda$, the asymmetry in the decay proton (antiproton) direction in the Λ ($\overline{\Lambda}$) rest frame is given by the product of the Λ ($\overline{\Lambda}$) and Ξ^- ($\overline{\Xi}^+$) alpha parameters:

$$\frac{dP}{d\cos\theta} = \frac{1}{2}(1 + \alpha_\Lambda \alpha_\Xi \cos\theta), \tag{9}$$

where θ is the polar angle the proton (antiproton) makes with respect to the Λ ($\overline{\Lambda}$) polarization direction. It should be emphasized that ***in the absence of CP violation the proton and antiproton distributions should be identical***, as should be every other kinematic variable from the Ξ^- and $\overline{\Xi}^+$ decays.

Because we measure the product of the Λ and Ξ alpha parameters, the *CP* asymmetry extracted is the sum of the Λ and Ξ asymmetries given in Eq. (4) (see Appendix 1):

$$\mathcal{A} = \frac{\alpha_\Lambda \alpha_\Xi - \alpha_{\overline{\Lambda}} \alpha_{\overline{\Xi}}}{\alpha_\Lambda \alpha_\Xi + \alpha_{\overline{\Lambda}} \alpha_{\overline{\Xi}}} = A_\Lambda + A_\Xi, \tag{10}$$

where A_Λ and A_Ξ are defined by:

$$A_\Lambda = \frac{\alpha_\Lambda + \alpha_{\overline{\Lambda}}}{\alpha_\Lambda - \alpha_{\overline{\Lambda}}}, \tag{11}$$

$$A_\Xi = \frac{\alpha_\Xi + \alpha_{\overline{\Xi}}}{\alpha_\Xi - \alpha_{\overline{\Xi}}}. \tag{12}$$

Hence the measured asymmetry is sensitive to *CP* violation in both Λ and Ξ^- alpha parameters. Theoretical predictions indicate that any cancellation is highly unlikely.

2.3 Theoretical Predictions

Model independent expressions for the observables given in Eqs. (3)-(6) have been explicitly calculated [9]. To leading order they are, for $\Lambda \to p\pi^-$ decay:

$$\Delta \cong \sqrt{2}\frac{S_3}{S_1}\sin(\delta_3^S - \delta_1^S)\sin(\phi_3^S - \phi_1^S) \tag{13}$$

$$A \cong -\tan(\delta_1^P - \delta_1^S)\sin(\phi_1^P - \phi_1^S), \tag{14}$$

$$B \cong \cot(\delta_1^P - \delta_1^S)\sin(\phi_1^P - \phi_1^S), \tag{15}$$

$$B' \cong -\sin(\phi_1^P - \phi_1^S), \tag{16}$$

and for $\Xi^- \to \Lambda\pi^-$ decay:

$$\Delta = 0, \tag{17}$$

$$A \cong -\tan(\delta_3^P - \delta_3^S)\sin(\phi_1^P - \phi_1^S), \tag{18}$$

$$B \cong \cot(\delta_3^P - \delta_3^S)\sin(\phi_1^P - \phi_1^S). \tag{19}$$

The *CP* asymmetry Δ results from the interference between the $|\Delta I| = 1/2$ and $|\Delta I| = 3/2$ amplitudes whereas the other asymmetries are due to the interference of *S*- and *P*-waves. Δ vanishes in Ξ decays because there is only one isospin channel. Note that *CPT* invariance only guarantees the total decay width or lifetime be the same for the particle and the anti-particle.

Calculations of *CP* asymmetries in hyperon decays are difficult and the predicted asymmetries vary (see Ref. [9,10,11,12,13,14,15,16,17]). For example, predictions of the asymmetry *A* given by Eq. (4) range from 10^{-3} to 10^{-5}. To calculate the magnitude of the asymmetries requires the values of ϵ, ϵ', the top quark mass and the hadronic matrix elements. Results are not reliable to better than an order of magnitude [16].

The hierarchy of the observables given above can be reliably estimated. Because the $|\Delta I| = 1/2$ amplitudes are about 20 times larger than the $|\Delta I| = 3/2$ amplitudes and because $\sin(\delta_i) \approx 1/10$, Donoghue *et al.* find that $\Delta \approx A/10 \approx B'/100$ [9]. In only B' do the strong interaction final state phases cancel out, and the predicted magnitude is the largest of all the asymmetries. *A* is suppressed by the small value of the final state

phase shifts whereas Δ is further suppressed by the $|\Delta I| = 1/2$ rule. Unfortunately, as mentioned in the previous section, measuring B or B' is prohibitively difficult because a hyperon parent with precisely known polarization is needed.

The magnitudes of the predicted *CP* asymmetries are model dependent. Theories with no $|\Delta S| = 1$ *CP*-odd effects, such as the superweak model and models with a very heavy neutral Higgs, predict no *CP* asymmetries [9]. Models in which $|\Delta S| = 1$ *CP* nonconservation is dominant, such as the Weinberg model [18], predict asymmetries which are on the order of those calculated in the standard model.

In the standard model *CP* violation effects are due solely to the complex phase in the Cabbibo–Kobayashi–Maskawa matrix [19] and hence *CP* asymmetries can only arise from matrix elements which involve transitions to the third quark generation. These are thought to be dominated by the gluon penguin diagram [20] shown in Fig. 1 for both kaon and hyperon decays. The standard model predictions vary quite a bit. For example, Donoghue [14] predicts asymmetries in A which range from $-(0.3 \rightarrow 4.0)\times 10^{-4}$ for Λ ($\overline{\Lambda}$) hyperons and $-(0.4 \rightarrow 4.8)\times 10^{-4}$ for Ξ^- ($\overline{\Xi}^+$) hyperons, where much of the uncertainty is due to the incomplete knowledge of the hadronic matrix elements. To illustrate the range of expected values in the standard model, Valencia [21] has compiled predictions based on the method of Xe, Steger, and Valencia [16] with the matrix elements calculated using several different models. These are shown in Fig. 2. Non standard models further widen the range.

2.3.1 Differences Between Direct *CP* Violation in Kaons and Hyperons

Although there is a close relationship between direct *CP* violation in kaon and hyperon decays, the differences are important. The most promising method of looking for direct *CP* violation in neutral kaons is by measuring ϵ'/ϵ where:

$$1 - 6Re(\frac{\epsilon'}{\epsilon}) \approx \left| \frac{\frac{A(K_l \rightarrow \pi^0\pi^0)}{A(K_s \rightarrow \pi^0\pi^0)}}{\frac{A(K_l \rightarrow \pi^+\pi^-)}{A(K_s \rightarrow \pi^+\pi^-)}} \right| . \tag{20}$$

The ratio ϵ'/ϵ can be written in the form [23]:

$$\frac{\epsilon'}{\epsilon} = -\frac{1}{\sqrt{2}|\epsilon|}\frac{1}{ReA_0}\frac{ReA_2}{ReA_0}\left[ImA_0 - \frac{ReA_0}{ReA_2}ImA_2\right], \tag{21}$$

where A_0 and A_2 are the amplitudes leading to isospin-zero and isospin-two final states. Direct *CP* violation in kaon decays arises from the interference of isospin $I = 0$ and $I = 2$ final states whereas the direct *CP* violation which is responsible for the difference in alpha parameters between hyperon and antihyperon is due to the interference between *S*-wave and *P*-wave final states.

Another difference between the two different examples of direct *CP* violation is that in standard model calculations the value of ϵ'/ϵ is very sensitive to the top quark mass

whereas $A = (\alpha + \overline{\alpha})/(\alpha - \overline{\alpha})$ is not. The reason for this sensitivity in kaon decays is that the two terms in Eq. 21 with opposite sign have been shown to have the same phase [22] and hence tend to cancel. The amplitude A_0 is due to the *QCD* penguin diagram whereas amplitude A_2 is due to the electroweak penguin diagram, which involves exchanges of Z° and γ. Although the latter amplitude is expected to be much smaller than the former, its importance in Eq. 21 is amplified by the fact that the factor ReA_0/ReA_2 is quite large due to the small size of ReA_2 relative to ReA_0. The electroweak penguin also has a contribution that increases as m_t^2. Hence ϵ'/ϵ diminishes with increasing top mass, vanishing at a top quark mass of about 220 GeV/c^2 and becoming negative thereafter [23]. The dependence on the top quark mass is shown in Fig. 3 for both ϵ'/ϵ and $A_\Lambda = (\alpha_\Lambda + \alpha_{\overline{\Lambda}})/(\alpha_\Lambda - \alpha_{\overline{\Lambda}})$. Should the top quark mass be very heavy — and the CDF and D0 limits are getting ever higher — then we have the unfortunate situation where, even if the standard model explanation of direct *CP* violation is correct, the theory mimics the superweak theory for ϵ'/ϵ.

3 Comparison with Other Past and Proposed Hyperon CP Violation Experiments

The only data on *CP* violation in hyperon decays comes from the comparison of the alpha parameters in Λ and $\overline{\Lambda}$ decays. The experimental limits are weak: the world average compiled by the Particle Data Group is $A = (\alpha_\Lambda + \alpha_{\overline{\Lambda}})/(\alpha_\Lambda - \alpha_{\overline{\Lambda}}) = -0.03 \pm 0.06$ [7]. The three published results are given in Table 2 below. Each of the three experiments used a different technique — and none used the technique we propose here. Their bounds are all limited by statistical, not systematic errors. The first result in Table 2 is from an ISR experiment (R608) which produced Λ and $\overline{\Lambda}$ in $pp \rightarrow \Lambda X$ and $p\overline{p} \rightarrow \overline{\Lambda} X$ reactions. They quote $\alpha P(\overline{\Lambda})/\alpha P(\Lambda) = -1.04 \pm 0.29$. We have converted their result to a limit on A assuming the polarization is the same for Λ and $\overline{\Lambda}$. The data sample consisted of 10,000 $\overline{\Lambda}$'s and 17,000 Λ's. The large error is due to the small polarization of the Λ and $\overline{\Lambda}$.

The second result is from the DM2 detector in the Orsay e^+e^- colliding ring DCI. They ran on the J/ψ resonance and used the decays $J/\psi \rightarrow \Lambda\overline{\Lambda}$. The branching ratio is small — 1.4×10^{-3} [7] — which is why with a total of 8.6×10^6 J/ψ decays only 770 events were used in the analysis. Nevertheless, because of the large Λ polarization, their sensitivity is comparable to the R608 measurement. The third result is from a LEAR experiment (PS185) producing Λ hyperons in the threshold reaction $p\overline{p} \rightarrow \Lambda\overline{\Lambda}$. The polarization of the two Λ's is assumed to be equal by C-parity conservation in strong interactions. A total of 4,063 $\Lambda\overline{\Lambda}$ pairs was used in the analysis.

Table 2: Experimental limits on $A = (\alpha_\Lambda + \alpha_{\overline{\Lambda}})/(\alpha_\Lambda - \alpha_{\overline{\Lambda}})$.

Mode	Limit	Experiment
$p\overline{p} \rightarrow \Lambda X$, $p\overline{p} \rightarrow \overline{\Lambda} X$	0.02 ± 0.14	R608 [24]
$e^+e^- \rightarrow J/\psi \rightarrow \Lambda\overline{\Lambda}$	0.01 ± 0.10	DM2 [25]
$p\overline{p} \rightarrow \Lambda\overline{\Lambda}$	-0.07 ± 0.09	PS185 [26]

There has been considerable interest at CERN in pursuing these measurements to better precision with an improved higher luminosity LEAR (SuperLEAR) [27]. CERN has decided not to pursue this, largely due to budget constraints, and it appears that the LEAR program will end in 1995. A proposal has also been submitted to Fermilab to construct a similar facility dedicated to searching for *CP* violation in Λ ($\overline{\Lambda}$) decays [28]. This experiment requires the main ring injector upgrade to produce the necessary amount of antiprotons as well as the construction of a dedicated storage ring. Hence it entails a large financial commitment on the part of the lab. Both the LEAR and Fermilab storage ring proposals claim a sensitivity on the order of this proposal.

There has also been interest in pursuing hyperon *CP* violation at a tau-charm factory through the decay process $J/\psi \to \Lambda\overline{\Lambda}$. Even with optimistic assumptions on the luminosity and monochromaticity, the expected asymmetry reach is only 5×10^{-4} [29] and hence is not competitive with this proposal.

Only in fixed target experiments at either Fermilab or CERN can sufficient statistics be collected to provide a sensitivity at the 1×10^{-4} level.

4 Yields

4.1 Required Yields

The goal of this experiment is to search for direct *CP* violation in Λ and Ξ^- decays by determining the observable $\mathcal{A} = (\alpha_\Lambda\alpha_\Xi - \alpha_{\overline{\Lambda}}\alpha_{\overline{\Xi}})/(\alpha_\Lambda\alpha_\Xi + \alpha_{\overline{\Lambda}}\alpha_{\overline{\Xi}})$ with a sensitivity at the 10^{-4} level. The number of events needed to measure the asymmetry to this precision is 2×10^9 each for Ξ^- and $\overline{\Xi}^+$ (see Appendix 2). For a nominal Fermilab fixed target run of 200 days; 2×10^7 events per day, 14,000 events per spill, or 700 events per spill second are required. Assuming a 50% duty factor 1,400 *reconstructed* Ξ events per spill second are needed.

4.2 Ξ^- and $\overline{\Xi}^+$ Yields

A magnetic channel with a solid angle of 4.88 μsr selects Ξ^- and $\overline{\Xi}^+$ hyperons with small x_F and a mean p_t of 0 GeV/c, ensuring that the average production polarization is very small if not zero. The $\overline{\Xi}^+$ to π^+ ratio has been measured in p + Cu collisions at 400 GeV [30]. The ratio is about 1×10^{-3} at an x_F of 0.27 and a p_t between 0.0 GeV/c and 0.8 GeV/c which is approximately the kinematic acceptance of the magnetic channel. The π, K, and p yields can be estimated fairly reliably using the parameterization of Malensek [31] which has been used extensively at Fermilab in the design of beam lines. They have been cross-checked with a Pythia simulation which agrees to about 20%. Table 3 is a summary of the yields entering and exiting the magnetic channel for a production angle of 0 mrad and for 1×10^{10} 800 GeV protons incident on a 8.84 cm long (0.21 λ_I) Be target. The acceptance of the magnetic channel is shown in Fig. 8. The estimated number of $\overline{\Xi}^+$'s, with momentum between 110 GeV and 215 GeV, entering the collimator is 65,000 per 1×10^{10} protons. This yields 8,500 $\overline{\Xi}^+$'s at the exit of the collimator where the loss due to decay in the channel has been taken into account.

We have cross-checked the $\overline{\Xi}^+$ yield in several different ways, all of which agree to within a factor of two. The most straightforward estimate is based on E756 measurements. In four full days of running E756 collected 8×10^4 $\overline{\Xi}^+$'s. An increase in yield of about 25,000 over E756 is needed. How that increase is attained is given in Table 4. Note that only a factor of 20 increase in proton intensity is needed. Much of the increase in yield comes from running the experiment for 100 full days rather than 4. Decreasing both the p_T (necessary to produce unpolarized Ξ's) and x_F also provides substantial increases in the yield.

The Ξ^- cross section at low x_F and small transverse momentum has not been measured at high energies. However, the invariant cross section of Ξ^- hyperons produced by 800 GeV protons on Be at 2.5 mrad has been measured by E756. The result is similar to the E495 measurement of the Ξ° cross section at 5 mrad with 400 GeV protons [32]. (In the CERN hyperon experiment the Ξ^- and Ξ° production cross sections were found

Table 3: Ξ, π, K, and p yields per 10^{10} protons[a].

Particle	Yields at Collimator Entrance[b]	Exit[c]
Negative Beam		
Ξ^-	1.1×10^5	1.5×10^4
π^-	3.6×10^7	1.5×10^7
K^-	2.9×10^6	1.2×10^6
Total:	3.9×10^7	1.6×10^7
Positive Beam		
$\overline{\Xi}^+$	6.5×10^4	8.5×10^3
π^+	6.5×10^7	2.7×10^7
K^+	6.5×10^6	2.7×10^6
p	3.2×10^7	1.3×10^7
Total:	1.0×10^8	4.3×10^7

[a] Assuming a 21% λ_I Be target.
[b] Inside a cone with a solid angle of 4.88 μsr centered along the incident beam direction.
[c] Decay loss and channel acceptance have been taken into account.

to be identical [33].) Hence we use the parameterization given by E495 for Ξ^0 production to estimate the Ξ^- yield at 0 mrad. The number of Ξ^-'s at the collimator exit is approximately 15,000.

After correcting for the probability that the Ξ^- ($\overline{\Xi}^+$) and Λ ($\overline{\Lambda}$) decay in the vacuum region, the spectrometer acceptance, and the branching fraction of $\Lambda \to p\pi^-$ (64%), approximately 4,100 (2,300) events remain. Taking the trigger efficiency, reconstruction efficiency and event selection cuts into account, the final number of Ξ^- ($\overline{\Xi}^+$) is about 2,500 (1,400) per 1×10^{10} protons (see Table 5). The thoroughly tested E756 Monte Carlo and reconstruction programs have been used to estimate the efficiencies.

4.3 Muon Background

Muon background has not been a serious problem for any of the hyperon experiments done at Fermilab the past 15 years. For example, E555 [34], E756, and E800 have all run at much higher target interaction rates than contemplated in P871 with no untoward effects. Nevertheless, we have taken care in the design of the P871 spectrometer to minimize effects due to muon halo.

To estimate the actual muon flux we again rely on data from E756. In that experi-

Table 4: Comparison of P871 and E756 $\bar{\Xi}^+$ yields.

	E756	P871	Gain
Run time	4 days	50 days	12.5
Channel solid angle	2.36 μsr	4.88 μsr	2
$< x_F >$	0.4	0.2	7
$< p_T >$	0.75 GeV/c	0.0 GeV/c	7
Proton intensity (s^{-1})	5×10^8	1×10^{10}	20
Lifetime	0.5	0.6	1.2
Total:			29,400

ment ungated scalers recorded: 1) the singles rate in an upstream wire chamber (a 2 mm pitch MWPC (*C4*) with an active area of 10"×20" and located at 26 m from the exit of the hyperon magnet), 2) the singles rate in a downstream wire chamber (a 2 mm pitch MWPC (*C12*) with an active area of 15"×47" and positioned behind the analysis magnet at 49 m from the exit of the hyperon magnet), and 3) a single track trigger ("*pion*") defined by a small aperture scintillator telescope. Approximately 90% of the "*pion*" triggers were fully reconstructed in the offline analysis and were successfully traced back to the target. In Fig. 4 is shown the muon fluence in the upstream and downstream wire chambers as a function of number of protons for three different hyperon magnetic field settings. The targeting angle in all cases was 0 degrees. The muon fluence is defined as the difference between the singles rate of the MWPC and the "*pion*" trigger rate. The muon fluence has little dependence on the hyperon magnetic field integral: it increases slightly as the hyperon magnet field integral decreases. An independent measurement of the muon fluence using a lead-scintillator telescope agrees with these results [35]. We also cross-checked the rates with those measured by E800 in similar conditions [36] and find comparable rates.

From these measurements we estimate a muon rate in P871 of approximately 7×10^6 Hz in the upstream chambers and 2×10^6 Hz in the downstream chambers. The reduction in rate in the downstream chambers is due to the shielding and sweeping of the analysis magnet since the solid angles subtended by the upstream and downstream chambers are approximately the same. This rate will not be a problem for the wire chambers. Nor is it a problem for the trigger elements: the pion hodoscope is subdivided such that the muon rate in any individual counter is small, and the calorimeter used for the proton (antiproton) trigger is essentially muon blind.

Table 5: Ξ^- and $\overline{\Xi}^+$/ acceptance and yields per 10^{10} protons.

	Ξ^-	$\overline{\Xi}^+$
Total entering collimator:	110,000	65,000
Total exiting collimator:	15,000	8,500
Spectrometer Acceptance		
BR ($\Xi^- \to \Lambda\pi^-$)	1.00	
BR ($\Lambda \to p\pi^-$)	0.641	
Ξ^- & Λ decay in vacuum region	0.50	
Geometric acceptance	0.87	
Trigger acceptance	0.99	
Reconstruction efficiency	0.73	
Software selection cuts	0.84	
Overall acceptance (and BR):	0.17	
Total events passing all cuts:	2,540	1,440

5 Experimental Design

The design of the apparatus is based on 15 years of experience in doing hyperon physics at Fermilab, and in particular, the experience gathered in E756 [6]. The spectrometer is relatively simple. The emphasis is on good acceptance, high efficiency, and high-rate capability. The Ξ^- and $\overline{\Xi}^+$ events will be produced, trigger selected and analyzed under almost identical conditions.

Although the spectrometer described in this section is similar to E756, it is vastly superior in rate capability. The wire chambers and readout used in E756 were built 20 years ago and are not suitable for high-rate experiments. The maximum trigger rate in E756 was about 500 Hz. We intend to increase this rate by over two orders of magnitude.

Figures 5 and 6 show the plan and elevation views of the apparatus. The spectrometer, approximately 60 m long and 2 m wide, consists of a hyperon magnet (M1), 8 wire chamber stations (C1–C8), a pair of momentum analyzing magnets (M2), a hodoscope for triggering on the pions from Ξ and Λ decay, and a small hadronic calorimeter for triggering on the proton (antiproton) from Λ ($\overline{\Lambda}$) decay. To change from Ξ^- to $\overline{\Xi}^+$ running will require that the polarity of all the magnets be changed and that the target be changed.

5.1 Beam

The hyperons will be produced by an 800 or 900 GeV primary proton beam with an intensity of 2×10^{11} per 20 second spill. The beam should have a Gaussian profile with a full width at half maximum of about 1 mm when it is focussed on the target. The beam divergence should be kept as small as possible. The beam position immediately upstream of the target will be monitored with two 0.5 mm wire pitch SWIC's separated by 2 m. This arrangement determines the targeting angle to better than 0.5 mrad. For particles produced with a momentum of 150 GeV/c, the resolution in the transverse momentum due to the uncertainty in the targeting angle is only 75 MeV/c. Although we plan to take most of the data at 0 mrad production angle, it is important that the primary proton beam can be targeted at a production angle up to approximately ± 5 mrad in the vertical and horizontal planes for systematic studies as well as Ξ^- and $\overline{\Xi}^+$ yield measurements.

5.2 Target

Two targets, one for Ξ^- and the other for $\overline{\Xi}^+$ production, will be mounted on a target holder that can be moved remotely in the vertical as well as the horizontal direction. This allows fine tuning of the target position with respect to the spectrometer so that the secondary beam is symmetrically produced with respect to the nominal production direction. The targets, identical in size, will be short to minimize potential target size

effects, and will have different interaction lengths in order to produce the same charged particle flux in the spectrometer. A high-A target will be used because: 1) the physical length of the target can be made shorter, 2) fewer primary protons are needed to produce the required number of Ξ's, and 3) the relative yield of hyperons at low x_F is higher with heavy target material [32].

5.3 Hyperon Channel

After the primary protons interact in the target, a secondary charged beam is defined by a curved channel embedded in a dipole magnet with a uniform vertical field. The channel consists of brass and tungsten blocks as shown in Fig. 7. The 90 cm-long upstream tungsten block serves as a dump for the beam protons which strike the upstream face of the defining collimator at 7.5 mm to the left of the central orbit. The defining aperture is 5 mm wide in the bend view and 1 cm high in the vertical direction, giving a solid angle acceptance of 4.88 μsr.

The design of the magnetic channel has been optimized to maximize the Ξ to charged particle ratio and to select a narrow momentum bite. The central orbit of the channel has a radius of 270.27 m and a bend angle, defined by the tangents to the central orbit at the entrance and exit of the channel, of 22.56 mrad. With a field of 1.85 T, the central orbit corresponds to the trajectory of a 150 GeV/c charged particle. The channel acceptance — defined as the fraction of particles within the solid angle that emerge from the exit of the channel — is shown in Fig. 8 as a function of the secondary beam momentum.

At 0 mrad production angle, positively charged secondaries are mainly protons with momenta greater than 200 GeV/c. Because of the narrow and lower momentum bite of the channel, these high energy protons are not transported to the spectrometer, effectively increasing the fraction of $\overline{\Xi}^+$'s in the beam.

When the magnetic field of the sweeping magnet is reversed, a negatively charged beam is selected. With an NMR probe permanently installed in the collimator, it is possible to reproduce the field to high precision. In E756, even without an NMR, the momentum acceptance of the channel between the two charge modes agreed to 0.25 GeV/c, or better than one part in 10^3.

5.3.1 Decay Region

To minimise the number of interactions in the spectrometer, the 25 m long decay region will be evacuated using a 60 cm diameter vacuum pipe with thin windows at the ends. Space between the chambers will be filled with helium bags.

5.4 Spectrometer

Measuring the asymmetry to the 10^{-4} level requires a large flux of Ξ's which are accompanied by a much larger flux of charged pions (and protons). The limiting factor in

the number of Ξ's that can be accumulated is not the production cross section of the Ξ, which is quite large, but the maximum charged fluence the wire chambers can tolerate. In order to collect 1,400 reconstructed $\overline{\Xi}^+$ decays per second the spectrometer must be able to tolerate the passage of 4.3×10^7 Hz of protons and pions when a positively charged beam is selected (the fraction of Ξ^-'s in the negative beam is larger with the same fluence).

5.4.1 Wire Chambers

The wire chambers must have low mass and high-rate capability. There will be four wire chambers upstream of the analysis magnet and four behind. Table 6 is a summary of the geometry of the wire chambers that has been used in the Monte Carlo studies. Each chamber will contain three views, one having vertically strung wires and the other two having wires inclined at a stereo angle. The stereo angle will be chosen so that the resolutions in the bend and non–bend views are comparable. Since there are multiple planes in each view, there is sufficient redundancy to allow the chamber efficiencies to be measured accurately and the tracking efficiency is thus a weak function of the individual plane efficiency.

Table 6: Geometry of the wire chambers.

Z (m)[a]	Width (cm)	Height (cm)	Pitch (cm)	No. of Channels
26.0	76.8	45	0.1	3 × 768
30.0	76.8	45	0.1	3 × 768
34.0	76.8	45	0.1	3 × 768
38.0	76.8	45	0.1	3 × 768
44.0	76.8	45	0.1	3 × 768
46.0	198.4	60	0.2	3 × 992
49.0	198.4	60	0.2	3 × 992
52.0	198.4	60	0.2	3 × 992
Total channels:				20,448

[a] From the exit of the collimator

The chambers upstream of the analysis magnet will have small diameter ($12-15\,\mu$m) anode wires spaced at 1 mm and an anode-cathode gap of 3 mm or less. Since the particle density after the analysis magnet is reduced, it is possible to use chambers having a more conventional wire spacing of 2 mm at that location. All chambers will use either a fast gas such as $CF_4(80\%)/i-C_4H_{10}(20\%)$ or a traditional magic gas $Ar/i-C_4H_{10}/CF_3Br+$ Methylal at a gain of less than 10^5. The latter mixture may

be preferred in the higher flux chambers since only ionization within ~1 mm of the anode would undergo avalanche multiplication.

The rate limitation is given by the flux in the most upstream chamber which is 26 m downstream of the exit of the collimator. From the Monte Carlo simulation, the beam size at the first chamber is about 10 cm high and 25 cm wide. The rate is approximately 4×10^5 $s^{-1}cm^{-2}$ in the busiest region. If a 1 mm wire spacing MWPC is used, the highest rate per wire will be about 0.4 MHz. This is a high intensity, but not above that encountered in other high-rate experiments. Wire chambers operating at rates of several times 10^7 $s^{-1}cm^{-2}$ have successfully been built [37].

Another concern is radiation damage over the course of a 10^7 second run. Assuming that all of the ionization in a 6 mm path length is amplified at a maximal gain of 10^5, we estimate a deposited charge of ~ 0.08 C/cm on the hottest wires. This is within the accepted limit of $\sim$ 1C/cm for 25 μm wires in traditional chamber gases.

Chamber Electronics

A low input impedance preamplifier will be mounted close to the wire followed by an Amplifier/Discriminator incorporating shaping circuitry to reduce the ion tail. Experience in E771 has shown that separating these two stages with approximately 30 feet of cable suppresses parasitic feedback sufficiently well to have stable operation at an anode threshold of $\sim 12,000e$. The discriminators will have a delayed output going to the data aquisition system as well as an optional prompt output for trigger purposes.

5.4.2 Analysis Magnet

The momentum analyzing magnet will be made up of two standard BM109 dipoles, each with an aperture of 61 cm wide by 30 cm high and an effective length of 2 m. The total transverse momentum kick is 1.8 GeV/c. The field is known to be uniform and can be easily mapped with the Fermilab ziptrack. From the experience gained in E756, the relative field values can be determined to better than 1×10^{-3}. As shown in Figs. 9 and 10, the agreement in the Ξ^- and $\overline{\Xi}^+$ as well as the Λ and $\overline{\Lambda}$ masses measured in E756 is excellent.

5.4.3 Hadronic Calorimeter

A simple hadronic calorimeter, used only to distinguish protons (antiprotons) (from Ξ decays) from background muons, is situated 70 meters downstream of the exit of the collimator, far enough downstream that the charged beam exiting the collimator is well separated from it. A schematic of the calorimeter is shown in Fig. 11. Its lateral size is 105×90 cm^2, and it is $6\lambda_I$ deep. It is a sampling calorimeter with scintillator as the active medium and lead as the absorber. There are a total of 50 layers of 0.5 cm scintillator and 2.0 cm lead, giving an interaction length of 20.3 cm and a radiation

length of 0.70 cm. Lead was chosen rather than iron as the absorber material because it gives a better energy resolution [38] and has a shorter radiation length, which confines electromagnetic showers from muon radiative processes to a smaller volume, allowing them to be discriminated against in the trigger rather easily.

The calorimeter is segmented laterally into seven horizontal and two vertical sections, and longitudinally into two sections, for a total of 28 channels. Each module is 62.5 × 45 × 15 cm^3. Essentially all of the protons from Λ decay which clear the spectrometer magnet enter a fiducial region which is at least one interaction length from the edge of the calorimeter. Protons entering at the edge of the calorimeter fiducial region have over 90% of their energy contained within the lateral extent of the calorimeter [39]. The longitudinal containment is better: only 2.5% of the shower energy will leak out the back [40].

The light is read out using photomultipliers coupled to wavelength shifter light guides on the top and the bottom of the calorimeter. We anticipate using Bicron BC-408 scintillator and Bicron BC-482A wavelength shifter (WLS) [41], which has a long attenuation length, good light output, and shows little degradation in light output when exposed to air for long periods of time. The wavelength shifter absorption spectrum is well matched to the emission spectrum of the BC-408, and the emission spectrum is well matched to the sensitivity of bialkali photomultipliers. Photomultipliers with a transistor base design [42] will be used to provide good gain stability with rate. We currently favor using the R-580 photomultiplier manufactured by Hamamatsu because of its excellent high rate characteristics [43]. The calorimeter response will be fast, with a FWHM of approximately 25 ns.

In the design shown in Fig. 11 the light is only read out on one end of the module in order that the calorimeter be hermetic. Because the light output at the WLS side of the scintillator tiles depends on the distance of the shower from the WLS, a special wrapping will be used to recover lateral uniformity of response. This will be done using Tyvek (Q173D) wrapping paper, from Du Pont [44], with a uniformity correction pattern, applied using a silk screen printing technique as has been done with the Zeus calorimeter [45]. A test rig will be constructed to determine the required pattern and test scintillator uniformity.

Calorimeter Energy Resolution

The hadronic energy resolution will be approximately $\sigma/\mathrm{E} = 60\%/\sqrt{E}$ [46], independent of energy as the calorimeter is compensating [47]. (If an iron absorber is used, with the same ratio of scintillator to absorber, the energy resolution would be worse: $\sigma/\mathrm{E} = 80\%/\sqrt{E}$ at 100 GeV. [38]) The electromagnetic resolution should be approximately $\sigma/\mathrm{E} = 30\%/\sqrt{E}$ [48]. The uncertainty in the muon energy loss is dominated by sampling fluctuations and hence should be similar to the electromagnetic energy resolution.

Calorimeter Muon Discrimination

The minimum proton (antiproton) momentum from Λ ($\overline{\Lambda}$) decay is 70 GeV (see Fig. 12). The resolution of the calorimeter at that energy is $\sigma = 5$ GeV. We wish to have very good efficiency for these protons, so the energy threshold will be set at approximately 20 GeV or 20σ away. (Note that the real-time energy resolution of the calorimeter will be worse than $60\%/\sqrt{E}$ and there will be some uncertainty in the trigger energy threshold due to drifts in the phototube gains.)

Muons deposit an energy of 1.9 GeV in the calorimeter due to ionization (assuming an *e/mip* ratio of 0.70, which is true for low momentum muons [49]). The uncertainty in the measurement of this energy is approximately $\sigma = 0.5$ GeV, assuming a Gaussian distribution. The distribution is better described by a Landau distribution, particularly at higher energies, where radiative processes are no longer rare. Note that the critical energy for muons in lead is approximately 250 GeV, well above our Monte Carlo estimate of 25 GeV for the mean muon momentum. Hence the tail of the Landau should not be pronounced. Experimental data taken with a similar calorimeter show that less than one out of a thousand muons of 20 GeV momentum deposit more than 8 GeV energy in the calorimeter [49].

To further discriminate against radiating high energy muons, the calorimeter trigger can be set to require a minimum energy in either adjacent calorimeter modules or in both the front and the back of the calorimeter. Electromagnetic showers induced by muon radiative processes are well localized, as is the ionization itself, whereas hadronic showers have a much longer and wider shower.

Calorimeter Radiation Damage

Radiation damage is not a problem. A hadron flux of approximately 10^5 per second over the period of a year gives a total flux of 6×10^{11} over an area of approximately 40×40 cm^2, or a dose of 10 Gy [50]. BC-408 scintillator has been measured to suffer little light reduction after a dose of 10 kGy [51].

Calorimeter Calibration

The calibration of the calorimeter will be easy. Every spill second over a thousand protons (or antiprotons) from Λ decays will be incident on the calorimeter. These have a momentum which is very well measured and will be used to calibrate the calorimeter and track its time dependence. An elaborate calibration system is not needed.

5.4.4 Hodoscope

A simple hodoscope, situated on the beam side of the spectrometer 60 meters from the exit of the collimator is used to trigger on pions from Ξ and Λ decay (see Fig 14). It

consists of 21 scintillation counters, each of 14×60 cm^2 area and 2 cm thickness. Each counter overlaps its neighbor by 2 cm giving a total width of 252 cm. The light is read out with phototubes placed at both ends. With these short, thick counters we expect a very high efficiency. We anticipate using Bicron BC-404 for the scintillator because of its fast response, and fast phototubes, such as the EMI 9814B [52] which has a FWHM of 3 ns. The hodoscope provides the timing for the experiment.

5.5 Trigger

The trigger has been kept simple in order to minimize potential biases. It relies on the fact that the decay of a Ξ^- ($\overline{\Xi}^+$) produces two pions with the same sign charge, but less momentum, than the beam exiting the hyperon channel, and a proton (antiproton) with the *opposite* sign charge. Because the polarity of the analysis magnet will be set equal to that of the hyperon magnet, the pions from the Ξ decay will be bent in the same direction (beam side) as the charged beam exiting the collimator, and the proton (antiproton) will be bent in the opposite direction to the charged beam. At the rear of the spectrometer both of the pions from the Ξ decay are well separated from the proton (antiproton), and both the pions and the proton (antiproton) are well separated from the charged beam exiting the collimator (see Fig. 13).

The trigger requires: 1) the presence, at the rear of the spectrometer, of a charged hadron in a hadronic calorimeter on the side opposite to the beam side of the spectrometer; and 2) the presence, again at the rear of the spectrometer, of at least one charged particle in a scintillator hodoscope on the beam side of the spectrometer. These two requirements — respectively called the proton and pion triggers — together are called the left-right trigger.

Because of the possibility of a large muon flux at the rear of the spectrometer — up to 2 MHz at the last MWPC (based on E756 studies) — either the proton trigger or the pion trigger must be made "muon blind". This is best done using a hadronic calorimeter. Because the protons have a higher momentum and are more tightly bunched together, the proton trigger rather than the pion trigger is implemented with the calorimeter. The pion trigger uses a simple scintillation counter hodoscope. Both of these trigger elements are placed outside of the intense charged particle beam exiting the collimator which has a flux of: 1.6×10^7 (4.3×10^7) per second in Ξ^- ($\overline{\Xi}^+$) mode with a nominal 10^{10} protons per second on target (see Table 3). This beam corresponds to an average bucket occupancy of 0.30 and 0.81, respectively for Ξ^- and $\overline{\Xi}^+$ running, of charged particles exiting the collimator. (The bucket spacing at Fermilab is 18.9 ns).

5.5.1 Trigger Rate

The trigger rate is summarized in Table 7. The trigger rate will be dominated by interactions of the charged beam exiting the collimator with material in the spectrometer,

as has been found in E756 using a similar trigger. The trigger rate must be kept below 100 kHz, the bandwidth to tape of the data acquisition system, a factor of 160 (430) less than the charged particle flux exiting the collimator in the Ξ^- ($\overline{\Xi}^+$) mode.

With 1.4% of an interaction length of material in the spectrometer, a rate of approximately 220 kHz (600 kHz) interactions per 10^{10} protons/s is expected for Ξ^- ($\overline{\Xi}^+$) running. Less than 5% of these interactions satisfy the left-right trigger, giving a trigger rate of 8 kHz (22 kHz) for Ξ^- ($\overline{\Xi}^+$) running. This is based on a sophisticated Monte Carlo simulation that reproduces the E756 trigger rate to better than 50%.

The spectrometer acceptance for Ξ's is given in Table 5. The trigger acceptance for Ξ's is well matched to the geometric acceptance: 99% of all the Ξ's that have both Ξ and Λ decay vertices in the vacuum decay region and whose decay products make it through the spectrometer magnet are accepted by the trigger. A total of 4,100 (2,300) Ξ^- ($\overline{\Xi}^+$) events are triggered on per 10^{10} protons/s on target. Of these 2,540 and 1,440 respectively for the Ξ^- and $\overline{\Xi}^+$ modes pass all software selection cuts.

Table 7: Trigger rate (per 10^{10} protons/s on target).

	Negative Running	Positive Running
Background trigger rate	8,300 Hz	22,200 Hz
$\Xi^\pm \rightarrow \Lambda\pi^\pm$ trigger rate	4,100 Hz	2,300 Hz
$K^\pm \rightarrow \pi^\pm\pi^\pm\pi^\mp$ trigger rate	900 Hz	2,000 Hz
Total:	13,300 Hz	26,500 Hz

5.5.2 Proton Trigger

Because of the large muon rate, a hadronic calorimeter is used, rather than a hodoscope (as was used in E756), to detect the presence of a proton (antiproton) from the Λ ($\overline{\Lambda}$) decay. The muon rejection of the calorimeter has to be approximately two orders of magnitude in order that the data acquisition system not saturate. To be safe, an order of magnitude more rejection is desirable because of the large uncertainty in the estimate of the muon rates.

The calorimeter must be fast, have good energy resolution, and be large enough to insure a good efficiency over its entire fiducial area. It does not have to be particularly radiation hard, or well segmented, and calibration is easy due to the large flux of well-measured protons incident on it.

Although the muon rejection factor seems easy to attain, measuring an asymmetry to 1×10^{-4} makes a high trigger efficiency for both protons and antiprotons extremely desirable. Hence the energy threshold on the proton trigger must be set low enough

for good efficiency. Although the amount of energy a muon deposits in dense matter is small, at large enough energies, radiative processes become important [53]. These processes, unlike ionization, are characterized by large energy fluctuations, and produce electromagnetic showers.

We estimate that the average muon momentum at the calorimeter will be about 25 GeV. (The exact value depends somewhat on the details of the siting of the experiment.) As discussed in the section describing the hadronic calorimeter, this is well below the critical energy of lead and experimental data taken with a similar calorimeter indicates that a rejection factor of one in 10^3 should be easy to obtain which retaining a very high proton (antiproton) efficiency.

5.5.3 Pion Trigger

The pion trigger is implemented with a simple scintillator hodoscope situated on the beam side of the spectrometer, 60 meters from the exit of the collimator (see Fig. 5). The hodoscope intercepts all but the unwanted low momentum pions clearing the magnet aperture. It does not intercept any of the charged particle beam exiting the collimator.

5.5.4 Trigger Electronics

The trigger electronics will be simple. The hodoscope trigger will employ standard NIM electronics. Fast phototubes are used to provide good single bucket timing.

Signals from the calorimeter phototubes will be split in two, with part going to flash ADC's (or perhaps the fast ADC's being developed for the KTeV experiment [54]) and then to the data acquisition system. The digitization of the signals should take less than 5 microseconds. The dynamic range of the ADC's should be sufficient to allow the muon energy to be well measured. The other part of the phototube output will be used to form the trigger, which will be done with the analog sum of the total energy in the calorimeter, and perhaps, front and rear sums, or separate lateral sums as well. This needs to be done in about half a microsecond.

5.6 Data Acquisition

The design goal of the DAQ system is to read 20,000 channels with a maximum trigger rate of 100,000 per spill second, build events, and write them to tape. We assume a maximum event size of 416 bytes (a factor of 2 larger than that of E756), resulting in a sustained data logging requirement of about 14 Mbyte/s — a high rate, but no larger than has been previously logged at Fermilab. The overall system deadtime should not exceed 10%, meaning that we should be able to log comfortably at least 90,000 triggers per second, *a factor of three greater than the estimated $\bar{\Xi}^+$ trigger rate and a factor of seven greater than the estimated Ξ^- trigger rate.*

The maximum event size is calculated as follows. There are 8 chambers, each with 3 wire planes (X, U and V plane). The ideal hit multiplicity for an event of interest is 3 per plane. If we take double hits and noise hits into account, a maximum of 8 hits per plane is a reasonable estimate. To be even more conservative, we always consider this worst case in our throughput calculations. Since each wire channel needs 2 bytes for encoding, a maximum of 384 bytes will be read out from all the chambers. Furthermore, we assume that a total of 20 bytes are generated by scintillators and calorimeter. The run and event number, event length and end of event marker will take up another 12 bytes. Therefore a maximum event size of 416 Bytes presents a very conservative estimate.

The design of the acquisition system is driven by the requirements of modularity (new technologies should be implementable as they become available without affecting the overall system), and scalability (it should be possible to accommodate an increase in performance).

The layout of the acquisition system is given in Fig. 15. The centerpiece is a standard 6U VME crate (DAQ-crate) that holds one or more Front-End Interfaces (FEI) that communicate with Front-End Crates (FEC), Event Builders (EB), Interfaces to Tape units (TI), and a State Machine (StM) which controls and monitors the activities of the readout sequences. A group of FEC's form a read-out branch. Several such branches can be accessed in parallel. Auxiliary readout of scalars, magnetic field monitors and other slow control devices will be done separately but will be embedded into the standard data stream.

The FEC contains the Front-End Modules (FEM) that read and latch the signals from the MWPC's and counters. The FEI communicates with the DAQ-crate and a Front-End Processor (FEP) which executes a real time kernel (e.g. VxWorks) for time-critical operations. The main functions of the FEP are data collection from all FEM's in the FEC, data reduction through reformatting of the event fragment, and temporary storage of data until the EB pulls a new block of events into its local memory.

There are six system components:

1. Front-End Module: In Fig. 16 the 256 differential ECL detector signals are received by the FEM and converted to TTL logic. The data are latched into a FIFO array. The FIFO's are deep enough to derandomize the intensity fluctuations of the incoming beam. The hit is then encoded as absolute wire address by an address encoder such as a digital signal processor and stored in one of two VME accessible on-board buffers. At the end of encoding, the address encoder will put out a word to signal the End of Event (EOE), e.g. FFFF, and append it to the event fragment. Data are written into the same buffer until the FEP decides to read out the FEM. The FEP broadcasts a SWITCH_BUFFER signal on the VME bus to all FEM's in the FEC and subsequently performs a block-read of the full buffer. In summary, the FEM's act as VME slaves to the FEP and have a double buffer scheme implemented. A "busy" signal will be generated to disable the trigger when the readout sequence cannot keep up with the trigger rate. Also a minimum

deadtime will be imposed once a trigger is accepted. In the current design we set the deadtime to 100 ns, limiting the FIFO speed to 10 MHz.

2. Front-End Processor (FEP): The FEP retrieves data with chained VME block-reads from all FEM's. After the FEP has fetched all these packets it assembles the data belonging to the same trigger and forms a new event fragment containing event number and fragment length. The FEP has large on-board memory (maximum 128 MByte) to hold event fragments over one full spill. This enables the FEI to transfer data during the spill and in between spills.

3. Event Builder (EB): The EB fetches all the event fragments from all FEC's to the local memory. Then it builds the final event from the event fragments belonging to the same trigger before writing it out to the permanent storage.

4. State Machine (StM): This module will synchronize and arbitrate the related DAQ processes. For example, it coordinates the trigger signals and the data transport through the DAQ.

5. Front-End-Interface (FEI): One FEC has to communicate with the DAQ-crate at a sustained rate of almost 2 MByte/s. The total throughput from all FEC's to the EB is expected to be around 18 MByte/s. Thus we will employ a fast link that enables us to daisy-chain several or all FEC's with the DAQ-crate. In case the setup latency for transfers is substantial we will use the State Machine to control the data flow.

6. Data Logging: We expect to log up to 14 MByte of data per second to the permanent storage. An array of five Exabyte Mammoth tape drives [55], which will be available at the end of 1994, and which write (in non-compressed mode) 3 MByte/s and pack 20 GByte per tape will be used.

5.7 Total Ξ Yields

The total Ξ^- and $\overline{\Xi}^+$ yield is limited by the bandwidth of the data acquisition system and by the requirement that we run on positives and negatives with the same fluence through the wire chambers. In order to saturate the bandwidth of the DAQ (10% dead time) a trigger rate per spill second of 90,000 is needed. In Ξ^- running this corresponds to a total flux of 108 MHz exiting the collimator and a *reconstructed* Ξ^- yield of 17,100 per spill second. To keep the charged particle fluence through the wire chambers the same in $\overline{\Xi}^+$ running, a corresponding trigger rate is 67,000 per spill second is needed giving a *reconstructed* $\overline{\Xi}^+$ yield of 3,600 per spill second.

At these rates the total Ξ^- and $\overline{\Xi}^+$ yield in a 200 day run with 50% duty factor is 9×10^9 each (assuming 80% of the running is on $\overline{\Xi}^+$). This corresponds to an error in the asymmetry $\mathcal{A} = (\alpha_\Lambda \alpha_\Xi - \alpha_{\overline{\Lambda}} \alpha_{\overline{\Xi}})/(\alpha_\Lambda \alpha_\Xi + \alpha_{\overline{\Lambda}} \alpha_{\overline{\Xi}})$ of 0.5×10^{-4}.

Because of uncertainties in our yield estimates, and because of the uneven spill structure in fixed target running, we are being more conservative and claim a maximum trigger rate of only 30 kHz per spill second. In Ξ^- running this corresponds to 36 MHz of charged particles exiting the collimator and a *reconstructed* Ξ^- yield of 5,700 per spill second. The corresponding reconstructed $\overline{\Xi}^+$ yield per spill second is 1,200. The total yield at this trigger rate, again assuming that 80% of the running is on $\overline{\Xi}^+$, is 2.9×10^9 for both Ξ^- and $\overline{\Xi}^+$. This corresponds to an error in the asymmetry $\mathcal{A} = (\alpha_\Lambda \alpha_\Xi - \alpha_{\overline{\Lambda}} \alpha_{\overline{\Xi}})/(\alpha_\Lambda \alpha_\Xi + \alpha_{\overline{\Lambda}} \alpha_{\overline{\Xi}})$ of 0.8×10^{-4}.

6 Offline Computing Needs

A sustained rate of 10,000 events per second will be written to tape assuming a 30,000 Hz trigger rate. In 200 days of running with a duty factor of 50% the total number of events will be 86×10^9 on 1,800 8mm–20 GB tapes (assuming an event size twice that of E756). This is a data sample on the order of that taken by E791 in the 1991 fixed target run [56].

Our estimate of the offline computing requirements is summarized in Table 8. In the first pass analysis, which reconstructs events, the CPU time required to process the E756 data on a HP 9000/735 workstation (rated 81 SPEC_int92) is 3 ms/event (including I/O time). We expect it will take comparable time to analyze an event in this experiment. A total of 2,100 SPEC_int92 are needed if the entire data set is to be reconstructed in 10^7 seconds.

The data throughput required for event reconstruction in 10^7 seconds is 3.6 MB/s. We expect to acquire 15 of the Exabyte Mammoth tape drives which will leave us with a nominal bandwidth of 45 MB/s.

For the final analysis, again based on our experience gained in E756, it will take approximately 1 ms to process a DST event on a HP-735. Assuming 4×10^9 Ξ events, a total of 3.2×10^8 SPEC_int92-seconds are needed for the final analysis. This could be done in 70 hours on the University of Virginia Digital alpha cluster.

Note that the total amount of DST data is 2,400 GB, or 120 tapes, assuming a 600 byte event size. (The E756 DST event size is 68 bytes!) In order to read all of these events from tape in 70 hours requires a sustained rate of 9.5 MB/s, well within the 45 MB/s bandwidth of our 15 Mammoth drives.

For Monte Carlo studies two types of events are generated: complete events and hybrid events. In a complete Monte Carlo event the parent particle is generated at the target, tracked through the collimator and the spectrometer, and digitized. The sophisticated E756 Monte Carlo takes about 45 ms to generate such an event on a HP-735. Hybrid Monte Carlo events use the decay vertex and momentum of the real Ξ's. Only the decay products are generated by the Monte Carlo. This minimizes errors due to poor simulation of the parent particle kinematic parameters. This technique has been extensively used in many high statistics hyperon polarization experiments [57]. With 10 ms needed to generate a hybrid event (on a HP-735), it also reduces the amount of computer time needed to generate an event. To generate a number of Monte Carlo events that is equal to the amount of data requires a processor power of 810 SPEC_int92 in 10^7 seconds.

The total amount of processor power needed to reconstruct, analyze, and generate an equivalent number of Monte Carlo events is approximately 3,000 SPEC_int92 in 10^7 seconds. Available computer resources among the collaborating institutions is over 1,200 SPEC_int92 (see Table 9). (We have omitted the lower end platforms available to the collaboration in Table 9.) We expect that by the time we begin the data analysis —

Table 8: Estimate of offline computing requirements.

Event Reconstruction	
Total triggers:	86×10^9
Total bytes:	36,000 GB
Total tapes (20 GB):	1,800
Reconstruction time per event:	0.24 SPEC_int92-second[a]
Total CPU needed:	2.1×10^{10} SPEC_int92-second
CPU per 10^7 seconds:	2,100 SPEC_int92
Final Analysis	
Total Ξ events:	4×10^9
Analysis time per event:	0.081 SPEC_int92-second[b]
Total CPU needed:	3.2×10^8 SPEC_int92-second
CPU per 10^7 seconds:	32 SPEC_int92
Monte Carlo Studies	
Events needed:	1.0×10^{10}
Analysis time per event:	0.81 SPEC_int92-second[c]
Total CPU needed:	8.1×10^9 SPEC_int92-second
CPU per 10^7 seconds:	810 SPEC_int92
Total CPU per 10^7 seconds needed:	2,942 SPEC_int92

[a]Based on the E756 reconstruction time using an HP-735 (81 SPEC_int92).
[b]Based on the E756 DST analysis time using an HP-735 (81 SPEC_int92).
[c]Based on the E756 Monte Carlo using an HP-735 (81 SPEC_int92).

1997, assuming a long fixed target run — the available processor power will have at least doubled by planned upgrades to the existing hardware to 3,000 SPEC_int92. Additional computer acquisitions will further augment this. *Hence we expect to be able to analyze all of the data in approximately half a year without recourse to the Fermilab farm.* We would like, however, to have several hundred SPEC_int92 of offline Fermilab processor power available during the running of the experiment and a fraction of the Fermilab processor farm for the data analysis.

Table 9: Presently available computing resources.

			Performance (SPEC_int92)	
Institution	Model	Number	Unit	Total
Univ. Virginia	Digital Alpha 3000/400	12	75	900
Berkeley	HP 9000/735	3	81	243
	HP 9000/730	2	37	74
Total:				1,217

7 Systematics

The experimental apparatus is designed to minimize systematic biases that produce false *CP* asymmetries. Because the Ξ^- and Λ alpha parameters both change sign under the *CP* transformation, the distribution of the proton in the Λ rest frame should be identical to that of the antiproton in the $\overline{\Lambda}$ rest frame. (The Λ and $\overline{\Lambda}$ distributions in the Ξ^- and $\overline{\Xi}^+$ rest frames should also be identical because the Ξ's are produced with no polarization.) *Hence, in principle, the proton and antiproton distributions can be directly compared with no acceptance corrections to search for CP violation.* In practice, acceptance corrections with have to be made, but they will be very small.

Systematic effects which have the potential to cause false asymmetries are of great concern in light of the fact that we wish to measure an asymmetry to the 10^{-4} level. Sources of biases which can cause false *CP* asymmetries fall into three classes: 1) differences in acceptance between the Ξ^- and $\overline{\Xi}^+$ decay products, 2) nonzero polarization of the Ξ^- or $\overline{\Xi}^+$, and 3) differences between the p and $\bar{p}$ cross sections.

7.1 Effect of Differences in the Acceptance

There are many possible causes of differences in the Ξ^- and $\overline{\Xi}^+$ acceptance. For example, targeting differences, magnetic field differences, and differences in the chamber efficiencies. Every effort will be made to minimize such differences.

Targeting differences can result in differences in the secondary production of Ξ's in the collimator. Such events are eliminated by requiring that the Ξ's point back to the target. To compensate for slight differences in the positive and negative magnetic fields of the hyperon channel and spectrometer magnets we intend to measure the differences in the field values to a part in 10^4 or better. The earth's magnetic field, which won't be flipped, produces slight changes in the acceptance between Ξ^- and $\overline{\Xi}^+$. The effect is small: an added 25 μrad deflection to a 15 GeV/c particle (amounting to 1 part in 10^3), the lowest momentum accepted by the spectrometer. This effect can be compensated for or corrected for in the Monte Carlo.

Because the Ξ^- and $\overline{\Xi}^+$ data samples will not be taken simultaneously, temporal changes in the apparatus could give rise to false asymmetries. To minimize rate dependent efficiencies in the chambers, we will be careful to run both positive and negative beams such that the charged particle flux at the exit of the collimator is always the same. Nevertheless, at the high charged particle fluences anticipated for the experiment, chamber efficiencies are not expected to be extremely high and localized inefficiencies producing false asymmetries at the 10^{-4} level are conceivable. In order to minimize such effects we have added redundant chamber planes at every measurement station. This allows the individual plane efficiencies to be measured to the desired accuracy and reduces the dependence of the tracking efficiency on the individual plane efficiency.

7.1.1 How the Analysis Method Minimizes Potential Biases

Despite efforts taken to minimize acceptance differences, some small differences will remain. Our method of analyzing the Λ polarization — which is different than that used previously by the hyperon group at Fermilab — greatly reduces the effect of these differences. Recall that to measure the product of the Ξ and Λ alpha parameters one needs to measure the distribution of polar angles that the protons makes with respect to the Λ polarization. This distribution is given by:

$$\frac{dP}{d\Omega} = \frac{1}{4\pi}(1 + \alpha_\Lambda \vec{P}_\Lambda \cdot \hat{p}_p), \tag{22}$$

where $\vec{P}_\Lambda$ is the Λ polarization and $\hat{p}_p$ is the proton momentum direction in the Λ rest frame. In previous hyperon polarization experiments measuring the Λ polarization and magnetic moment, the projection of this distribution on rest frame axes parallel to the lab frame x, y, and z axes has been measured. This was done because the Λ polarization in those experiments was fixed in space.

The situation in P871 is quite different. The Λ polarization is not fixed: its direction differs from event to event, and is given by the direction of the Λ momentum in the Ξ rest frame (see Fig. 17). The magnitude is always the same and is given by α_Ξ. The slope of the proton $\cos\theta$ distribution is equal to $\alpha_\Xi \alpha_\Lambda$,

$$\frac{dP}{d\cos\theta} = \frac{1}{2}(1 + \alpha_\Xi \alpha_\Lambda \cos\theta), \tag{23}$$

only in that frame in which the polar axis is determined by the direction of the Λ polarization. Hence we do not analyze the Λ polarization along axes fixed with respect to the lab axes, but in a coordinate frame in which the Λ polarization defines the polar axis.

Because the Λ direction changes from event to event over the 4π solid angle in the Ξ^- rest frame and because the acceptance along the helicity axis in the Λ rest frame is very uniform, acceptance differences localized in a particular part of the apparatus do not map onto any particular part of the $\cos\theta$ distribution of the proton. This will become evident in the following discussion.

7.1.2 Estimating Biases from E756 Data

In order to get a quantitative estimate of the effect of acceptance differences on the asymmetry measurement, we have chosen pairs of Ξ^- data sets from E756 with large acceptance differences and compared their proton distributions in the Λ rest frame. Since all of the events are Ξ^-'s, any difference between the proton distributions is solely due to acceptance differences between the two samples and not due to *CP* violation. *No attempt was made to correct for acceptance differences between the data sets.* Over 10 million Ξ^- events were analyzed.

We have chosen to investigate systematic effects using real rather than Monte Carlo data for several reasons. First, real data, unlike Monte Carlo data, has *all* effects which might cause biases — those known as well as those we have not yet thought of. Second, generating millions of Monte Carlo events is very time consuming. And finally, one can always correct for any biases put into the Monte Carlo since their source is exactly known. We have used all Ξ^- events rather than both Ξ^- and $\overline{\Xi}^+$ events from E756 because there are more of them, and because they have precisely the same $\cos\theta$ slope: $\alpha_\Lambda\alpha_\Xi$. *Any differences are due to biases and not CP violation!*

The data samples we have compared were taken at different hyperon magnet settings, producing different momentum distributions, and at different targeting angles, producing different values of the Ξ^- polarization. Samples with non-zero production angles are known to be polarized with a magnitude of about 12%.

The difference in the proton cosine distributions of any two samples is determined by taking the ratio:

$$R(\cos\theta) = \frac{A_1(\cos\theta)(1+a\cos\theta)}{A_2(\cos\theta)(1+a\cos\theta)}, \tag{24}$$

$$= \frac{A_1(\cos\theta)}{A_2(\cos\theta)}, \tag{25}$$

where $A_1(\cos\theta)$ and $A_2(\cos\theta)$ are the acceptances as a function of $\cos\theta$ of the two samples, $a = \alpha_\Xi\alpha_\Lambda$, and $\cos\theta$ is the polar angle the proton makes relative to the Λ polarization direction (which is the Λ momentum direction in the Ξ rest frame). Since $R(\cos\theta)$ is very uniform in $\cos\theta$, we parameterize it as

$$R(\cos\theta) = a + b\cos\theta \tag{26}$$

where the slope b is a measure of how well the acceptances of the two samples agree with each other. The intercept a is unity when the samples are properly normalized and the slope b is zero if the acceptances are identical *and* the fit is good.

Table 10 and Fig. 18 summarize the difference in $\cos\theta$ acceptance for data samples with comparable Ξ^- polarization but different average Ξ^- momentum. The acceptance mismatch strongly depends on the difference in momentum of the samples down to a momentum difference of $\Delta p = 20$ GeV/c, below which there is no statistically significant difference. It is important to note that in the insensitive region the proton $\cos\theta$ distributions in the Λ rest frame already agree to better than a few parts per thousand although the samples have significant acceptance differences in the laboratory frame and were taken at different times.

In P871 we will control the acceptance differences to well over an order of magnitude better than the differences shown above and we will correct any known acceptance differences. In order to minimize the bias due to a difference between the Ξ^- and $\overline{\Xi}^+$ momentum distributions we have a small collimator aperture which selects a narrow

Table 10: Acceptance difference as a function of momentum mismatch.

$< p_1 >^a$	$< p_2 >^b$	Δp^c	$\Delta P_\Xi{}^d$	$\lvert b \rvert$	χ^2/DOF
318.74	458.83	140.1	0.04	0.1442 ± 0.0041	3.76
318.74	427.34	108.6	0.03	0.1271 ± 0.0027	6.54
318.74	385.48	66.8	0.01	0.0923 ± 0.0024	4.10
385.48	427.34	41.9	0.02	0.0355 ± 0.0022	1.47
427.34	458.83	31.5	0.01	0.0183 ± 0.0039	0.74
458.83	478.98	20.2	0.04	0.0032 ± 0.0048	0.74
467.13	462.41	4.7	0.00	0.0029 ± 0.0051	1.54

[a]Mean Ξ^- momentum of sample 1 (GeV/c).
[b]Mean Ξ^- momentum of sample 2 (GeV/c).
[c]Difference in Ξ^- momentum (GeV/c).
[d]Difference in the Ξ^- polarisation.

momentum bite. As a result, the Ξ^- and $\overline{\Xi}^+$ momenta are determined largely by the collimator acceptance rather than by their production properties (which are different). To get an idea of how well the Ξ^- and $\overline{\Xi}^+$ acceptances match we have normalized the momentum spectra of the E756 Ξ^- and $\overline{\Xi}^+$ data to each other and then compared various Ξ^- and $\overline{\Xi}^+$ kinematic quantities. (The normalization is necessary because the momentum bite of the E756 magnetic channel was much broader than the P871 design and hence the Ξ^- and $\overline{\Xi}^+$ momentum spectra were different.) As shown in Figs. 19–21, the comparison is almost perfect — chi-squares per degree of freedom indicate no difference — even though the two data samples were taken at widely different times. In particular, in the comparison between the $\cos\theta$ distributions of the proton polar angle with respect to the Λ momentum in the Λ rest frame — the asymmetry we need to measure to search for *CP* violation — the slope b is -0.001 ± 0.009 with a χ^2/DOF of 0.67, indicating no statistically significant difference (see Fig. 22).

By extrapolation from the studies of the E756 data, we expect that the acceptance contribution in P871 to the measurement of the $\cos\theta$ slope will be considerably less than 10^{-4}.

7.2 Effect of Non-zero Ξ Polarization

Another potential source of bias is from non-zero Ξ^- and $\overline{\Xi}^+$ polarizations. The most probable source of such polarization would be a slight mistargetting. The resultant polarization would be extremely small due to the low p_T and small x_f of the Ξ. Any source of Ξ polarization can be measured to the 10^{-3} level and can be corrected for. A non-zero Ξ polarization results in a small fixed component to the Λ polarization in

addition to its helicity. Unlike the helicity, which changes from event to event, this new component is fixed in space. The effect of any fixed component of Ξ polarization on the measurement of the Λ helicity is diluted by our method of analysis — where the analysis polar axis changes from event to event. Because of the near uniform acceptance along the Λ momentum in the Λ rest frame, sources of polarization that are fixed in space average to almost identically zero.

The best evidence for this comes from another analysis of the E756 data. Samples of Ξ^-'s with equal and opposite production angles (± 2.5 mrad) were analyzed for differences in their proton $\cos\theta$ distributions. The data samples were chosen to have widely different polarizations: on average +12% and −12%, and widely different acceptances. This is partially due to the different polarizations, but mainly due to the tendency of the Ξ^- to follow the direction of the incident beam. The +2.5 mrad Ξ^- decay products tend to inhabit the upper part of the apparatus whereas the −2.5 mrad Ξ^- decay products inhabit the lower part. The magnitude of the difference is illustrated in Fig. 24 showing the vertical position of the proton at the spectrometer magnet center. The difference is huge.

How do these large differences in acceptance in the laboratory affect the measurement of the slope of the $\cos\theta$ distribution? Fig. 25 shows the proton $\cos\theta$ distributions from two samples. Fitting the ratio of the two to the form given by Eq. 26 shows no significant difference: the slope b of this comparison is $(2.3 \pm 2.9) \times 10^{-3}$ with a χ^2/DOF = 16.3/18. In Table 11 we show the same comparison for several similar samples of different Ξ polarization. There are no statistically significant differences in the proton $\cos\theta$ distributions between the two samples in each case despite the large differences in acceptance.

Table 11: Acceptance difference for samples of opposite polarization.

$< p_{+\theta} >^a$	$< p_{-\theta} >^b$	Δp^c	$\Delta P_\Xi{}^d$	b	χ^2/DOF
317.67	319.07	−1.40	0.23	-0.0017 ± 0.0027	1.02
318.74	319.34	−0.60	0.25	$+0.0023 \pm 0.0029$	0.90
385.48	383.45	2.03	0.26	-0.0016 ± 0.0017	1.20
427.34	425.85	1.49	0.28	-0.0030 ± 0.0024	0.74
458.83	454.32	4.51	0.29	-0.0063 ± 0.0047	0.93
478.98	478.42	0.56	0.25	-0.0125 ± 0.0044	1.03

[a] Mean momentum of positive production angle sample (GeV/c).
[b] Mean momentum of negative production angle sample (GeV/c).
[c] Difference in momentum (GeV/c).
[d] Difference in the Ξ^- polarisation.

Combining all the above samples we find $b = (2.5 \pm 10.4) \times 10^{-4}$, i.e. there is no

significant difference between the two $\cos\theta$ slopes of interest at the 10^{-3} level. Hence the dilution of the effect of the Ξ polarization is large and we expect that even smaller polarizations — on the order of a few tenths of a percent — will contribute less than 10^{-4} to the measured asymmetry.

In any case, we do not intend to only hope for a small Ξ polarization, but to actually measure it. Measuring it to the required 10^{-3} level is possible and would require only a fraction of the total data sample. We expect to find no polarization, but in fact could extract the *CP* asymmetry even in the presence of a Ξ polarization greater than 10^{-3}.

7.3 Differences in the p and $\bar{p}$ Cross Sections

Secondary interactions of the Ξ^- and $\overline{\Xi}^+$ decay products in the spectrometer can cause differences in the Ξ^- and $\overline{\Xi}^+$ reconstruction efficiencies. If such differences favor on part of the proton $\cos\theta$ distribution over another then false *CP* asymmetries can result.

In order to study this effect we have generated 5 million Ξ^- and $\overline{\Xi}^+$ Monte Carlo events in the P871 apparatus (using a modified version of the well-tested E756 Monte Carlo). Each proton or antiproton from a Ξ decay was forced to interact in the spectrometer with a distribution according to the amount of material at each location. PYTHIA was used to generate the number, type, and momentum of the resulting secondaries which were tracked through the spectrometer by the P871 Monte Carlo. The events were then reconstructed and the $\cos\theta$ distributions of the proton and antiproton were compared for those events that were successfully reconstructed. Only 120,000 events survived. The difference in the slopes of the $\cos\theta$ distributions ($\alpha_\Xi\alpha_\Lambda$ for both the Ξ^- and $\overline{\Xi}^+$ samples) was found to be -0.017 ± 0.010. Because P871 will have approximately 1.4% of an interaction length of material, this translates to a sensitivity of about $(2.9 \pm 1.7) \times 10^{-4}$ in the asymmetry A. Again, no attempt was made to correct for acceptance differences between the two data sets.

7.4 Other Potential Biases and Checks

There are other potential sources of biases. The radiative decays $\Lambda \to p\pi^-\gamma$ or $\overline{\Lambda} \to p\pi^+\gamma$ occur with a branching ratio of only 10^{-3} and don't contribute to the asymmetry A at the 10^{-4} level. Backgrounds from other sources are very small, as is evident in Fig. 23 which shows the $p\pi^-$ and $\bar{p}\pi^+$ invariant masses. Most of the continuum in the invariant mass distribution is due to poorly reconstructed Ξ events. This kind of background is reproduced in the Monte Carlo simulation in E756. With better position resolution and more redundant tracking measurements in this experiment, we expect this background to be highly suppressed.

To test the level of the systematics we intend to compare the Ξ^- and $\overline{\Xi}^+$ as well as Λ and $\overline{\Lambda}$ masses as well as their lifetimes as a function of the hyperon momentum. They should be identical if *CPT* is conserved. We will also have a sample of $K^- \to \pi^-\pi^-\pi^+$

and $K^+ \to \pi^+\pi^+\pi^-$ decays on the order of the Ξ sample. These can be analyzed as if they are $\Xi^\pm$ decays to search for false asymmetries.

8 Future Improvements

The *CP* sensitivity of this proposal, assuming systematic errors are not a problem, is not limited by the number of Ξ^- and $\overline{\Xi}^+$ hyperons that can be produced, but by the rates that the wire chambers can handle, the trigger selectivity, and the bandwidth of the data acquisition system. New technologies are being developed that are pushing these limits to higher levels. Wire chambers have been built that can take an order of magnitude more flux than we anticipate with no untoward effects [37]. The development of gas microstrip chambers [58] promises an even higher rate capability. Recently an experiment, NA12, has run at high intensities for 100 days with 8 microstrip gas chambers at CERN [59]. The chambers have a rate capability higher than 5×10^7 cm^{-2}s^{-1}. Vigorous R&D efforts are underway to increase the size and lower the mass of these chambers. If these efforts are successful, fluxes of two orders of magnitude higher than we anticipate in this proposal could be tolerated.

Similar improvements are being made in the data acquisition systems and triggers. Hence we expect in the future that large increases in the yield will be possible and the *CP* sensitivity of the experiment can be pushed beyond 10^{-4}.

9 Other Physics

9.1 CP Violation in Charged Kaon Decays

Direct *CP* violation can also show up in differences between K^+ and K^- decays. Two observables sensitive to *CP* asymmetries are:

$$\Delta\Gamma(\tau) = \frac{[\Gamma(K^+ \to \pi^+\pi^+\pi^-) - \Gamma(K^- \to \pi^-\pi^-\pi^+)]}{[\Gamma(K^+ \to \pi^+\pi^+\pi^-) + \Gamma(K^- \to \pi^-\pi^-\pi^+)]}, \tag{27}$$

and the asymmetry Δg in the slope parameter of the Dalitz plot which measures the energy dependence of the odd pion. The Dalitz plot of $K_{3\pi}$ decay is conventionally parameterized [7] with the form:

$$|M^2| \propto 1 + g\frac{(s_3 - s_0)}{m_\pi^2} + h\frac{(s_3 - s_0)^2}{m_\pi^2} + j\frac{(s_2 - s_1)}{m_\pi^2} + k\frac{(s_2 - s_1)^2}{m_\pi^2} + \ldots, \tag{28}$$

with

$$s_i = (m_K - m_i)^2 - 2m_K T_i, \; i = 1,2,3, \tag{29}$$

$$s_0 = \frac{1}{3}({m_K}^2 + {m_1}^2 + {m_2}^2 + {m_3}^2), \tag{30}$$

where m_i and T_i are the mass and the kinetic energy of the i^{th} pion, and the index 3 is used for the opposite sign pion in the decay. The coefficient j is zero if *CP* is conserved. Furthermore, if any of the other slope parameters, g, h, and k for $K^+ \to \pi^+\pi^+\pi^-$ is not the same as that for $K^- \to \pi^-\pi^-\pi^+$ decay, then *CP* symmetry is violated.

Because standard model estimates of $\Delta\Gamma(\tau)$ are very small ($< 10^{-6}$) [60], it seems unlikely that *CP* violating asymmetries will be observed there. The situation is more favorable for the slope parameters. Experimentally, the values of h and k are found to be very small [7]. Hence it will be very difficult to observe *CP*-odd effect by determining the difference in either h or k between $K^+ \to 3\pi$ and $K^- \to 3\pi$ decays. The slope parameter g is large (-0.2154 ± 0.0035 [7]) and hence interest in searching for direct *CP* violation in $K_{3\pi}$ decay has focused on it. The asymmetry of the slope parameter g is defined by

$$\Delta g = \frac{g(K^+) - g(K^-)}{g(K^+) + g(K^-)}. \tag{31}$$

Theoretical predictions of Δg vary from 1.4×10^{-3} to the order of 10^{-6} [61,62,63]. The best measurement of Δg is from a BNL experiment done in the late 60's which, with about 3.2 million $K^\pm \to 3\pi$ decays, determined Δg to be -0.0070 ± 0.0053 [64].

Our anticipated charged Kaon yields are given in Table 12. Despite the small acceptance due to the long $K^\pm$ lifetime — on average 2.2% of the $K^\pm$'s will decay in the decay region with the π's inside the spectrometer active area — the yields are very high; comparable to the Ξ yields. (About 50% of the $K_{3\pi}$ events pass reconstruction and

selection cuts.) In a 200 day run (assuming a 50% duty factor) we will collect 1.5×10^9 $K^+ \to \pi^+\pi^+\pi^-$ and 0.7×10^9 $K^- \to \pi^-\pi^-\pi^+$ decays. This implies a sensitivity for *CP* violation of about 1×10^{-4}.

There are several competing proposals. The NA48 collaboration has entertained using their apparatus to investigate charged-K decays. In a one-year run they would accumulate approximately 2×10^8 $K^+ \to \pi^+\pi^+\pi^-$ and $K^- \to \pi^-\pi^-\pi^+$ decays to get an error of 5×10^{-4} in Δg [65]. The E865 collaboration at Brookhaven is also considering measuring Δg [66]. They hope to collect 10^{10} decays in a few weeks of running. Finally, the Φ factory hopes to collect about 10^9 K^+K^- decays to allow a measurement of $\Delta g = 5 \times 10^{-4}$ [67].

Table 12: Charged Kaon yields (per 10^{10} protons).

	$K^+ \to \pi^+\pi^+\pi^-$	$K^- \to \pi^-\pi^-\pi^+$
Yield at target[a] (Hz)	6.5×10^6	2.9×10^6
Yield at collimator exit[b] (Hz)	2.7×10^6	1.2×10^6
Branching ratio	0.0559	
Lifetime acceptance	0.022	
Trigger acceptance	0.61	
Reconstruction efficiency	0.64	
Event selection cut efficiency	0.80	
Total (per spill second)	1,040	460
Total (200 day run)[c]	1.5×10^9	0.66×10^9

[a] Inside a cone with a solid angle of 4.88 μsr centered along the incident beam direction.
[b] Decay loss and channel acceptance have been taken into account.
[c] Assuming a 30% spill duty factor and a 50% experimental duty factor.

9.2 Other Physics

There are other physics topics that can be addressed by P871. We list some of them here.

- Precision measurements of the decay parameter α of Ξ and Ω^- decays.
- Tests of *CPT* in the differences in masses and lifetimes of particle and antiparticle in the $\Xi^\pm$, $\Omega^\pm$, Λ, and kaon systems.
- Search for the $\Delta S = 2$ decay: $\Xi^- \to p\,\pi^-\pi^-$.
- Search for the $\Delta S = 2$ decay: $\Omega^- \to \Lambda\pi^-$.

- Search for the $\Delta S = 3$ decay: $\Omega^- \to p\,\pi^-\pi^-$.
- Precise measurements of the polarization of the Ξ^- and $\overline{\Xi}^+$ at very small production angles and low x_F.
- Measurements of the Ξ^- and $\overline{\Xi}^+$ production cross sections.

If we were to add a muon station to the spectrometer then other interesting physics topics would become available including:

- Search for $K^\pm \to \pi^\pm\mu^+\mu^-$.
- Search for $K^- \to \pi^+\mu^-\mu^-$. (This mode is probably limited by the π/μ rejection that is possible.)
- Search for $\Xi^- \to p\mu^-\mu^-$.

With silicon strip detectors, or gas microstrip chambers at the exit of the collimator, at least two more rare decays can be searched for:

- Search for $\Sigma^- \to p\mu^-\mu^-$.
- Search for $\Sigma^+ \to p\mu^+\mu^-$.

Some of the above decays can also be searched for in the charged conjugate modes.

10 Costs

In this section we give our best estimates of the costs of the experiment. We expect these costs to be accrued over a period of two years. A detailed breakdown of the cost of constructing the spectrometer — wire chambers, calorimeter, hodoscope, readout electronics, and data acquisition system — is given in Table 18. The total cost is \$1,246K excluding \$146K needed for electronics from PREP. (Note that the cost per channel of the wire chamber electronics is \$37 excluding the cost of the data acquisition system.) The costs of the spectrometer are to be born by the collaborating institutions according to the breakdown given in Table 14. As of this writing we are somewhat short what is needed, but are confident that once approved new collaborators will make up the difference.

The total cost of constructing and mounting the experiment depends on the beam line used. An investigation by the beam group at Fermilab [68] found three beam lines that are well matched to the needs of the experiment: P-Center, P-West, and M-Center. Costs estimates for mounting the experiment in each of these beam lines are given in Tables 15, 16, and 17 [69]. Note that some of the rigging costs in the tables for P-West and M-Center must be done irrespective of P871. The total cost of mounting the experiment, for each of the three beam lines, is given in Table 13. Note that the Fermilab contribution in each case includes \$146K of existing PREP electronics.

We have omitted costs of running the experiment, which would be accrued in 1996 and 1997, and would be relatively minor (\$20K for tapes, for example). We have also omitted costs associated with analyzing the experiment, which would be accrued following 1997. Both LBL and the University of Virginia have substantial existing computer resources, so we expect these costs to be less than \$100K.

Table 13: P-871 Cost Summary.

Component	P-Center		P-West		M-Center	
	Fermilab	Collaboration	Fermilab	Collaboration	Fermilab	Collaboration
Beam line equipment	250,000		520,000		320,000	
Wire chamber fabrication		115,000		115,000		115,000
Chamber readout electronics	3,000	792,000	3,000	792,000	3,000	792,000
Hadronic calorimeter	12,000	73,000	12,000	73,000	12,000	73,000
Pion hodoscope	41,000	24,000	41,000	24,000	41,000	41,000
Trigger logic	90,000		90,000		90,000	
DAQ System		242,000		242,000		242,000
Total:	396,000	1,246,000	666,000	1,246,000	466,000	1,246,000

Table 14: Collaborating institution cost breakdown [$].

Institution	Funding Source	Year 1	Year 2
LBL	DOE University	250,000	250,000
Academia Sinica	Taiwan Research Council	?	100,000
University of Virginia	DOE University	100,000	100,000
University of Wisconsin	DOE University	50,000	50,000
Illinois Inst. of Tech.	DOE University	75,000	75,000
University of S. Alabama	DOE University	10,000	10,000
University of Houston	DOE University	?	?
Total:		485,000 + ?	585,000 + ?

Table 15: P-Center cost estimate [$].

Beam, Target, and Hyperon Channel	
Hyperon channel (fab. and install.)	50,000
Vacuum decay pipe (fab. and install.)	20,000
Fab. and install. muon spoilers	20,000
Cost of rapid removal of all E781 detectors	30,000
Interlock modifications	5,000
Experiment	
Move existing BM109's	10,000
Move E781 calorimeter	10,000
Install cable trays	10,000
Miscellaneous electrical	5,000
Provide counting rooms	90,000
Total:	$250,000

Table 16: P-West cost estimate [$].

Beam, Target, and Hyperon Channel	
Primary beamline: remove spoilers and install angle varying bends	40,000
Target and shielding	
Target mechanism	10,000
Reconfigure existing shielding	40,000
Hyperon channel (fab. and install.)	50,000
Install hyperon channel B2	20,000
Extra transerexes and busswork for AVB and hyperon	100,000?
Move toroids 1' east	20,000
Vacuum decay pipe inside existing toroids	20,000
Move SELMA 10 m downstream, remove polepiece	50,000
Remove E705/E771 (labourers, carpenters, etc.)	40,000
Remove Rosie	25,000
Remove E705/E771 muon wall	50,000
Interlock modifications	5,000
Experiment	
Install calorimeter	20,000
Modify cable trays	10,000
Modify existing counting rooms	20,000
Total:	$520,000 + ?

Table 17: M-Center cost estimate [$].

Beam, Target, and Hyperon Channel	
Primary beamline	
Add vertical AVB bend magnet (10')	20,000
Target and shielding	
Target mechanism	10,000
Remove Eartly magnets and dump	40,000
Hyperon channel (fab. and install.)	50,000
Install B2 hyperon magnet	20,000
Reshield hyperon cave	20,000
Reuse E799 vacuum decay pipe (fab. and install.)	10,000
Move existing MC7 experimental shielding	20,000
Remove existing MC7 experimental equipment	20,000
Modify existing MC7 muon spoilers	10,000
Construct secondary beam stop	5,000
Interlock modifications	5,000
Experiment	
Install 2 BM109 magnets	40,000
Install calorimeter	10,000
Install cable trays	10,000
Small upstream (MC7) counting room	30,000
Total:	**$320,000**

Table 18: Detector costs.

Hadronic Calorimeter							
Component	Unit	Unit Cost [$]	Ref.	# of units	Fermilab	Collab.	Total Cost [$]
Scintillator	$0.5 \times 45.0 \times 62.5$ cm^3	54	1	560		30,240	30,240
Waveshifter	$1.0 \times 15.0 \times 62.5$ cm^3	84	2	28		2,352	2,352
Lead	lb	0.47	3	24,000		11,280	11,280
Photomultiplier	channel	350	4	28		9,800	9,800
Bases	channel	100	5	28		2,800	2,800
Linear fan-In	16 channels	860	6	2	1,720		1,720
Discriminator	16 channels	1,650	7	3	4,950		4,950
Camac crate	each	5,000	8	1	5,000		5,000
Flash ADC	channel	50	9	28		1,400	1,400
Miscellaneous			10			15,000	15,000
Subtotal:					11,670	72,872	84,542

Pion Hodoscope							
Component	Unit	Unit Cost [$]	Ref.	# of units	Fermilab	Collab.	Total Cost [$]
Scintillator	$2.0 \times 14.0 \times 60.0$ cm^3	259	11	21		5,439	5,439
Photomultiplier	channel	350	12	42		14,700	14,700
Bases	channel	100	13	42		4,200	4,200
High voltage	80 channels	11,067	14	1	11,067		11,067
Discriminator	16 channels	1,650	15	4	6,600		6,600
Delay	16 channels	2,720	16	3	8,160		8,160
Coincidence unit	16 channels	1,869	17	2	3,738		3,738
Logic unit	32 channels	2,321	18	1	2,321		2,321
Camac crate	each	5,000	19	1	5,000		5,000
Miscellaneous			20		4,000		4,000
Subtotal:					40,886	24,339	65,225

Wire Chambers							
Component	Unit	Unit Cost [$]	Ref.	# of units	Fermilab	Collab.	Total Cost [$]
PWC	45×77 cm^2	10,000	21	5		50,000	50,000
PWC	60×200 cm^2	15,000	21	3		45,000	45,000
Amplifier	4 channels	44	22	5,250		231,000	231,000
Discriminator	32 channels	352	23	656		230,912	230,912
Latch	256 channels	2,200	24	82		180,400	180,400
Cable	16 channels/200 ft	100	25	1,300		130,000	130,000
High voltage	per pair	800	26	4	3,200		3,200
Low voltage	each	1,000	27	20		20,000	20,000
Gas system	system	20,000	28	1		20,000	20,000
Subtotal:					3,200	907,000	910,200

Data Acquisition System							
Component	Unit	Unit Cost [$]	Ref.	# of units	Fermilab	Collab.	Total Cost [$]
F.E. VME Crate	each	5,000	29	9		45,000	45,000
F.E. Interface	card	2,200	30	10		22,000	22,000
F.E. Processor	card	5,000	31	9		45,000	45,000
Memory Module	128 MB	6,500	32	9		58,500	58,500
DAQ VME Crate	each	2,500	33	1		2,500	2,500
State Machine	card	3,000	34	1		3,000	3,000
Event Builder	card	15,000	35	2		30,000	30,000
Tape Interface	card	2,500	36	4		10,000	10,000
Software License	each	600	37	10		6,000	6,000
Exabyte drive	each	4,000	38	5		20,000	20,000
Subtotal:						242,000	242,000

Trigger							
Component	Unit	Unit Cost [$]	Ref.	# of units	Fermilab	Collab.	Total Cost [$]
NIM electronics	module	1,500	—	40	60,000		60,000
CAMAC Crate	crate	5,000	—	2	10,000		10,000
NIM Bin	crate	2,000	—	10	20,000		20,000
Subtotal:					90,000		90,000

References

1. Bicron BC-408 scintillator; Bicron, 12345 Kinsman Rd., Newbury OH 44065.
2. Bicron BC-482A wavelength shifter; Bicron, 12345 Kinsman Rd., Newbury OH 44065.
3. Calcium Lead; Vulcan Lead Resources, Inc., 1400 W. Pierce St., Milwaukee, WI 53204.
4. Hamamatsu R-590; Hamamatsu Corp., 360 Foothill Rd., Bridgewater, NJ 08807-0910.
5. To be home built.
6. LeCroy 428F; LeCroy Corp., 700 Chestnut Ridge Rd., Chestnut Ridge, NJ 10977-6499.
7. LeCroy 4413; LeCroy Corp., 700 Chestnut Ridge Rd., Chestnut Ridge, NJ 10977-6499.
8. CAMAC crate and controller. Vendor not specified.
9. Type not yet selected.
10. Fabrication jig and prototype plus miscellaneous supplies.
11. Bicron BC-404 scintillator; Bicron, 12345 Kinsman Rd., Newbury OH 44065.
12. EMI 9814B; THORN EMI Gencom Inc., 23 Madison Rd., Fairfield, NJ 07006.
13. To be home built.
14. The high voltage supply will be used for both the hodoscope and calorimeter. LeCroy 1449, 1442N high voltage supply; LeCroy Corp., 700 Chestnut Ridge Rd., Chestnut Ridge, NJ 10977-6499.
15. LeCroy 4413; LeCroy Corp., 700 Chestnut Ridge Rd., Chestnut Ridge, NJ 10977-6499.

16. LeCroy 4518; LeCroy Corp., 700 Chestnut Ridge Rd., Chestnut Ridge, NJ 10977-6499.
17. LeCroy 4516; LeCroy Corp., 700 Chestnut Ridge Rd., Chestnut Ridge, NJ 10977-6499.
18. LeCroy 4532; LeCroy Corp., 700 Chestnut Ridge Rd., Chestnut Ridge, NJ 10977-6499.
19. CAMAC crate and controller. Vendor not specified.
20. Cables, etc.
21. Based on the KTeV estimates, *Conceptual Design Report: Kaons at the Main Injector*, FN-568.
22. This is based on a quote from LeCroy on the price of their PCOS IV preamp. It includes a tail cancelling shaper.
23. Design similar to E789 silicon strip detector readout system with the addition of a one-shot pulse stretcher. See B. Turko et al., IEEE Trans. Nucl. Sci. **39** (1992) 758.
24. To be home built. The estimate includes the costs of design, parts and fabrication.
25. Three sections of 34 conductor twist-n-flat having total length 200'.
26. Fermilab standard chamber high voltage power supply.
27. 100 amp Lambda power supply.
28. To be home built.
29. 9U VME crate (1.5kW); Dawn VME Products, 47073 Warm Springs Blvd., Fremont, CA 94539.
30. PTI 940; Performance Technologies, 315 Science Parkway, Rochester, NY 14620.
31. MVME 167.
32. Micro Memory Inc., 9540 Vassar Avenue, Chatsworth, CA 91311.
33. Standard 6U VME crate; Dawn VME Products, 47073 Warm Springs Blvd., Fremont, CA 94539.
34. MVME 162.
35. SPARC CPU-10; Themis Computer, 6681 Owens Drive, Pleasanton, CA 94588.
36. Performance Technologies, 315 Science Parkway, Rochester, NY 14620.
37. LBL sitewide licence.
38. Estimated cost of the new Exabyte Mammoth tape drive due out in the fall of 1994.

Appendix 1: What do we Actually Measure?

The angular distribution of the proton in the decay chain: $\Xi^- \to \Lambda\pi^-$, $\Lambda \to p\,\pi^-$, where the Ξ^- is produced unpolarized, is given by:

$$\frac{dP}{d\cos\theta} = \frac{1}{2}(1 + a\cos\theta), \tag{1}$$

where $a = \alpha_\Lambda\alpha_\Xi$ and θ is the polar angle of the proton in the Λ rest frame relative to the Λ momentum direction in the Ξ rest frame. Similarly, the angular distribution of the antiproton in the antiprocess: $\overline{\Xi}^+ \to \overline{\Lambda}\pi^+$, $\overline{\Lambda} \to \overline{p}\,\pi^+$, where the $\overline{\Xi}^+$ is produced unpolarized, is given by:

$$\frac{dP}{d\cos\theta} = \frac{1}{2}(1 + \overline{a}\cos\theta), \tag{2}$$

where $\overline{a} = \alpha_{\overline{\Lambda}}\alpha_{\overline{\Xi}}$. We write the expressions for the alpha parameters of the antiparticles as:

$$\begin{aligned} \alpha_{\overline{\Lambda}} &= -\alpha_\Lambda + \Delta\alpha_\Lambda, \\ \alpha_{\overline{\Xi}} &= -\alpha_\Xi + \Delta\alpha_\Xi. \end{aligned}$$

It is $\Delta\alpha_\Lambda$ and $\Delta\alpha_\Xi$ that we wish to measure: if CP is violated they must be nonzero. Measuring the angular distributions of Eq. (1) and Eq. (2) gives:

$$\begin{aligned} a &= \alpha_\Lambda\alpha_\Xi, \\ \overline{a} &= (-\alpha_\Lambda + \Delta\alpha_\Lambda)(-\alpha_\Xi + \Delta\alpha_\Xi). \end{aligned}$$

The difference between the two asymmetries is:

$$\begin{aligned} \mathcal{A} = \frac{a - \overline{a}}{a + \overline{a}} &= \frac{\alpha_\Lambda\alpha_\Xi - (-\alpha_\Lambda + \Delta\alpha_\Lambda)(-\alpha_\Xi + \Delta\alpha_\Xi)}{\alpha_\Lambda\alpha_\Xi + (-\alpha_\Lambda + \Delta\alpha_\Lambda)(-\alpha_\Xi + \Delta\alpha_\Xi)}, \\ &= \frac{+\alpha_\Lambda\Delta\alpha_\Xi + \alpha_\Xi\Delta\alpha_\Lambda - \Delta\alpha_\Lambda\Delta\alpha_\Xi}{2\alpha_\Lambda\alpha_\Xi - \alpha_\Lambda\Delta\alpha_\Xi - \alpha_\Xi\Delta\alpha_\Lambda + \Delta\alpha_\Lambda\Delta\alpha_\Xi}. \end{aligned}$$

Leaving out terms which are second order in $\Delta\alpha_\Lambda$ and $\Delta\alpha_\Xi$ in the numerator and first order in the denominator gives:

$$\begin{aligned} \mathcal{A} &\cong \frac{\alpha_\Lambda\Delta\alpha_\Xi + \alpha_\Xi\Delta\alpha_\Lambda}{2\alpha_\Lambda\alpha_\Xi}, \\ &\cong \frac{\Delta\alpha_\Xi + \Delta\alpha_\Lambda(\alpha_\Xi/\alpha_\Lambda)}{2\alpha_\Xi}. \end{aligned}$$

We wish to relate this to the individual asymmetries in the Ξ and Λ alpha parameters:

$$A_\Lambda = \frac{\alpha_\Lambda+\alpha_{\overline{\Lambda}}}{\alpha_\Lambda-\alpha_{\overline{\Lambda}}} = \frac{\Delta\alpha_\Lambda}{2\alpha_\Lambda},$$

$$A_\Xi = \frac{\alpha_\Xi+\alpha_{\overline{\Xi}}}{\alpha_\Xi-\alpha_{\overline{\Xi}}} = \frac{\Delta\alpha_\Xi}{2\alpha_\Xi}.$$

Plugging these in gives:

$$\frac{a-\overline{a}}{a+\overline{a}} = A_\Xi + A_\Lambda. \tag{3}$$

We have gone through this simple derivation in some detail in order to emphasize that what we are sensitive to is the *CP* asymmetry in both the Ξ and the Λ alpha parameters. In fact there is no way the two alpha parameters can be deconvoluted if one measures the Λ polarization through its self-analyzing weak decay. Although in theory $\Delta\alpha_\Lambda$ and $\Delta\alpha_\Xi$ could be equal and opposite in sign, the chances of such a conspiracy are remote: most calculations predict that A_Λ and A_Ξ have equal sign, and in fact the standard model prediction of [9] shows them to be roughly equal in magnitude as well, doubling the size of the measured asymmetry.

Appendix 2: Error in the Asymmetry Measurement

We wish to measure the difference between the the product of the Λ and Ξ^- alpha parameters and the $\overline{\Lambda}$ and $\overline{\Xi}^+$ alpha parameters:

$$\mathcal{A} = \frac{\alpha_\Lambda \alpha_\Xi - \alpha_{\overline{\Lambda}} \alpha_{\overline{\Xi}}}{\alpha_\Lambda \alpha_\Xi + \alpha_{\overline{\Lambda}} \alpha_{\overline{\Xi}}} = \frac{a - \overline{a}}{a + \overline{a}} = A_\Lambda + A_\Xi.$$

The error in this measurement is given by:

$$\begin{aligned} \delta\mathcal{A} &= \sqrt{\left(\frac{d\mathcal{A}}{da}\Delta a\right)^2 + \left(\frac{d\mathcal{A}}{d\overline{a}}\Delta\overline{a}\right)^2}, \\ &= \frac{2}{(a+\overline{a})^2}\sqrt{(\overline{a}\Delta a)^2 + (a\Delta\overline{a})^2}, \\ &= \frac{1}{2a}\sqrt{\Delta a^2 + \Delta\overline{a}^2}, \end{aligned}$$

where we have set $a = \overline{a}$. The product of the two alpha parameters is measured by measuring the asymmetry a in the proton (antiproton) decay distribution:

$$\frac{dP}{d\cos\theta} = \frac{1}{2}(1 + a\cos\theta).$$

The error in a is estimated using [70]:

$$\begin{aligned} \Delta a &= \frac{1}{\sqrt{N}}\sqrt{2a^3/(\log(1+a) - \log(1-a) - 2a)}, \\ &\cong \sqrt{\frac{3}{N}}, \end{aligned}$$

where the expression strictly applies only when the acceptance is uniform. We find:

$$\delta\mathcal{A} = \frac{1}{2a}\sqrt{\frac{3}{N_{\Xi^-}} + \frac{3}{N_{\overline{\Xi}^+}}},$$

where N_{Ξ^-} and $N_{\overline{\Xi}^+}$ are respectively the number of Ξ^- and $\overline{\Xi}^+$. If the two data samples are equal then:

$$\delta\mathcal{A} = \frac{1}{a}\sqrt{\frac{3}{2N}}.$$

The number of events needed to measure $\mathcal{A}$ to $\delta\mathcal{A}$ precision is:

$$\begin{aligned} N &= \frac{3}{2a^2}\frac{1}{(\delta\mathcal{A})^2}, \\ &= \frac{17.5}{(\delta\mathcal{A})^2}, \end{aligned}$$

where we have substituted $a = \alpha_\Lambda\alpha_\Xi = (-0.456)(0.642) = -0.293$. To measure an asymmetry with an error of $\delta\mathcal{A} = 1 \times 10^{-4}$ requires 1.8×10^9 Ξ^- events and the same number of $\overline{\Xi}^+$ events.

References

[1] J.H. Christenson, J.W. Cronin, V.L. Fitch and R. Turlay, Phys. Rev. Lett. **13** (1964) 138.

[2] L. Wolfenstein, Phys. Rev. Lett. **13** (1964) 562.

[3] L.K. Gibbons et al. (E731), Phys. Rev. Lett. **70** (1993) 1203.

[4] H. Burkhardt et al. (NA31), Phys. Lett **B206** (1988) 169.

[5] A. Pais, Phys. Rev. Lett. **3** (1959) 242.
O.E. Overseth and S. Pakvasa, Phys. Rev. **184**, (1969) 1663.

[6] P.M. Ho et al., Phys. Rev. **D44** (1991) 3402.

[7] Review of Particle Properties, Phys. Rev. **D45** 1992) 1.

[8] T.D. Lee and C.N. Yang, Phys. Rev. **108** (1957) 1645.

[9] John F. Donoghue, Xiao-Gang He and Sandip Pakvasa, Phys. Rev. **D34** (1986) 833.

[10] Tim Brown, S.F. Tuan and Sandip Pakvasa, Phys. Rev. Lett. **51** (1983) 1823.

[11] Ling-Lie Chau and Hai-Yang Cheng, Phys. Lett. **B131** (1983) 202.

[12] John F. Donoghue and Sandip Pakvasa, Phys. Rev. Lett. **55** (1985) 162.

[13] John F. Donoghue, Barry R. Holstein and German Valencia, Phys. Lett. **B178** (1986) 319.

[14] John F. Donoghue, Third Conf. on the Intersections between Particle and Nuclear Physics, Rockport ME, 14–19 May, 1988.

[15] M.J. Iqbal and G.A. Miller, Phys. Rev. **D41** (1990) 2817.

[16] X.G. He, H. Steger and G. Valencia, Phys. Lett. **B272** (1991) 411.

[17] E.A. Paschos and Y.L. Wu, Mod. Phys. Lett. **A6** (1991) 93.

[18] S. Weinberg, Phys. Rev. Lett. **37** (1976) 657.
T.D. Lee, Phys. Rev. **D8** (1973) 1226; Phys. Rep. **96** (1974) 143.

[19] M. Kobayashi and T. Maskawa, Prog. Theor. Phys. **49** (1973) 652.

[20] M. Shifman, A. Vainshtein, and V. Zakharov, Nucl. Phys. **B120** (1977) 316.
F. Gilman and M. Wise, Phys. Lett. **B93** (1980) 129.

[21] G. Valencia, private communication.

[22] J.M. Flynn and L. Randall, Phys. Lett. **B224** (1989) 221.

[23] G. Buchalla, A. Buras and M. Harlander, Nucl. Phys. **B337** (1990) 313.

[24] P. Chauvat et al., Phys. Lett. **163B** (1985) 273.

[25] M.H. Tixier et al., Phys. Lett. **B212** (1988) 523.

[26] P.D. Barnes et al., Phys. Lett. **B199** (1987) 147.

[27] N. Hamann et al., CERN/SPSLC 92-19, 30 March 1992.

[28] S.Y. Hsueh, "Search for direct *CP* violation in $\bar{p} + p \rightarrow \bar{\Lambda} + \Lambda \rightarrow \bar{p}\pi^+ + p\pi^-$", Proposal to Fermilab, January 2, 1992.

[29] E.M. Gonzalez, Proceedings of the Meeting on the Tau-charm Factory Detector and Machine, University of Seville, Andalucia, Spain, 29 April – 2 May 1991, Ed. by J. Kirkby and J.M. Quesada.

[30] T.R.Cardello et al., Phys. Rev. **D32** (1985) 1.

[31] A.J. Malensek, Fermilab note FN-341 (1981), unpublished.

[32] A. Beretvas et al., Phys. Rev. **D34** (1986) 53.

[33] M. Bourquin et al., Z. Phys. **C5** (1980) 275.

[34] B. Lundberg et al., Phys. Rev. **D40** (1989) 3557.

[35] J. Lach and Y. Li, Fermilab note TM-1555 (1989), unpublished.

[36] G. Guglielmo, private communication.

[37] J. Fischer, A. Hrisoho, V. Radeka and P. Rehak, Nucl. Instr. and Meth. **A238** (1985) 249.

[38] R. Wigmans, Nucl. Instr. and Meth. **A259** (1987) 389.

[39] D. Acosta et al., Nucl. Instr. and Meth. **A316** (1992) 184.

[40] H. Abramowicz et al., Nucl. Instr. and Meth. **180** (1981) 429.

[41] Bicron, 12345 Kinsman Rd., Newbury OH 44065.

[42] C.R. Kerns, IEEE Trans. on Nucl. Science, *NS-24* (1973) 353.

[43] Hamamatsu Corp., 360 Foothill Rd. Bridgewater, NJ 08807-0910.

[44] DuPont, P.O. Box 80016, Wilmington, DE 19880-0016.

[45] The Zeus Detector, Status Report, March 1989.

[46] G. Drews et al., Nucl. Instr. and Meth. **A290** (1990) 335.

[47] P.K. Job et al., Nucl. Instr. and Meth. **A316** (1992) 174.

[48] J. Del Peso and E. Ros, Nucl.. Instr. and Meth. **A276** (1989) 456.

[49] D. Acosta et al., Nucl. Instr. and Meth. **A320** (1992) 128.

[50] D.E. Groom, "Radiation Levels in the SSC Interaction Regions", SSC-SR-1033, June 10, 1988.

[51] C. Zorn et al., Nucl. Instr. and Meth. **A276** (1989) 58.

[52] THORN EMI Gencom Inc., 23 Madison Rd., Fairfield, NJ 07006.

[53] W. Lohmann, R. Kopp, and R. Voss, "Energy Loss of Muons in the Energy Range 1–10,000 GeV," CERN Report 85–03 (1985).

[54] KTeV Design Report, FN-580, Fermilab, January 22, 1992.

[55] Exabyte Corp., 1685 38th Street, Boulder CO 80301.

[56] S. Amato et al., Nucl. Instr. and Meth. **A324** (1993) 535.

[57] G. Bunce, Nucl. Instr. Meth. **172** (1980) 553.

[58] A. Oed, Nucl. Instr. and Meth. **A263** (1988) 351.
F. Angelini et al., Nucl. Instr. and Meth. **A283** (1989) 755.

[59] F. Angelini et al., Nucl. Instr. and Meth. **A315** (1992) 21.

[60] B. Grinstein, S.J. Reg, and M.B. Wise, Phys. Rev. **D33** (1986) 1495.

[61] A.A. Bel'kov et al., Phys. Lett. **B300** (1993) 283.

[62] G. D'Ambrosio, G. Isidori, and N. Puver, Phys. Lett. **B273** (1991) 497.

[63] Hai-Yang Cheng Phys. Rev. **D44** (1991) 919.

[64] W.T. Ford et al., Phys. Rev. Lett. **25** (1970) 1370.

[65] G.D. Barr *et al.,* Proposal for NA48, CERN/SPSC/90-22.

[66] M. Zeller *et al.,* BNL proposal E865 (1991).

[67] P. Franzini, INFN preprint LNF-92/024 (P) (1992).

[68] A. Malensek and R. Tokarek, *Possible Beam Locations for P-871*, March 4, 1994.

[69] C.N. Brown, *P871: Preliminary Cost Guesstimate*, March 24, 1994.

[70] A.G. Frodesen, O. Skjeggestad and H. Tofte, "Probability and Statistics in Particle Physics" (Universitetsforlaget, Oslo, 1979) p. 219.

List of Figures

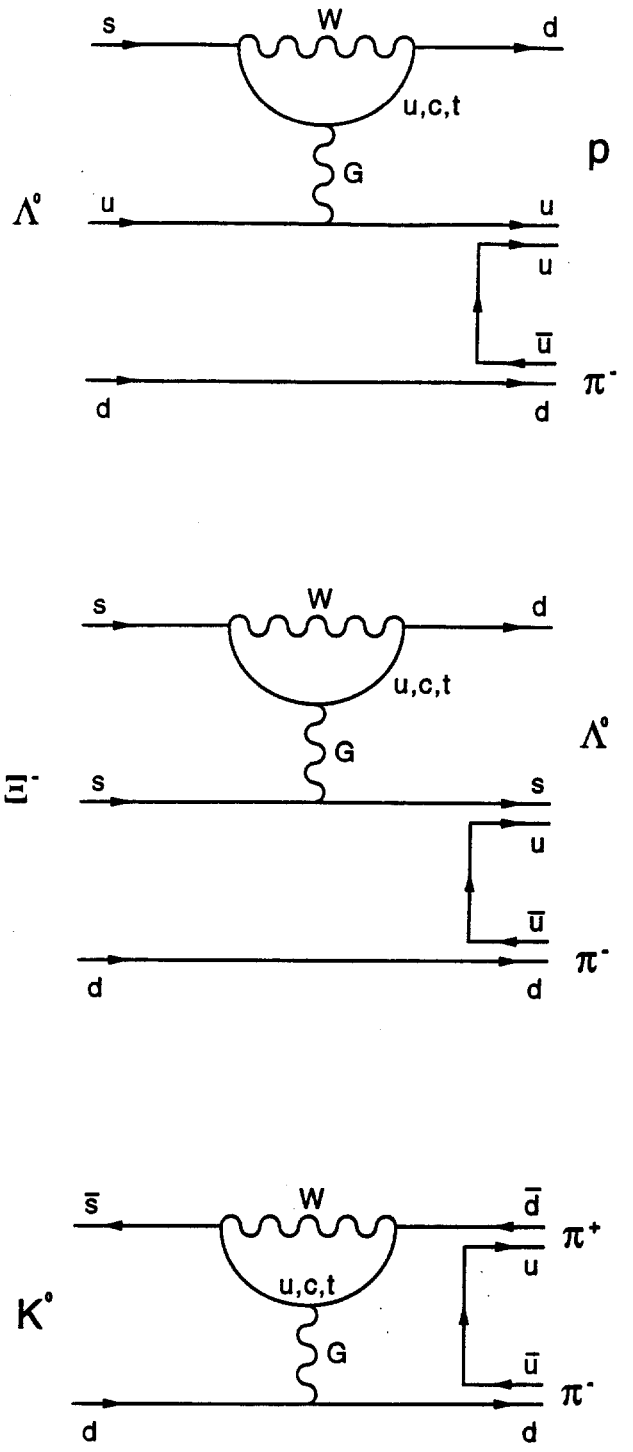

Figure 1: Penguin diagrams responsible for $|\Delta S| = 1$ direct CP violation in $\Lambda \to p\pi^-$, $\Xi^- \to \Lambda\pi^-$ and $K \to \pi^+\pi^-$ decays according to the standard model.

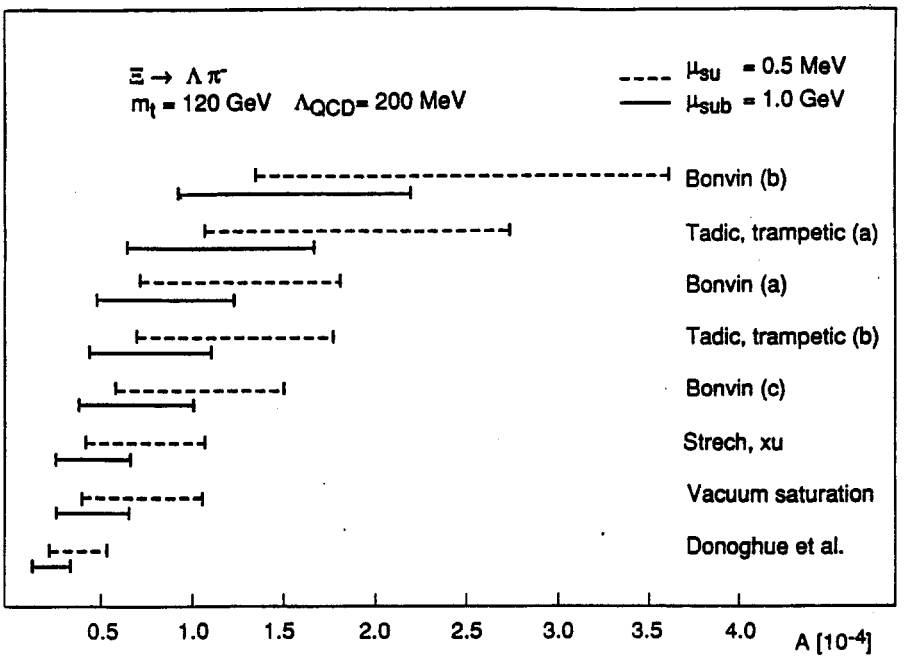

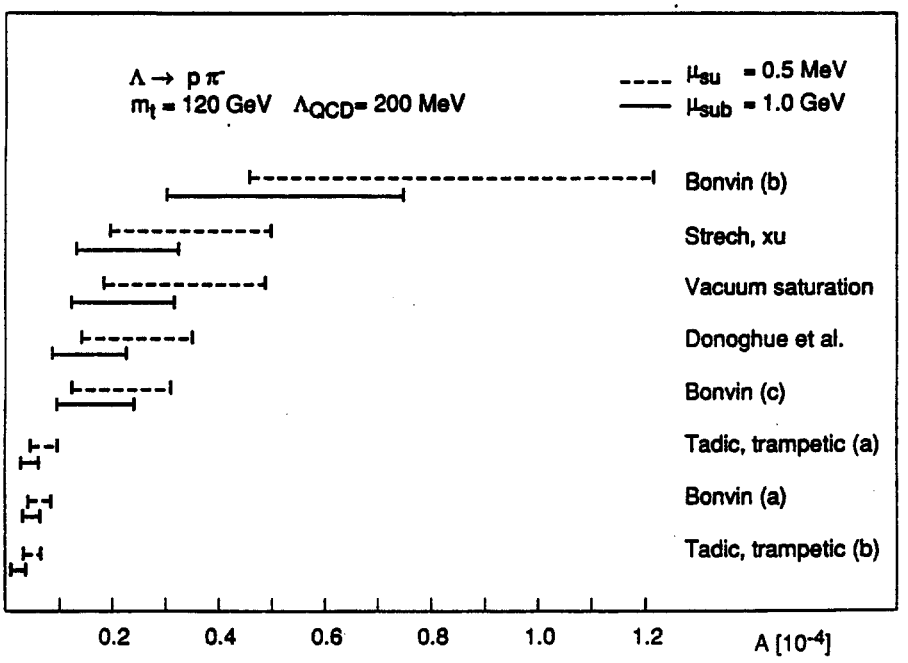

Figure 2: Range of standard model predictions of (a) $(\alpha_\Xi + \alpha_{\bar{\Xi}})/(\alpha_\Xi - \alpha_{\bar{\Xi}})$ and (b) $(\alpha_\Lambda + \alpha_{\bar{\Lambda}})/(\alpha_\Lambda - \alpha_{\bar{\Lambda}})$ from the model of Xe, Steger, and Valencia [21] using matrix elements calculated from various models.

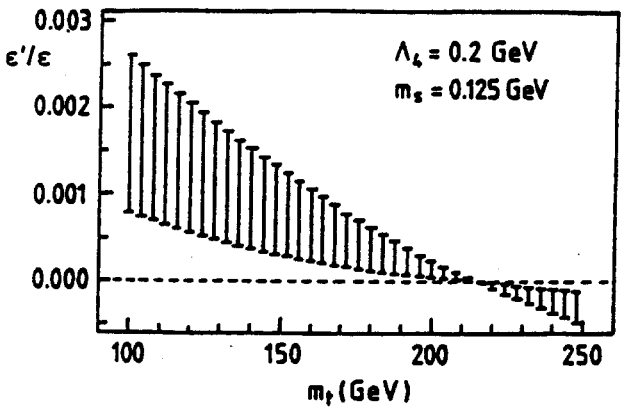

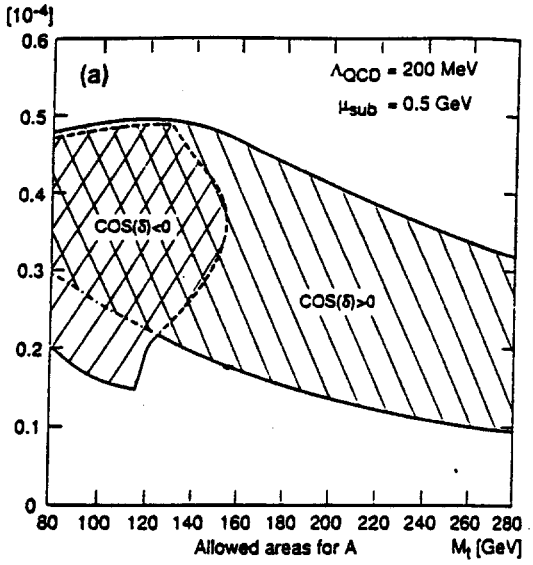

Figure 3: Standard model predictions for (a) ϵ'/ϵ [17] and (b) $(\alpha_\Lambda + \alpha_{\overline{\Lambda}})/(\alpha_\Lambda - \alpha_{\overline{\Lambda}})$ [16] showing the dependence on the top quark mass.

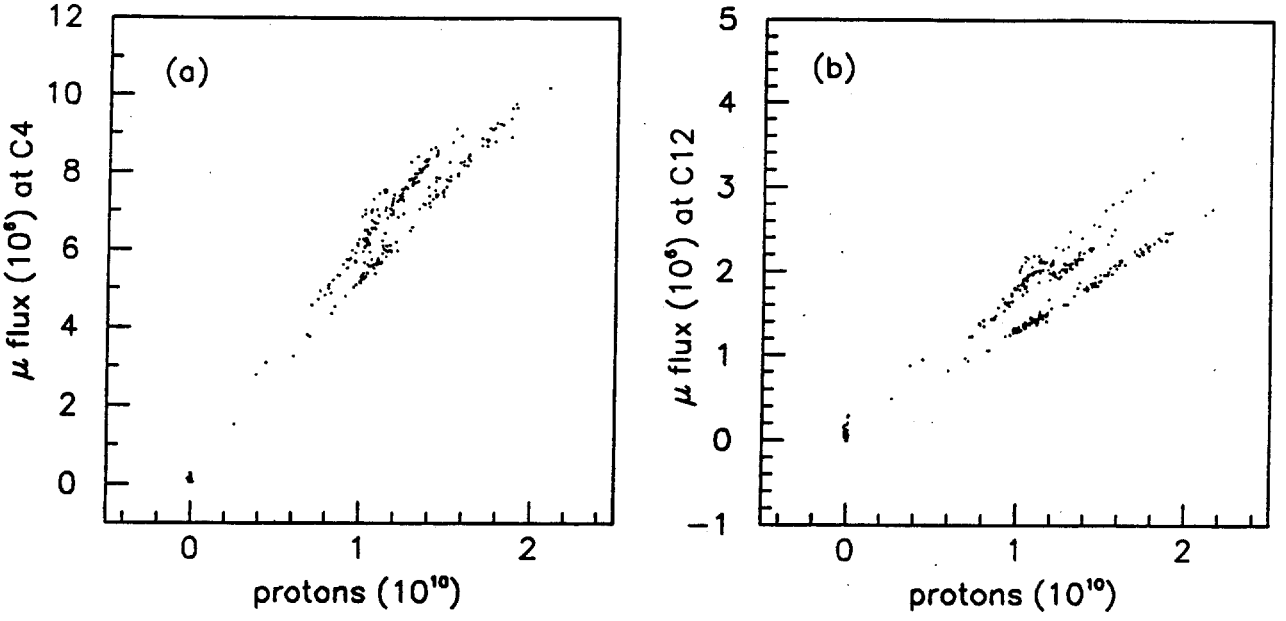

Figure 4: Muon fluence measured in E756 at (a) an upstream chamber (*C4*: 26 m from the collimator exit), and (b) a downstream chamber (*C12*: 49 m from exit).

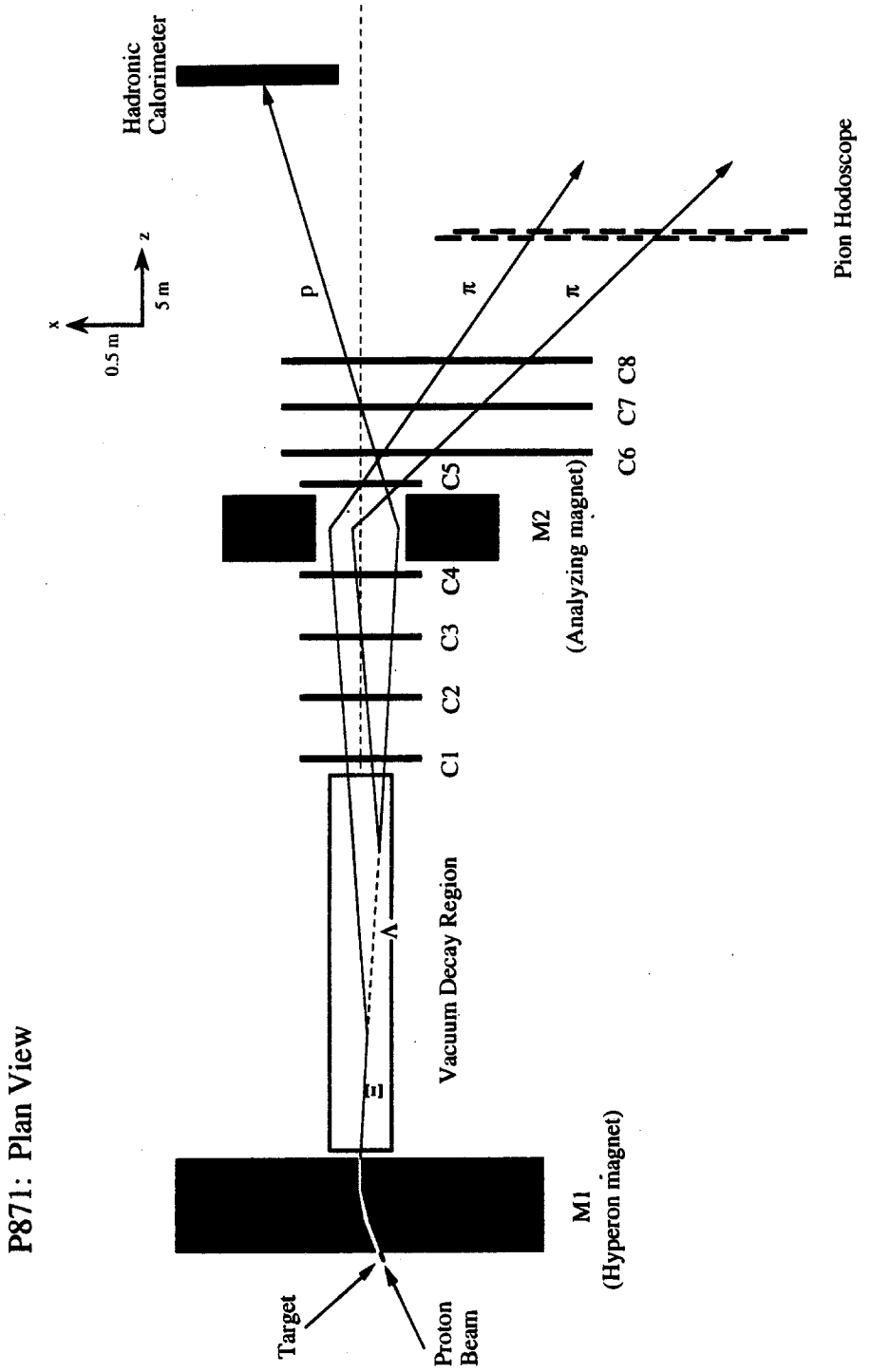

Figure 5: Plan view of the P871 spectrometer.

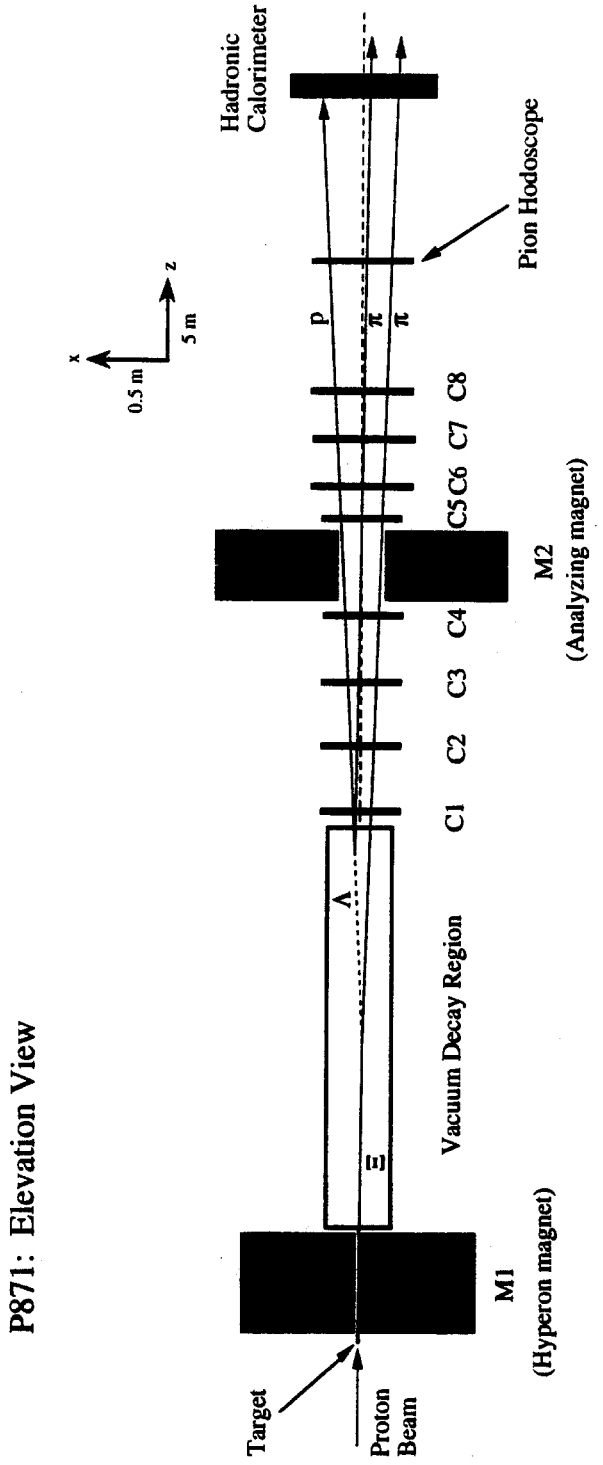

Figure 6: Elevation view of the P871 spectrometer.

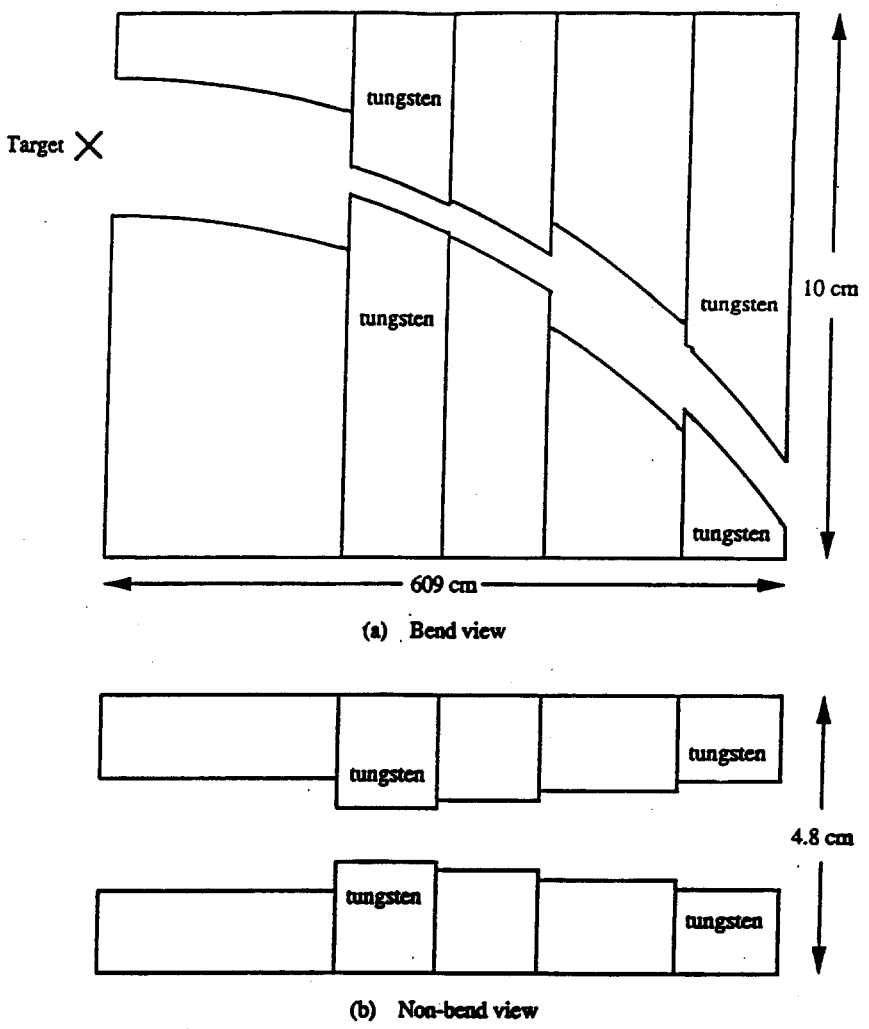

Figure 7: The P871 hyperon channel.

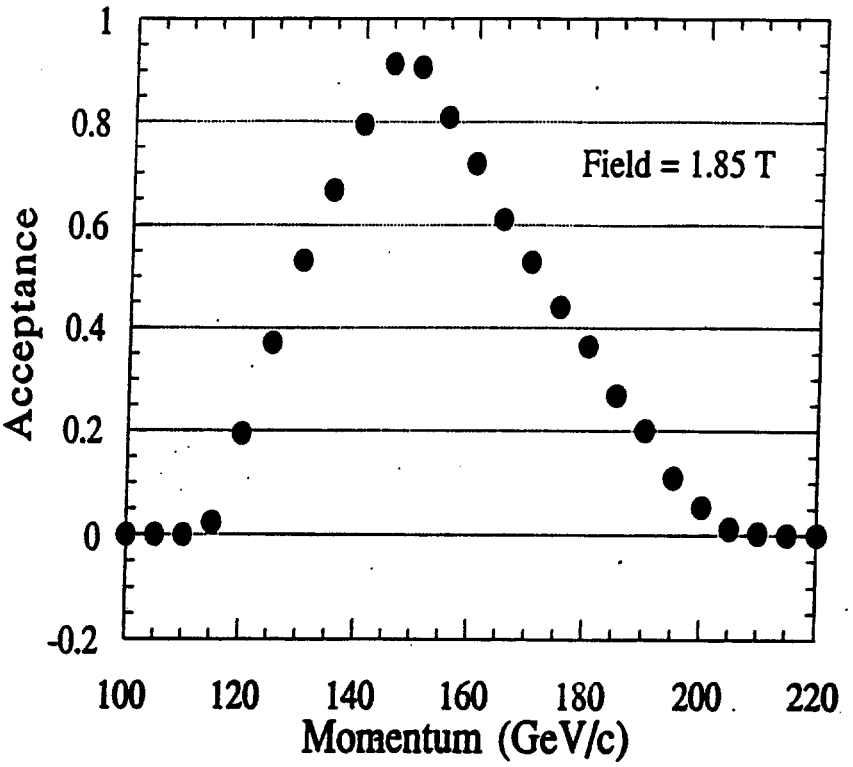

Figure 8: The hyperon channel acceptance.

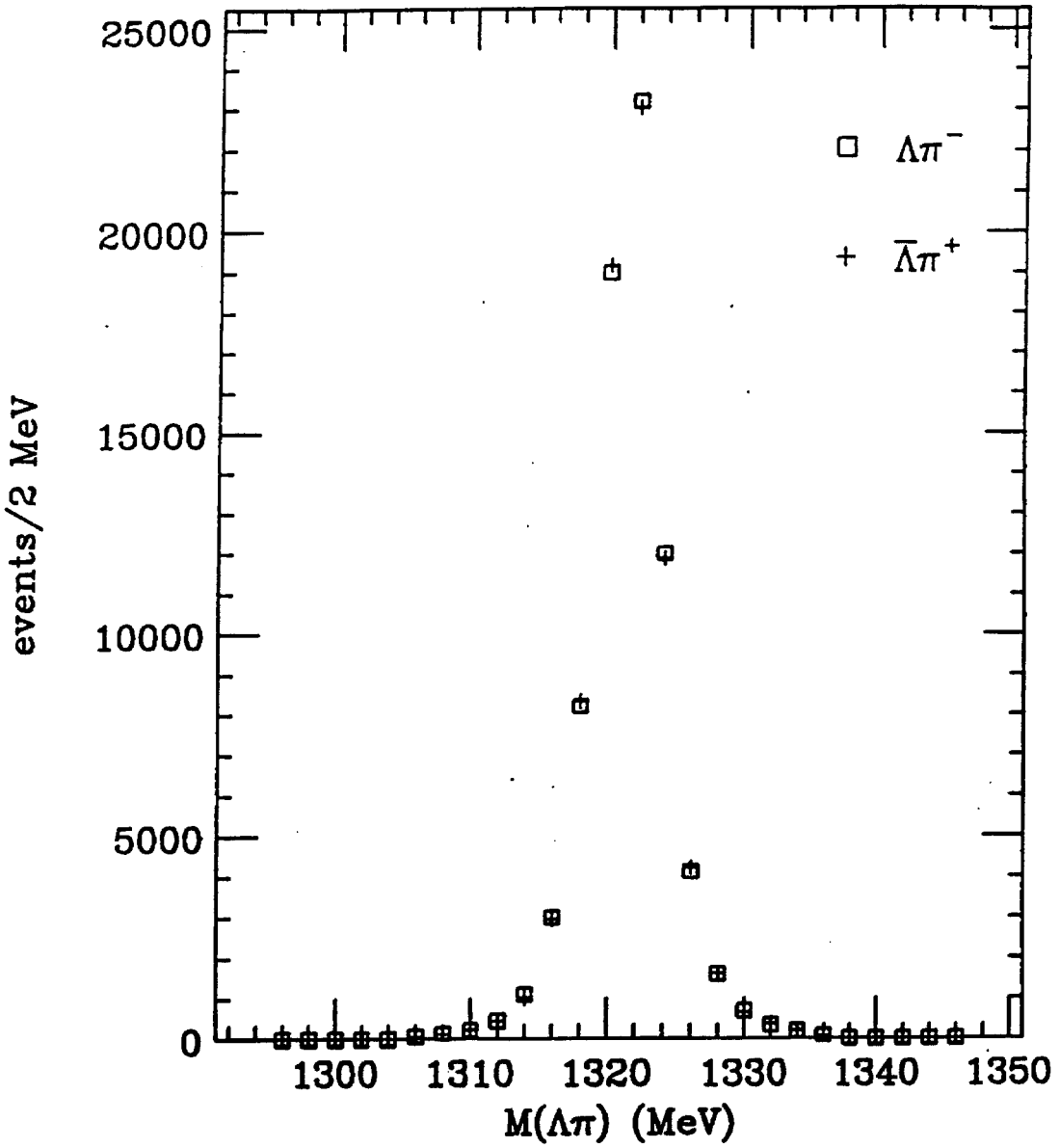

Figure 9: Comparison between the $\Lambda\pi^-$ and $\overline{\Lambda}\pi^+$ invariant masses from E756.

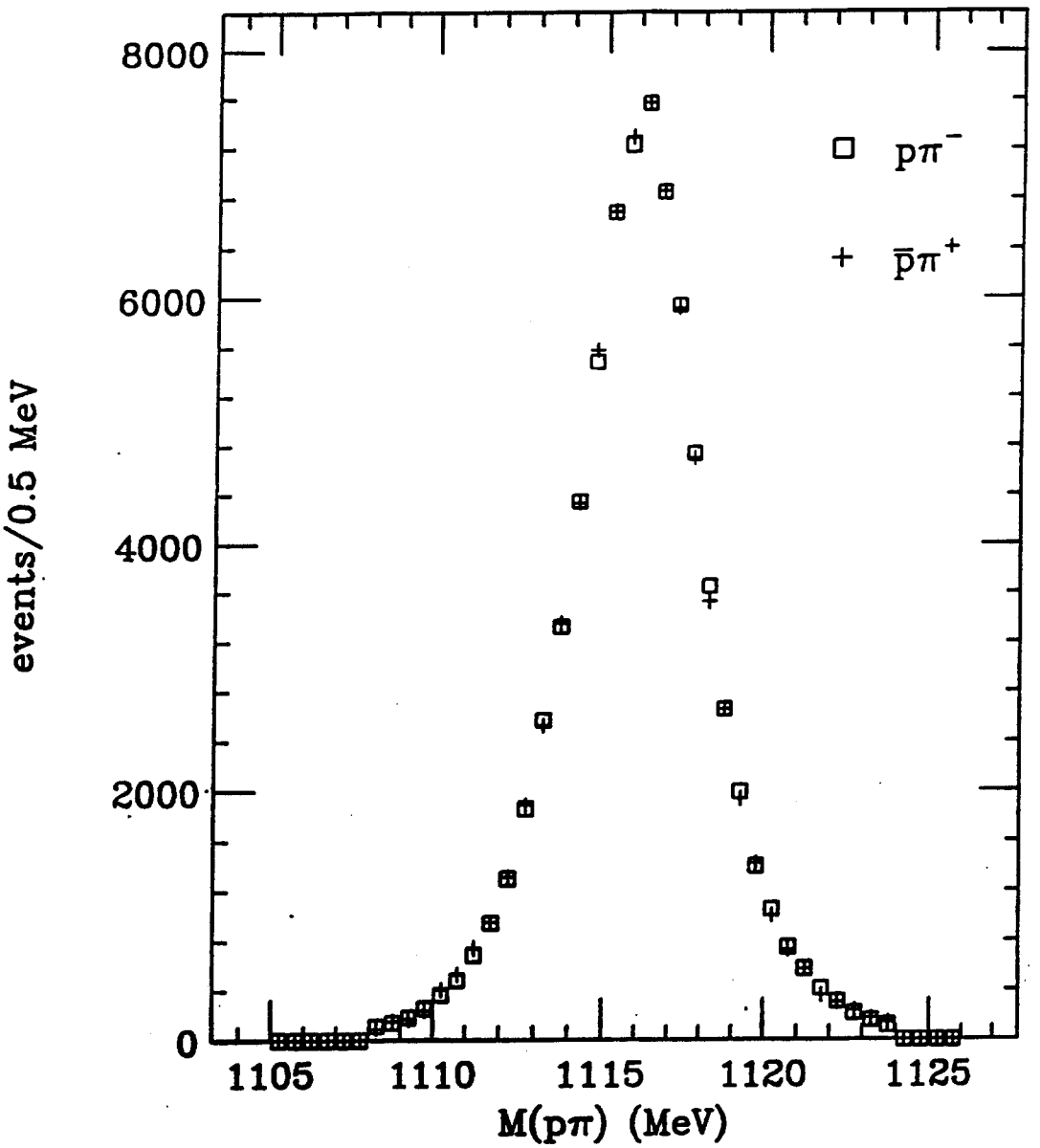

Figure 10: Comparison between the $p\pi^-$ and $\bar{p}\pi^+$ invariant masses from E756.

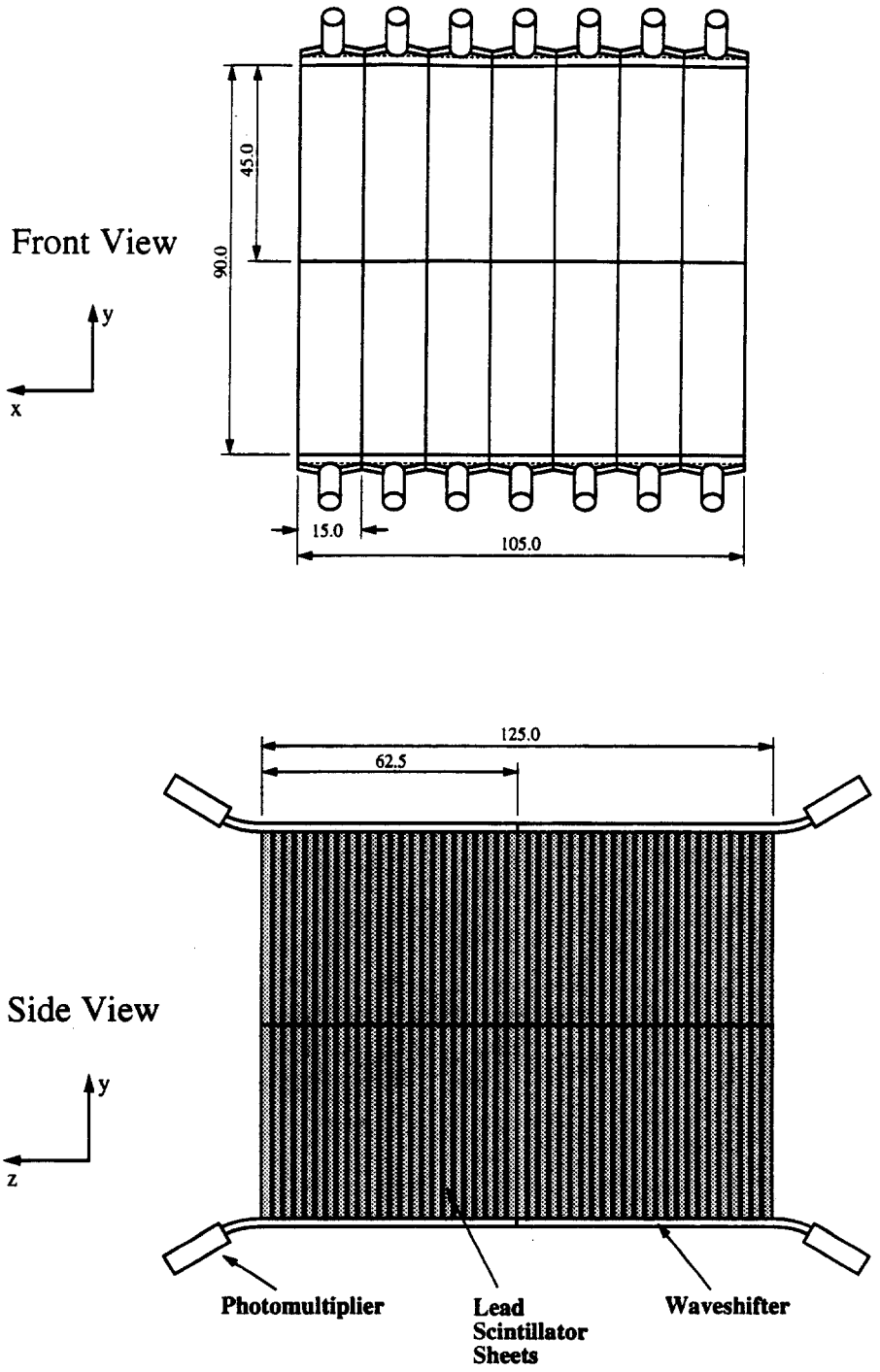

Figure 11: Front and side views of the hadronic calorimeter. Units are cm.

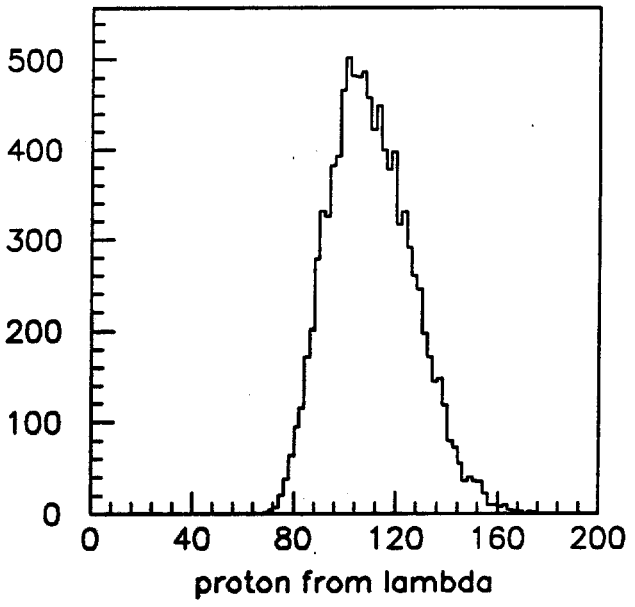

Figure 12: The proton momentum (in GeV/c) from Λ decays.

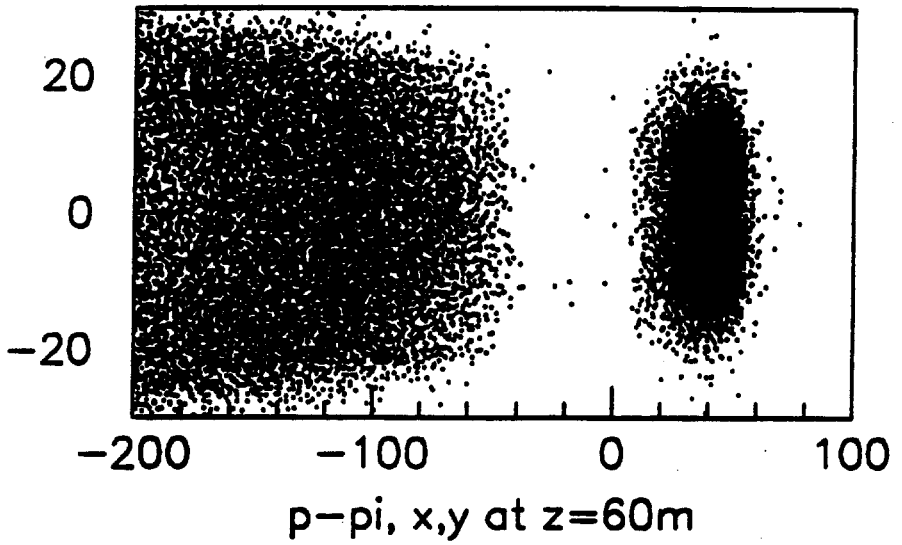

Figure 13: The x and y distributions of the charged particles from $\Xi \rightarrow \Lambda\ \pi$, and $\Lambda \rightarrow p\pi$ decays at the rear of the spectrometer (position of the pion hodoscope). The proton inhabits the right side and the the pions the left. Units are cm.

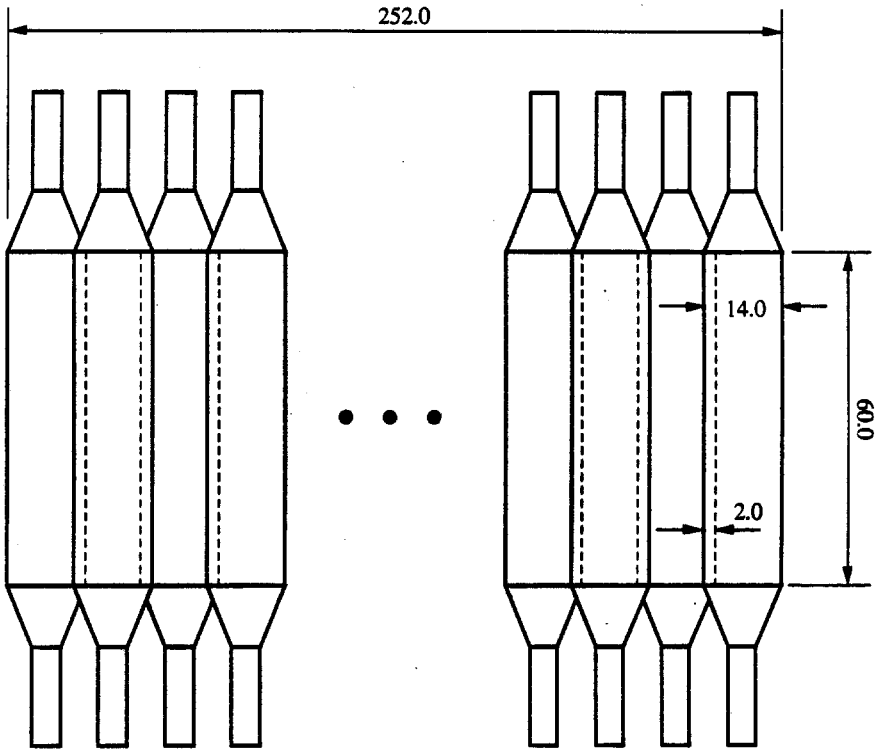

Figure 14: The pion hodoscope. Units are cm.

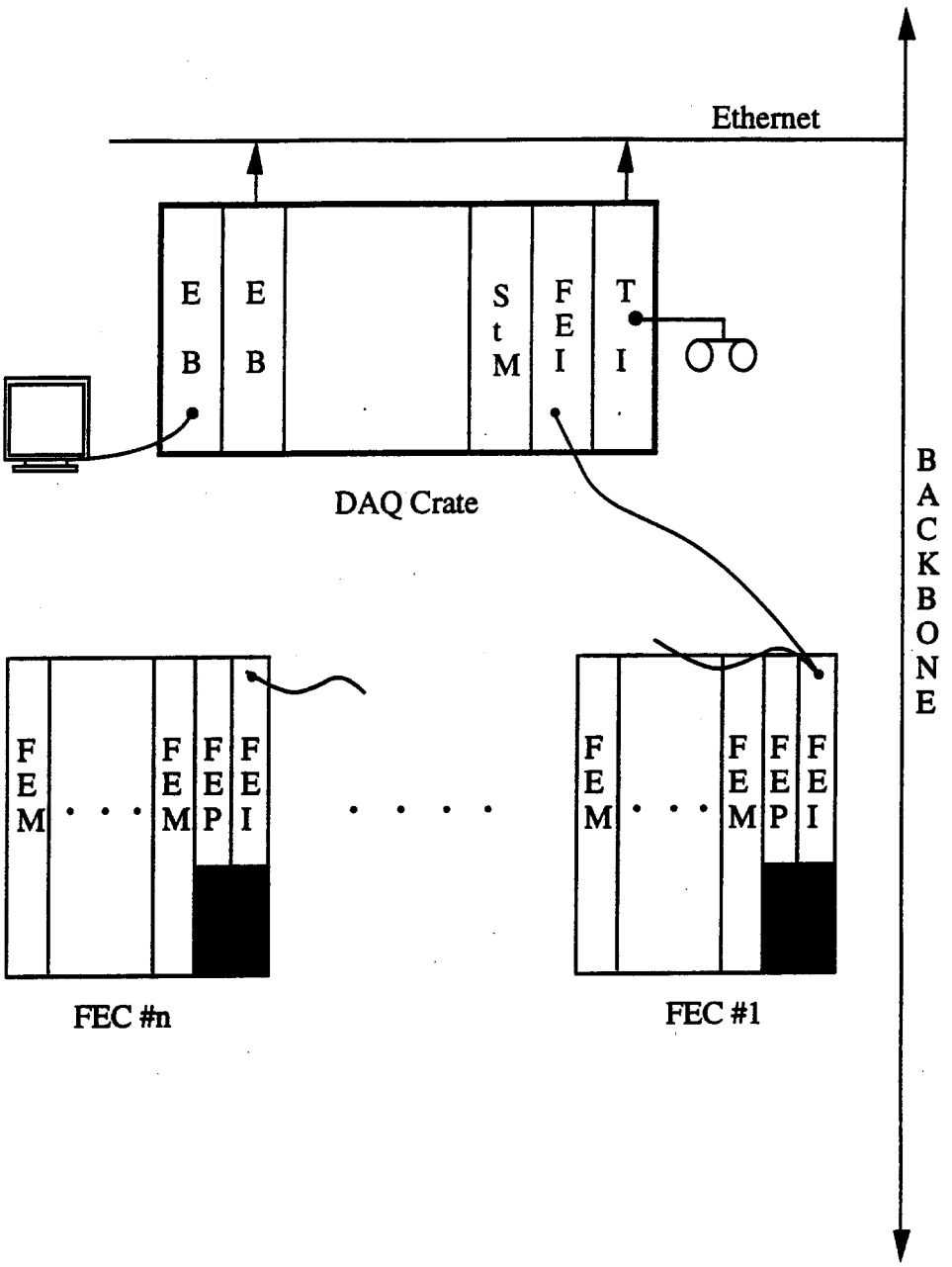

Figure 15: Layout of the data acquisition system.

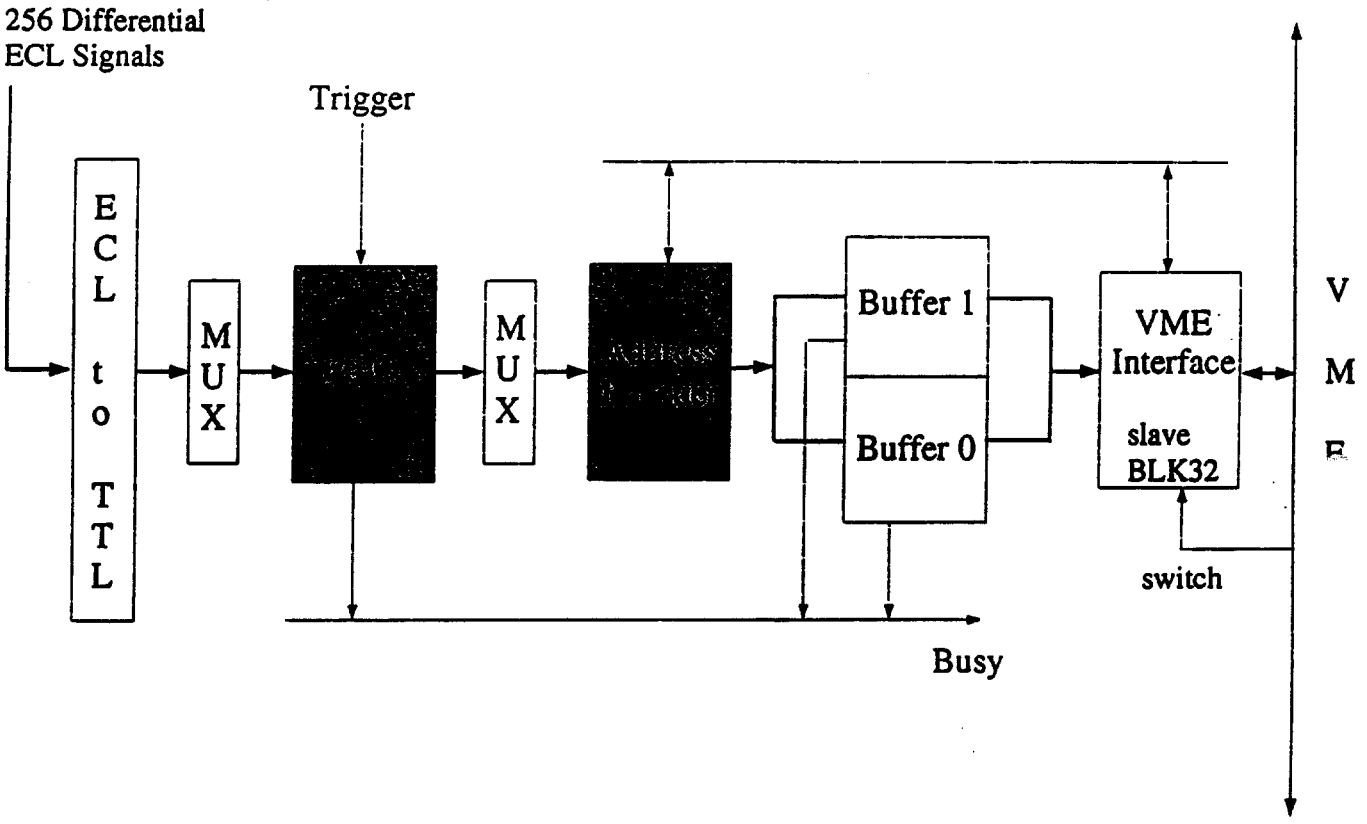

Figure 16: Block diagram of a front-end module.

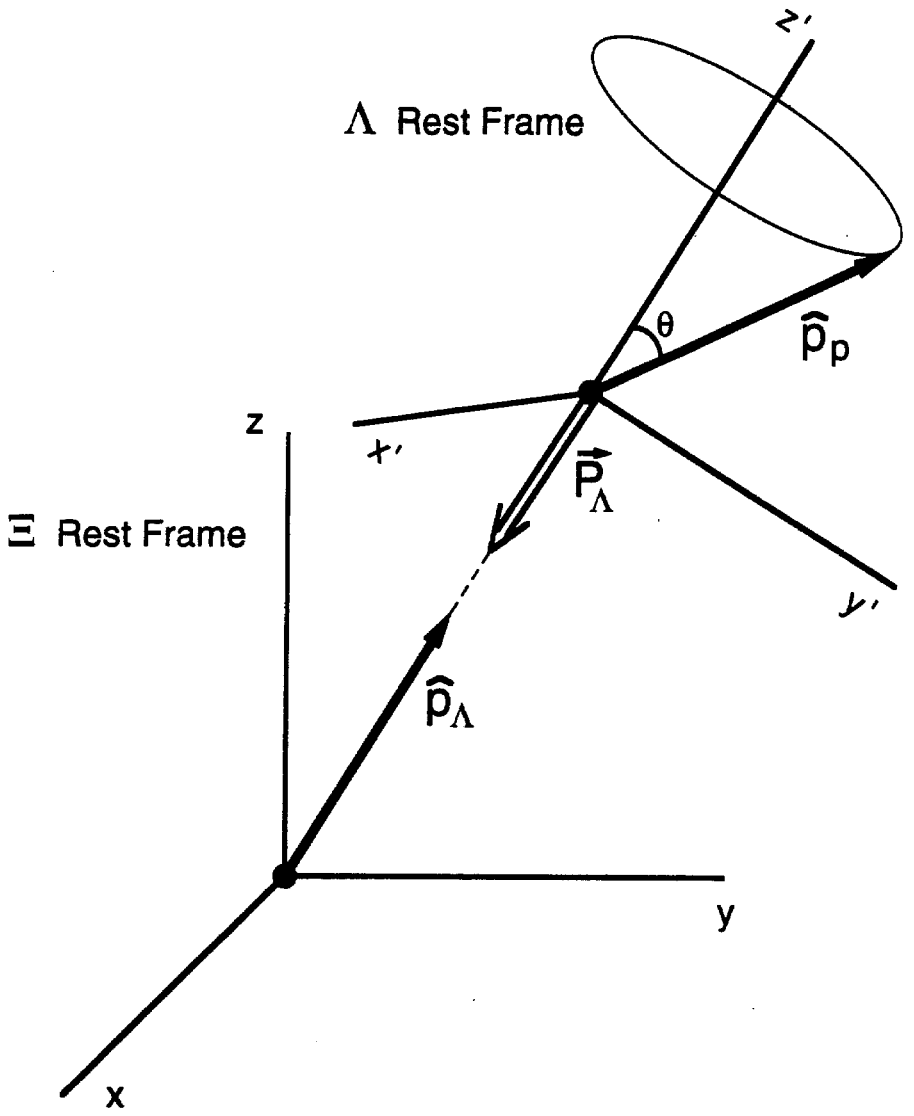

Figure 17: Analysis frames used in the Λ polarization analysis. The Λ polarization ($\vec{P}_\Lambda$) is antiparallel to the Λ momentum in the Ξ rest frame (α_Ξ is negative). The Λ momentum defines the polar (z') axis in the frame in which the proton $\cos\theta$ distribution is measured.

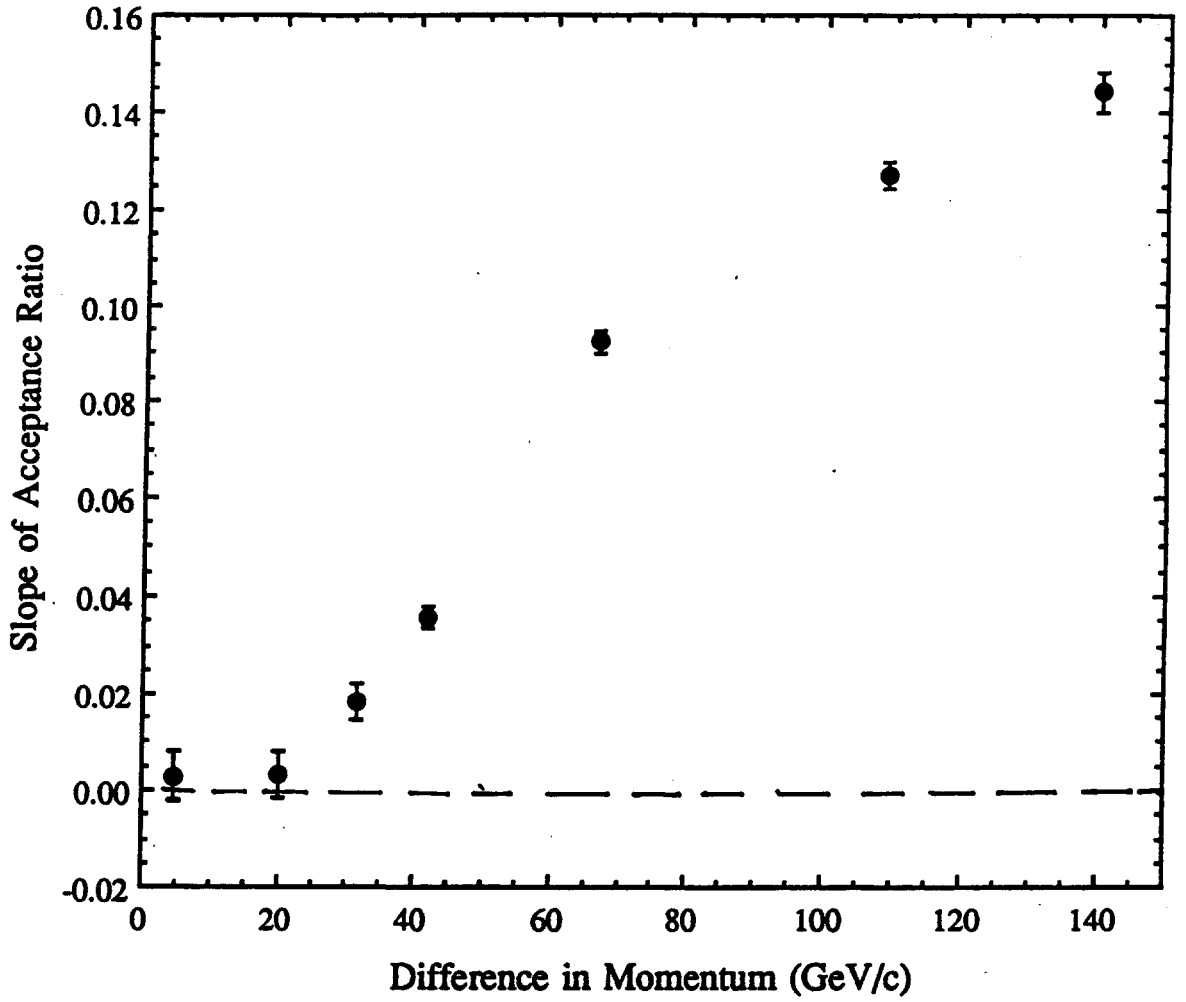

Figure 18: Difference in the proton $\cos\theta$ distributions for pairs of E756 Ξ^- data samples with different average momentum. The slope b of the ratio, $R = a + b\cos\theta$, of the two $\cos\theta$ distributions is given as a function of the momentum difference.

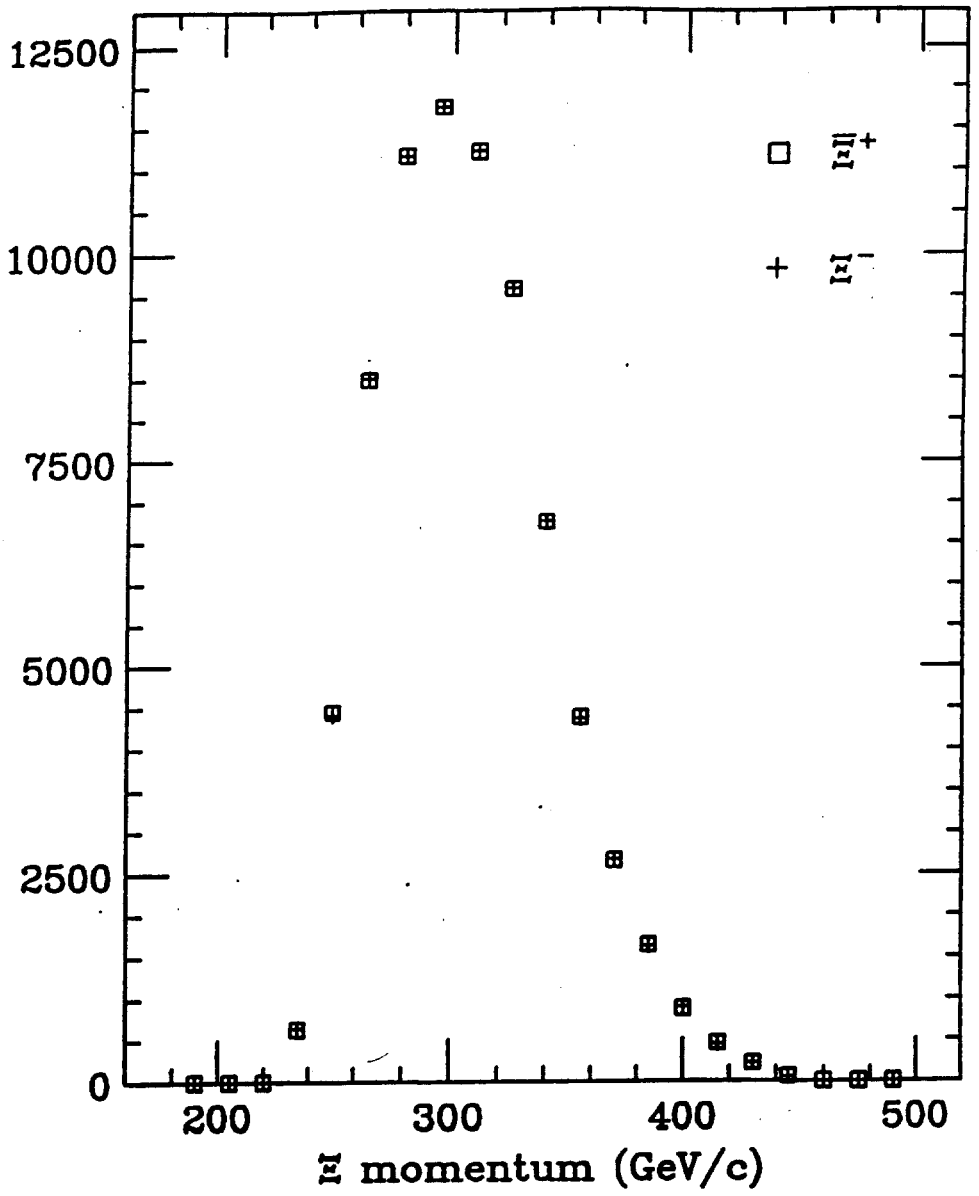

Figure 19: Comparison between the Ξ^- and $\bar{\Xi}^+$ momenta from E756, after normalization.

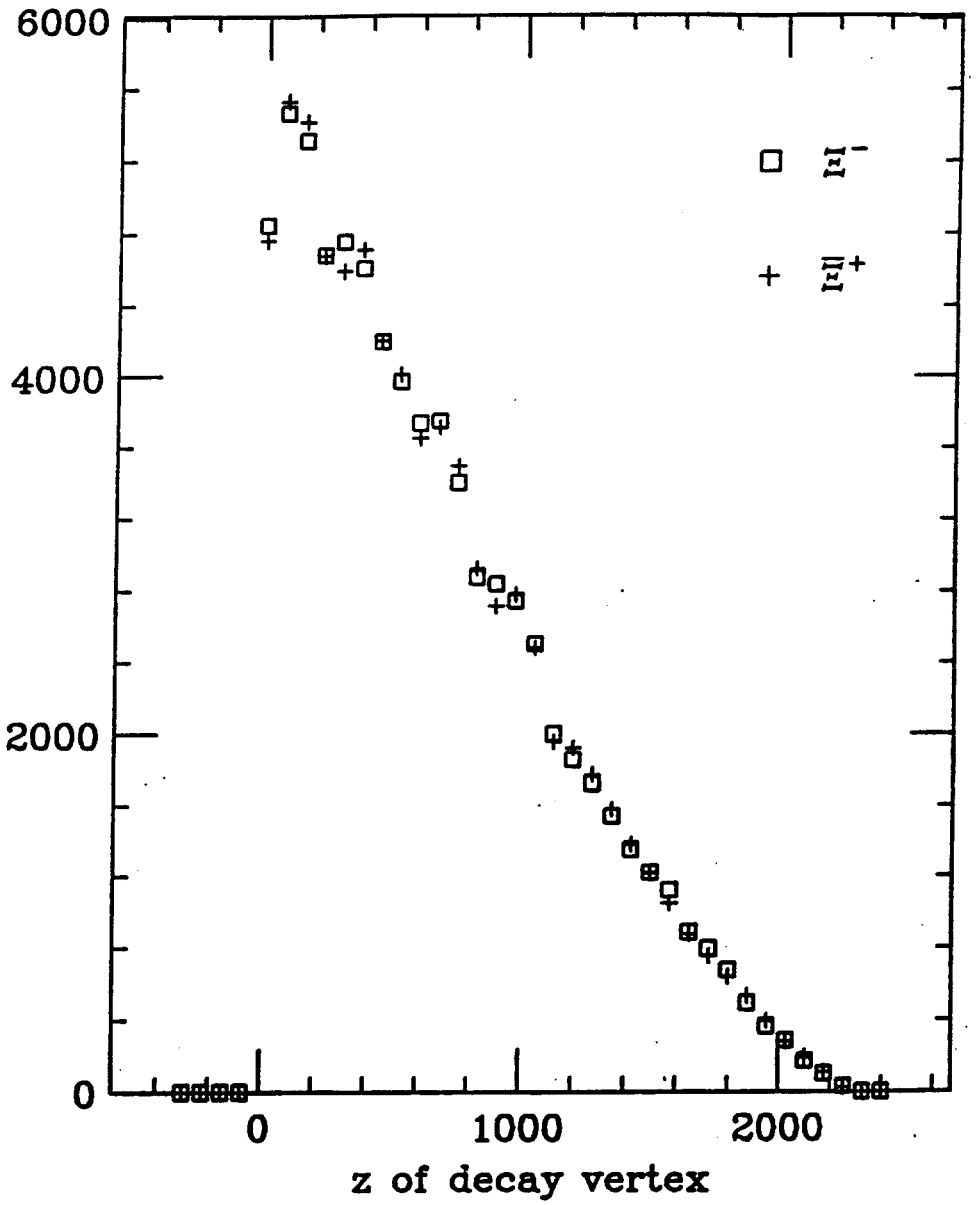

Figure 20: Comparison between the Ξ^- and $\bar{\Xi}^+$ z decay vertices for E756.

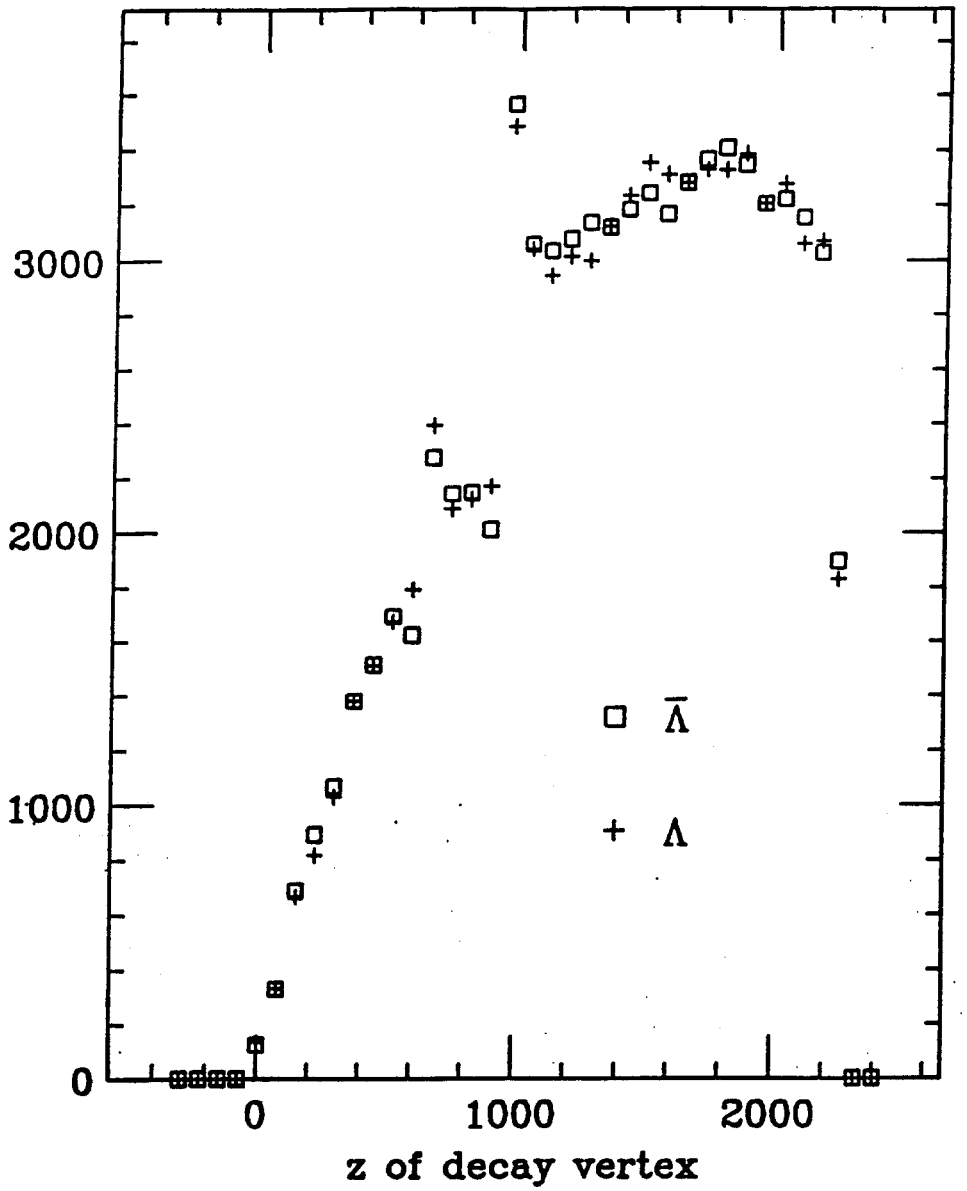

Figure 21: Comparison between the Λ and $\overline{\Lambda}$ z decay vertices from E756.

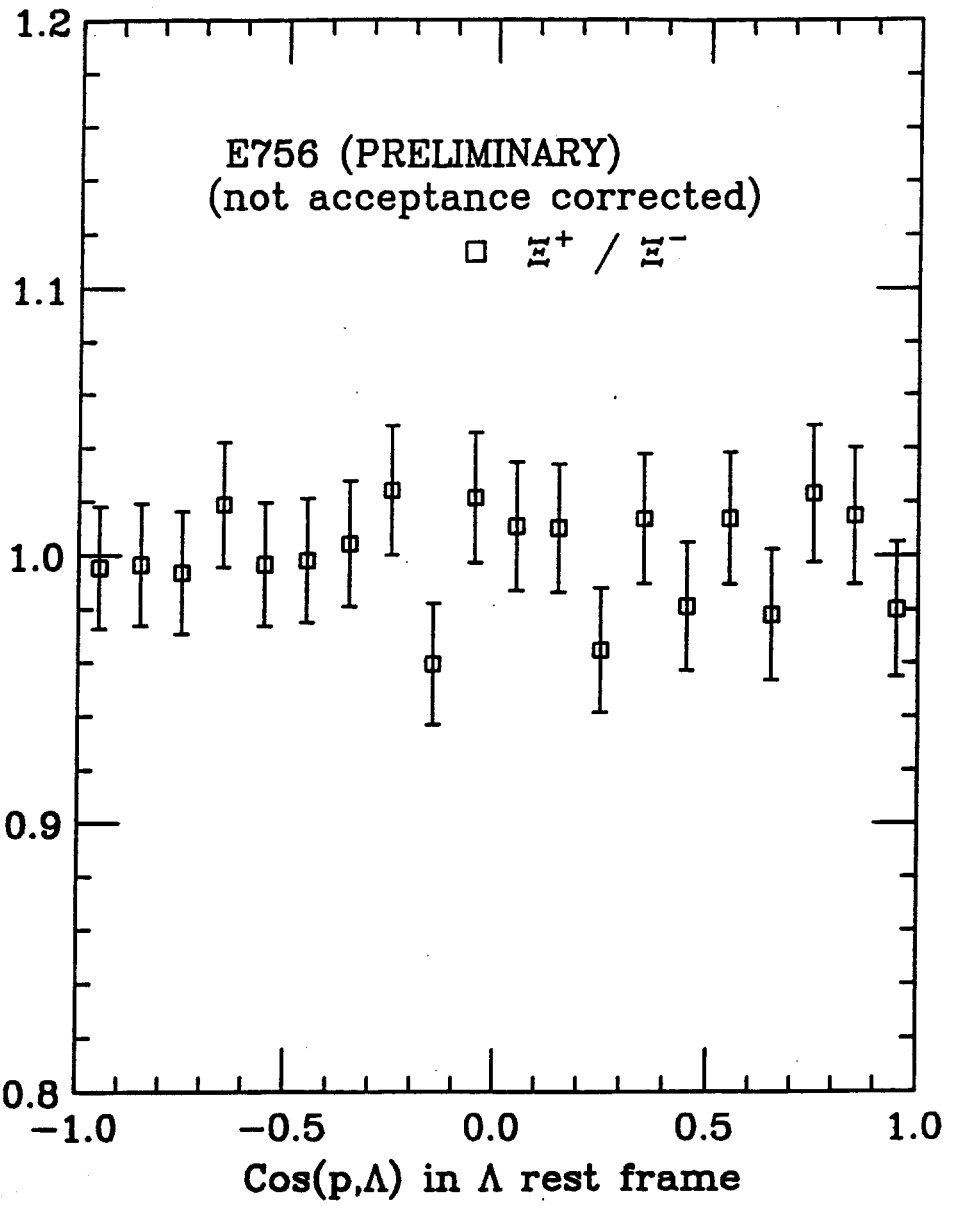

Figure 22: The ratio of the proton and antiproton $\cos\theta$ distributions from the E756 Ξ^- and $\bar{\Xi}^+$ data samples. No significant difference is evident despite the fact that no acceptance corrections have been made. (The sign of the cosine has been reversed.)

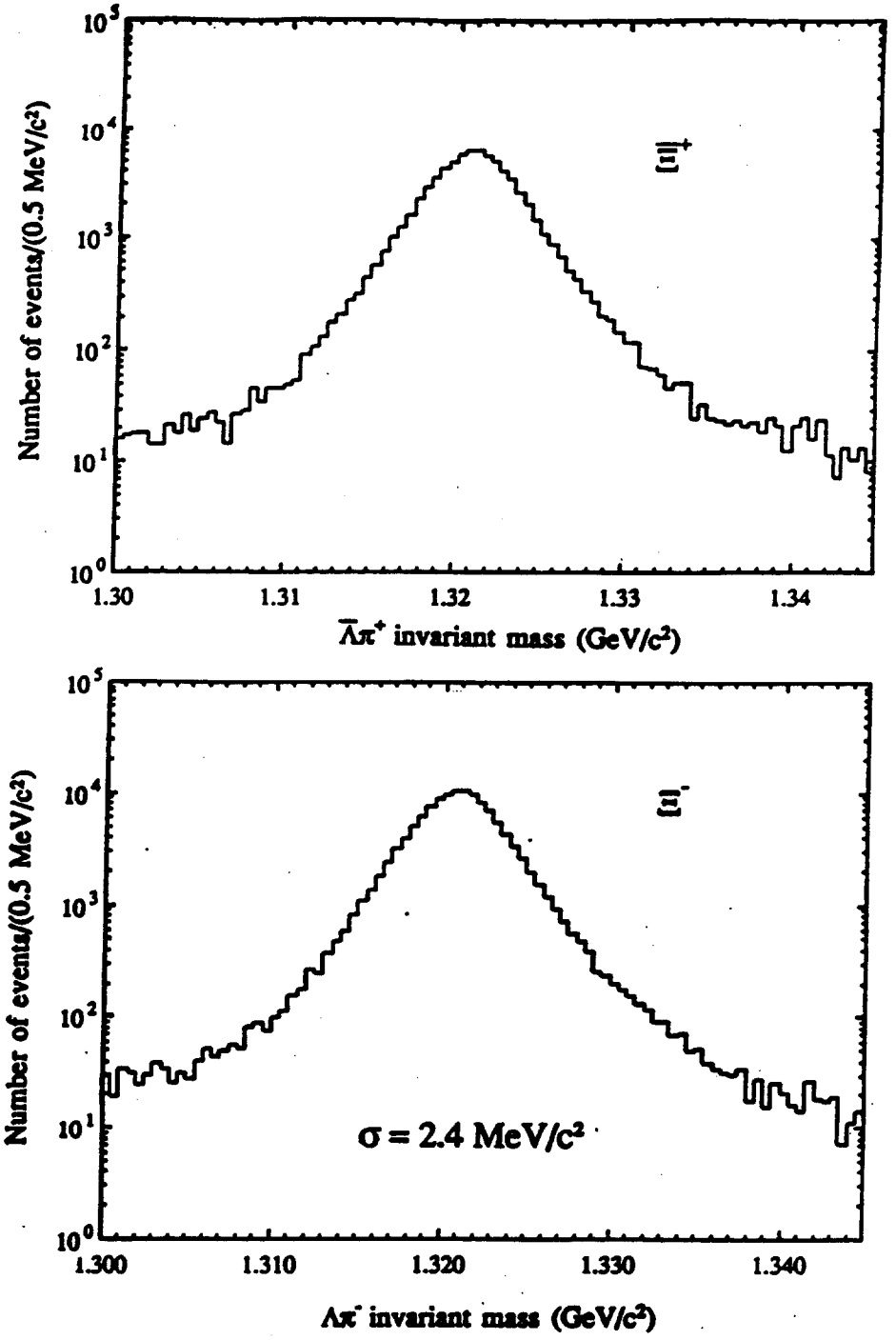

Figure 23: The $\Lambda\pi^-$ and $\bar{\Lambda}\pi^+$ invariant masses from E756, showing the level of the background.

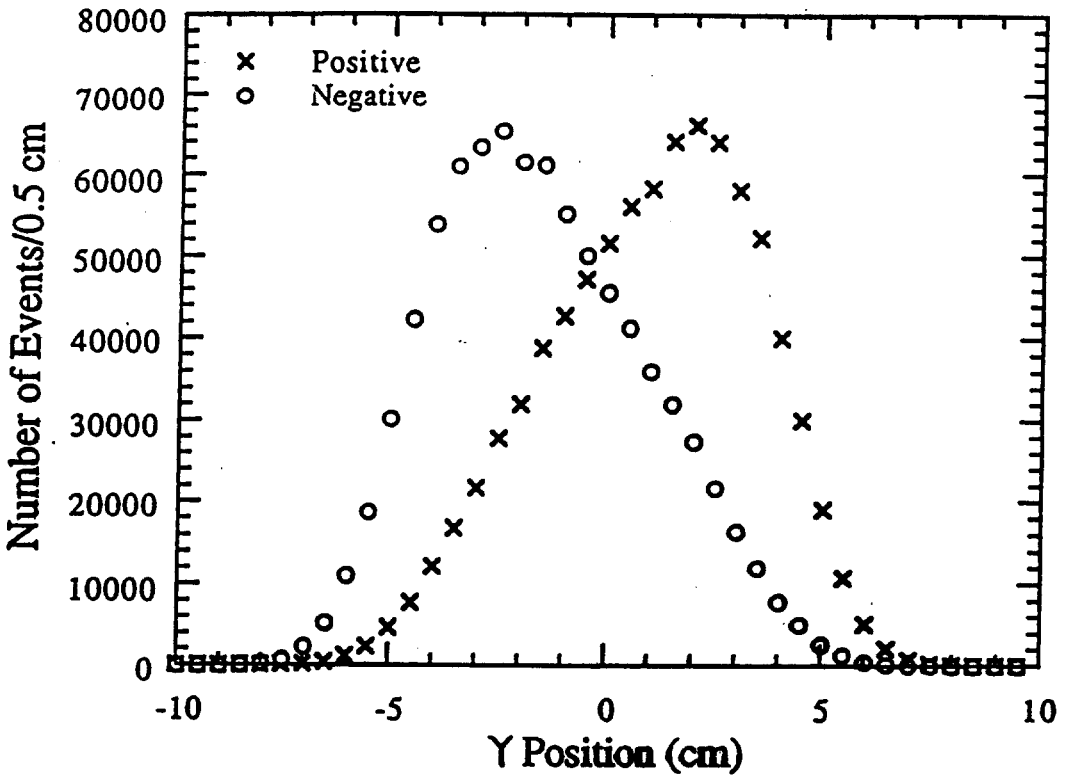

Figure 24: The y position of the proton at the analyzing magnet for +2.5 mrad and −2.5 mrad production angles in E756.

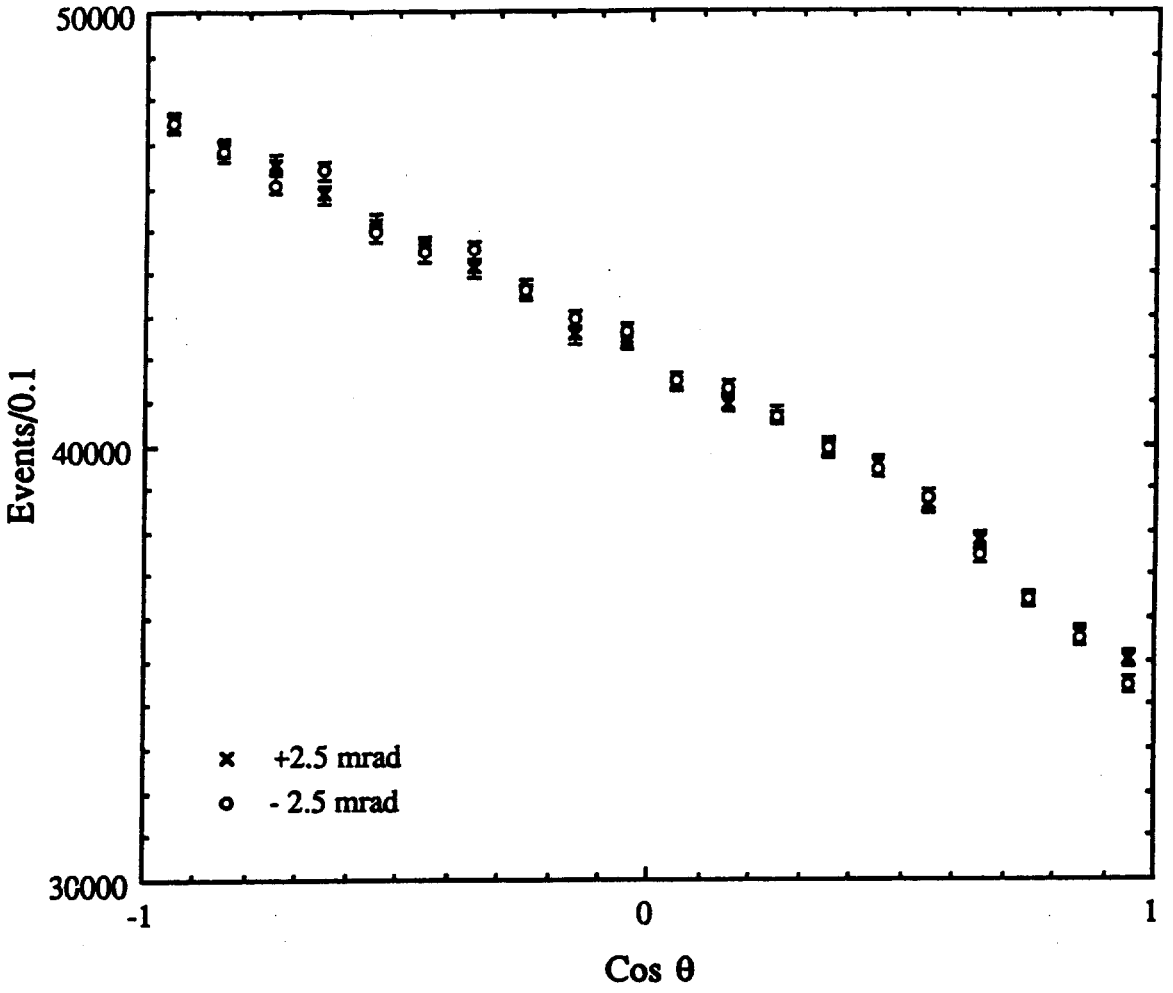

Figure 25: The proton $\cos\theta$ distribution from $\Xi^- \rightarrow \Lambda\pi^-$, $\Lambda \rightarrow p\pi^-$ decays in E756. The X's (O's) are protons from Ξ^-'s that were produced from protons targeted at +2.5 mrad (–2.5 mrad). No acceptance corrections have been made.

Fermilab Proposal P-871

Search for CP Violation in the Decays of $\Xi^-/\overline{\Xi}^+$ and $\Lambda^\circ/\overline{\Lambda}^\circ$ Hyperons

J. Antos, Y.C. Chen, C.N. Chiou, C. Ho, A. Sumarokov, and P.K. Teng

Academia Sinica, Nankang, Taipei 11529, Taiwan, Republic of China

G. Abrams, H. Bingham, G. Gidal, P.M. Ho, and K.B. Luk[1]

Lawrence Berkeley Laboratory and the University of California, Berkeley, CA 94720, USA

M. Botlo and E. Wang

Superconducting Super Collider, Dallas, TX 75237, USA

E.C. Dukes[2]

University of Virginia, Charlottesville, VA 22901, USA

T. Alexopoulos, A. Erwin, and M. Thompson

University of Wisconsin, Madison, WI 53706, USA

October 14, 1993

[1]Spokesperson: LUK@CSA.LBL.GOV, (510)486-7054

[2]Spokesperson: DUKES@UVAHEP.PHYS.VIRGINIA.EDU, (804)982-5376

Abstract

We propose to perform a sensitive search for *CP* violation in Ξ and Λ decays. Unpolarized Ξ^- and $\overline{\Xi}^+$ hyperons are produced by protons and momentum selected with a magnetic channel. The decay sequences $\Xi^- \to \Lambda^\circ\pi^-$; $\Lambda^\circ \to p\pi^-$ and $\overline{\Xi}^+ \to \overline{\Lambda}^\circ\pi^+$; $\overline{\Lambda}^\circ \to \overline{p}\pi^+$ are detected with a simple wire chamber spectrometer with high-rate capability. By studying the angular distribution of $p(\overline{p})$ with respect to the helicity axis in the $\Lambda^\circ(\overline{\Lambda}^\circ)$ rest frame, the product of the decay parameters $\alpha_\Lambda\alpha_\Xi(\alpha_{\overline{\Lambda}}\alpha_{\overline{\Xi}})$ can be extracted. Any difference between $\alpha_\Lambda\alpha_\Xi$ and $\alpha_{\overline{\Lambda}}\alpha_{\overline{\Xi}}$ is evidence that *CP* symmetry is violated. In a typical Fermilab fixed target run, 4×10^9 Ξ^- and $\overline{\Xi}^+$ decays can be collected, enabling a measurement of the relevant asymmetry to 10^{-4} sensitivity, comparable to the level of theoretical predictions for the asymmetry and well over two orders of magnitude better than the present limit. A non-zero asymmetry would be the first evidence of *CP* violation outside of the neutral kaon system and would be evidence of direct *CP* violation.

Contents

1 Introduction

In almost 30 years since the discovery of *CP* violation [1], our understanding of the phenomenon has improved little despite a long series of beautiful experiments. It still remains a small peculiarity unique to the neutral kaon system. Although *CP* violation can be accommodated nicely within the framework of the standard model, its origin and magnitude remain a profound mystery and many questions need to be answered before we can claim to have an understanding of it. Perhaps foremost among these is whether *CP* violation is a phenomenon unique to the neutral kaon system or a property shared by other particles. The standard model tells us that it should be evident elsewhere — in the decays of hyperons and neutral B mesons for example — but no experiment has been able to achieve the necessary sensitivity to see *CP* violation outside of the neutral kaon system. Another outstanding question is whether *CP* violation occurs only in $|\Delta S| = 2$ weak decays — as is predicted by the superweak model of Wolfenstein [3] — or is also evident in direct $|\Delta S| = 1$ transitions, as is predicted by the standard model. Despite an impressive experimental effort, both at Fermilab [4] and CERN [5], the question remains open.

For some time it has been known that *CP* violation should manifest itself in the decays of hyperons: in differences in the angular distribution of the daughter baryons between particle and antiparticle [6]. The asymmetries are expected to be small and were presumed to be difficult if not impossible to measure experimentally. In the past decade, however, considerable advances have been made in the development and operation of very high-rate spectrometers. It is no longer inconceivable for an experiment to acquire in a year's time the order of a billion events needed to measure such asymmetries. Recently E756 at Fermilab — an experiment measuring both the $\overline{\Xi}^+$ magnetic moment and polarization [7] — has shown that copious numbers of $\overline{\Xi}^+$ hyperons can be acquired with a simple trigger and with very little background. Analysis of the difference between the daughter decay distributions in the Ξ^- and the $\overline{\Xi}^+$ samples — the signature for *CP* asymmetry — shows no evidence of false asymmetries. This is extremely encouraging considering the fact that the experiment was by no means optimized to measure small asymmetries between Ξ^- and $\overline{\Xi}^+$ decays. The E756 collaboration expects to report a result with a sensitivity of about 10^{-2} which is better than any previous measurement.

In light of these facts, we have examined the possibility of measuring *CP* violation in a dedicated experiment analyzing the non-leptonic decays of charged Ξ and Λ hyperons. We find that in a standard Fermilab fixed target run a sensitivity of 10^{-4} can be achieved in the comparison of the α decay parameters of the $\Xi^-(\overline{\Xi}^+)$ and

$\Lambda^\circ(\overline{\Lambda}^\circ)$. This is a sensitivity on the order of the theoretical predictions of the standard model (as well as other models of *CP* violation), and over two orders of magnitude better than the world average experimental limit of -0.03 ± 0.06 [2] in $\Lambda^\circ(\overline{\Lambda}^\circ)$ decays. Observation of an asymmetry would provide the first evidence of *CP* violation outside of the neutral kaon system as well as evidence of direct *CP* violation. Because of the importance of *CP* violation to our understanding of the standard model we feel that this experiment should be pursued vigorously at Fermilab. We emphasize that the experiment can be done with relatively modest effort and expenditure.

2 Signatures for CP Violation in Hyperon Decays

The phenomenology of *CP* violation in hyperon decays has been discussed in several excellent references (see Ref. [12] for example). We briefly review it here. Because the nonleptonic weak decays of spin 1/2 hyperons violate parity they can decay into admixtures of both *S*- and *P*-wave final states:

$$\begin{aligned} S &= +S_1 e^{i(\delta_1^S+\phi_1^S)} + S_3 e^{i(\delta_3^S+\phi_3^S)}, \\ \overline{S} &= -S_1 e^{i(\delta_1^S-\phi_1^S)} - S_3 e^{i(\delta_3^S-\phi_3^S)}, \\ P &= +P_1 e^{i(\delta_1^P+\phi_1^P)} + P_3 e^{i(\delta_3^P+\phi_3^P)}, \\ \overline{P} &= +P_1 e^{i(\delta_1^P-\phi_1^P)} + P_3 e^{i(\delta_3^P-\phi_3^P)}. \end{aligned}$$

Here δ and ϕ are the strong and weak phases, and the subscripts 1 and 3 refer to the $\Delta I = 1/2$ and $\Delta I = 3/2$ isospin transitions. Note that under the combined operation of *CP* the *S*-waves and the weak phases change sign.

In terms of the *S*- and *P*-wave amplitudes, the hyperon non–leptonic decays are conventionally described by the Lee–Yang variables: α, β, and γ [8]:

$$\begin{aligned} \alpha &= \frac{2\mathrm{Re}(S^*P)}{|S|^2+|P|^2}, \\ \beta &= \frac{2\mathrm{Im}(S^*P)}{|S|^2+|P|^2}, \\ \gamma &= \frac{|S|^2-|P|^2}{|S|^2+|P|^2}, \end{aligned}$$

where $\alpha^2 + \beta^2 + \gamma^2 = 1$. Often one sees (in the Particle Data Booklet, for example) the parametrization given in terms of α and ϕ where:

$$\begin{aligned} \beta &= \sqrt{1-\alpha^2}\sin\phi, \\ \gamma &= \sqrt{1-\alpha^2}\cos\phi. \end{aligned}$$

Note that ϕ given above is not the same as the weak phase defined previously. Measured values of α, β, γ, and ϕ are given in the Table 1 for the Ξ^- and Λ° hyperons.

Table 1: Ξ^- and Λ° Hyperon Decay Parameters [2].

Mode	α	β	γ	ϕ
$\Xi^- \to \Lambda^\circ\pi^-$	-0.456 ± 0.014	0.062 ± 0.062	0.888 ± 0.008	$(4 \pm 4)^\circ$
$\Lambda^\circ \to p\pi^-$	0.642 ± 0.013	-0.087 ± 0.047	0.762 ± 0.012	$(-6.5 \pm 3.5)^\circ$

The decay distribution of the daughter spin 1/2 baryon in the rest frame of the parent hyperon (the Λ° in the decay $\Xi^- \to \Lambda^\circ\pi^-$, for example) is given by:

$$\frac{dP}{d\Omega} = \frac{1}{4\pi}(1 + \alpha \vec{P}_p \cdot \hat{p}_d), \tag{1}$$

where $\vec{P}_p$ is the parent hyperon polarization and $\hat{p}_d$ is the daughter baryon momentum direction in the rest frame of the parent. The daughter itself is polarized with a polarization given by:

$$\vec{P}_d = \frac{(\alpha + \vec{P}_p \cdot \hat{p}_d)\hat{p}_d + \beta(\vec{P}_p \times \hat{p}_d) + \gamma(\hat{p}_d \times (\vec{P}_p \times \hat{p}_d))}{(1 + \alpha \vec{P}_p \cdot \hat{p}_d)}. \tag{2}$$

Note that in the case of an unpolarized parent the daughter is in a helicity state with a polarization given by the parent α.

Under the operation of CP both α and β reverse sign whereas γ is unchanged. If CP is conserved, the magnitudes of α and β remain the same under the transformation. Hence to search for CP violation in hyperon decays one looks for a difference in either the α or β parameters, or in the partial decay rate ($\Gamma \propto |S|^2 + |P|^2$) between the particle and antiparticle. Observables that are sensitive to CP asymmetries include :

$$\Delta = \frac{\Gamma - \overline{\Gamma}}{\Gamma + \overline{\Gamma}}, \tag{3}$$

$$A = \frac{\alpha + \overline{\alpha}}{\alpha - \overline{\alpha}}, \tag{4}$$

$$B = \frac{\beta + \overline{\beta}}{\beta - \overline{\beta}}, \tag{5}$$

$$B' = \frac{\beta + \overline{\beta}}{\alpha - \overline{\alpha}}, \tag{6}$$

where overlined quantities refer to the antihyperon.

3 Theoretical Predictions

Nonzero values for the observables given in Eqs. (3)–(6) above result from interference between either the S- and P-waves or the $|\Delta I| = 1/2$ and $|\Delta I| = 3/2$ amplitudes.

Model independent expressions for the observables have been explicitly calculated [12]. To leading order they are, for $\Lambda^\circ \to p\pi^-$ decay:

$$\begin{aligned}
\Delta &\cong \sqrt{2}\frac{S_3}{S_1}\sin(\delta_3^S - \delta_1^S)\sin(\phi_3^S - \phi_1^S) \\
A &\cong -\tan(\delta_1^P - \delta_1^S)\sin(\phi_1^P - \phi_1^S), \\
B &\cong \cot(\delta_1^P - \delta_1^S)\sin(\phi_1^P - \phi_1^S), \\
B' &\cong -\sin(\phi_1^P - \phi_1^S),
\end{aligned}$$

and for $\Xi^- \to \Lambda^\circ\pi^-$ decay:

$$\begin{aligned}
\Delta &= 0, \\
A &\cong -\tan(\delta_3^P - \delta_3^S)\sin(\phi_1^P - \phi_1^S), \\
B &\cong \cot(\delta_3^P - \delta_3^S)\sin(\phi_1^P - \phi_1^S).
\end{aligned}$$

The *CP* asymmetry Δ results from the interference between the $|\Delta I| = 1/2$ and $|\Delta I| = 3/2$ amplitudes whereas the other asymmetries are due to the interference of *S*- and *P*-waves. Δ vanishes in Ξ decays because there is only one isospin channel. Note that CPT invariance only guarantees the total decay width or lifetime be the same for the particle and the anti-particle.

Calculations of *CP* asymmetries in hyperon decays are difficult and the predicted asymmetries vary (see Ref. [9] - [16]). For example, predictions of the asymmetry A given by Eq. (4) range from 10^{-3} to 10^{-5}. To calculate the magnitude of the asymmetries requires the values of ϵ, ϵ', the top quark mass and the hadronic matrix elements. Results are not reliable to better than an order of magnitude [16]. However because the $|\Delta I| = 1/2$ amplitudes are about 20 times larger than the $|\Delta I| = 3/2$ amplitudes and because $\sin(\delta_i) \approx 1/10$, Donoghue *et al.* find that $\Delta \approx A/10 \approx B'/100$ [12]. B' is clearly the asymmetry one would want to measure. In only B' do the strong interaction final state phases cancel out, and the predicted magnitude is the largest of all the asymmetries. A is suppressed by the small value of the final state phase shifts whereas Δ is further suppressed by the $|\Delta I| = 1/2$ rule. Unfortunately, as we shall see below, measuring B' is prohibitively difficult.

The magnitudes of the predicted *CP* asymmetries are model dependent. Theories with no $|\Delta S| = 1$ *CP*-odd effects, such as the superweak model and models with a very heavy neutral Higgs, predict no *CP* asymmetries [12]. Models in which $|\Delta S| = 1$ *CP* nonconservation is dominant, such as the Weinberg model [18], predict asymmetries which are on the order of those calculated in the standard model. In the standard model *CP* violation effects are due solely to the complex phase in the Cabbibo–Kobayashi–Maskawa matrix [19], and penguin diagrams are the source of $|\Delta S| = 1$ *CP* asymmetries [20]. The standard model predictions vary quite a bit. For example, Donoghue [14] predicts asymmetries in A which range from $-(0.3 \to 4.0) \times 10^{-4}$ for $\Lambda^\circ(\overline{\Lambda}^\circ)$ hyperons and $-(0.4 \to 4.8) \times 10^{-4}$ for $\Xi^-(\overline{\Xi}^+)$ hyperons, where much of the uncertainty is due to the incomplete knowledge of the hadronic matrix elements.

To illustrate the range of expected values in the standard model, Valencia [17] has compiled predictions based on the method of Xe, Steger, and Valencia [16] with these matrix elements calculated in several models. These are shown in Fig. 1. Non standard models further widen this range. Experiments in progress as well as this experiment should give more precise values of the hyperon decay parameters and so more closely constrain these predictions.

We should point out that standard model calculations of *CP* violation in hyperon decays are less sensitive to the top quark mass than similar $|\Delta S| = 1$ calculations in $K^\circ \rightarrow \pi^-\pi^+$ decays [16]. The value of ϵ'/ϵ in K° decays decreases with increasing top quark mass, essentially vanishing at a top mass of about 220 GeV/c^2 [21].

4 Comparison with Other Past and Proposed Hyperon CP Violation Experiments

The only data on *CP* violation in hyperon decays comes from the comparison of the alpha parameters in Λ° and $\overline{\Lambda}^\circ$ decays. The experimental limits are weak: the world average compiled by the Particle Data Group is $A = (\alpha_\Lambda + \alpha_{\overline{\Lambda}})/(\alpha_\Lambda - \alpha_{\overline{\Lambda}}) = -0.03 \pm 0.06$ [2]. The three published results are given in Table 2 below. Each of the three experiments used a different technique — and none used the technique we propose here. Their bounds are all limited by statistical, not systematic errors. The first result in Table 2 is from an ISR experiment (R608) which produced Λ° and $\overline{\Lambda}^\circ$ in $pp \rightarrow \Lambda^\circ X$ and $p\overline{p} \rightarrow \overline{\Lambda}^\circ X$ reactions. They quote $\alpha P(\overline{\Lambda}^\circ)/\alpha P(\Lambda^\circ) = -1.04 \pm 0.29$. We have converted their result to a limit on A assuming the polarization is the same for Λ° and $\overline{\Lambda}^\circ$. The data sample consisted of 10,000 $\overline{\Lambda}^\circ$'s and 17,000 Λ°'s. The large error is due to the small polarization of the Λ° and $\overline{\Lambda}^\circ$.

The second result is from the DM2 detector in the Orsay e^+e^- colliding ring DCI. They ran on the J/ψ resonance and used the decays $J/\psi \rightarrow \Lambda^\circ\overline{\Lambda}^\circ$. The branching ratio is small — 1.4×10^{-3} [2] — that is why with a total of 8.6×10^6 J/ψ decays only 770 events were used in the analysis. Nevertheless, because of the large Λ° polarization, their sensitivity is comparable to the R608 measurement. The third result is from a LEAR experiment (PS185) producing Λ° hyperons in the threshold reaction $p\overline{p} \rightarrow \Lambda^\circ\overline{\Lambda}^\circ$. The polarization of the two Λ°'s is assumed to be equal by C-parity conservation in strong interactions. A total of 4,063 $\Lambda^\circ\overline{\Lambda}^\circ$ pairs was used in the analysis.

There has been considerable interest at CERN in pursuing these measurements to better precision with an improved higher luminosity LEAR (SuperLEAR) [25]. (A proposal has also been submitted to Fermilab to construct a similar facility dedicated to searching for *CP* violation in $\Lambda^\circ(\overline{\Lambda}^\circ)$ decays [26].) Unfortunately, due to budget constraints it appears that SuperLEAR will not be built.

There has also been interest in pursuing hyperon *CP* violation at a tau-charm factory through the decay process $J/\psi \rightarrow \Lambda^\circ\overline{\Lambda}^\circ$. Even with optimistic assumptions on

Table 2: Experimental Limits on $A = (\alpha_\Lambda + \alpha_{\overline{\Lambda}})/(\alpha_\Lambda - \alpha_{\overline{\Lambda}})$.

Mode	Limit	Experiment
$p\overline{p} \to \Lambda^\circ X$, $p\overline{p} \to \overline{\Lambda}^\circ X$	0.02 ± 0.14	R608 [22]
$e^+e^- \to J/\psi \to \Lambda^\circ\overline{\Lambda}^\circ$	0.01 ± 0.10	DM2 [23]
$p\overline{p} \to \Lambda^\circ\overline{\Lambda}^\circ$	-0.07 ± 0.09	PS185 [24]

the luminosity and monochromaticity, the expected asymmetry reach is only 5×10^{-4} [27] and hence is not competitive with this proposal.

Only in fixed target experiments at either Fermilab or CERN can sufficient statistics be collected to provide a sensitivity of the 1×10^{-4} level. Furthermore, preliminary analysis of the Fermilab E756 data, based on 74,000 $\overline{\Xi}^+$'s and 1.5×10^5 Ξ^-'s, indicates that our approach is free of systematic errors at the $\sim 1\%$ level.

5 Experimental Strategy

The four observables for hyperon decays that are sensitive to *CP* asymmetries are given in Eqs. (3)-(6). The small theoretical predictions for Δ and the difficulty in measuring small differences in rates makes the possibility of finding *CP* violation through Δ very unlikely. To search for *CP* violations through measurements of either B or B' requires hyperons and antihyperons with identical or precisely determined polarizations because the β decay parameter can only be determined by measuring the daughter polarization from a polarized parent. Both Ξ^- and $\overline{\Xi}^+$ hyperons have been shown to be polarized when produced with finite transverse momentum by protons in inclusive production [7]. However, the magnitude of the polarizations is only 10% at a p_t of about 1 GeV/c and an x_F of 0.4, requiring a prohibitive number of Ξ^- and $\overline{\Xi}^+$ hyperons to measure the *CP* asymmetry in β. Furthermore, the polarizations of the Ξ^- and $\overline{\Xi}^+$ are almost certainly different at the required sensitivity level, making measurements of the differences in β extremely difficult. Hence we propose to search for *CP*-odd asymmetries in the parameter A of Eq. (4).

Determining A requires measuring the α parameters of the hyperon and antihyperon. The α parameter can either be determined by measuring the decay asymmetry of a hyperon of known polarization or by measuring the daughter polarization from either a polarized or unpolarized parent. Measurement of the α parameter is much easier with unpolarized hyperons (or samples with a mean polarization of zero which can be made by combining data sets with equal and opposite polarizations) if the daughter decay analyzes its own polarization. The Ξ^- and $\overline{\Xi}^+$ hyperons are ideal candidates because they decay with large branching ratios (100%) into Λ° and $\overline{\Lambda}^\circ$ whose polarizations can be measured through their weak decay. Unpolarized Ξ^-

and $\overline{\Xi}^+$ hyperons are produced by targeting at 0° incident angle. The daughter Λ polarization from an unpolarized Ξ is simply:

$$\vec{P}_\Lambda = \alpha_\Xi \hat{p}_\Lambda. \tag{7}$$

The $\Lambda°(\overline{\Lambda}^\circ)$ is found in a helicity state with polarization given by the $\Xi^-(\overline{\Xi}^+)$ alpha parameter: $|\vec{P}_\Lambda| = 0.456$. A difference between the $\Lambda°$ and $\overline{\Lambda}^\circ$ polarizations is direct evidence of *CP* violation.

The $\Lambda°$ and $\overline{\Lambda}^\circ$ polarizations are measured through the decay asymmetry given by Eq. (1). The asymmetry in the decay proton (antiproton) direction in the $\Lambda°$ $(\overline{\Lambda}^\circ)$ rest frame is given by the product of the $\Lambda°$ and Ξ^- $(\overline{\Lambda}^\circ$ and $\overline{\Xi}^+)$ alpha parameters. We emphasize that *in the absence of CP violation the proton and antiproton distributions should be identical*, as should be every other kinematic variable from the Ξ^- and $\overline{\Xi}^+$ decays.

Because we measure the product of the Λ and Ξ alpha parameters, the *CP* asymmetry extracted is the sum of the Λ and Ξ asymmetries given in Eq. (4) (see Appendix 1):

$$\mathcal{A} = \frac{\alpha_\Lambda \alpha_\Xi - \alpha_{\overline{\Lambda}} \alpha_{\overline{\Xi}}}{\alpha_\Lambda \alpha_\Xi + \alpha_{\overline{\Lambda}} \alpha_{\overline{\Xi}}} = A_\Lambda + A_\Xi, \tag{8}$$

where A_Λ and A_Ξ are defined by:

$$\begin{aligned} A_\Lambda &= \frac{\alpha_\Lambda + \alpha_{\overline{\Lambda}}}{\alpha_\Lambda - \alpha_{\overline{\Lambda}}}, \\ A_\Xi &= \frac{\alpha_\Xi + \alpha_{\overline{\Xi}}}{\alpha_\Xi - \alpha_{\overline{\Xi}}}. \end{aligned}$$

Hence the measured asymmetry is sensitive to *CP* violation in both $\Lambda°$ and Ξ^- alpha parameters. Any cancellation is highly unlikely.

6 Goal

The goal of this experiment is to search for direct *CP* violation in $\Lambda°$ and Ξ^- decay by determining the observable $\mathcal{A}$ with a sensitivity at the 10^{-4} level. The number of events needed to measure the asymmetry to a precision of 1×10^{-4} is 2×10^9 each for Ξ^- and $\overline{\Xi}^+$(see Appendix 2). For a nominal Fermilab fixed target run of 200 days; 2×10^7 events per day, 14,000 events per spill, or 700 events per second are required. Assuming a 50% duty factor 1,400 *reconstructed* events per second are needed.

7 Yields

7.1 Ξ^- and $\overline{\Xi}^+$ Yields

A magnetic channel selects Ξ^- and $\overline{\Xi}^+$ hyperons with small x_F and a mean p_t of 0 GeV/c, ensuring that the average production polarization is very small if not zero.

The $\overline{\Xi}^+$ to π^+ ratio has been measured in p + Cu collisions at 400 GeV [28]. The ratio is about 1×10^{-3} at an x_F of 0.27 and a p_t between 0.0 GeV/c and 0.8 GeV/c which is approximately the kinematic acceptance of the magnetic channel. The π, K, and p yields can be calculated fairly reliably with the parametrization of Malensek [29]. They have been cross-checked with a Pythia simulation with agrees within 20%. Table 3 is a summary of the yields between 110 GeV and 215 GeV (the momentum bite of the magnetic channel) at 0 mrad for 1×10^{10} 800 GeV protons incident on a 8.84 cm long Be target. The solid angle is taken to be 4.88 μsr. The estimated number

Table 3: Ξ, π, K, and p yields per 10^{10} protons.

Particle	At target[1]	At exit of channel[2]
Positive Beam		
$\overline{\Xi}^+$	6.5×10^4	8.5×10^3
π^+	6.5×10^7	2.7×10^7
K^+	6.5×10^6	2.7×10^6
p	3.2×10^7	1.3×10^7
Total:	1.0×10^8	4.3×10^7
Negative Beam		
Ξ^-	1.1×10^5	1.5×10^4
π^-	3.6×10^7	1.5×10^7
K^-	2.9×10^6	1.2×10^6
Total:	3.9×10^7	1.6×10^7

of $\overline{\Xi}^+$'s, with momentum between 110 GeV and 215 GeV, entering the collimator is 65,000 per 1×10^{10} protons. This yields 8,500 $\overline{\Xi}^+$'s at the exit of the collimator where the loss due to decay in the channel has been taken into account. After correcting for the probability that the $\overline{\Xi}^+$ and $\overline{\Lambda}$ decay in the vacuum region, the spectrometer acceptance, and the branching fraction of $\Lambda^\circ \rightarrow p\pi^-$ (64%), approximately 2,100 events remain. Taking the trigger efficiency, reconstruction efficiency and event selection cuts into account, the final number of $\overline{\Xi}^+$'s is about 1,500 per 1×10^{10} protons (see Table 4). The thoroughly tested E756 Monte Carlo and reconstruction programs have been used to estimate the efficiencies.

We have cross-checked the $\overline{\Xi}^+$ yield in several different ways, all of which agree to within a factor of two. The most straightforward estimate is based on the fact that in E756 we collected 8×10^4 $\overline{\Xi}^+$'s in four full days of running (the equivalent of 8 calendar days with a 50% duty factor). The following table shows how we intend to increase the yield of $\overline{\Xi}^+$ hyperons in P871. An increase in yield of 25,000 over

[1]Inside a cone with a solid angle of 4.88 μsr centered along the incident beam direction.

[2]Decay loss and channel acceptance have been taken into account.

Table 4: Ξ^- and $\overline{\Xi}^+$/ acceptance and yields per 10^{10} protons.

	Ξ^-	$\overline{\Xi}^+$
Total entering collimator:	110,000	65,000
Total exiting collimator:	15,000	8,500
BR ($\Xi^- \rightarrow \Lambda^\circ\pi^-$)	1.00	1.00
BR ($\Lambda^\circ \rightarrow p\pi^-$)	0.641	0.641
Ξ & Λ decaying in vacuum region	0.84	0.84
Geometric acceptance	0.79	0.79
Trigger acceptance	0.88	0.88
Reconstruction efficiency	0.87	0.87
Software event selection cuts	0.88	0.88
Total events passing all cuts:	2,650	1,500

E756 is needed. How that increase is attained is given in Table 5. Note that only a factor of 20 increase in proton intensity is needed. Much of the increase in yield comes from running the experiment for the full duration of a Fermilab fixed target run. Decreasing the x_F from 0.4 to 0.2 gives a factor of 7 increase in the Ξ cross section.

Table 5: Comparison of P871 and E756 $\overline{\Xi}^+$ Yields.

	E756	P871	Gain
Run time	8 days	100 days	12.5
Channel solid angle	2.36 μsr	4.88 μsr	2
$< x_F >$	0.4	0.2	7
$< p_T >$	0.75 GeV/c	0.0 GeV/c	7
Proton intensity	1×10^{10}	2×10^{11}	20
Lifetime	0.5	0.6	1.2
Total:			29,400

The Ξ^- cross section at low x_F and small transverse momentum has not been measured at high energies. However, the invariant cross section of Ξ^- hyperons produced by 800 GeV protons on Be at 2.5 mrad has been measured by E756. The result is similar to the E495 measurement of the Ξ° cross section at 5 mrad with 400 GeV protons [30]. (In the CERN hyperon experiment the Ξ^- and Ξ° production cross sections were found to be identical [31].) Hence we use the parametrization given by E495 for Ξ° production to estimate the Ξ^- yield at 0 mrad. The number of Ξ^-'s

at the collimator exit is approximately 1.5×10^4. With all efficiencies folded in, the expected number of Ξ^-'s is 2,650 per 1×10^{10} protons.

7.2 Muon background

Muon background has not been a serious problem for any of the hyperon experiments done at Fermilab the past 15 years. For example, E555 [32], E756, and E800 have all run at much higher target interaction rates than contemplated in P871 with no untoward effects.

To estimate the actual muon flux we again rely on the data from E756. In that experiment ungated scalers recorded (1) the singles rate of a 2 mm pitch MWPC (*C4*) with an active area of 10" x 20" and located at 26 m from the exit of a 7.3 m long hyperon magnet, (2) the singles rate of another 2 mm wire spacing MWPC (*C12*) with an area of 15" x 47" and positioned at 49 m from the exit, and (3) a single track trigger ("*pion*") defined by a small aperture scintillator telescope (90% of these triggers were fully reconstructed in the offline analysis and were successfully traced back to the target). In Figures 2 (a) and (b) we show the muon fluence at the locations of *C4* and *C12* as a function of number of protons for three different hyperon magnet field integrals. The targeting angle was 0 degree. The muon fluence was calculated as the difference between the singles rate of the MWPC and the "*pion*" trigger. The muon fluence increases slowly as the hyperon magnet field integral decreases. An independent measurement of the muon fluence using a scintillator telescope agrees with our results [33]. We also cross-checked the rates with those in E800 under similar conditions The difference between E756 and E800 is the design of the channel. The bend angle of the E800 channel is 18.37 mrad rather than 14.60 mrad as in E756 and the solid angle acceptance is about a factor of two larger than that of the E756 channel. The singles rate of *C4* in E800 also at 26 m from the exit is comparable to that recorded in E756 at the highest field integral and similar beam intensities [34]. From Figure 2, we extrapolate the muon rate to a proton intensity of 1×10^{10} per second and a field integral of about 12 T-m for this experiment. The estimated muon rates are about 7×10^6 Hz for *C4* and 2×10^6 Hz for *C12*. Since the solid angles subtended by *C4* and *C12* are similar, the reduction of muon rate at *C12* is likely due to the shielding and sweeping of the analysis magnet. In summary, all measurements available to date give consistent estimation of muon fluence in P871. Extra shielding around the hyperon decay region is expected to reduce the muon background in P871.

8 Experimental Design

The design of the apparatus is based on 15 years of experience in doing hyperon physics at Fermilab, and in particular, the experience gathered in E756 [7]. The spectrometer is relatively simple. The emphasis is on good acceptance, high efficiency, and high-rate capability. The Ξ^- and $\overline{\Xi}^+$ events will be produced, trigger

selected and analyzed under almost identical conditions. This approach has been tested successfully in E756.

Although the spectrometer described in this section is similar to E756, it is vastly superior in rate capability. The wire chambers and readout used in E756 were built 20 years ago and are not suitable for high-rate experiments. The maximum trigger rate in E756 was about 500 Hz. We intend to increase this rate by over two orders of magnitude.

Figures 3 and 4 are the plan and elevation views of the apparatus. The spectrometer, approximately 60 m long and 2 m wide, consists of a hyperon magnet (M1), 8 wire chamber stations (C1–C8), a momentum analyzing magnet (M2), two planes of hodoscopes (H1–H2) for timing and triggering purposes, and a hadronic calorimeter for triggering.

8.1 Beam

The hyperons will be produced by an 800 or 900 GeV primary proton beam with an intensity of 2×10^{11} per 20 second spill. The beam should have a Gaussian profile with a full width at half maximum of about 1 mm when it is focussed on the target. The beam divergence should be kept as small as possible. Similar to the layout in E756, the beam position immediately upstream of the target is monitored with two 0.5 mm wire pitch SWIC's separated by 2 m. This arrangement determines the targeting angle to better than 0.5 mrad. For particles produced with a momentum of 150 GeV/c, the resolution in the transverse momentum due to the uncertainty in the targeting angle is only 75 MeV/c. Although we plan to take most of the data at 0 mrad production angle, it is important that the primary proton beam can be targeted at a production angle up to ± 5 mrad in the vertical and horizontal planes for systematic studies as well as Ξ^- and $\overline{\Xi}^+$ yield measurements.

8.2 Target

Two targets, one for Ξ^- and the other for $\overline{\Xi}^+$ production, will be mounted on a target holder that can be moved remotely in the vertical as well as the horizontal direction. This allows fine tuning of the target position with respect to the spectrometer so that the secondary beam is symmetrically produced with respect to the nominal production direction. The targets, identical in size, will be short to minimize potential target size effects, and will have different interaction lengths in order to produce the same charged particle flux in the spectrometer. A high-A target will be used because: 1) the physical length of the target can be made shorter, 2) fewer primary protons are needed to produce the required number of Ξ's, and 3) the relative yield of hyperons at low x_F is higher with heavy target material [30].

8.3 Hyperon Channel

After the primary protons interact in the target, a secondary charged beam is defined by a curved channel embedded in a dipole magnet with a uniform vertical field. The channel consists of brass and tungsten blocks as shown in Fig. 5. The 90 cm-long upstream tungsten block serves as a dump for the beam protons. The defining aperture is 5 mm wide in the bend view and 1 cm high in the vertical direction, giving a solid angle acceptance of 4.9 μsr.

The design of the magnetic channel has been optimized to maximize the Ξ to charged particle ratio and to select a narrow momentum bite. The central orbit of the channel has a radius of 41.89 m and a bend angle, defined by the tangents to the central orbit at the entrance and exit of the channel, of 22.56 mrad. With a field of 1.85 T, the central orbit corresponds to the trajectory of a 150 GeV/c charged particle. The channel acceptance — defined as the fraction of particles within the solid angle that emerge from the exit of the channel — is shown in Fig. 6 as a function of the secondary beam momentum.

At 0 mrad production angle, positively charged secondaries are mainly protons with momenta greater than 200 GeV/c. Because of the narrow and lower momentum bite of the channel, these high energy protons are not transported to the spectrometer, effectively increasing the fraction of $\overline{\Xi}^+$'s in the beam. The 800 GeV primary protons not impacting the target strike the upstream face of the defining collimator at 7.5 mm to the left of the central orbit.

When the magnetic field of the sweeping magnet is reversed, a negatively charged beam is selected. With an NMR probe permanently installed in the collimator, it is possible to reproduce the field to high precision. In E756, even without an NMR, the momentum acceptance of the channel between the two charge modes agreed to 0.25 GeV/c, better than the 10^{-3} level.

8.4 Magnetic Spectrometer

Measuring the asymmetry to the 10^{-4} level requires a large flux of Ξ's which are accompanied by a much larger flux of charged pions (and protons). The limiting factor in the number of Ξ's that can be accumulated is not the production cross section of the Ξ, which is quite large, but the maximum charged fluence the wire chambers can tolerate. In order to collect 1,400 reconstructed $\overline{\Xi}^+$ decays per second the spectrometer must be able to tolerate the passage of 4.3×10^7 Hz of protons and pions when a positively charged beam is selected (the fraction of Ξ^-'s in the negative beam is larger with the same fluence).

8.4.1 Wire Chambers

The wire chambers must have low mass and high-rate capability. There will be four wire chambers upstream of the analysis magnet and four behind. Table 6 is

a summary of the geometry of the wire chambers that has been used in the Monte Carlo studies. Each chamber will contain three views, one having vertically strung wires and the other two having wires inclined at a stereo angle. The stereo angle will be chosen so that the resolutions in the bend and non–bend views are comparable. Since there are multiple planes in each view, there is sufficient redundancy to allow the chamber efficiencies to be measured accurately and the tracking efficiency is thus a weak function of the individual plane efficiency.

Table 6: Geometry of the wire chambers.

Z (m)	Width (cm)	Height (cm)	Pitch (cm)	No. of Channels
26.0	76.8	45	0.1	3 × 768
30.0	76.8	45	0.1	3 × 768
34.0	76.8	45	0.1	3 × 768
38.0	76.8	45	0.1	3 × 768
41.0	76.8	45	0.1	3 × 768
44.0	198.4	60	0.2	3 × 992
47.0	198.4	60	0.2	3 × 992
50.0	198.4	60	0.2	3 × 992
Total channels:				20,448

The chambers upstream of the analysis magnet will have small diameter ($12 - 15\,\mu$m) anode wires spaced at 1 mm and an anode-cathode gap of 3 mm or less. Since the particle density after the analysis magnet is reduced, it is possible to use chambers having a more conventional wire spacing of 2 mm at that location. All chambers will use either a fast gas such as $CF_4(80\%)/i - C_4H_{10}(20\%)$ or a traditional magic gas $Ar/i - C_4H_{10}/CF_3Br +$ Methylal at a gain $< 10^5$. The latter mixture may be preferred in the higher flux chambers since only ionization within $\sim 1mm$ of the anode would undergo avalanche multiplication.

The rate limitation is given by the flux in the most upstream chamber which is 26 m downstream of the exit of the collimator. From the Monte Carlo simulation, the beam size at the first chamber is about 10 cm high and 25 cm wide. The rate is approximately $4 \times 10^5 s^{-1} cm^{-2}$ in the busiest region. If a 1 mm wire spacing MWPC is used, the highest rate per wire will be about 0.4 MHz. This is a high intensity, but not above that encountered in other high-rate experiments. Wire chambers operating at rates of several times $10^7 s^{-1} cm^{-2}$ have successfully been built [36].

Perhaps another concern is radiation damage over the course of a 10^7sec run. Assuming that all of the ionization in a 6 mm path length is amplified at a maximal gain of 10^5, we estimate a deposited charge of ~ 0.08 C/cm on the hottest wires. This is within the accepted limit of ~ 1C/cm for 25 μm wires in traditional chamber gases.

8.4.2 Chamber Electronics

A low input impedance preamplifier will be mounted close to the wire followed by an Amplifier/Discriminator incorporating shaping circuitry to reduce the ion tail. Experience in E771 has shown that separating these two stages with $\sim 30'$ of cable suppresses parasitic feedback sufficiently well to have stable operation at an anode threshold of $\sim 12,000e$. The discriminators will have a delayed output going to the data aquisition system as well as an optional prompt output for use in the multiplicity trigger described below.

8.4.3 Analysis Magnet

The momentum analyzing magnet can be made up of two standard BM109 dipoles,each with an aperture of 61 cm wide by 30 cm high and an effective length of 2 m. The total transverse momentum kick is approximately 0.75 GeV/c. The field is known to be uniform and can be easily mapped with the Fermilab ziptrack. From the experience gained in E756, the relative field values can be determined to better than 1×10^{-3}. As shown in Figs. 7–8, the agreement in the Ξ^- and $\overline{\Xi}^+$ as well as the Λ° and $\overline{\Lambda}^\circ$ masses measured in E756 is excellent.

8.4.4 Hadronic Calorimeter

A simple hadronic calorimeter, used only to distinguish protons (antiprotons) (from Ξ decays), from background muons, is situated 10 meters downstream of the last wire chamber. Its size is 60 cm $\times$ 80 cm by 108 cm deep ($6\lambda_I$). It is constructed of 24 alternating layers of 4.0 cm iron and 0.5 cm thick scintillator sheets and subdivided transversely into four submodules. The submodules are read out using photomultipliers coupled to waveshifting scintillators. A total of 16 photomultipliers are needed giving a segmentation of four in the longitudinal direction.

To match the calorimeter fiducial region to that of the last wire chamber its transverse size extends beyond the chambers by one interaction length, except on the side adjacent to the beam exiting the collimator. Hence all protons (antiprotons) passing through the wire chamber will have at least 90% of their energy contained within the calorimeter [39]. The energy resolution is expected to be $85\%/\sqrt{E}$ at 100 GeV. Because it is non-compensating, the 85% will improve to approximately 70% at 15 GeV [40]. To estimate the radiation dose the calorimeter has to suffer, we assume an incident hadron flux of 10^5 per second, which corresponds to 2.9×10^{11} per year. This flux is spread over an area of approximately 60 cm $\times$ 30 cm = 1,800 cm^2. The dose per incident hadron per cm^2 is given by $3.8 \times 10^{-10} p^{0.89}$ Gy cm^2 [41]. This corresponds to a maximum dose of 66 Gy in a 200 day run.

8.4.5 Hodoscopes

Two vertical planes of hodoscopes, back to back and offset by a small amount from each other in the horizontal direction, will be positioned downstream of the last wire chamber. Each plane is 2 m wide by 0.6 m high and has 32 scintillation counters. The individual counters will have a dimension of 0.6 m by 6.35 cm. They will be used for timing and serve as fast trigger elements.

8.4.6 Decay Region

To minimize the number of interactions in the spectrometer, the 25 m long decay region will be evacuated using a 60 cm diameter vacuum pipe with thin windows at the ends. Space between the chambers will be filled with helium bags.

8.5 Trigger

8.5.1 Trigger Philosophy

The trigger has been kept simple in order to minimize potential biases. It relies on the fact that the decay of a Ξ^- ($\overline{\Xi}^+$) produces two pions with the same sign charge as the beam exiting the hyperon channel and a proton (antiproton) with the *opposite* sign charge. Because the polarity of the analysis magnet will be set equal to that of the hyperon magnet, the pions from the Ξ^- ($\overline{\Xi}^+$) decay will be bent in the same direction (beam side) as the charged beam exiting the collimator, and the proton (antiproton) will be bent in the opposite direction to the charged beam. At the z position of the last wire chamber the proton (antiproton) will be well separated from both the pions from the Ξ^- ($\overline{\Xi}^+$) decay as well as from the charged beam exiting the collimator. The trigger will require: 1) the presence of at least two charged particles in the first two wire chambers; 2) the presence, at the rear of the spectrometer, of at least one charged particle on the beam side; and 3) the presence, at the rear of the spectrometer, of a charged hadron on the side opposite the beam side.

The trigger is very similar to that used in E756, which was logic combination of: 1) a small upstream scintillation counter surrounded by a veto counter, 2) a hit in the right and left side of the last wire chamber, and 3) a signal corresponding to, between two and five minimum ionizing particles, in a 1 cm thick scintillator at the end of the decay region. The major difference between the E756 and the P871 triggers is the addition of a small hadronic calorimeter, situated 10 meters downstream of the last wire chamber, to detect the proton (antiproton). The reason for using a calorimeter to detect the proton (antiproton), rather than simply using a hodoscope, is because of the possibility of a large muon background in the spectrometer. The threshold on the energy deposited in the calorimeter will be kept just above that expected for a muon.

8.5.2 Trigger Backgrounds

In E756 the yield of fully reconstructed Ξ^-'s from this trigger was 32%, but only 0.25% for $\overline{\Xi}^+$'s. The yield was much less for the $\overline{\Xi}^+$ mode for the following reason. The momentum bite accepted by the E756 channel was between 240 GeV/c and 500 GeV/c for the $\overline{\Xi}^+$ run. In this range, the flux of protons exiting the collimator was very large, at $\sim 0.5 \times 10^6$ per second. With 3.5% of an interaction length of material in the spectrometer, the trigger rate of 8×10^3 per spill was totally dominated by secondary interactions of these protons. On the other hand, when running in the Ξ^- mode, the ratio of Ξ's to π^-'s was much higher and secondary interactions were far less a problem.

In order to increase the $\overline{\Xi}^+$ trigger yield for P871 the fraction of $\overline{\Xi}^+$'s in the beam exiting the hyperon channel is maximized and the amount of material in the spectrometer minimized. The former is done by selecting lower momentum particles, where the ratio of $\overline{\Xi}^+$'s to protons is much higher, with the magnetic channel. The latter is accomplished by eliminating the trigger counters which were at the end of the decay region in E756. The amount of material has been cut by a factor of four from the E756 value, to 0.8% of an interaction length.

8.5.3 Left-Right Trigger

A left-right trigger is formed by the coincidence of an amount of energy in the hadronic calorimeter consistent with the presence of a hadron, and a signal in a scintillation counter hodoscope situated on the beam side at the end of the spectrometer. Redundancy in the hodoscope planes should ensure an efficiency close to 100%. The rate of this trigger is primarily due to genuine Ξ decays and interactions of the secondary beam in the spectrometer. When producing a positively charged secondary beam, 4.3×10^7 particles per second exit the collimator (see Table 3). About 3.5×10^5 of these particles per second will have interactions in the spectrometer but only 9×10^4 per second will satisfy the left-right trigger along with about 4,000 $\overline{\Xi}^+$'s. This trigger rate has been estimated by the same Monte Carlo program that reproduces the E756 $\overline{\Xi}^+$ trigger rate to better than 50%.

8.5.4 Multiplicity Trigger

Much of the trigger rate is due to interactions in the downstream wire chambers. Hence, the requirement of a multiplicity in the upstream chambers consistent with the Ξ, Λ decay chain can reduce the trigger rate. Monte Carlo studies show that requiring at least two hits in each of the front two chambers reduces the hodoscope trigger rate to approximately 16,000 Hz.

The vertical wires in the first two chambers will be used to form the multiplicity trigger. Prompt discriminator fan-outs from every group of 64 wires will drive line receivers in one current summing module. (See Fig. 9.) Each PWC hit received by a

module switches a current step into the daisy-chained outputs of the modules. Preset comparators (See Fig. 10.) monitor the current sum and give separate outputs for greater than 1, 2, 3, or 4 hits. Scalers will be used to monitor the relative rate from the 4 comparators to insure trigger conditions do not change with time. The size of the active area of the multiplicity trigger will be made small enough to eliminate the possibility that particles from sources other than the collimator satisfy the trigger.

The time resolution of the upstream chambers is excellent due to the millimeter wire spacing, which allows charge collection in a time comparable to the spacing of RF buckets ($\sim$ 20 nsec). Accidental wire hits from previous events or 'hot' wires should be very low. For example, with a beam intensity of 5×10^7 per second in E771, 99% of random triggers were free of hits in chambers with a similar wire pitch.

The efficiency of the multiplicity trigger in reducing the trigger rate from events where an interaction in the spectrometer satisfies the left-right hodoscope requirement is limited by the rate in which multiple charged particles exit the collimator within the time resolution of the trigger. There are two sources of multiple charged particles exiting the collimator: two or more interactions each producing a secondary which makes it through the collimator, and single interactions in which two or more secondaries make it through the collimator. The probability of the latter — from a Pythia Monte Carlo simulation of primary proton interactions in the target — is negligible for the interaction rates of P871. The probability of the former is determined by dividing the 43 MHz rate of secondaries exiting the collimator (see Table 3) by 5.3×10^7 buckets per second. The mean bucket occupancy of 0.81 secondary particle at the exit corresponds to a 20% probability of having more than one particle exiting the collimator in the same bucket. This is assuming a perfect spill structure, something the Tevatron does not provide any of the external beam lines. Hence we estimate a reduction of only a factor of two in the left-right trigger rate when the multiplicity trigger is added. In other words, the trigger rate will be 45,000 Hz, rather than the 16,000 Hz calculated with the Monte Carlo which did not take into account multiple charged particles exiting the collimator.

8.5.5 Further Improvements

To increase the sensitivity of *CP* asymmetry measurement beyond 10^{-4} we need to further reduce the trigger rate due to accidentals. This can be done by incorporating an online processor that would find decay vertices and select events consistent with decays inside the vacuum decay region. We are investigating the use of a processor similar to those used in E605 and E789, which reconstructed complicated event topologies in about 10 μsec, with rejection factors as high as 10 [42].

8.6 Data Acquisition

The design goal of the DAQ system is to read 20,000 channels with a maximum trigger rate of 100,000 Hz, build events, and write them to tape. We assume a

maximum event size of 416 Byte (a factor of 2 larger than that of E756), resulting in a sustained data logging requirement of almost 14 Mbyte/sec. The overall system deadtime should not exceed 10%, meaning that we should be able to log comfortably at least 90,000 triggers per second.

The maximum event size is calculated as follows. There are 8 chambers, each with 3 wire planes (X, U and V plane). The ideal hit multiplicity for an event of interest is 3 per plane. If we take double hits and noise hits into account, a maximum of 8 hits per plane is a reasonable estimate. To be even more conservative, we always consider this worst case in our throughput calculations. Since each wire channel needs 2 bytes for encoding, a maximum of 384 bytes will be read out from all the chambers. Furthermore, we assume that a total of 20 bytes are generated by scintillators and calorimeter. The run and event number, event length and end of event marker will take up another 12 bytes. Therefore a maximum event size of 416 Bytes presents a very conservative estimate.

The design of the Acquisition System is driven by the requirements of modularity (new technologies should be implementable as they become available without affecting the overall system), and scalability (it should be possible to accommodate an increase in performance).

The layout of the acquisition system is given in Fig. 11. The centerpiece is a standard 6U VME crate (DAQ-crate) that holds one or more Front-End Interfaces (FEI) that communicate with Front-End Crates (FEC), Event Builders (EB), Interfaces to Tape units (TI), and a State Machine (StM) which controls and monitors the activities of the readout sequences. A group of FEC's form a read-out Branch. Several such branches can be accessed in parallel. Auxiliary readout of scalars, magnetic field monitors and other slow control devices will be done separately but will be embedded into the standard data stream.

The FEC contains the Front-End Modules (FEM) that read and latch the signals from the MWPC's and counters. The FEI communicates with the DAQ-crate and a Front-End Processor (FEP) which executes a real time kernel (e.g. VxWorks) for time-critical operations. The main functions of the FEP are data collection from all FEM's in the FEC, data reduction through reformatting of the event fragment, and temporary storage of data until the EB pulls a new block of events into its local memory.

There are six system components:

1. Front-End Module: In Fig. 12 the 256 differential ECL detector signals are received by the FEM and converted to TTL logic. The data are latched into a FIFO array. The FIFO's are deep enough to derandomize the intensity fluctuations of the incoming beam. The hit is then encoded as absolute wire address by an address encoder such as a DSP and stored in one of two VME accessible on-board buffers. At the end of encoding, the address encoder will put out a word to signal the End of Event (EOE), e.g. FFFF, and append it to the event fragment. Data are written into the same buffer until the FEP decides

to read out the FEM. The FEP broadcasts a SWITCH_BUFFER signal on the VME bus to all FEM's in the FEC and subsequently performs a block-read of the full buffer. In summary, the FEM's act as VME slaves to the FEP and have a double buffer scheme implemented. A "busy" signal will be generated to disable the trigger when the readout sequence cannot keep up with the trigger rate. Also a minimum deadtime will be imposed once a trigger is accepted. In the current design we set the deadtime to 100ns, limiting the FIFO speed to 10MHz.

2. Front-End Processor (FEP): The FEP retrieves data with chained VME block-reads from all FEM's. After the FEP has fetched all these packets it assembles the data belonging to the same trigger and forms a new event fragment containing event number and fragment length. The FEP has large on-board memory (maximum 128 MByte) to hold event fragments over one full spill. This enables the FEI to transfer data during the spill and in between spills.

3. Event Builder (EB): The EB fetches all the event fragments from all FEC's to the local memory. Then it builds the final event from the event fragments belonging to the same trigger before writing it out to the permanent storage.

4. State Machine (StM): This module will synchronize and arbitrate the related DAQ processes. For example, it coordinates the trigger signals and the data transport through the DAQ.

5. Front-End-Interface (FEI): One FEC has to communicate with the DAQ-crate at a sustained rate of almost 2 MByte/sec. The total throughput from all FEC's to the EB is expected to be around 18 MByte/sec. Thus we will employ a fast link that enables us to daisy-chain several or all FEC's with the DAQ-crate. In case the setup latency for transfers is substantial we will use the State Machine to control the data flow.

6. Data Logging: We expect to log up to 14 MByte of data per second to the permanent storage. Currently we pursue two options to solve the technical challenge that is posed by such a high data rate. Option 1 is the use of a high speed tape-drive with a VME interface capable of recording 16 MByte/sec. Several such drives are on the market and we have already gained some experience with the AMPEX DD2 that is available at the SSCL. Option 2 uses an array of five Exabyte Mammoth tape drives [38]. These are an upgraded version of the Exabyte 8505 drives, and will be available at the end of 1994. They write (in non-compressed mode) 3 MByte/sec and pack 20 GByte per tape.

9 Offline Computing Needs

A sustained rate of 1.5×10^4 events per second will be written to tape assuming a 45 kHz trigger rate. In 200 days of running with a duty factor of 50% the total number of events will be 1.3×10^{10} on 2,700 8mm–20Gb tapes (assuming an event size twice that of E756). This is a data sample on the order of that taken by E791 in the 1991 fixed target run [37].

In the first pass analysis, which reconstructs and selects events with interesting decay topologies, the CPU time required to process the E756 data on a HP-735 workstation (rated 76 SPECint92) is 3 msec/event (including I/O time). We expect it will take comparable time to analyze an event in this experiment. With a cluster of 20 HP-735 workstations, the first pass analysis of the entire data set in this experiment can be processed in one calendar year with a processing duty factor of 60%. With one HP-735 workstation, we can analysis 5% of the raw data during the run. For the final analysis, based on our experience gained in E756, it will take 1 ms to process a DST event on a HP-735 machine or about four weeks to analyse all the DST events.

For Monte Carlo studies two types of events are generated: complete events and hybrid events. In a complete Monte Carlo event the parent particle is generated at the target, tracked through the collimator and the spectrometer, and digitized. It takes about 45 ms to generate such an event. The Hybrid Monte Carlo events use the decay vertex and momentum of the real Ξ's. Only the decay products are generated by the Monte Carlo. Usually ten or so Monte Carlo events are generated per one real Ξ. The hybrid Monte Carlo minimizes errors due to poor simulation of the parent particle kinematic parameters. It has been extensively used in many high statistics Hyperon polarization experiments [35]. With 10 ms needed to generate a hybrid event, it also reduces the amount of computer time needed to generate an event. With a cluster of 10 HP-735 workstations, 47 CPU days will be needed to generate 4×10^9 events.

10 Systematics

The experimental apparatus has been designed to minimize systematic biases that produce false *CP* asymmetries. Because the Ξ^- and Λ° alpha parameters both change sign under the *CP* transformation, the distribution of the proton in the Λ° rest frame should be identical to that of the antiproton in the $\overline{\Lambda}^\circ$ rest frame. (The Λ° and $\overline{\Lambda}^\circ$ distributions in the Ξ^- and $\overline{\Xi}^+$ rest frames should also be identical because the Ξ's are produced with no polarization.) Hence the proton and antiproton distributions can be directly compared with no acceptance corrections to searching for *CP* violation.

Systematic effects giving rise to false asymmetries are of great concern in light of the fact that we wish to measure an asymmetry to the 10^{-4} level. Sources of biases which can cause false *CP* asymmetries fall into three classes: 1) differences in acceptance between the Ξ^- and $\overline{\Xi}^+$ decay chains, 2) nonzero polarization of the Ξ^-

or $\bar{\Xi}^+$, and 3) differences between the p and $\bar{p}$ cross sections.

10.1 Effect of differences in the acceptance

There are many possible causes of differences in the Ξ^- and $\bar{\Xi}^+$ acceptance. For example, targeting differences, magnetic field differences, and differences in the chamber efficiencies. Our method of analyzing the Λ° polarization — by measuring the $\cos\theta$ distribution of the proton in the Λ° rest frame — greatly reduces the effect of these differences. Because the Λ° direction changes from event to event over the 4π solid angle in the Ξ^- rest frame and because the acceptance along the helicity axis in the Λ° rest frame is very uniform, problems localized in a particular part of the apparatus do not map onto any particular part of the $\cos\theta$ distribution of the proton. This will become evident in the following discussion.

In order to get a quantitative estimate of the effect of acceptance differences on the asymmetry measurement, we have chosen pairs of Ξ^- data sets from E756 with large acceptance differences and compared their proton distributions in the Λ° rest frame. Since these are all Ξ^-'s, any difference between the proton distributions is solely due to acceptance differences between the two samples and not due to *CP* violation. *No attempt was made to correct for acceptance differences between the data sets.* Over 10 million Ξ^- events were analyzed.

The difference in the proton cosine distribution is determined by taking the ratio:

$$R(\cos\theta) = \frac{A_1(\cos\theta)(1 + a\cos\theta)}{A_2(\cos\theta)(1 + a\cos\theta)}, \tag{9}$$

$$= \frac{A_1(\cos\theta)}{A_2(\cos\theta)}, \tag{10}$$

where $A_1(\cos\theta)$ and $A_2(\cos\theta)$ are the acceptance functions of the two samples, $a = \alpha_\Xi\alpha_\Lambda$, and $\cos\theta$ is the polar angle the proton makes relative to the Λ° polarization direction (which is the Λ° momentum direction in the Ξ rest frame).

Since $R(\cos\theta)$ is very uniform in $\cos\theta$, we parametrize it as

$$R(\cos\theta) = a + b\cos\theta \tag{11}$$

where the slope b is a measure of how well the acceptances of the two samples agree with each other. The intercept a is unity when the samples are properly normalized and the slope b is zero if the acceptances are identical. The E756 data samples were taken at six different hyperon magnet settings, corresponding to six different momentum bites. One of the settings has two polarized samples produced by a high energy polarized neutral beam at 0 mrad. Most of the other Ξ^- data were produced by primary protons at +2.5 mrad and -2.5 mrad in the vertical plane. For some magnet settings small samples were taken at 0 mrad, +1.3 mrad and -1.3 mrad as well as +1.2 mrad and -1.2 mrad in the horizontal direction. Samples with non-zero production angles are known to be polarized with a magnitude of about 12%.

Table 7 and Fig. 13 summarize the difference in acceptance for samples with comparable Ξ^- polarization but different average Ξ^- momentum. The acceptance differences strongly depend on the difference in momentum of the samples down to a few GeV/c. Below that, the slope b is less sensitive to the momentum mismatch. It is important to note that in this insensitive region the proton distributions in the Λ° rest frame already agree to better than a few parts per thousand although the samples have different acceptance in the laboratory frame and were taken at different times.

Table 7: Acceptance difference as a function of momentum mismatch.

$< p_1 >$ [1]	$< p_2 >$ [2]	Δp (GeV/c) [3]	ΔP_Ξ [4]	$\lvert b \rvert$	χ^2/DOF
318.739	458.834	140.1	0.04	0.1442 ± 0.0041	3.76
318.739	427.339	108.6	0.03	0.1271 ± 0.0027	6.54
318.739	385.484	66.75	0.01	0.0923 ± 0.0024	4.10
385.484	427.339	41.86	0.02	0.0355 ± 0.0022	1.47
427.339	458.834	31.50	0.01	0.0183 ± 0.0039	0.74
458.834	478.983	20.15	0.04	0.0032 ± 0.0048	0.74
467.132	462.409	4.72	0.00	0.0029 ± 0.0051	1.54

In P871 we will control the acceptance differences to well over an order of magnitude better than the differences show above. In order to minimize the bias due to a difference between the Ξ^- and $\overline{\Xi}^+$ momentum distributions we have a small collimator aperture which selects a narrow momentum bite. As a result, the Ξ^- and $\overline{\Xi}^+$ momenta are determined largely by the collimator acceptance rather than by their production properties (which are different). To get an idea of how well the Ξ^- and $\overline{\Xi}^+$ acceptances match we have normalized the momentum spectra of the E756 Ξ^- and $\overline{\Xi}^+$ data to each other and then compared various Ξ^- and $\overline{\Xi}^+$ kinematic quantities. (The normalization is necessary because the momentum bite of the E756 magnetic channel was much broader than the P871 design and hence the Ξ^- and $\overline{\Xi}^+$ momentum spectra were different.) As shown in Figs. 14–16, the comparison is almost perfect — chi-squares per degree of freedom indicate no difference — even though the two data samples were taken at widely different times. (For this experiment we intend to switch between Ξ^- and $\overline{\Xi}^+$ running every hour, if not more often.) In particular the comparison between the cosine distributions of the proton polar angle with respect to the Λ° momentum in the Λ° rest frame, shown in Fig. 17, — the asymmetry we want to measure to search for CP violation — the slope b is -0.001 ± 0.009 with a χ^2/DOF

[1] Mean momentum of sample 1.
[2] Mean momentum of sample 2.
[3] Difference in momentum.
[4] Difference in the Ξ^- polarization.

of 0.67, showing no statistically significant difference. The backgrounds are also negligible, as is evident in Fig. 18 which shows the $p\pi^-$and $\bar{p}\pi^+$ invariant masses. Most of the continuum in the invariant mass distribution is due to poorly reconstructed Ξ events. This kind of background is reproduced in the Monte Carlo simulation in E756. With better position resolution and more redundant tracking measurements in this experiment, we expect this background to be highly suppressed.

Another potential source of bias is slight differences in the positive and negative magnetic fields of the hyperon channel and spectrometer magnets. The BM109 dipole magnets are known to have uniform fields. We intend to measure the differences in the field values to a part in 10^4 or better in order to control such biases and to reverse the magnet polarities as often as possible.

Because the Ξ^- and $\overline{\Xi}^+$ data samples will not be taken simultaneously, temporal changes in the apparatus could give rise to false asymmetries. To minimize rate dependent efficiencies in the chambers, we will be careful to run both positive and negative beams such that the charged particle flux at the exit of the collimator is always the same. Nevertheless, at the high charged particle fluences anticipated for the experiment, duty factors and chamber efficiencies are not expected to be extremely high and localized inefficiencies producing false asymmetries at the 10^{-4} level are conceivable. In order to minimize such effects we have added redundant chamber planes at every measurement station. This will allow the individual plane efficiencies to be measured to the desired accuracy and will reduce the dependence of the tracking efficiency on the individual plane efficiency.

Hence, by extrapolation from the studies of the E756 data, we expect that the acceptance contribution to the measurement of the $\cos\theta$ will be considerably less than 10^{-4}.

10.2 Effect of non-zero Ξ polarization

Another potential source of bias is from non-zero Ξ^- and $\overline{\Xi}^+$ polarizations. The most probable source of such polarization is slight mistargetting. The resultant polarization would be extremely small due to the low p_T and small x_f of the Ξ. Any source of Ξ polarization can be measured to the 10^{-3} level. The effect of such polarization on the measured Λ polarization is diluted by our method of analysis — the Ξ polarization is fixed in space whereas the helicity component of the polarization of the Λ changes from event to event. Because of the uniform acceptance along the Λ momentum in the Λ rest frame, sources of polarization that are fixed in space average to zero.

The best evidence for this comes from another analysis of the E756 data. Samples with equal and opposite production angles have widely different polarizations: about +12% and -12%. More importantly, the acceptance of the two samples is quite different. This is because the Ξ^- tends to follow the direction of the incident beam. Hence the +2.5 mrad Ξ^- decay products tend to inhabit the upper part of the apparatus whereas the -2.5 mrad Ξ^- decay products inhabit the lower part. The

difference is best illustrated in Fig. 19 showing the vertical position of the proton at the spectrometer magnet center. How does this large difference in acceptance in the laboratory affect the measurement of the product of the two α parameters? Fig. 20 shows a comparison of the proton $\cos\theta$ distribution from two samples with equal and opposite production angles. Slope b of this comparison is $(2.3 \pm 2.9) \times 10^{-3}$ with a $\chi^2/\mathrm{DOF} = 16.3/18$. In Table 8 we show the same comparison for several similar samples. There are no statistically significant differences between the two samples in each case despite the large differences in acceptance.

Table 8: Acceptance difference for samples of opposite polarization.

$< p_{+\theta} >$[1]	$< p_{-\theta} >$[2]	Δp (GeV/c)[3]	ΔP_Ξ[4]	b	χ^2/DOF
317.665	319.066	-1.40	0.23	-0.0017 ± 0.0027	1.02
318.739	319.342	-0.60	0.25	$+0.0023 \pm 0.0029$	0.90
385.484	383.453	2.03	0.26	-0.0016 ± 0.0017	1.20
427.339	425.845	1.49	0.28	-0.0030 ± 0.0024	0.74
458.834	454.323	4.51	0.29	-0.0063 ± 0.0047	0.93
478.983	478.419	0.56	0.25	-0.0125 ± 0.0044	1.03

Combining all the above samples we get $b = 0.00025 \pm 0.00104$, i.e. there is no significant difference between the two $\cos\theta$ slopes of interest at the 10^{-3} level. Hence the dilution of the polarization is large and we expect that even smaller polarizations — on the order of a few tenths of a percent — will contribute less than 10^{-4} to the measured asymmetry.

In any case, we do not intend to only hope for a small Ξ polarization, but to actually measure it. Measuring it to the required 10^{-3} level is possible and would require only a fraction of the total data sample. We expect to find no polarization, but in fact could extract the *CP* asymmetry even in the presence of a polarization greater than 10^{-3}.

10.3 Differences in the p and $\bar{p}$ cross sections

Secondary interactions of the Ξ^- and $\overline{\Xi}^+$ decay products in the spectrometer can cause differences in the Ξ^- and $\overline{\Xi}^+$ reconstruction efficiencies. If such differences manifest themselves in the proton distributions then false *CP* asymmetries may result.

In order to study this effect we have generated 5 million Ξ^- and $\overline{\Xi}^+$ Monte Carlo events in the P871 apparatus (using a modified version of the well-tested E756 Monte

[1] Mean momentum of positive production angle sample.
[2] Mean momentum of negative production angle sample.
[3] Difference in momentum.
[4] Difference in the Ξ^- polarization.

Carlo). Each proton or antiproton from a Ξ decay was forced to interact in the spectrometer with a distribution according to the amount of material at each location. PYTHIA was used to generate the number, type, and momentum of the resulting secondaries which were tracked through the spectrometer by the P871 Monte Carlo. The events were then reconstructed and the $\cos\theta$ distributions of the proton and antiproton were compared for those events that were successfully reconstructed. Only 120,000 events survived. The difference in the slopes of the $\cos\theta$ distributions ($\alpha_\Xi\alpha_\Lambda$ for both the Ξ^- and $\overline{\Xi}^+$ samples) was found to be -0.017 ± 0.010. Because P871 will have less than 1% of an interaction length of material, this translates to a sensitivity of about $(2.9 \pm 1.7) \times 10^{-4}$ in the asymmetry A. We intend to push this result to beyond the 10^{-4} level.

10.4 Other Potential Biases and Checks

There are other potential sources of biases. Secondary production of Ξ's in the collimator could produce biases. Such events are eliminated by requiring that the Ξ's point back to the target. The earth's magnetic field, which won't be flipped, produces slight changes in the acceptance between Ξ^- and $\overline{\Xi}^+$. The effect is small: an added 25 μrad deflection to a 15 GeV/c particle (amounting to 1 part in 10^3), the lowest momentum accepted by the spectrometer. This effect must be compensated or corrected for in the Monte Carlo.

To test the level of the systematics we intend to compare the Ξ^- and $\overline{\Xi}^+$ as well as Λ° and $\overline{\Lambda}^\circ$ lifetimes as a function of the hyperon momentum and angular distributions in the Ξ and Λ rest frames. They should be identical if *CPT* is conserved.

11 Future Improvements

As we have emphasized, the *CP* sensitivity of the experiment is not limited by the number of Ξ^- and $\overline{\Xi}^+$ hyperons that can be produced, but by the rates that the wire chambers can handle, the trigger selectivity, and the bandwidth of the data acquisition system (assuming systematic errors can be controlled). New technologies are being developed that are pushing these limits to higher levels. Wire chambers have been built that can take an order of magnitude more flux than we anticipate with no untoward effects [36]. The development of gas microstrip chambers [43] promises an even higher rate capability. Recently an experiment, NA12, has run at high intensities for 100 days with 8 microstrip gas chambers at CERN [44]. The chambers have a rate capability higher than $5 \times 10^7 cm^{-2}s^{-1}$. Vigorous R&D efforts are underway to increase the size and lower the mass of these chambers. If these efforts are successful, fluxes of two orders of magnitude higher than we anticipate in this proposal could be tolerated.

Similar improvements are being made in the data acquisition systems and triggers. Hence we expect in the future that large increases in the yield will be possible and

the CP sensitivity of the experiment can be pushed beyond 10^{-4}.

12 Other Physics

12.1 CP Violation in Charged Kaon Decays

Direct CP violation can also show up in charged K decays. The Dalitz plot of $K_{3\pi}$ decay is conventionally parametrized with the form [2]

$$|M^2| \propto 1 + g\frac{(s_3 - s_0)}{m_\pi^2} + h\frac{(s_3 - s_0)^2}{m_\pi^2} + j\frac{(s_2 - s_1)}{m_\pi^2} + k\frac{(s_2 - s_1)^2}{m_\pi^2}, \tag{12}$$

with

$$s_i = (m_K - m_i)^2 - 2m_K T_i, \quad i = 1, 2, 3, \tag{13}$$

$$s_0 = \frac{1}{3}({m_K}^2 + {m_1}^2 + {m_2}^2 + {m_3}^2), \tag{14}$$

where m_i and T_i are the mass and the kinetic energy of the i^{th} pion, and the index 3 is used for the opposite sign pion in the decay. The coefficient j is zero if CP is conserved. Furthermore, if any of the slope parameters, g, h, and k for $K^+ \to \pi^+\pi^+\pi^-$ is not the same as that for $K^- \to \pi^-\pi^-\pi^+$ decay, then CP symmetry is again violated.

Experimentally, the values of h and k are found to be very small [2]. As with the observables B or B' in hyperon decays, it is very difficult to search for CP-odd effect by determining the difference in either h or k between $K^+ \to 3\pi$ and $K^- \to 3\pi$ decays. Interest in searching for direct CP violation in $K_{3\pi}$ decay is focused on the charge asymmetry of the slope parameter g defined by

$$\Delta g = \frac{g(K^+) - g(K^-)}{g(K^+) + g(K^-)}. \tag{15}$$

Theoretical predictions of Δg vary from 1.4×10^{-3} to the order of 10^{-6} [45][46]. The best measurement of Δg is from a BNL experiment done in the late 60's. With about 3.2 million $K^\pm \to 3\pi$ decays, Δg was determined to be -0.0070 ± 0.0053 [47].

In our experiment, on the average 2.2% of the $K^\pm$'s will decay in the decay region with the π's inside the spectrometer active area. About 50% of the $K_{3\pi}$ events can be reconstructed and pass all selection cuts. From the yield calculation, it is very likely that in one Fermilab fixed target run we can collect 2×10^9 $K^+ \to \pi^+\pi^+\pi^-$ and 1×10^9 $K^- \to \pi^-\pi^-\pi^+$ decays, along with the Ξ^- and $\overline{\Xi}^+$ events. This implies a sensitivity for CP violation of about 1×10^{-4}, comparable to what can be achieved with a ϕ factory [48].

13 Cost Estimate

While many aspects of the experiment are yet to be determined we can make a rough estimate of the costs. The estimates are given in two columns: the first contains new equipment costs; the second the costs of items available at Fermilab and rigging charges that would be accrued to Fermilab. We expect the outside collaborating institutions to contribute to all of the costs in the first column and Fermilab to contribute to all of the costs in the second column. The estimates of the Fermilab contribution depend greatly upon the location of the experiment. They could be substantially less for an existing beam line with a modest amount of equipment. The $200K estimated for PREP electronics is only for NIM equipment and a small amount of CAMAC equipment.

The LBL contribution will be $250K per year for two years. The remaining institutions would contribute $565K per year total.

	New Equipment	Available Equipment and Labor
Beam line equipment and setup costs		200K
Hyperon magnet		100K
Hyperon channel	50K	
Evacuated decay pipe		10K
Installation of analysis magnet		10K
Portacamp facility		50K
Mechanical and Electrical support		50K
Electronics from PREP		200K
Terminals and network hookups required for online and offline computing		20K
DAQ system	200K	
Wire chamber fabrication and testing	200K	
Cables for chamber readout	100K	
Chamber readout electronics	800K	
Scintillators and associated electronics	30K	
8mm tapes	50K	
Offline computers and peripherals	100K	
Hadronic calorimeter	100K	
Total cost	\$1,630K	\$640K

Appendix 1: What do we Actually Measure?

The angular distribution of the proton in the decay chain: $\Xi^- \to \Lambda^\circ \pi^-$, $\Lambda^\circ \to p\,\pi^-$, where the Ξ^- is produced unpolarized, is given by:

$$\frac{dP}{d\cos\theta} = \frac{1}{2}(1 + a\cos\theta), \tag{1}$$

where $a = \alpha_\Lambda \alpha_\Xi$ and θ is the polar angle of the proton in the Λ° rest frame relative to the Λ direction in the Ξ rest frame. Similarly, the angular distribution of the antiproton in the antiprocess: $\overline{\Xi}^+ \to \overline{\Lambda}^\circ \pi^+$, $\overline{\Lambda}^\circ \to \overline{p}\,\pi^+$, where the $\overline{\Xi}^+$ is produced unpolarized, is given by:

$$\frac{dP}{d\cos\theta} = \frac{1}{2}(1 + \overline{a}\cos\theta), \tag{2}$$

where $\overline{a} = \alpha_{\overline{\Lambda}}\alpha_{\overline{\Xi}}$. We write the expressions for the alpha parameters of the antiparticles as:

$$\begin{aligned} \alpha_{\overline{\Lambda}} &= -\alpha_\Lambda + \Delta\alpha_\Lambda, \\ \alpha_{\overline{\Xi}} &= -\alpha_\Xi + \Delta\alpha_\Xi. \end{aligned}$$

It is $\Delta\alpha_\Lambda$ and $\Delta\alpha_\Xi$ that we wish to measure: if CP is violated they must be nonzero. Measuring the angular distributions of Eq. (1) and Eq. (2) gives:

$$\begin{aligned} a &= \alpha_\Lambda \alpha_\Xi, \\ \overline{a} &= (-\alpha_\Lambda + \Delta\alpha_\Lambda)(-\alpha_\Xi + \Delta\alpha_\Xi). \end{aligned}$$

The difference between the two asymmetries is:

$$\begin{aligned} \mathcal{A} = \frac{a - \overline{a}}{a + \overline{a}} &= \frac{\alpha_\Lambda\alpha_\Xi - (-\alpha_\Lambda + \Delta\alpha_\Lambda)(-\alpha_\Xi + \Delta\alpha_\Xi)}{\alpha_\Lambda\alpha_\Xi + (-\alpha_\Lambda + \Delta\alpha_\Lambda)(-\alpha_\Xi + \Delta\alpha_\Xi)}, \\ &= \frac{+\alpha_\Lambda\Delta\alpha_\Xi + \alpha_\Xi\Delta\alpha_\Lambda - \Delta\alpha_\Lambda\Delta\alpha_\Xi}{2\alpha_\Lambda\alpha_\Xi - \alpha_\Lambda\Delta\alpha_\Xi - \alpha_\Xi\Delta\alpha_\Lambda + \Delta\alpha_\Lambda\Delta\alpha_\Xi}. \end{aligned}$$

Leaving out terms which are second order in $\Delta\alpha_\Lambda$ and $\Delta\alpha_\Xi$ in the numerator and first order in the denominator gives:

$$\begin{aligned} \mathcal{A} &\cong \frac{\alpha_\Lambda\Delta\alpha_\Xi + \alpha_\Xi\Delta\alpha_\Lambda}{2\alpha_\Lambda\alpha_\Xi}, \\ &\cong \frac{\Delta\alpha_\Xi + \Delta\alpha_\Lambda(\alpha_\Xi/\alpha_\Lambda)}{2\alpha_\Xi}. \end{aligned}$$

We wish to relate this to the individual asymmetries in the Ξ and Λ alpha parameters:

$$A_\Lambda = \frac{\alpha_\Lambda + \alpha_{\overline{\Lambda}}}{\alpha_\Lambda - \alpha_{\overline{\Lambda}}} = \frac{\Delta\alpha_\Lambda}{2\alpha_\Lambda},$$

$$A_\Xi = \frac{\alpha_\Xi + \alpha_{\overline{\Xi}}}{\alpha_\Xi - \alpha_{\overline{\Xi}}} = \frac{\Delta\alpha_\Xi}{2\alpha_\Xi}.$$

Plugging these in gives:

$$\frac{a - \overline{a}}{a + \overline{a}} = A_\Xi + A_\Lambda. \tag{3}$$

We have gone through this simple derivation in some detail in order to emphasize that what we are sensitive to is the *CP* asymmetry in both the Ξ and the Λ alpha parameters. In fact there is no way the two alpha parameters can be deconvoluted if one measures the Λ polarization through its self-analyzing weak decay. Although in theory $\Delta\alpha_\Lambda$ and $\Delta\alpha_\Xi$ could be equal and opposite in sign, the chances of such a conspiracy are remote: most calculations predict that A_Λ and A_Ξ have equal sign, and in fact the standard model prediction of [12] shows them to be roughly equal in magnitude as well, doubling the size of the measured asymmetry.

Appendix 2: Error in the Asymmetry Measurement

We wish to measure the difference between the the product of the Λ° and Ξ^- alpha parameters and the $\overline{\Lambda}^\circ$ and $\overline{\Xi}^+$ alpha parameters:

$$\mathcal{A} = \frac{\alpha_\Lambda \alpha_\Xi - \alpha_{\overline{\Lambda}} \alpha_{\overline{\Xi}}}{\alpha_\Lambda \alpha_\Xi + \alpha_{\overline{\Lambda}} \alpha_{\overline{\Xi}}} = \frac{a - \overline{a}}{a + \overline{a}} = A_\Lambda + A_\Xi. \tag{1}$$

The error in this measurement is given by:

$$\begin{aligned} \delta\mathcal{A} &= \sqrt{\left(\frac{d\mathcal{A}}{da}\Delta a\right)^2 + \left(\frac{d\mathcal{A}}{d\overline{a}}\Delta\overline{a}\right)^2}, \\ &= \frac{2}{(a+\overline{a})^2}\sqrt{(\overline{a}\Delta a)^2 + (a\Delta\overline{a})^2}, \\ &= \frac{1}{2a}\sqrt{\Delta a^2 + \Delta\overline{a}^2}, \end{aligned}$$

where we have set $a = \overline{a}$. The product of the two alpha parameters is measured by measuring the asymmetry a in the proton (antiproton) decay distribution:

$$\frac{dP}{d\cos\theta} = \frac{1}{2}(1 + a\cos\theta).$$

The error in a is estimated using [49]:

$$\begin{aligned} \Delta a &= \frac{1}{\sqrt{N}}\sqrt{2a^3/(\log(1+a) - \log(1-a) - 2a)}, \\ &\cong \sqrt{\frac{3}{N}}, \end{aligned}$$

where the expression strictly applies only when the acceptance is uniform. We find:

$$\delta\mathcal{A} = \frac{1}{a}\sqrt{\frac{3}{2N}}.$$

The number of events needed to measure $\mathcal{A}$ to $\delta\mathcal{A}$ precision is:

$$\begin{aligned} N &= \frac{3}{2a^2}\frac{1}{(\delta\mathcal{A})^2}, \\ &= \frac{17.5}{(\delta\mathcal{A})^2}, \end{aligned}$$

where we have substituted $a = \alpha_\Lambda \alpha_\Xi = (-0.456)(0.642) = -0.293$. To measure an asymmetry with an error of $\delta\mathcal{A} = 1 \times 10^{-4}$ requires 1.8×10^9 Ξ^- events and the same number of $\overline{\Xi}^+$ events.

References

[1] J.H. Christenson, J.W. Cronin, V.L. Fitch and R. Turlay, Phys. Rev. Lett. **13** (1964) 138.

[2] Review of Particle Properties, Phys. Rev. **D45** 1992) 1.

[3] L. Wolfenstein, Phys. Rev. Lett. **13** (1964) 562.

[4] L.K. Gibbons et al. (E731), Phys. Rev. Lett. **70** (1993) 1203.

[5] H. Burkhardt et al. (NA31), Phys. Lett **B206** (1988) 169.

[6] A. Pais, Phys. Rev. Lett. **3** (1959) 242.
O.E. Overseth and S. Pakvasa, Phys. Rev. **184**, (1969) 1663.

[7] P.M. Ho et al., Phys. Rev. **D44** (1991) 3402.

[8] T.D. Lee and C.N. Yang, Phys. Rev. **108** (1957) 1645.

[9] Tim Brown, S.F. Tuan and Sandip Pakvasa, Phys. Rev. Lett. **51** (1983) 1823.

[10] Ling-Lie Chau and Hai-Yang Cheng, Phys. Lett. **B131** (1983) 202.

[11] John F. Donoghue and Sandip Pakvasa, Phys. Rev. Lett. **55** (1985) 162.

[12] John F. Donoghue, Xiao-Gang He and Sandip Pakvasa, Phys. Rev. **D34** (1986) 833.

[13] John F. Donoghue, Barry R. Holstein and German Valencia, Phys. Lett. **B178** (1986) 319.

[14] John F. Donoghue, Third Conf. on the Intersections between Particle and Nuclear Physics, Rockport ME, 14–19 May, 1988.

[15] M.J. Iqbal and G.A. Miller, Phys. Rev. **D41** (1990) 2817.

[16] X.G. He, H. Steger and G. Valencia, Phys. Lett. **B272** (1991) 411.

[17] G. Valencia, private communication.

[18] S. Weinberg, Phys. Rev. Lett. **37** (1976) 657.
T.D. Lee, Phys. Rev. **D8** (1973) 1226; Phys. Rep. **96** (1974) 143.

[19] M. Kobayashi and T. Maskawa, Prog. Theor. Phys. **49** (1973) 652.

[20] M. Shifman, A. Vainshtein, and V. Zakharov, Nucl. Phys. **B120** (1977) 316.
F. Gilman and M. Wise, Phys. Lett. **B93** (1980) 129.

[21] G. Buchalla, A. Buras and M. Harlander, Nucl. Phys. **B337** (1990) 313.
E.A. Paschos and Y.L. Wu, Mod. Phys. Lett. **A6** (1991) 93.

[22] P. Chauvat et al., Phys. Lett. **163B** (1985) 273.

[23] M.H. Tixier et al., Phys. Lett. **B212** (1988) 523.

[24] P.D. Barnes et al., Phys. Lett. **B199** (1987) 147.

[25] N. Hamann et al., CERN/SPSLC 92–19, 30 March 1992.

[26] S.Y. Hsueh, "Search for direct *CP* violation in $\bar{p} + p \rightarrow \bar{\Lambda} + \Lambda \rightarrow \bar{p}\pi^+ + p\pi^-$", Proposal to Fermilab, January 2, 1992.

[27] E.M. Gonzalez, Proceedings of the Meeting on the Tau-charm Factory Detector and Machine, University of Seville, Andalucia, Spain, 29 April – 2 May 1991, Ed. by J. Kirkby and J.M. Quesada.

[28] T.R.Cardello et al., Phys. Rev. **D32** (1985) 1.

[29] A.J. Malensek, Fermilab note FN-341 (1981), unpublished.

[30] A. Beretvas et al., Phys. Rev. **D34** (1986) 53.

[31] M. Bourquin et al., Z. Phys. **C5** (1980) 275.

[32] B. Lundberg et al., Phys. Rev. **D40** (1989) 3557.

[33] J. Lach and Y. Li, Fermilab note TM-1555 (1989), unpublished.

[34] G. Guglielmo, private communication.

[35] G. Bunce, Nucl. Instr. Meth. **172** (1980) 553.

[36] J. Fischer, A. Hrisoho, V. Radeka and P. Rehak, Nucl. Instr. and Meth. **A238** (1985) 249.

[37] S. Amato et al., Nucl. Instr. and Meth. **A324** (1993) 535.

[38] Exabyte Corp., Boulder CO.

[39] D. Acosta et al., Nucl. Instr. and Meth. **A316** (1992) 184.

[40] R. Wigmans, Nucl. Instr. and Meth. **A259** (1987) 389.

[41] D.E. Groom, "Radiation Levels in the SSC Interactions Regions", SSC-SR-1033, June 10, 1988.

[42] Y.B. Hsiung et al., Nucl. Instr. Meth. **A245** (1986) 338.

[43] A. Oed, Nucl. Instr. and Meth. **A263** (1988) 351.
F. Angelini et al., Nucl. Instr. and Meth. **A283** (1989) 755.

[44] F. Angelini et al., Nucl. Instr. and Meth. **A315** (1992) 21.

[45] A.A. Bel'kov et al., Phys. Lett. **B300** (1993) 283.

[46] Hai-Yang Cheng Phys. Rev. **D44** (1991) 919.

[47] W.T. Ford et al., Phys. Rev. Lett. **25** (1970) 1370.

[48] P. Franzini, INFN preprint LNF-92/024 (P) (1992).

[49] A.G. Frodesen, O. Skjeggestad and H. Tofte, "Probability and Statistics in Particle Physics" (Universitetsforlaget, Oslo, 1979) p. 219.

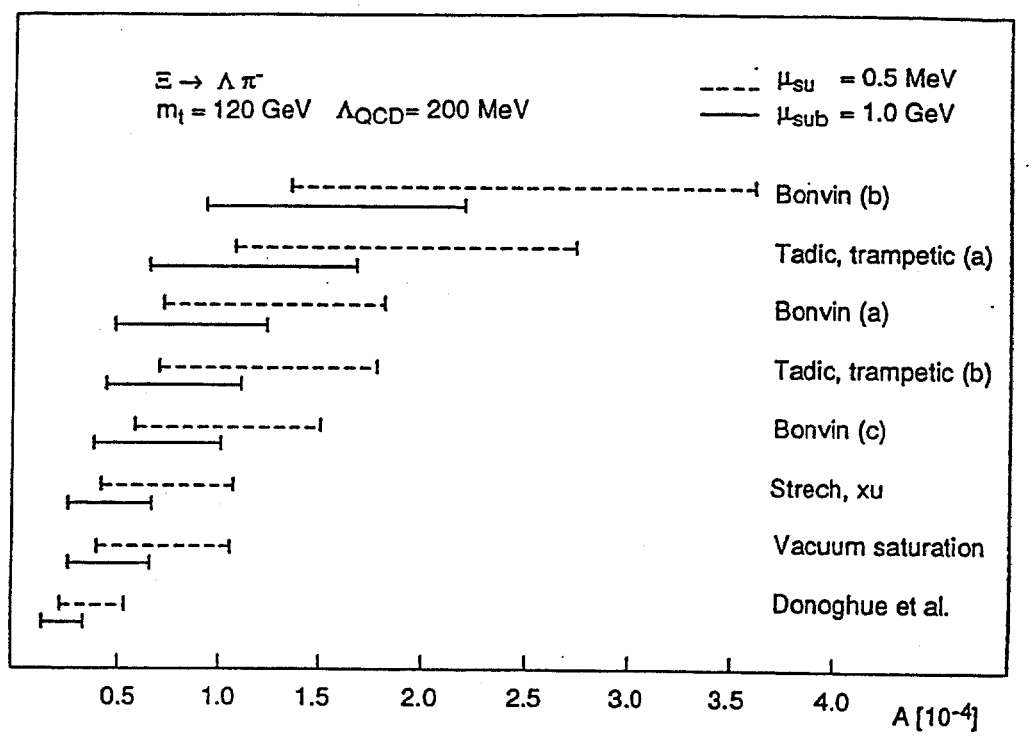

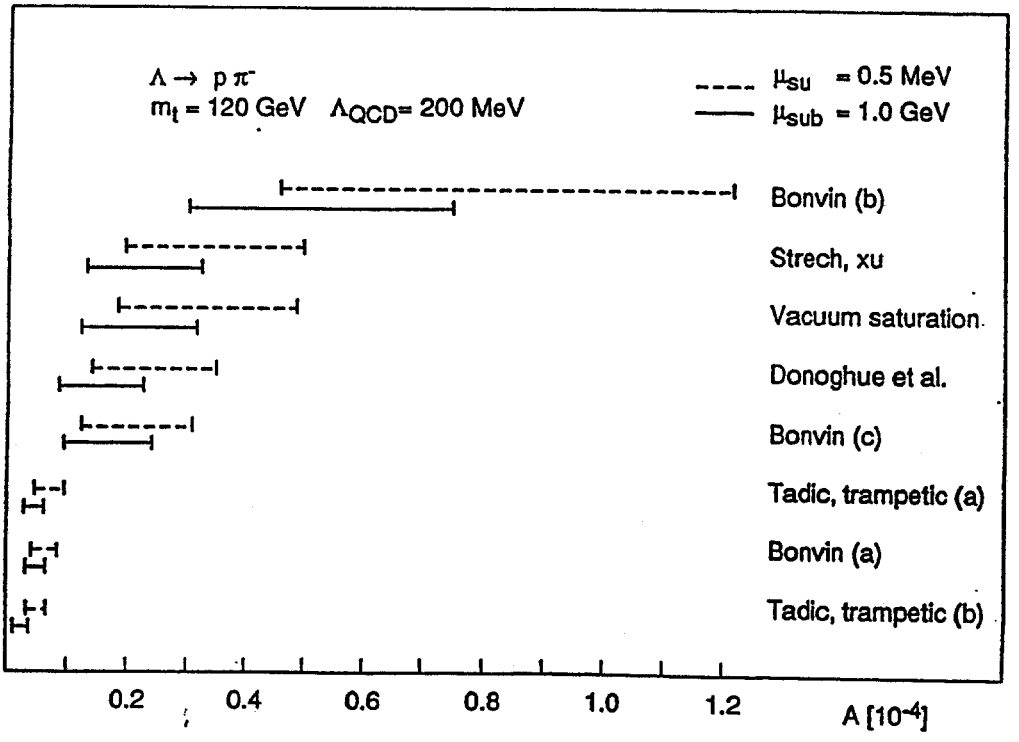

Figure 1: Standard Model predictions for (a) Ξ decay and (b) Λ decay.

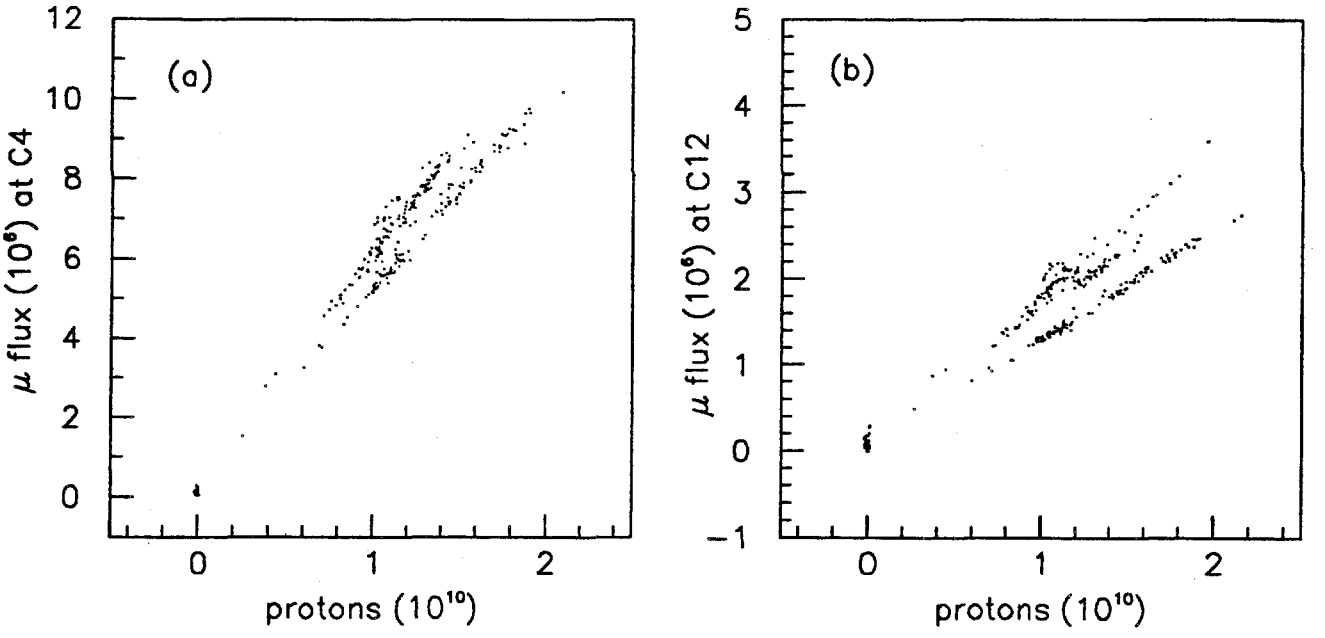

Figure 2: Muon fluence at (a) $C4$ (26 m from channel exit), and (b) $C12$ (49 m from exit).

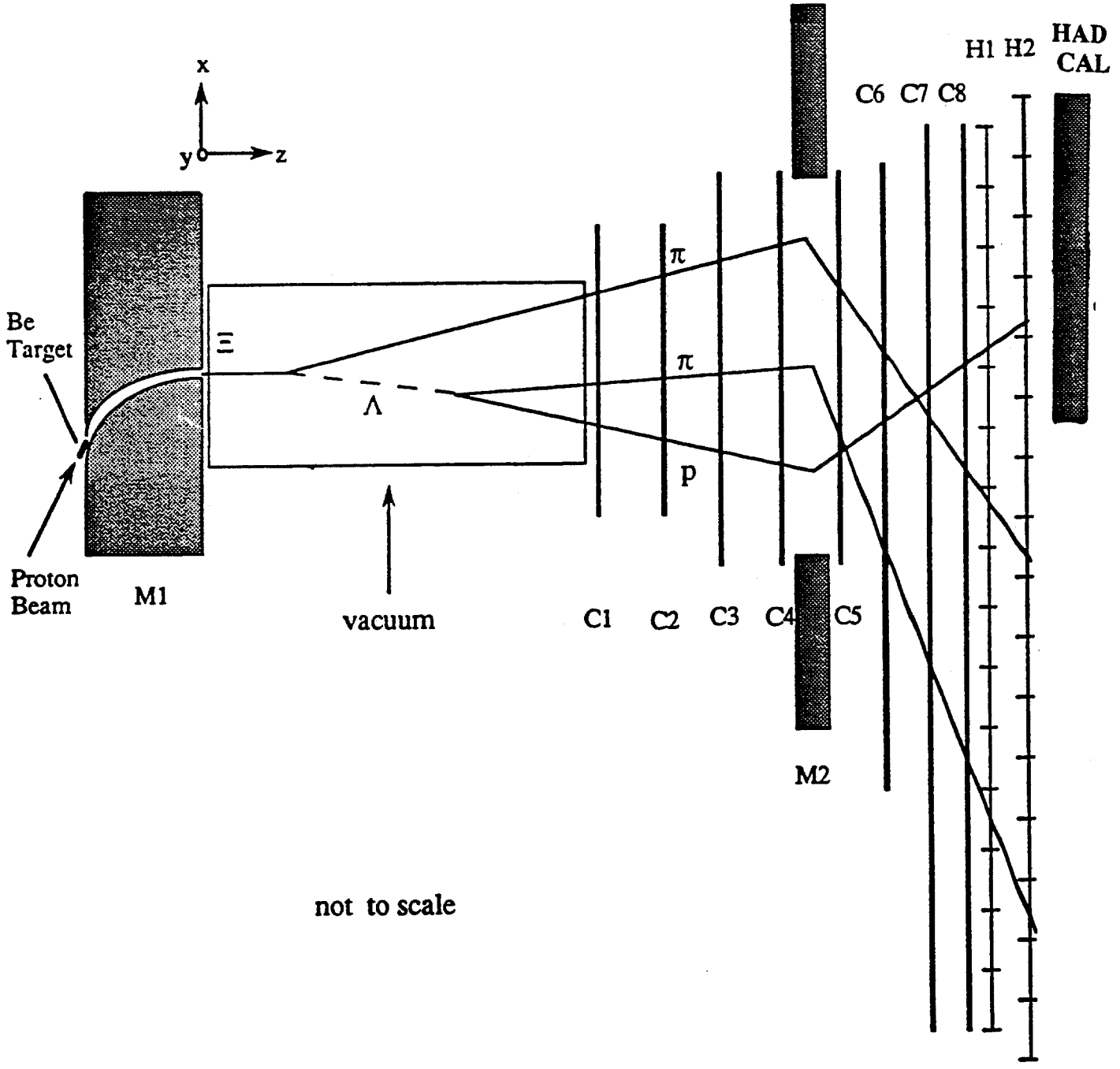

Figure 3: Plan view of spectrometer.

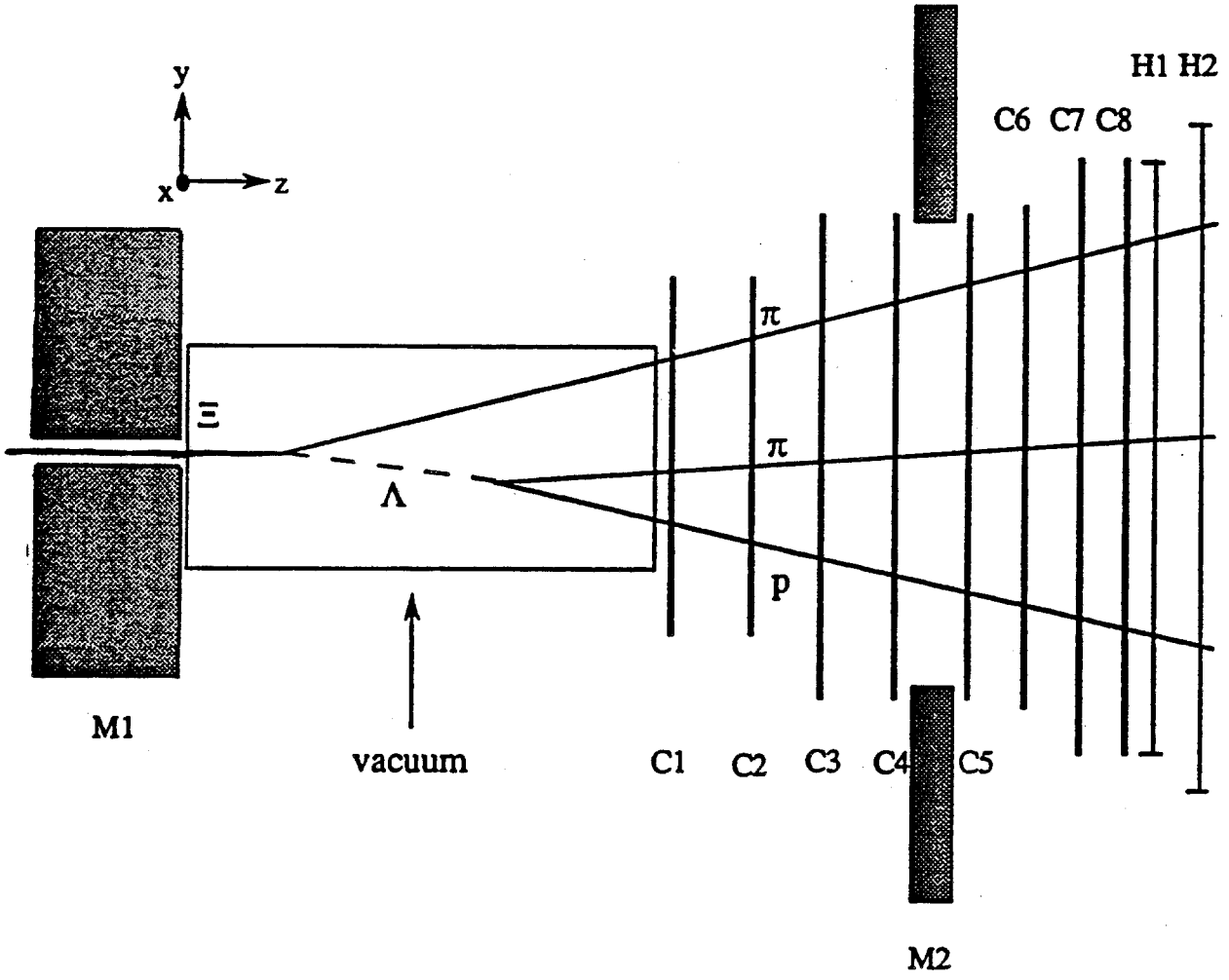

not to scale

Figure 4: Elevation view of spectrometer.

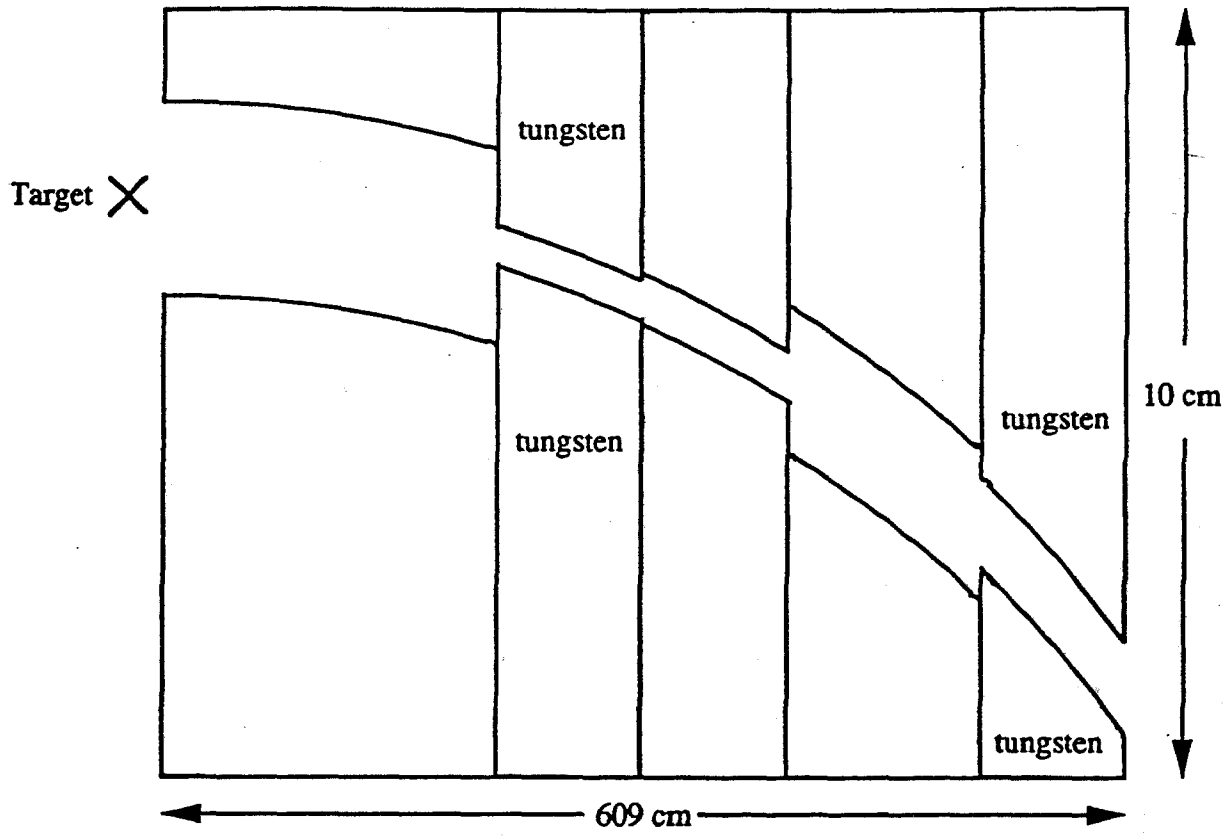

(a) Bend view

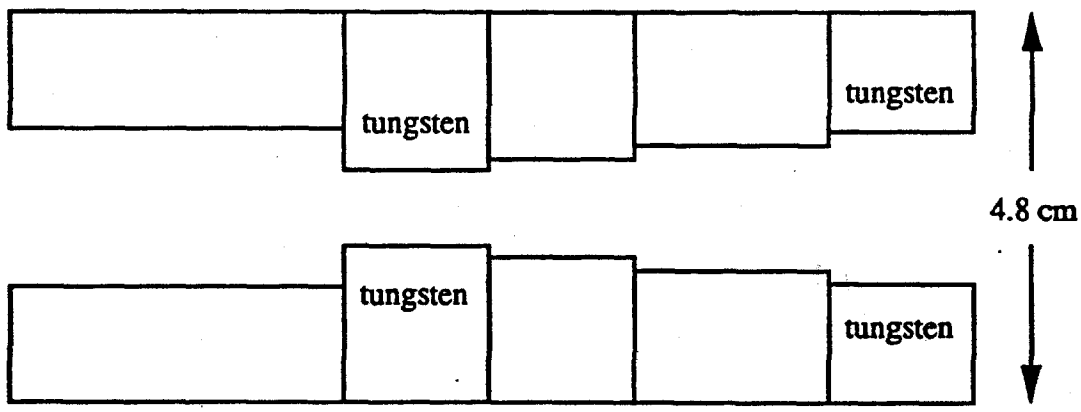

(b) Non-bend view

Figure 5: Hyperon channel.

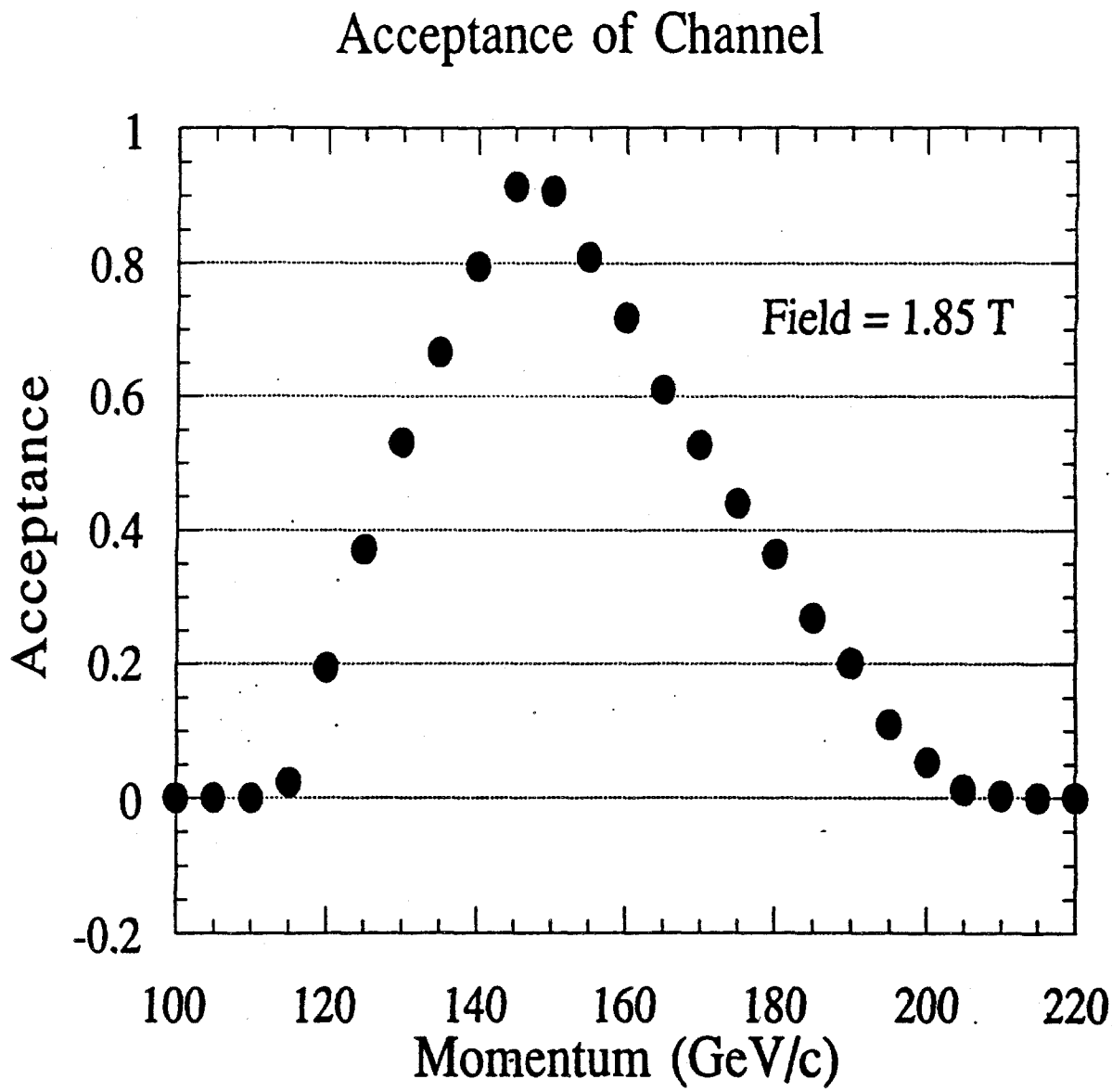

Figure 6: Hyperon channel acceptance.

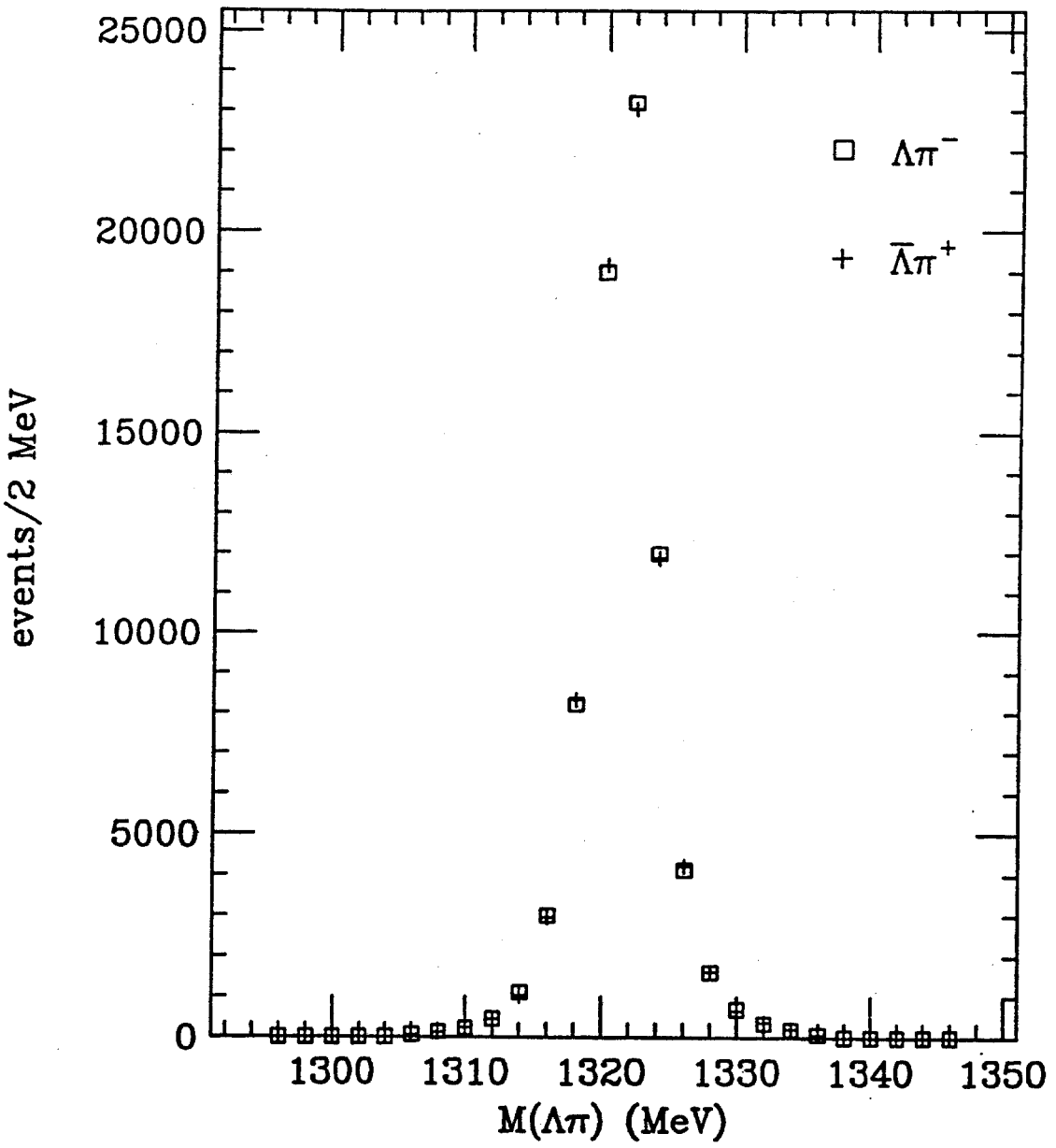

Figure 7: Comparison between the $\Lambda^{\circ}\pi^{-}$ and $\overline{\Lambda}^{\circ}\pi^{+}$ invariant masses from E756.

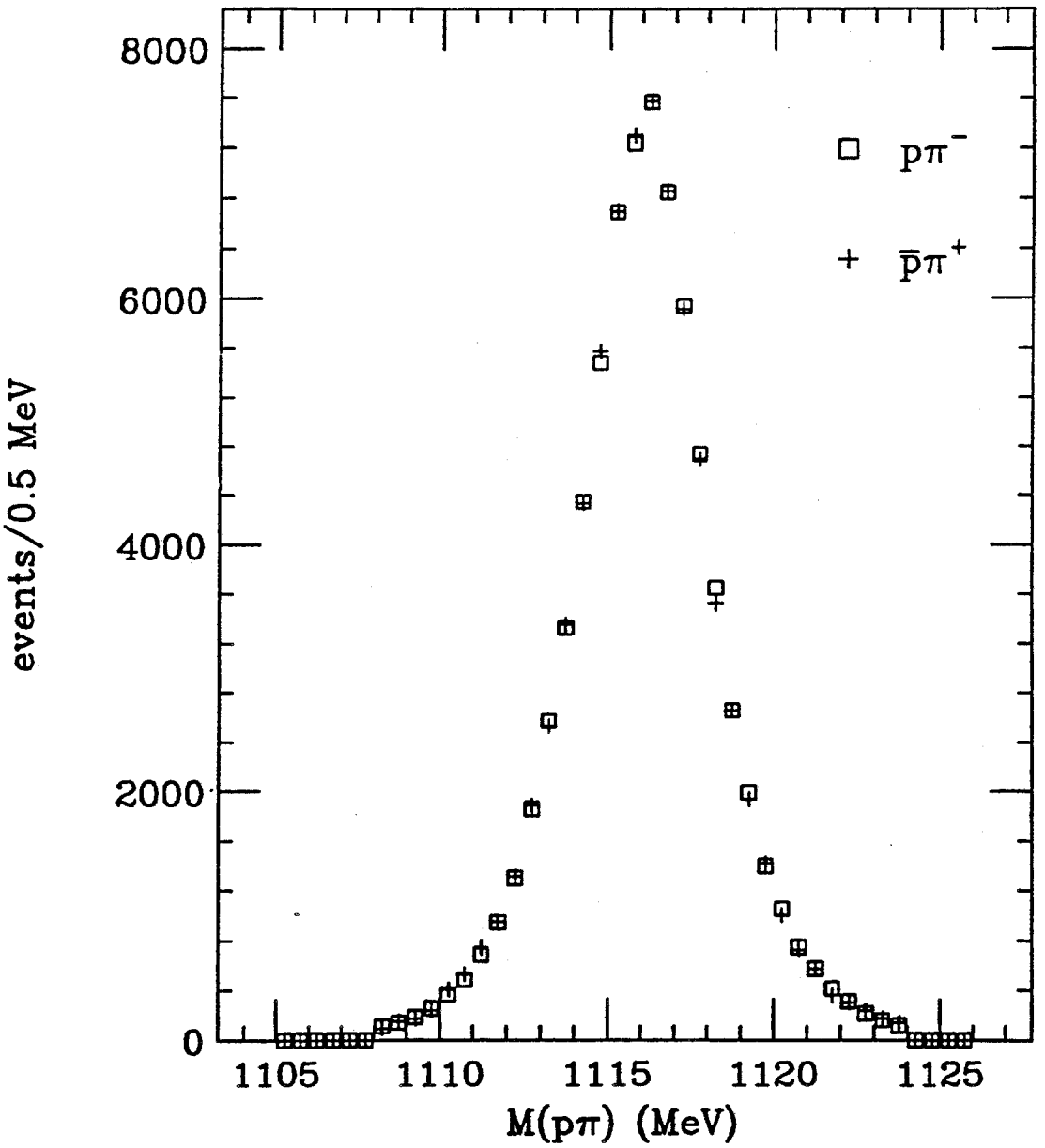

Figure 8: Comparison between the $p\pi^-$ and $\bar{p}\pi^+$ invariant masses from E756.

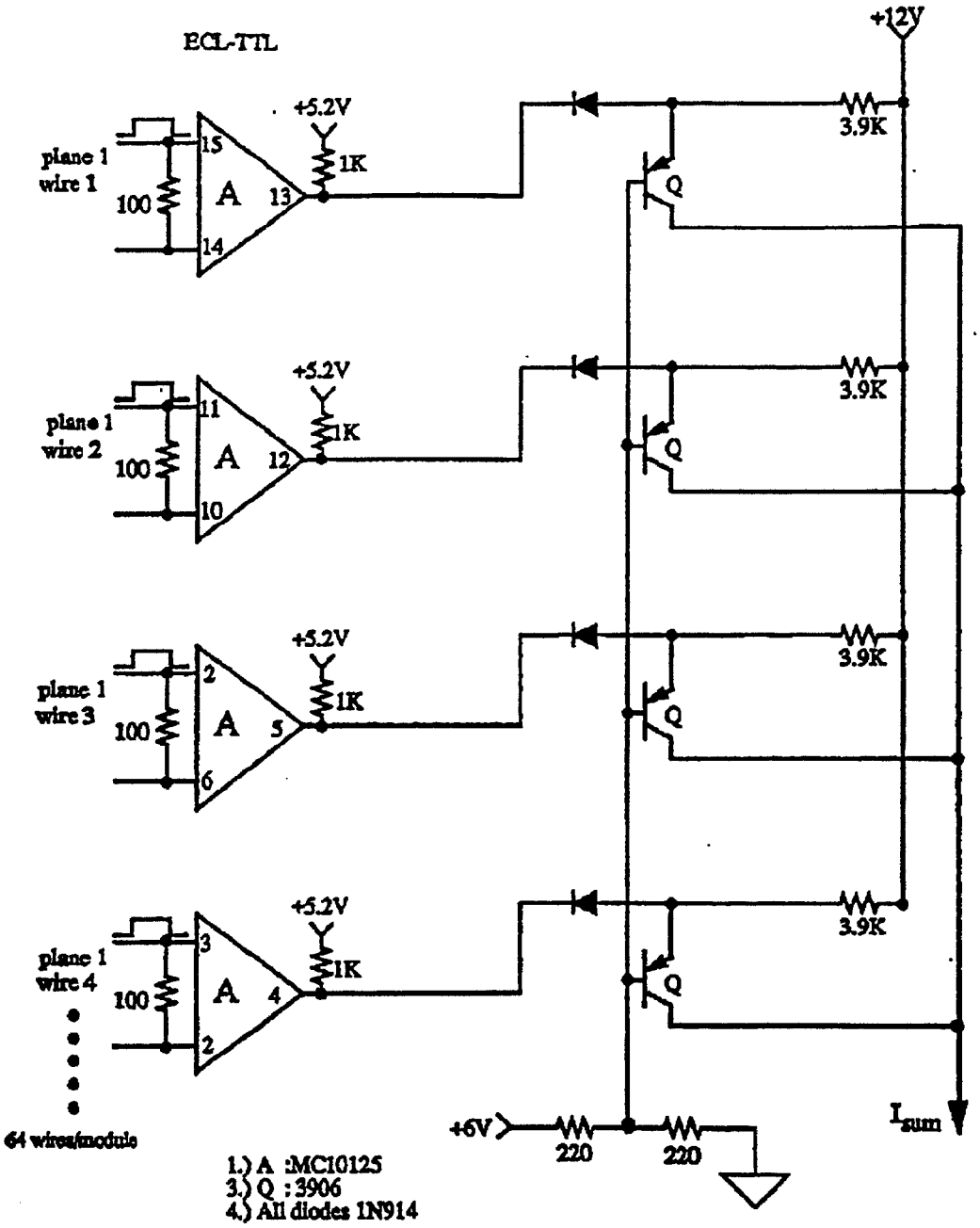

Figure 9: A set of line receivers and currents switches used to form a current sum proportional to the number of PWC wire hits. One NIM module of this type would serve 64 wires.

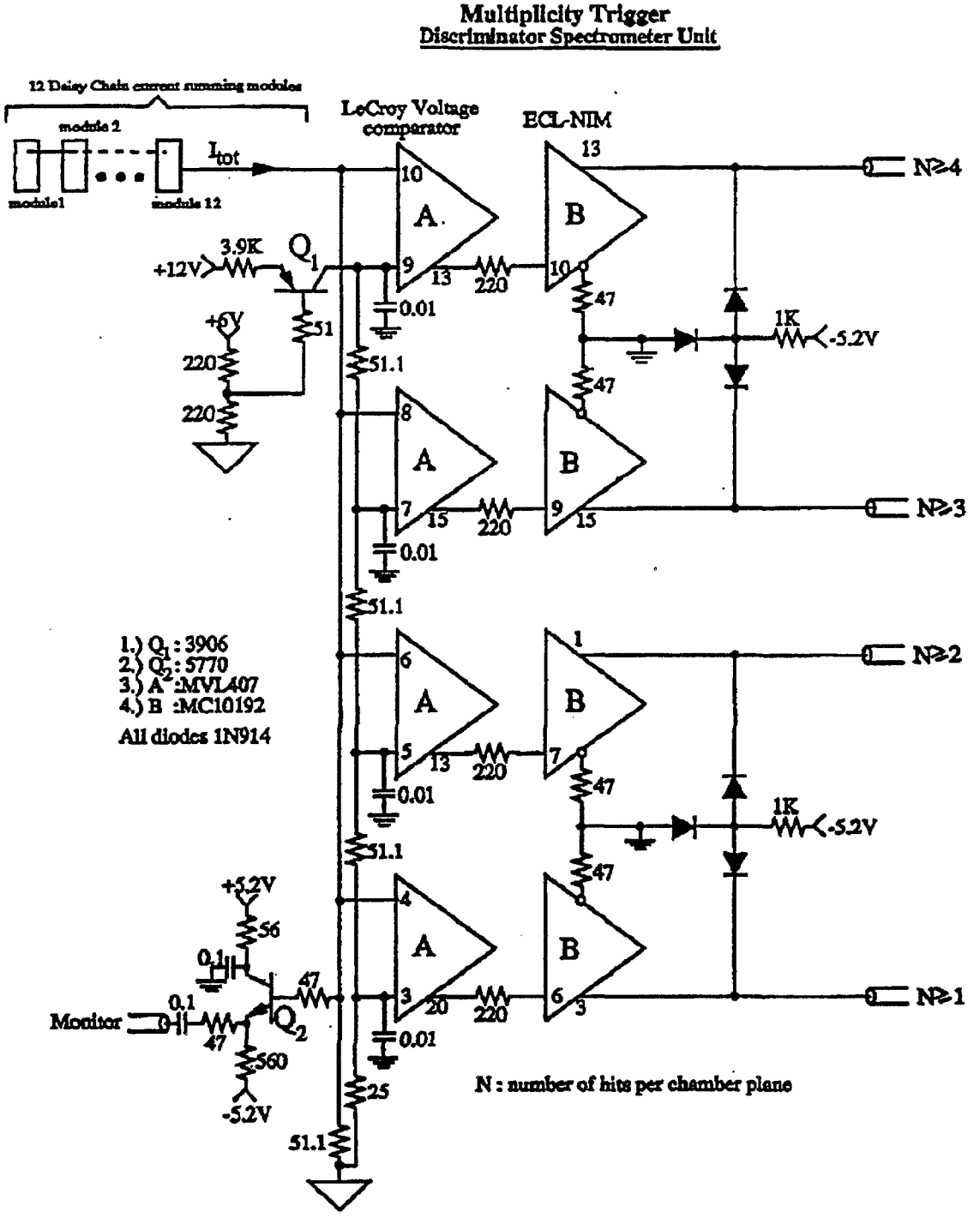

Figure 10: A comparator which gives separate outputs for current sums corresponding to more than 1, 2, 3, or 4 hits in a plane.

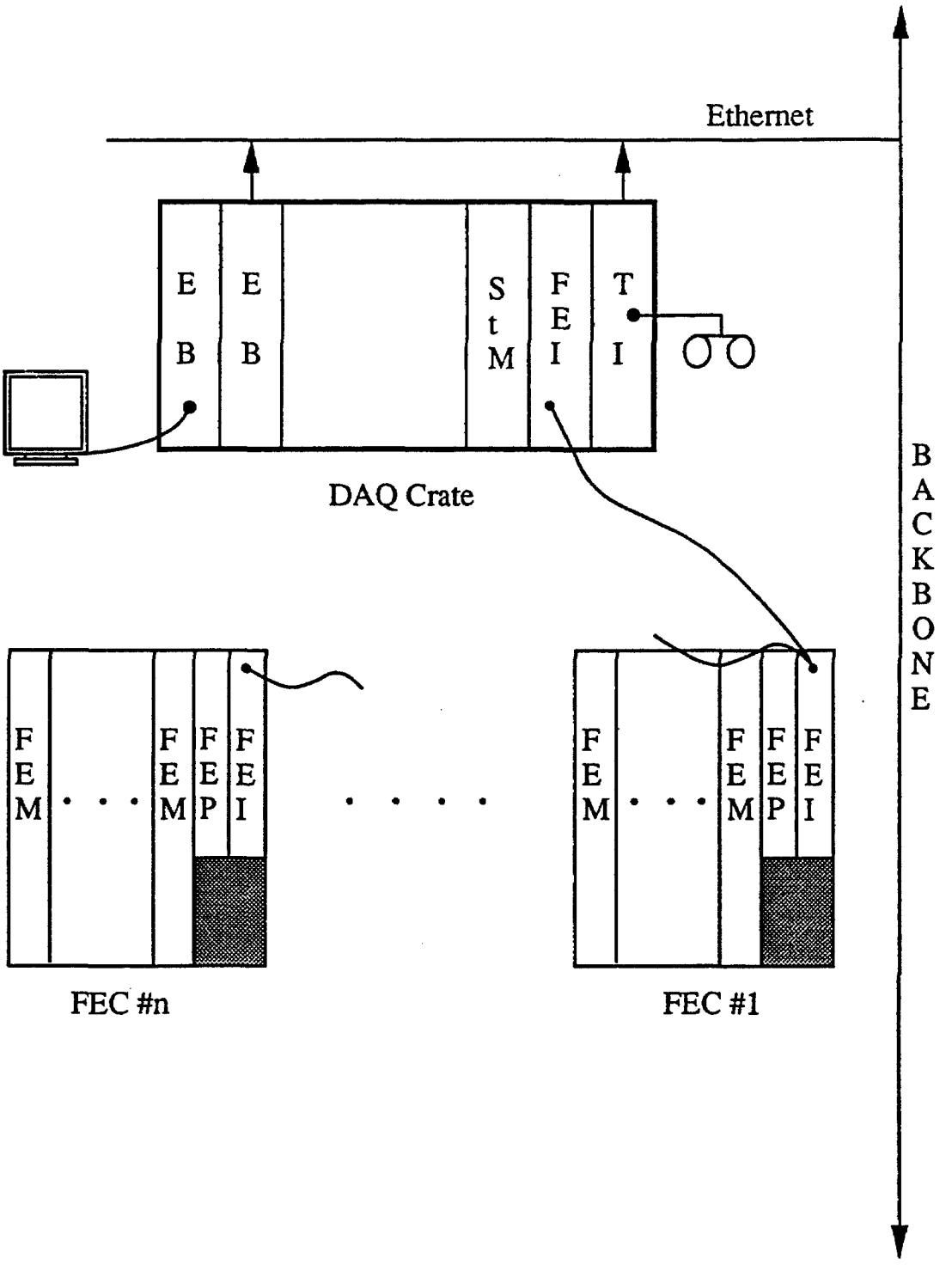

Figure 11: Layout of the data acquisition system.

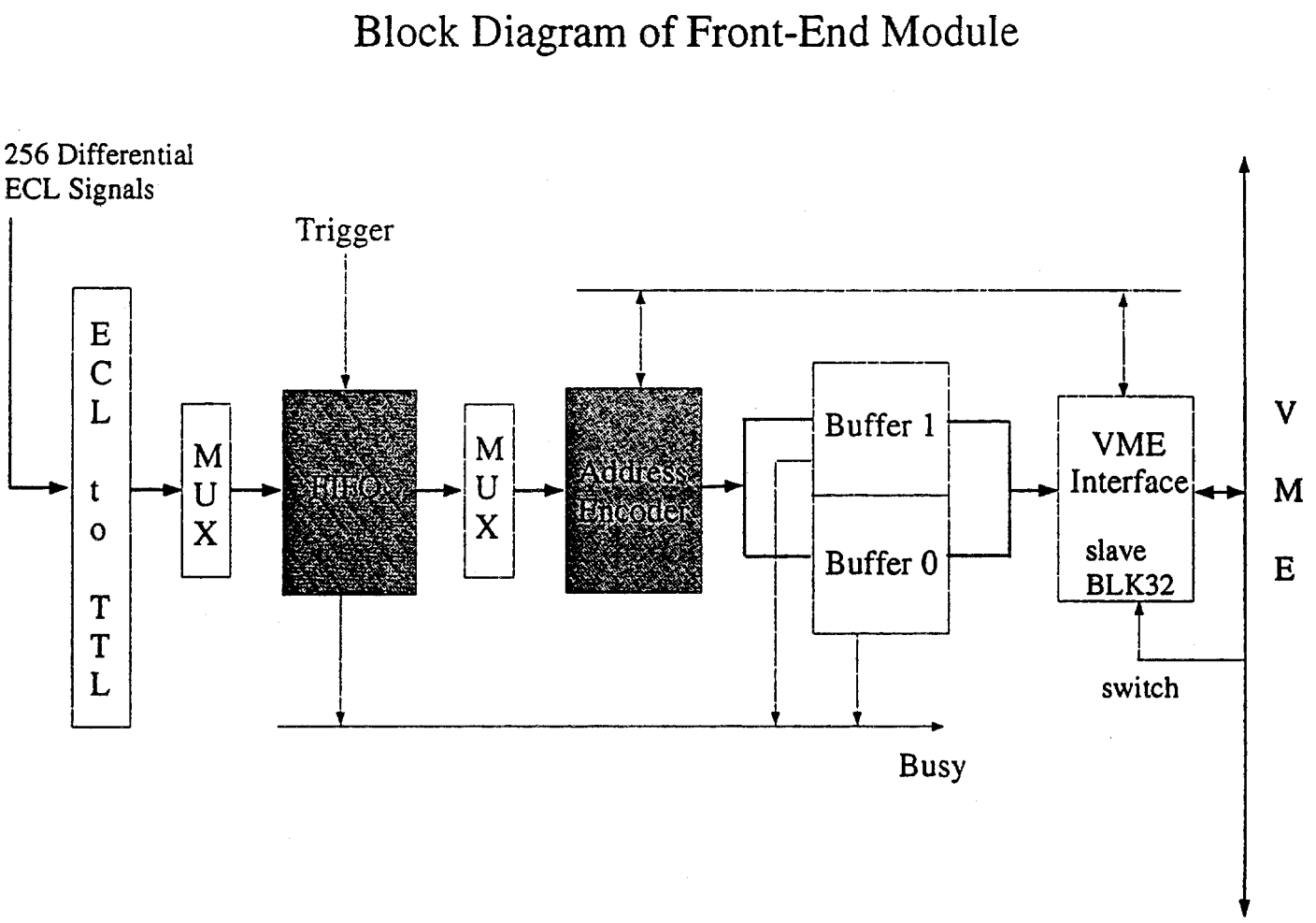

Figure 12: Block diagram of a front-end module.

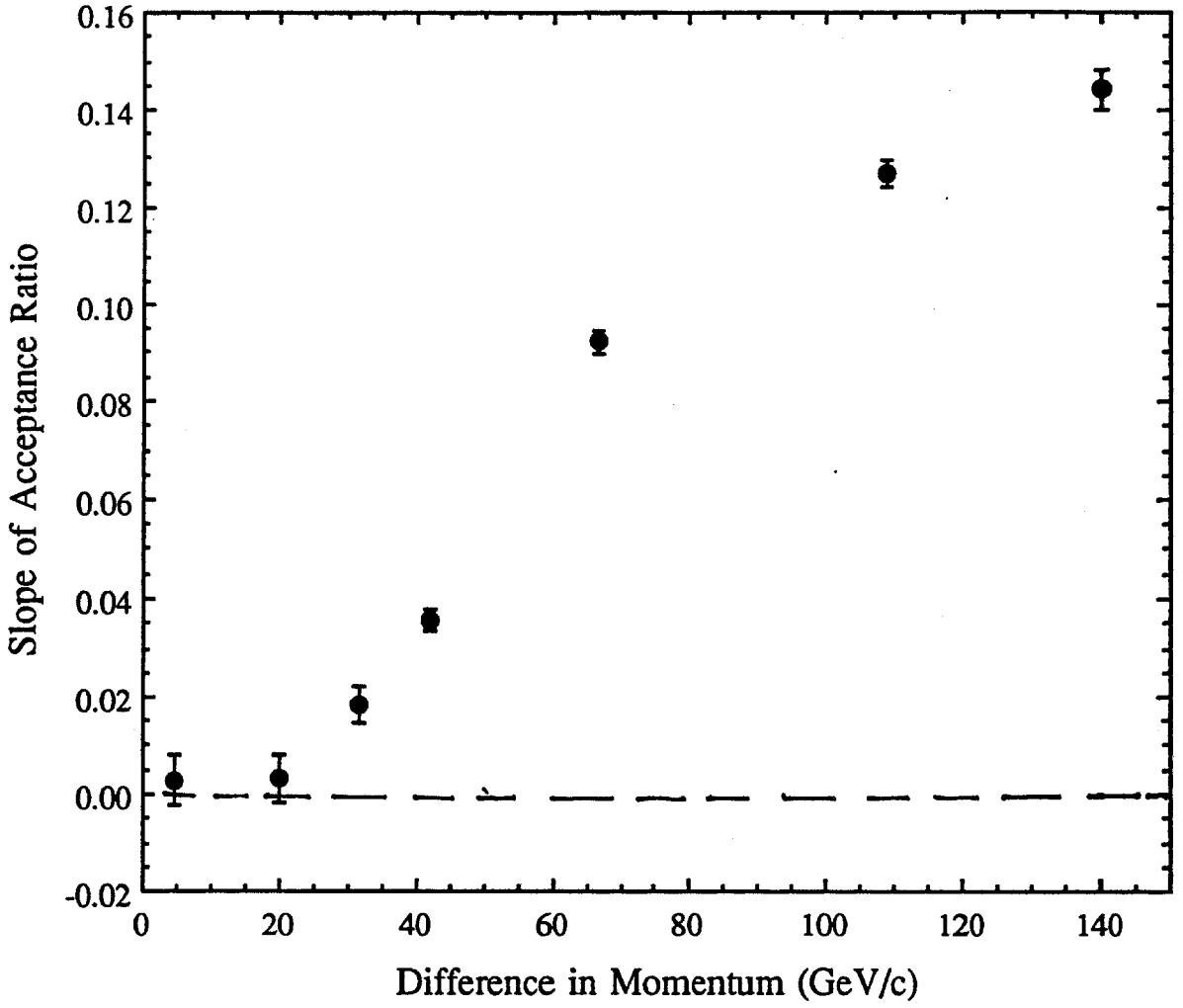

Figure 13: Acceptance difference along the Λ° helicity axis in the Λ° rest frame as a function of momentum difference between two Ξ^- samples

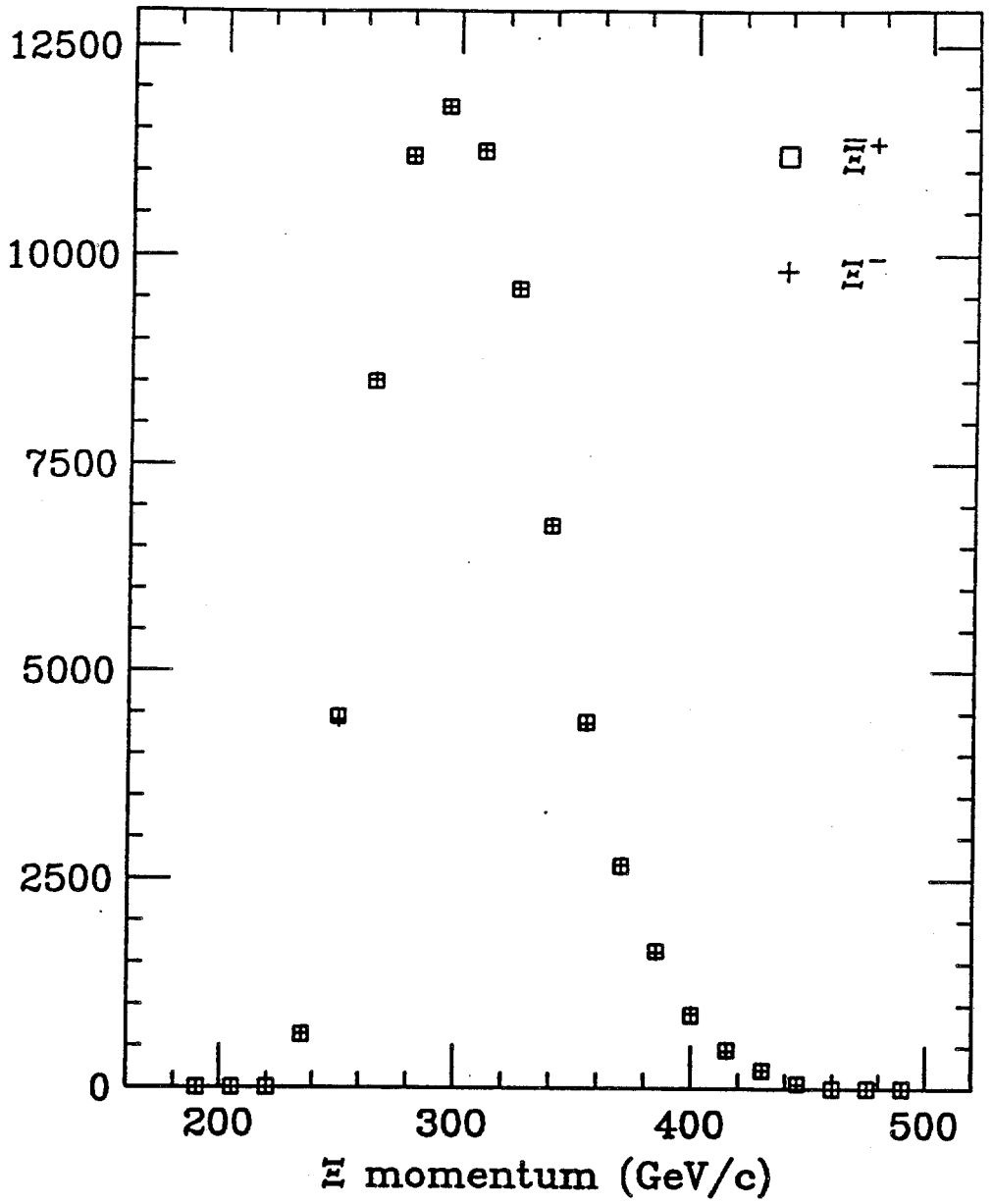

Figure 14: Comparison between the Ξ^- and $\overline{\Xi}^+$ momenta from E756, after normalization.

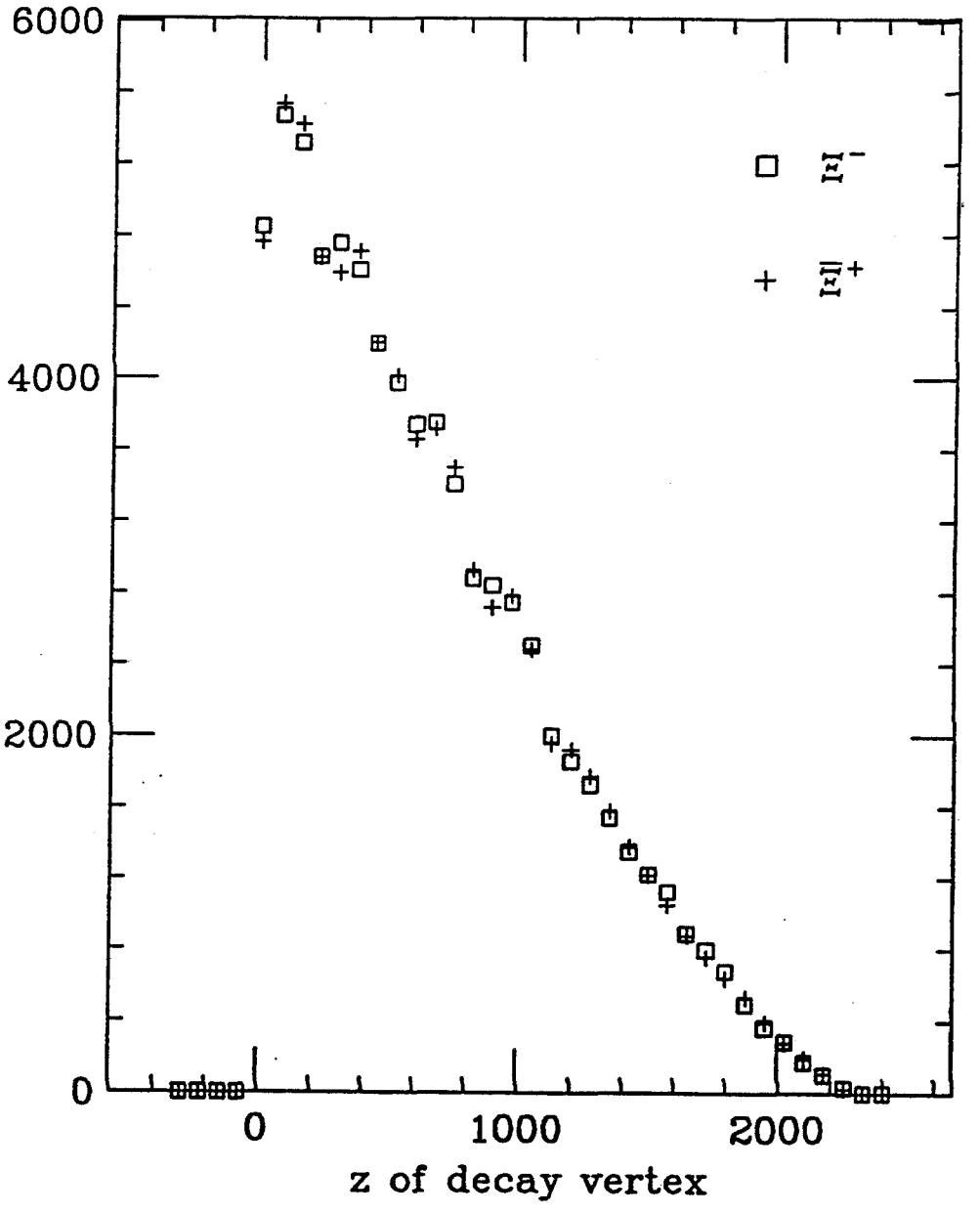

Figure 15: Comparison between the Ξ^- and $\bar{\Xi}^+$ z decay vertices for E756.

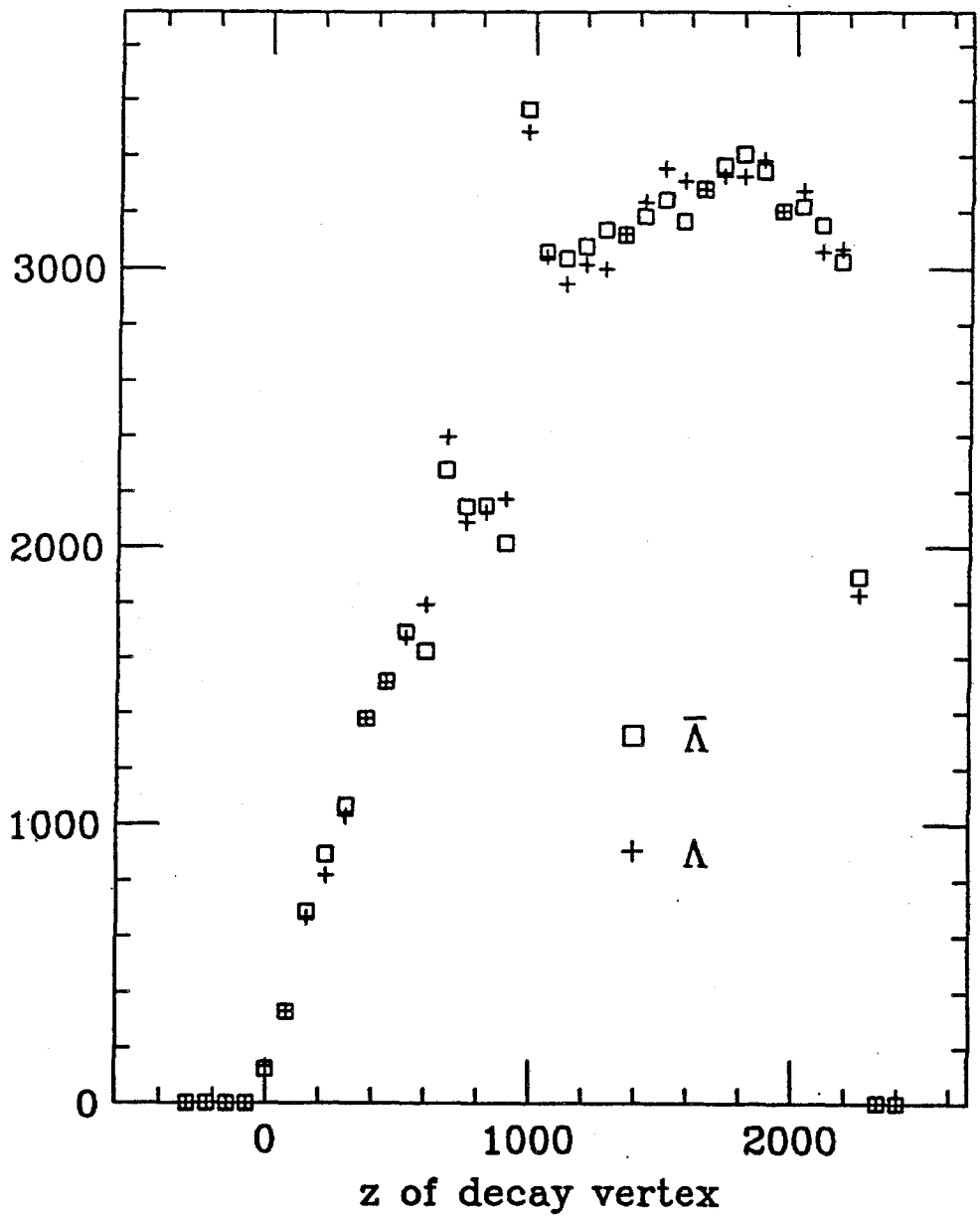

Figure 16: Comparison between the Λ^0 and $\overline{\Lambda^0}$ z decay vertices from E756.

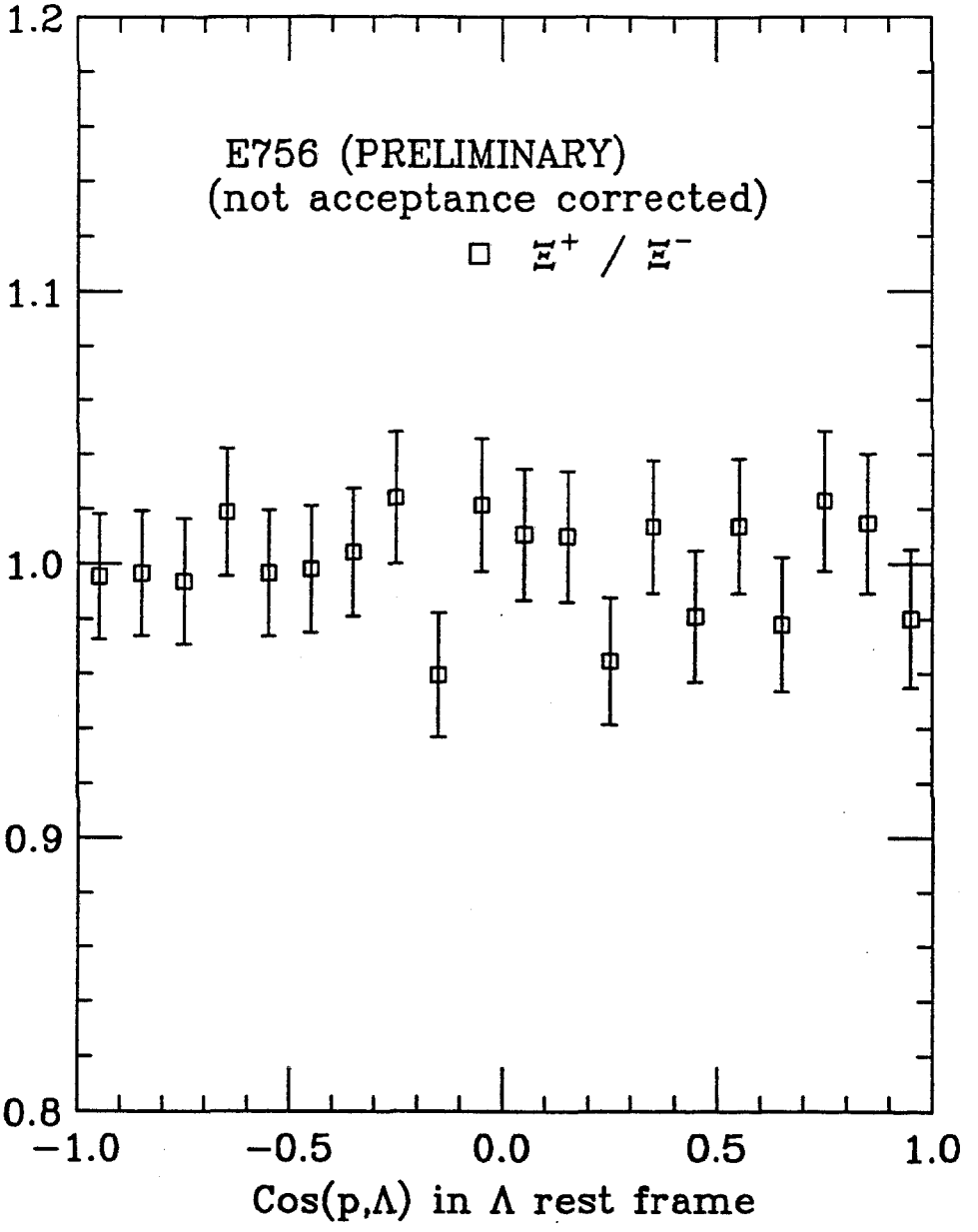

Figure 17: The Comparison between the cosine of the proton and antiproton polar angles in the Λ° and $\overline{\Lambda}^\circ$ rest frames. (The sign of the cosine has been reversed.) No significant difference is evident.

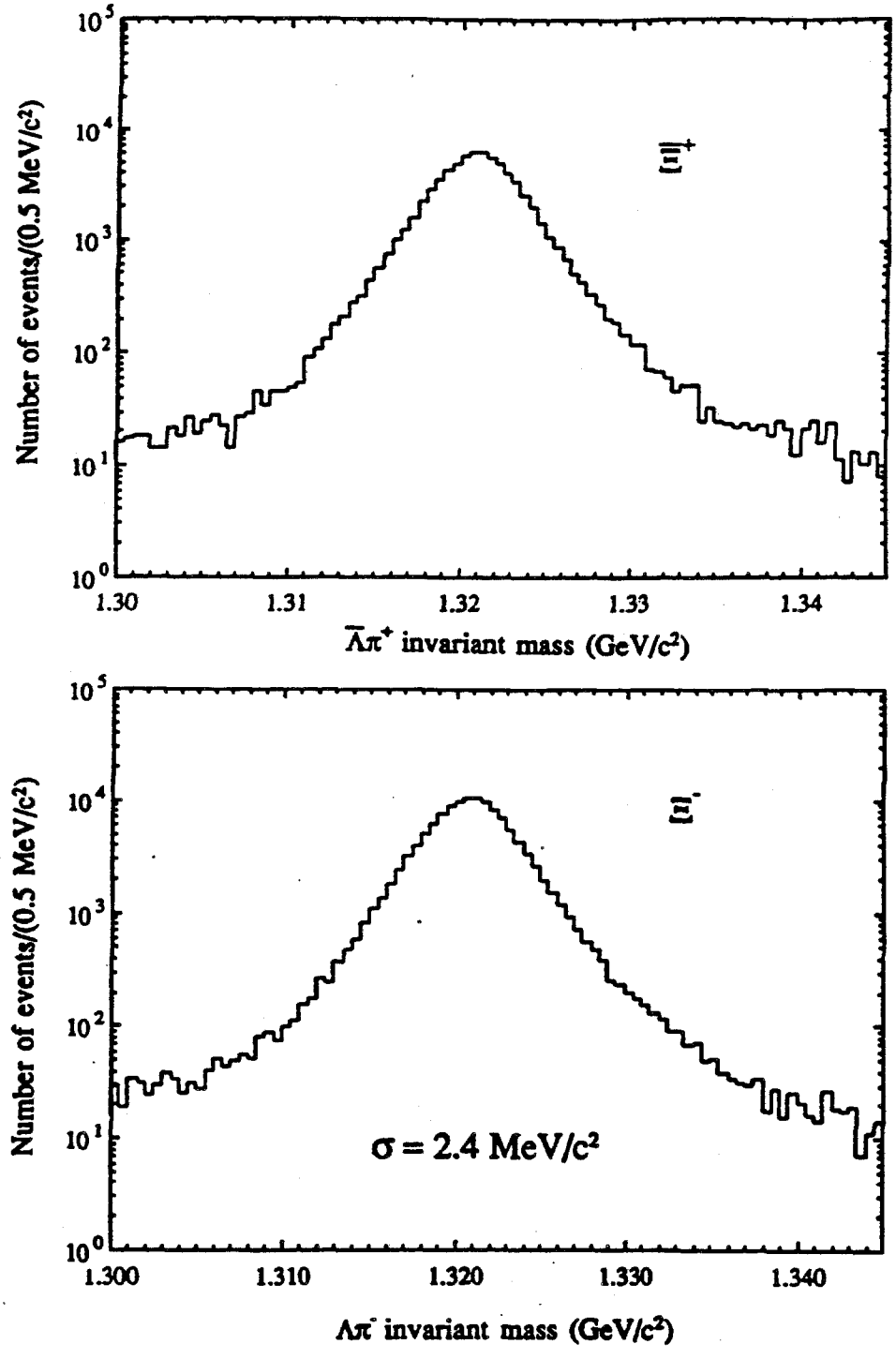

Figure 18: The $\Lambda^\circ\pi^-$ and $\overline{\Lambda}^\circ\pi^+$ invariant masses from E756 showing the level of the background.

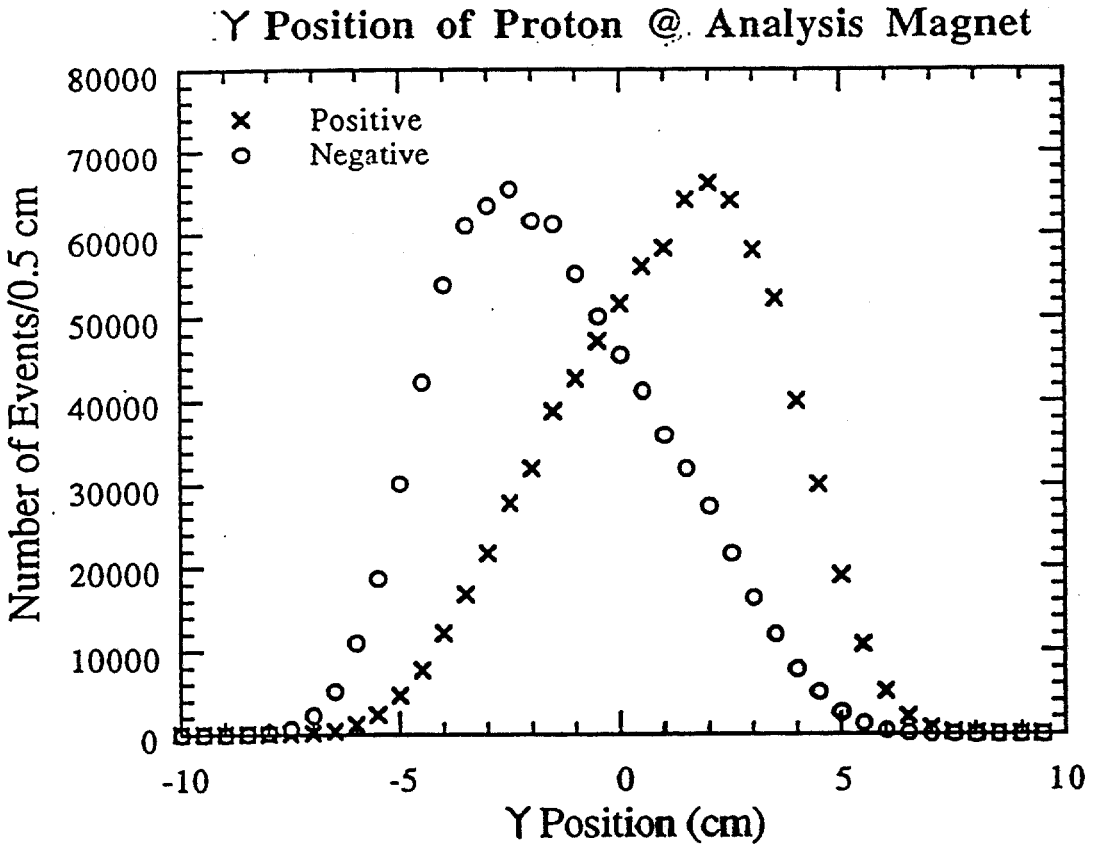

Figure 19: The y position of the proton at the analyzing magnet. The solid (dashed) curve is protons from Ξ^- decays that were produced from protons targeted at +2.5 mrad (-2.5 mrad).

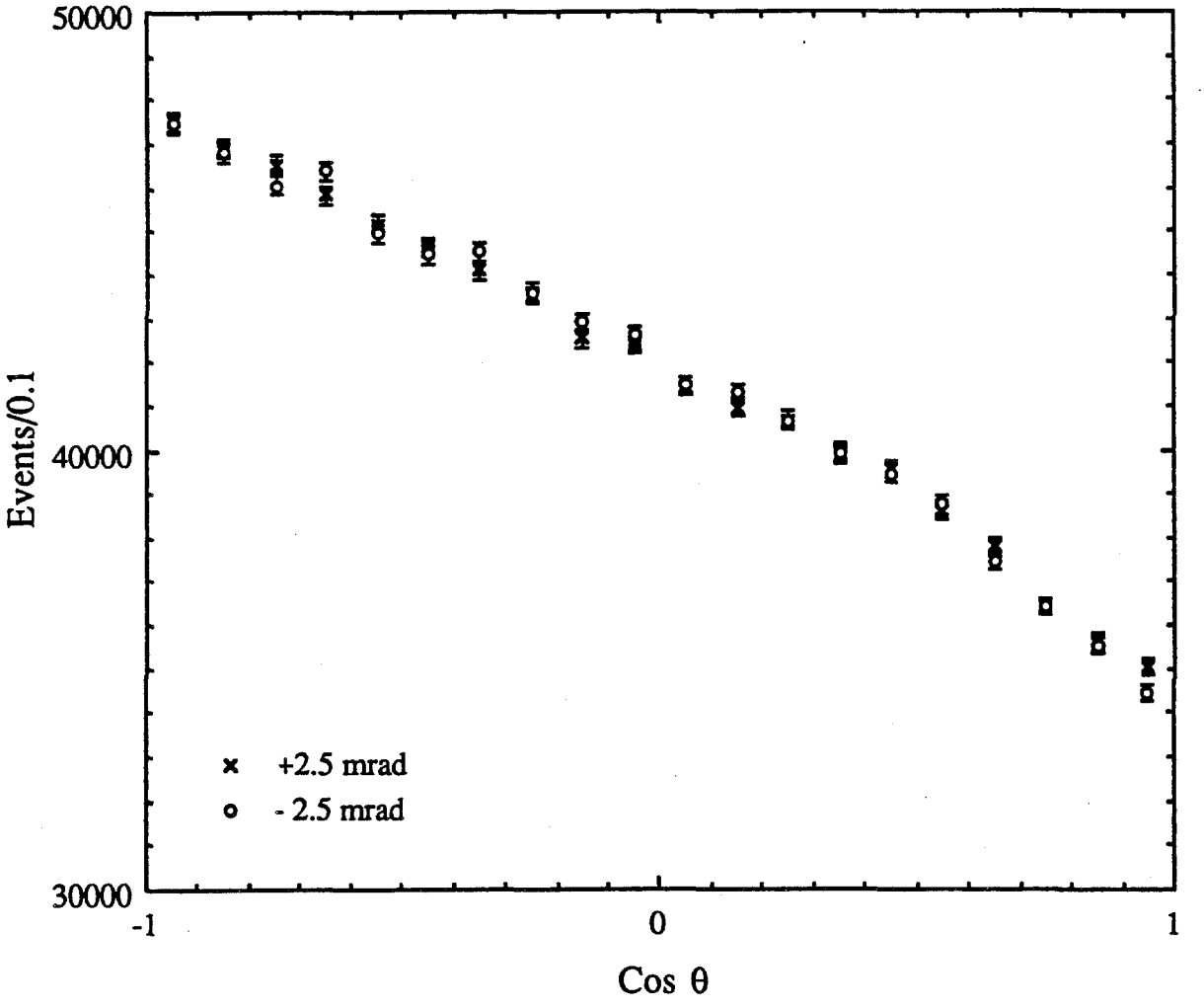

Figure 20: The cosine of the proton polar angle in the rest frame where the Λ^0 defines the z-axis. The solid (dashed) curve is protons from Ξ^- decays that were produced from protons targeted at +2.5 mrad (–2.5 mrad).

871

UNIVERSITY OF CALIFORNIA, BERKELEY

BERKELEY • DAVIS • IRVINE • LOS ANGELES • RIVERSIDE • SAN DIEGO • SAN FRANCISCO

SANTA BARBARA • SANTA CRUZ

DEPARTMENT OF PHYSICS
TEL: 510/642-7166
FAX: 510/643-8497

BERKELEY, CALIFORNIA 94720

March 27, 1993

Dr. John Peoples
Director
Fermilab
Batavia, IL 60510

Dear John,

Enclosed please find a copy of a new proposal outlining a search for direct CP violation in hyperon decay at a significant level of sensitivity. While we are talking to potential collaborators, and continuing to refine the details, especially with regard to the trigger, data acquisition and systematics, we feel that the upcoming PAC meeting should consider this exciting possibility.

Sincerely,

Kam-Biu Luk
Associate Professor of Physics

AA0447

Fermilab Proposal P-871

A Search for CP Violation in the Decays of $\Xi^-/\overline{\Xi}^+$ and $\Lambda^\circ/\overline{\Lambda}^\circ$ Hyperons

G. Gidal, P.M. Ho, and K.B. Luk[1]

Lawrence Berkeley Laboratory and the University of California, Berkeley, CA 94720

E.C. Dukes[2]

University of Virginia, Charlottesville, VA 22901

March 21, 1993

[1]Spokesperson
[2]Deputy Spokesperson

Abstract

We propose to perform a sensitive search for *CP* violation in Ξ and Λ decays. Unpolarized Ξ^- and $\overline{\Xi}^+$ hyperons are produced by protons and momentum selected with a magnetic channel. The decay sequences $\Xi^- \to \Lambda^\circ\pi^-$; $\Lambda^\circ \to p\pi^-$ and $\overline{\Xi}^+ \to \overline{\Lambda}^\circ\pi^+$; $\overline{\Lambda}^\circ \to \overline{p}\pi^+$ are detected with a simple wire chamber spectrometer with high-rate capability. By studying the angular distribution of $p(\overline{p})$ with respect to the helicity axis in the $\Lambda^\circ(\overline{\Lambda}^\circ)$ rest frame, the product of the decay parameters $\alpha_\Lambda\alpha_\Xi(\alpha_{\overline{\Lambda}}\alpha_{\overline{\Xi}})$ can be extracted. Any difference between $\alpha_\Lambda\alpha_\Xi$ and $\alpha_{\overline{\Lambda}}\alpha_{\overline{\Xi}}$ is evidence that *CP* symmetry is violated. In a typical Fermilab fixed target run, 4×10^9 Ξ^- and $\overline{\Xi}^+$ decays can be collected, enabling a measurement of the relevant asymmetry to 10^{-4} sensitivity; the level of theoretical predictions for the asymmetry, and well over two orders of magnitude better than at present. A non-zero asymmetry would be the first evidence of *CP* violation outside of the neutral kaon system and would be evidence of direct *CP* violation.

1 Introduction

In the almost 30 years since the discovery of *CP* violation [1], our understanding of the phenomenon has improved little despite a long series of beautiful experiments. It still remains a small peculiarity unique to the neutral kaon system. Although *CP* violation can be accommodated nicely within the framework of the standard model, its origin and magnitude remain a profound mystery and many questions need to be answered before we can claim to have an understanding of it. Perhaps foremost among these is whether *CP* violation is a phenomenon unique to the neutral kaon system or a property shared by other particles. The standard model tells us that it should be evident elsewhere — in the decays of hyperons and neutral B mesons for example — but no experiment has been able to achieve the necessary sensitivity to see *CP* violation outside of the neutral kaon system. Another outstanding question is whether *CP* violation occurs only in $|\Delta S| = 2$ weak decays — as is predicted by the superweak model of Wolfenstein [3] — or is also evident in direct $|\Delta S| = 1$ transitions, as is predicted by the standard model. Despite an impressive experimental effort, both at Fermilab [4] and CERN [5], the question remains open.

For some time it has been known that *CP* violation should manifest itself in the decays of hyperons: in differences in the angular distribution of the daughter baryons between particle and antiparticle [6]. The asymmetries are expected to be small and were presumed to be difficult if not impossible to measure experimentally. In the past decade, however, considerable advances have been made in the development and operation of very high-rate spectrometers. It is no longer inconceivable for an experiment to acquire in a year's time the order of a billion events needed to measure such asymmetries. Recently E756 at Fermilab — an experiment measuring both the $\overline{\Xi}^+$ magnetic moment and polarization [7] — has shown that copious numbers of $\overline{\Xi}^+$ hyperons can be acquired with a simple trigger and with very little background. Analysis of the difference between the daughter decay distributions in the Ξ^- and the $\overline{\Xi}^+$ samples — the signature for *CP* asymmetry — shows no evidence of false asymmetries. This is extremely encouraging considering the fact that the experiment was by no means optimized to measure small asymmetries between Ξ^- and $\overline{\Xi}^+$ decays. The E756 collaboration expects to report a result with a sensitivity of 10^{-2} which is better than any previous measurement.

In light of these facts, we have examined the possibility of measuring *CP* violation in a dedicated experiment analyzing the non-leptonic decays of charged Ξ and Λ hyperons. We find that in a standard Fermilab fixed target run a sensitivity of 10^{-4} can be achieved in the comparison of the α decay parameters of the $\Xi^-(\overline{\Xi}^+)$ and $\Lambda^\circ(\overline{\Lambda}^\circ)$. This is a sensitivity on the order of the theoretical predictions of the standard

model (as well as other models of *CP* violation), and over two orders of magnitude better than the world average experimental limit of -0.03 ± 0.06 [2] in $\Lambda^\circ(\overline{\Lambda}^\circ)$ decays. Observation of an asymmetry would provide the first evidence of *CP* violation outside of the neutral kaon system as well as evidence of direct *CP* violation. Because of the importance of *CP* violation to our understanding of the standard model we feel that this experiment should be pursued vigorously at Fermilab. We emphasize that the experiment can be done with relatively modest effort and expenditure.

2 Signatures for CP Violation in Hyperon Decays

The phenomenology of *CP* violation in hyperon decays has been discussed in several excellent references (see Ref. [12] for example). We briefly review it here. Because the nonleptonic weak decays of spin 1/2 hyperons violate parity they can decay into admixtures of both *S*- and *P*-wave final states:

$$\begin{aligned} S &= +S_1 e^{i(\delta_1^S+\phi_1^S)} + S_3 e^{i(\delta_3^S+\phi_3^S)}, \\ \overline{S} &= -S_1 e^{i(\delta_1^S-\phi_1^S)} - S_3 e^{i(\delta_3^S-\phi_3^S)}, \\ P &= +P_1 e^{i(\delta_1^P+\phi_1^P)} + P_3 e^{i(\delta_3^P+\phi_3^P)}, \\ \overline{P} &= +P_1 e^{i(\delta_1^P-\phi_1^P)} + P_3 e^{i(\delta_3^P-\phi_3^P)}. \end{aligned}$$

Here δ and ϕ are the strong and weak phases, and the subscripts 1 and 3 refer to the $\Delta I = 1/2$ and $\Delta I = 3/2$ isospin transitions. Note that under the combined operation of *CP* the *S*-waves and the weak phases change sign.

In terms of the *S*- and *P*-wave amplitudes, the hyperon non–leptonic decays are conventionally described by the Lee–Yang variables: α, β, and γ [8]:

$$\begin{aligned} \alpha &= \frac{2\mathrm{Re}(S^*P)}{|S|^2+|P|^2}, \\ \beta &= \frac{2\mathrm{Im}(S^*P)}{|S|^2+|P|^2}, \\ \gamma &= \frac{|S|^2-|P|^2}{|S|^2+|P|^2}, \end{aligned}$$

where $\alpha^2 + \beta^2 + \gamma^2 = 1$. Often one sees (in the Particle Data Booklet, for example) the parameterization given in terms of α and ϕ where:

$$\begin{aligned} \beta &= \sqrt{1-\alpha^2}\sin\phi, \\ \gamma &= \sqrt{1-\alpha^2}\cos\phi. \end{aligned}$$

Note that ϕ given above is not the same as the weak phase defined previously. Measured values of α, β, γ, and ϕ are given in the Table 1 for the Ξ^- and Λ° hyperons.

Table 1: Ξ^- and Λ° Hyperon Decay Parameters [2].

Mode	α	β	γ	ϕ
$\Xi^- \to \Lambda^\circ\pi^-$	-0.456 ± 0.014	0.062 ± 0.062	0.888 ± 0.008	$(4 \pm 4)^\circ$
$\Lambda^\circ \to p\pi^-$	0.642 ± 0.013	-0.087 ± 0.047	0.762 ± 0.012	$(-6.5 \pm 3.5)^\circ$

The decay distribution of the daughter spin 1/2 baryon in the rest frame of the parent hyperon (the Λ° in the decay $\Xi^- \to \Lambda^\circ\pi^-$, for example) is given by:

$$\frac{dP}{d\Omega} = \frac{1}{4\pi}(1 + \alpha \vec{P}_p \cdot \hat{p}_d), \tag{1}$$

where $\vec{P}_p$ is the parent hyperon polarization and $\hat{p}_d$ is the daughter baryon momentum direction in the rest frame of the parent. The daughter itself is polarized with a polarization given by:

$$\vec{P}_d = \frac{(\alpha + \vec{P}_p \cdot \hat{p}_d)\hat{p}_d + \beta(\vec{P}_p \times \hat{p}_d) + \gamma(\hat{p}_d \times (\vec{P}_p \times \hat{p}_d))}{(1 + \alpha \vec{P}_p \cdot \hat{p}_d)}. \tag{2}$$

Note that in the case of an unpolarized parent the daughter is in a helicity state with a polarization given by the parent α.

Under the operation of CP both α and β reverse sign whereas γ is unchanged. Hence to search for CP violation in hyperon decays one looks for a difference in either the α or β parameters, or in the partial decay rate ($\Gamma \propto |S|^2 + |P|^2$) between the particle and antiparticle. Observables that are sensitive to CP asymmetries include :

$$\Delta = \frac{\Gamma - \overline{\Gamma}}{\Gamma + \overline{\Gamma}}, \tag{3}$$

$$A = \frac{\alpha + \overline{\alpha}}{\alpha - \overline{\alpha}}, \tag{4}$$

$$B = \frac{\beta + \overline{\beta}}{\beta - \overline{\beta}}, \tag{5}$$

$$B' = \frac{\beta + \overline{\beta}}{\alpha - \overline{\alpha}}, \tag{6}$$

where $\overline{\Gamma}$, $\overline{\alpha}$, and $\overline{\beta}$ refer to the antihyperon.

3 Theoretical Predictions

Nonzero values for the observables given in Eqs. (3)–(6) above result from interference between either the S- and P-waves or the $|\Delta I| = 1/2$ and $|\Delta I| = 3/2$ amplitudes.

Model independent expressions for the observables have been explicitly calculated [12]. To leading order they are, for $\Lambda^\circ \to p\pi^-$ decay:

$$\begin{aligned}
\Delta &\cong \sqrt{2}\frac{S_3}{S_1}\sin(\delta_3^S - \delta_1^S)\sin(\phi_3^S - \phi_1^S) \\
A &\cong -\tan(\delta_1^P - \delta_1^S)\sin(\phi_1^P - \phi_1^S), \\
B &\cong \cot(\delta_1^P - \delta_1^S)\sin(\phi_1^P - \phi_1^S), \\
B' &\cong -\sin(\phi_1^P - \phi_1^S),
\end{aligned}$$

and for $\Xi^- \to \Lambda^\circ\pi^-$ decay:

$$\begin{aligned}
\Delta &= 0, \\
A &\cong -\tan(\delta_3^P - \delta_3^S)\sin(\phi_1^P - \phi_1^S), \\
B &\cong \cot(\delta_3^P - \delta_3^S)\sin(\phi_1^P - \phi_1^S).
\end{aligned}$$

The *CP* asymmetry Δ results from the interference between the $|\Delta I| = 1/2$ and $|\Delta I| = 3/2$ amplitudes whereas the other asymmetries are due to the interference of *S*- and *P*-waves. Δ vanishes in Ξ decays because there is only one isospin channel.

Calculations of *CP* asymmetries in hyperon decays are difficult and the predicted asymmetries vary (see Ref. [9] - [16]). For example, predictions of the asymmetry A given by Eq. (4) range from 10^{-3} to 10^{-5}. To calculate the magnitude of the asymmetries requires the values of ϵ, ϵ', the top quark mass and the hadronic matrix elements. Results are not reliable to better than an order of magnitude [16]. However because the $|\Delta I| = 1/2$ amplitudes are about 20 times larger than the $|\Delta I| = 3/2$ amplitudes and because $\sin(\delta_i) \approx 1/10$, Donoghue *et al.* find that $\Delta \approx A/10 \approx B'/100$ [12]. B' is clearly the asymmetry one would want to measure. In only B' do the strong interaction final state phases cancel out, and the predicted magnitude is the largest of all the asymmetries. A is suppressed by the small value of the final state phase shifts whereas Δ is further suppressed by the $|\Delta I| = 1/2$ rule. Unfortunately, as we shall see below, measuring B' is prohibitively difficult.

The magnitudes of the predicted *CP* asymmetries are model dependent. Theories with no $|\Delta S| = 1$ *CP*-odd effects, such as the superweak model and models with a very heavy neutral Higgs, predict no *CP* asymmetries [12]. Models in which $|\Delta S| = 1$ *CP* nonconservation is dominant, such as the Weinberg model [17], predict asymmetries which are on the order of those calculated in the standard model. In the standard model *CP* violation effects are due solely to the complex phase in the Cabbibo–Kobayashi–Maskawa matrix [18], and penguin diagrams are the source of $|\Delta S| = 1$ *CP* asymmetries [19]. The standard model predictions vary quite a bit. For example, Donoghue [14] predicts asymmetries in A which range from $-(0.3 \to 4.0) \times 10^{-4}$ for $\Lambda^\circ(\overline{\Lambda}^\circ)$ hyperons and $-(0.4 \to 4.8) \times 10^{-4}$ for $\Xi^-(\overline{\Xi}^+)$ hyperons, where much of the uncertainty is due to the incomplete knowledge of the hadronic matrix elements.

We should point out that standard model calculations of *CP* violation in hyperon decays are less sensitive to the top quark mass than similar $|\Delta S| = 1$ calculations in $K^\circ \rightarrow \pi^-\pi^+$ decays [16]. The value of ϵ'/ϵ in K° decays decreases with increasing top quark mass, essentially vanishing at a top mass of about 220 GeV/c^2 [20].

4 Comparison with Other Proposed Hyperon CP Violation Experiments

The only data on *CP* violation in hyperon decays comes from the comparison of the alpha parameters in Λ° and $\overline{\Lambda}^\circ$ decays. The experimental limits are weak: the world average compiled by the Particle Data Group is $A = (\alpha_\Lambda + \alpha_{\overline{\Lambda}})/(\alpha_\Lambda - \alpha_{\overline{\Lambda}}) = -0.03 \pm 0.06$ [2]. The three published results are given in Table 2 below. Each of the three experiments used a different technique — and none used the technique we propose here. Their bounds are all limited by statistical, not systematic errors. The first result in Table 2 is from an ISR experiment (R608) which produced Λ° and $\overline{\Lambda}^\circ$ in $pp \rightarrow \Lambda^\circ X$ and $p\overline{p} \rightarrow \overline{\Lambda}^\circ X$ reactions. They quote $\alpha P(\overline{\Lambda}^\circ)/\alpha P(\Lambda^\circ) = -1.04 \pm 0.29$. We have converted their result to a limit on A assuming the polarization is the same for Λ° and $\overline{\Lambda}^\circ$. The data sample consisted of 10,000 $\overline{\Lambda}^\circ$'s and 17,000 Λ°'s. The large error is due to the small polarization of the Λ° and $\overline{\Lambda}^\circ$.

The second result is from the DM2 detector in the Orsay e^+e^- colliding ring DCI. They ran on the J/ψ resonance and used the decays $J/\psi \rightarrow \Lambda^\circ\overline{\Lambda}^\circ$. The branching ratio is small — 1.4×10^{-3} [2] — which is why with a total of 8.6×10^6 J/ψ decays only 770 events were used in the analysis. Nevertheless, because of the large Λ° polarization, their sensitivity is comparable to the R608 measurement. The third result is from a LEAR experiment (PS185) producing Λ° hyperons in the threshold reaction $p\overline{p} \rightarrow \Lambda^\circ\overline{\Lambda}^\circ$. The polarization of the two Λ°'s is assumed to be equal by C-parity conservation in strong interactions. A total of 4063 $\Lambda^\circ\overline{\Lambda}^\circ$ pairs were used in the analysis.

Table 2: Experimental Limits on $A = (\alpha_\Lambda + \alpha_{\overline{\Lambda}})/(\alpha_\Lambda - \alpha_{\overline{\Lambda}})$.

Mode	Limit	Experiment
$p\overline{p} \rightarrow \Lambda^\circ X$, $p\overline{p} \rightarrow \overline{\Lambda}^\circ X$	0.02 ± 0.14	R608 [21]
$e^+e^- \rightarrow J/\psi \rightarrow \Lambda^\circ\overline{\Lambda}^\circ$	0.01 ± 0.10	DM2 [22]
$p\overline{p} \rightarrow \Lambda^\circ\overline{\Lambda}^\circ$	-0.07 ± 0.09	PS185 [23]

There has been considerable interest at CERN in pursuing these measurements to better precision with an improved higher luminosity LEAR (SuperLEAR) [24]. (A proposal has also been submitted to Fermilab to construct a similar facility dedicated

to searching for CP violation in $\Lambda^\circ(\overline{\Lambda}^\circ)$ decays [25].) Unfortunately, due to budget constraints it appears that SuperLEAR will not be built and the LEAR program will end in 1995. Our method has several advantages over threshold experiments in $p\bar{p}$ interactions, which suffer from insufficient yield, large differences between the pN and $\bar{p}N$, as well as the π^+N and π^-N cross sections, and more severely, from the large acceptance corrections that have to be made because the Λ° and $\overline{\Lambda}^\circ$ decay products do not inhabit the same part of the spectrometer. Hence, we feel that our technique is superior to threshold $p\bar{p}$ experiments. Preliminary analysis of the Fermilab E756 data, based on 74,000 $\overline{\Xi}^+$'s and 1.5×10^6 Ξ^-'s, indicates that our approach is systematic-free at the 1% level.

There has also been interest in pursuing hyperon CP violation at a tau-charm factory through the decay process $J/\psi \to \Lambda^\circ\overline{\Lambda}^\circ$. Even with optimistic assumptions on the luminosity and monochromaticity, the expected asymmetry reach is only 5×10^{-4} [26] and hence is not competitive with this proposal.

Only in fixed target experiments at either Fermilab or CERN can sufficient statistics be collected to provide a sensitivity of the 1×10^{-4} level.

5 Experimental Strategy

The four observables for hyperon decays that are sensitive to CP asymmetries are given in Eqs. (3)–(6). The small theoretical predictions for Δ and the difficulty in measuring small differences in rates makes the possibility of finding CP violation through Δ very unlikely. To search for CP violations through measurements of either B or B' requires hyperons and antihyperons with identical or precisely determined polarizations because the β decay parameter can only be determined by measuring the daughter polarization from a polarized parent. Both Ξ^- and $\overline{\Xi}^+$ hyperons have been shown to be polarized when produced with finite transverse momentum by protons in inclusive production [7]. However, the magnitude of the polarizations is only 10% at a p_t of about 1 GeV/c and an x_F of 0.4, requiring a prohibitive number of Ξ^- and $\overline{\Xi}^+$ hyperons to measure the CP asymmetry in β. Furthermore, the polarizations of the Ξ^- and $\overline{\Xi}^+$ are almost certainly different at the required sensitivity level, making measurements of the differences in β extremely difficult. Hence we propose to search for CP-odd asymmetries in the parameter A of Eq. (4).

Determining A requires measuring the α parameters of the hyperon and antihyperon. The α parameter can either be determined by measuring the decay asymmetry of a hyperon of known polarization or by measuring the daughter polarization from either a polarized or unpolarized parent. Measurement of the α parameter is much easier with unpolarized hyperons (or samples with a mean polarization of zero which can be made by combining data sets with equal and opposite polarizations) if the daughter decay analyzes its own polarization. The Ξ^- and $\overline{\Xi}^+$ hyperons are ideal candidates because they decay with large branching ratios (100%) into Λ° and $\overline{\Lambda}^\circ$

whose polarizations can be measured through their weak decay. Unpolarized Ξ^- and $\overline{\Xi}^+$ hyperons are produced by targeting at 0° incident angle. The daughter Λ polarization from an unpolarized Ξ is simply:

$$\vec{P}_\Lambda = \alpha_\Xi \hat{p}_\Lambda. \tag{7}$$

The $\Lambda°(\overline{\Lambda}°)$ is found in a helicity state with polarization given by the $\Xi^-(\overline{\Xi}^+)$ alpha parameter: $|\vec{P}_\Lambda| = 0.456$. A difference between the $\Lambda°$ and $\overline{\Lambda}°$ polarizations is direct evidence of *CP* violation.

The $\Lambda°$ and $\overline{\Lambda}°$ polarizations are measured through the decay asymmetry given by Eq. (1). The asymmetry in the decay proton (antiproton) direction in the $\Lambda°$ $(\overline{\Lambda}°)$ rest frame is given by the product of the $\Lambda°$ and Ξ^- $(\overline{\Lambda}°$ and $\overline{\Xi}^+)$ alpha parameters. We emphasize that *in the absence of CP violation the proton and antiproton distributions should be identical*, as should be every other kinematic variable from the Ξ^- and $\overline{\Xi}^+$ decays.

Because we measure the product of the Λ and Ξ alpha parameters, the *CP* asymmetry extracted is the sum of the Λ and Ξ asymmetries given in Eq. (4) (see Appendix 1):

$$\mathcal{A} = \frac{\alpha_\Lambda \alpha_\Xi - \alpha_{\overline{\Lambda}} \alpha_{\overline{\Xi}}}{\alpha_\Lambda \alpha_\Xi + \alpha_{\overline{\Lambda}} \alpha_{\overline{\Xi}}} = A_\Lambda + A_\Xi, \tag{8}$$

where A_Λ and A_Ξ are defined by:

$$\begin{aligned} A_\Lambda &= \frac{\alpha_\Lambda + \alpha_{\overline{\Lambda}}}{\alpha_\Lambda - \alpha_{\overline{\Lambda}}}, \\ A_\Xi &= \frac{\alpha_\Xi + \alpha_{\overline{\Xi}}}{\alpha_\Xi - \alpha_{\overline{\Xi}}}. \end{aligned}$$

Hence the measured asymmetry is sensitive to *CP* violation in both $\Lambda°$ and Ξ^- alpha parameters. Any cancellation is highly unlikely.

We repeat that the goal of this experiment is to search for direct *CP* violation in $\Lambda°$ and Ξ^- decay by determining the observable $\mathcal{A}$ with a sensitivity at the 10^{-4} level.

6 Yields

The number of events needed to measure the asymmetry to a precision of 1×10^{-4} is 2×10^9 each for Ξ^- and $\overline{\Xi}^+$ (see Appendix 2). For a nominal Fermilab fixed target run of 200 days; 2×10^7 events per day, 14,000 events per spill, and 700 events per second are required. Assuming a 50% duty factor 1,400 *reconstructed* events per second are needed.

6.1 Ξ^- and $\overline{\Xi}^+$ Yields

A magnetic channel selects Ξ^- and $\overline{\Xi}^+$ hyperons with small x_F and a mean p_t of 0 GeV/c, ensuring that the average production polarization is very small if not zero. The $\overline{\Xi}^+$ to π^+ ratio has been measured in p + Cu collisions at 400 GeV [27]. The ratio is about 1×10^{-3} at an x_F of 0.27 and a p_t between 0.0 GeV/c and 0.8 GeV/c which is approximately the kinematic acceptance of the magnetic channel. The π, K, and p yields can be calculated fairly reliably with the parameterization of Malensek [28]. Table 3 is a summary of the yields between 110 GeV and 215 GeV (the momentum bite of the magnetic channel) at 0 mrad for 1×10^{10} 800 GeV protons incident on a 8.84 cm long Be target. The solid angle is taken to be 4.88 μsr.

Table 3: Ξ, π, K, and p yields per 10^{10} protons.

Particle	At target	At exit of channel
$\overline{\Xi}^+$	6.5×10^4	8.5×10^3
π^+	6.5×10^7	2.7×10^7
K^+	6.5×10^6	2.7×10^6
p	3.2×10^7	1.3×10^7
Ξ^-	1.1×10^5	1.5×10^4
π^-	3.6×10^7	1.5×10^7
K^-	2.9×10^6	1.2×10^6

The estimated number of $\overline{\Xi}^+$'s produced at the target is 65,000 per 1×10^{10} protons. This translates to about 8,500 $\overline{\Xi}^+$'s at the exit of the collimator where the loss due to decay in the channel has been taken into account. After correcting for the probability that the $\overline{\Xi}^+$ and $\overline{\Lambda}$ decay in the vacuum region, the spectrometer acceptance, and the branching fraction of $\Lambda^\circ \rightarrow p\pi^-$ (64%), approximately 2,100 events remain. Taking the trigger efficiency, reconstruction efficiency and event selection cuts into account, the final number of $\overline{\Xi}^+$'s is about 1,500 per 1×10^{10} protons. The thoroughly tested E756 Monte Carlo and reconstruction programs have been used to estimate the efficiencies.

The Ξ^- cross section at low x_F and small transverse momentum has not been measured at high energies. However, the invariant cross section of Ξ^- hyperons produced by 800 GeV protons on Be at 2.5 mrad has been measured by E756. The result is similar to the E495 measurement of the Ξ° cross section at 5 mrad with 400 GeV protons [29]. (In the CERN hyperon experiment the Ξ^- and Ξ° production cross sections were found to be identical [30].) Hence we use the parameterization given by E495 for Ξ° production to estimate the Ξ^- yield at 0 mrad. The number of Ξ^-'s at the collimator exit is approximately 1.5×10^4. With all efficiencies folded in, the expected number of Ξ^-'s is 2,650 per 1×10^{10} protons.

7 Experimental Design

The design of the apparatus is based on 15 years of experience in doing hyperon physics at Fermilab, and in particular, the experience gathered in E756 [7]. The spectrometer is simple with only the momentum of charged particles being measured: no calorimetry and no particle identification is needed. The emphasis is on good acceptance, high efficiency, and high-rate capability. The Ξ^- and $\overline{\Xi}^+$ events will be produced, trigger selected and analyzed under almost identical conditions. This approach has been tested successfully in E756.

Although the spectrometer described in this section is similar to E756, it is vastly superior in rate capability. The wire chambers and readout used in E756 were designed and built 20 years ago and are not suitable for high-rate experiments. The maximum trigger rate in E756 was 500 Hz. We intend to increase this rate by two orders of magnitude.

Figures 1 and 2 are the plan and elevation views of the apparatus. The spectrometer, approximately 60 m long and 2 m wide, consists of a hyperon magnet (M1), 8 wire chamber stations (C1–C8), a momentum analyzing magnet (M2) and two planes of hodoscopes (H1–H2) for timing and triggering purposes.

7.1 Beam

The hyperons will be produced by an 800 or 900 GeV primary proton beam with an intensity of 2×10^{11} per 20 second spill. The beam should have a Gaussian profile with a full width at half maximum of about 1 mm when it is focussed on the target. The beam divergence should be kept as small as possible. Similar to the layout in E756, the beam position immediately upstream of the target is monitored with two 0.5 mm wire pitch SWIC's separated by 2 m. This arrangement determines the targeting angle to better than 0.5 mrad. For particles produced with a momentum of 150 GeV/c, the resolution in the transverse momentum due to the uncertainty in the targeting angle is only 75 MeV/c. Although we plan to take most of the data at 0 mrad production angle, it is important that the primary proton beam can be targeted at a production angle up to ± 5 mrad in the vertical and horizontal planes for systematic studies as well as Ξ^- and $\overline{\Xi}^+$ yield measurements.

7.2 Target

Two targets, one for Ξ^- and the other for $\overline{\Xi}^+$ production, will be mounted on a target holder that can be moved remotely in the vertical as well as the horizontal direction. This allows fine tuning of the target position with respect to the spectrometer so that the secondary beam is symmetrically produced with respect to the nominal production direction. The targets will be identical in size, will be short to minimize potential target size effects, and will have different interaction lengths in order to produce the

same charged particle flux in the spectrometer. A high A target is preferred for several reasons. The physical length of the target can be made shorter and fewer primary protons are needed to produce the required number of Ξ's. The relative yield of hyperons at low x_F is higher with heavy target material [29]. Finally, the Λ° production polarization is known to decrease with increasing A. We expect the Ξ^- and $\overline{\Xi}^+$ production polarizations to have a similar behavior.

7.3 Hyperon Channel

After the primary protons interact with the target, a secondary charged beam is defined by a curved channel embedded in a dipole magnet with a uniform vertical field. The channel consists of brass and tungsten blocks as shown in Fig. 3. The 90 cm-long upstream tungsten block serves as a dump for the beam protons. The defining aperture is 5 mm wide in the bend view and 1 cm high in the vertical direction, giving a solid angle acceptance of 4.9 μsr.

The design of the magnetic channel has been optimized to maximize the Ξ to charged particle ratio and to select a narrow momentum bite. The central orbit of the channel has a radius of 41.89 m and a bend angle, defined by the tangents to the central orbit at the entrance and exit of the channel, of 22.56 mrad. With a field of 1.85 T, the central orbit corresponds to the trajectory of a 150 GeV/c charged particle. The channel acceptance — defined as the fraction of particles within the solid angle that emerge from the exit of the channel — is shown in Fig. 4 as a function of the secondary beam momentum. At 0 mrad production angle, positively charged secondaries are mainly protons with momenta greater than 200 GeV/c. Because of the narrow and lower momentum bite of the channel, these high energy protons are not transported to the spectrometer, effectively increasing the fraction of $\overline{\Xi}^+$'s in the beam.

The 800 GeV primary protons not impacting the target strike the upstream face of the defining collimator at 7.5 mm to the left of the central orbit.

When the magnetic field of the sweeping magnet is reversed, a negatively charged beam is selected. With an NMR probe permanently installed in the collimator, it is possible to reproduce the field to high precision. In E756, even without an NMR, the momentum acceptance of the channel between the two modes agreed to 0.25 GeV/c.

7.4 Magnetic Spectrometer

Measuring the asymmetry to the 10^{-4} level requires a large flux of Ξ's which are accompanied by a much larger flux of charged pions. The limiting factor in the number of Ξ's that can be accumulated is not the production cross section of the Ξ, which is quite large, but the maximum charged fluence the wire chambers can tolerate. In order to collect 1,400 reconstructed $\overline{\Xi}^+$ decays per second the spectrometer must be able to tolerate the passage of 4.2×10^7 Hz of protons and pions when a positively

charged beam is selected (the fraction of Ξ^-'s in the negative beam is larger with the same fluence).

7.4.1 Wire Chambers

The wire chambers must have low mass and high–rate capability. There will be four wire chambers upstream of the analysis magnet and four behind. Table 4 is a summary of the geometry of the wire chambers that has been used in the Monte Carlo studies. Each chamber will have three views, two of them with small vertical stereo angles and the third plane with wires strung vertically. The stereo angle will be chosen so that the resolutions in the bend and non–bend view are comparable. Since there are multiple planes in each view, there is sufficient redundancy to allow the chamber efficiencies to be measured accurately and the tracking efficiency is thus a weak function of the individual plane efficiency.

Table 4: Geometry of wire chambers.

Z (m)	Width (cm)	Height (cm)
26.0	64	30
30.0	64	30
34.0	72	45
38.0	72	45
41.0	72	45
44.0	160	45
47.0	200	60
50.0	200	60

The rate limitation is given by the most upstream chamber which is 26 m downstream of the exit of the collimator. From the Monte Carlo simulation, the beam size at the first chamber is about 10 cm high and 25 cm wide. The rate is approximately $4 \times 10^5 s^{-1} cm^{-2}$ in the busiest region. If a 1 mm wire spacing MWPC is used, the highest rate per wire will be about 0.4 MHz. This is a high intensity, but not above that encountered in other high-rate experiments. For example, the rate is about the same as that experienced in E799, the rare K^0 decay experiment at Fermilab [31]. Wire chambers operating at rates of several times $10^7 s^{-1} cm^{-2}$ have successfully been built [32].

The chambers upstream of the momentum analyzing magnet will have an anode-cathode gap of less than 3 mm, and a small anode wire diameter. Since the particle density after the analysis magnet is reduced, it is possible to use more conventional chambers at that location. All chambers will use a fast gas, for example 80% CF_4

and 20% isobutane, at a gain of a few times 10^4. The preamplifier will have a low input impedance, followed by shaping circuitry to reduce the ion tail.

7.4.2 Analysis Magnet

The momentum analyzing magnet can be a standard BM109 dipole with an aperture of 61 cm wide by 30 cm high and an effective length of 2 m. The transverse momentum kick is approximately 0.75 GeV/c. The field is known to be uniform and can be easily mapped with the Fermilab ziptrack. From the experience gained in E756, the relative field values can be determined to better than 1×10^{-3}. As shown in Fig. 7, the agreement in the Ξ^- and $\overline{\Xi}^+$ masses measured in E756 is excellent.

7.4.3 Hodoscopes

Two vertical planes of hodoscopes, back to back and offset by a small amount from each other in the horizontal direction, will be positioned downstream of the last wire chamber. Each plane is 2 m wide by 0.6 m high and has 32 scintillation counters. The individual counters will have a dimension of 0.6 m by 6.35 cm. They will be used for timing and serve as fast trigger elements.

7.4.4 Decay Region

To minimize the number of interactions in the spectrometer, the 25 m long decay region will be evacuated using a 60 cm diameter vacuum pipe with thin windows at the ends. Space between the chambers will be filled with helium bags or vacuum tanks if possible.

7.5 Trigger and Data Acquisition

We intend to use a trigger which is very similar to that used in E756. In E756 the trigger for selecting Ξ^- and $\overline{\Xi}^+$ decays was the logic combination of two small scintillation counters, two veto counters in anticoincidence, the fast OR signals from the left and right side of the last two chambers, along with a signal based on the pulse height, corresponding to two but less than five minimum ionizing particles, from a 1 cm thick scintillator at the end of the decay region. The yield of fully reconstructed Ξ^- from this trigger was 32%. The yield was much less for the $\overline{\Xi}^+$ mode for the following reasons. The momentum bite accepted by the E756 channel was between 240 GeV/c and 500 GeV/c. In this range, the number of p's and π^+'s was 1×10^6 per spill. With about 3.5% of an interaction length of material in the spectrometer, the trigger rate of 8×10^3 per spill was totally dominated by secondary interactions. Only 20 reconstructed $\overline{\Xi}^+$ decays per spill were left after all cuts. In other words, the trigger yield dropped to 0.25% for $\overline{\Xi}^+$. With PYTHIA coupled to the E756 Monte Carlo program, we can reproduce the trigger rates to within 50%.

We have made two changes to the E756 spectrometer to increase the $\overline{\Xi}^+$ trigger yield. First, by selecting lower momentum particles with the magnetic channel, the ratio of $\overline{\Xi}^+$'s to protons is much higher. Second, we have reduced the amount of material in the spectrometer. By moving the trigger counters which were at the end of the decay region in E756 to the rear of the spectrometer the amount of material has been cut by a factor of four to 0.8% of an interaction length. The multiplicity logic decision from each hodoscope will be ORed to give the fast trigger. The redundancy should ensure an efficiency close to 100%. With 4×10^7 p's and π^+'s going through the spectrometer per second, the trigger rate due to interactions is estimated by Monte Carlo to be 4×10^4 Hz along with 10% of the events written to tape being $\overline{\Xi}^+$'s.

With an event size of 400 bytes (the E756 event size), a bandwidth of at least 20 Mbyte/sec to tape is required during the spill or 7 Mbyte/sec averaged over the spill and interspill period. This is a high throughput data acquisition system, but is comparable to many high-rate fixed target experiments at Fermilab. For example, E791 wrote an average of 9.6 MByte/sec in their 1991 run [33].

We do not intend to, but if necessary we can further reduce the trigger rate by incorporating an online processor that would select events consistent with decays inside the vacuum decay region. A processor similar to those used in E605 and E789 can process a very high multiplicity event in a few μsec, with a rejection factor as high as 10 [34]. Since the hit multiplicity in this experiment is expected to be much lower than those two experiments because of the tight collimation of the hyperon channel, it is likely that the processing time would be lower and the deadtime of the processor should be insignificant. Furthermore, the architecture of such a processor would be very simple, compared with those in E789.

8 Offline Computing Needs

With no trigger processor 4.4×10^4 events/sec will be written to tape. In 200 days of running with a duty factor of 50% the total number of events will be 1.3×10^{11} on 12,000 8mm–5Gb tapes. This is a data sample on the order of that taken by E791 in the 1991 fixed target run [33]. The CPU time required to process the E756 data on a HP-730 workstation (rated 76 MIPS) is 2 msec/event. With a cluster of 10 HP-730 workstations, the entire data set can be processed easily in one calendar year. Workstations with twice the processor power of the HP-730 are currently available (the HP-735, for example).

9 Systematics

The experimental apparatus has been designed to minimize systematic biases producing false *CP* asymmetries. Because the Ξ^- and Λ° alpha parameters change sign under the operation of *CP*, the proton decay distribution in the Λ° rest frame should

be identical to the antiproton decay distribution in the $\overline{\Lambda}^{\circ}$ rest frame. (The Λ° and $\overline{\Lambda}^{\circ}$ distributions in the Ξ^- and $\overline{\Xi}^+$ rest frames should also be identical because the Ξ's are produced with no polarization.) Hence the proton and antiproton decay distributions can be directly compared with no acceptance corrections in order to search for *CP* violation. Extracting the magnitude of an effect, of course, requires knowledge of the acceptance.

The method of analysis minimizes the effects of potential biases. For example, if the $\Lambda(\overline{\Lambda})$ polarization were measured along fixed laboratory axes, small differences in the apparatus acceptance between positive and negative running could map into differences in the $\cos\theta$ distribution of the proton (antiproton), causing a false asymmetry. The Λ polarization, however, is not analyzed along fixed axes in this experiment, but along its momentum direction in the Ξ rest frame. Because of the good Λ acceptance, this direction populates 4π fairly uniformly and there is little correlation between any particular region of the apparatus and a particular part of $\cos\theta$.

There are several potential causes of false *CP* asymmetries. One example is differences between the Ξ^- and $\overline{\Xi}^+$ momentum distributions. In order to minimize such effects we have a small collimator aperture which selects a narrow momentum bite. As a result, the Ξ^- and $\overline{\Xi}^+$ momenta are determined largely by the collimator acceptance rather than by their production properties (which are different). To get an idea of how well the Ξ^- and $\overline{\Xi}^+$ acceptances match we have normalized the E756 momentum spectra to each other and then compared various Ξ^- and $\overline{\Xi}^+$ kinematic quantities from E756. (The momentum bite of the E756 magnetic channel was much broader than this design and hence the Ξ^- and $\overline{\Xi}^+$ momentum spectra were different.) As shown in Figs. 5–9, the comparison is almost perfect — chi-squares per degree of freedom indicate no difference — even though the two data samples were taken at widely different times. (For this experiment we intend to change from Ξ^- to $\overline{\Xi}^+$ running every hour, if not more often.) In particular the comparison between the proton polar angle in the Λ° rest frame, shown in Fig. 10, — the asymmetry we want to measure to search for *CP* violation — shows no statistically significant difference. The backgrounds are also negligible, as is evident in Fig. 11 which shows the $p\pi^-$and $\overline{p}\pi^+$ invariant masses. Most of the continuum in the invariant mass distribution is due to poorly reconstructed events.

Another potential source of bias are slight differences in the positive and negative magnetic fields of the hyperon channel and spectrometer magnets. The BM109 dipole magnets are known to have uniform fields. We intend to measure the differences in the field values to a part in 10^4 in order to control such biases.

Because the Ξ^- and $\overline{\Xi}^+$ data samples will not be taken simultaneously, temporal changes in the apparatus could give rise to false asymmetries. To minimize rate dependent efficiencies in the chambers, we will be careful to run both positive and negative beams such that the charged particle flux at the exit of the collimator is always the same. Nevertheless, at the high charged particle fluences anticipated for the experiment, duty factors and chamber efficiencies are not expected to be

extremely high and localized inefficiencies producing false asymmetries at the 10^{-4} level are conceivable. In order to minimize such effects we intend to add redundant chamber planes at every measurement station. This will allow the individual plane efficiencies to be measured to the desired accuracy and will reduce the dependence of the tracking efficiency on the individual plane efficiency.

The fact that the π^+ and π^- as well as the p and $\bar{p}$ absorption cross sections differ by up to 10% in the momentum region of interest can cause systematic errors. Secondary interactions of the Ξ^- and $\overline{\Xi}^+$ decay products in the wire chambers and helium gas will cause differences in the Ξ^- and $\overline{\Xi}^+$ reconstruction efficiencies. The effects of such differences is being carefully simulated. Preliminary estimates indicate that with material equivalent to less than 1% of an interaction length and a 10% error in the Monte Carlo calculation we can account for the difference in yield to better than a part in 10^4. Corresponding differences in $\alpha_\Xi\alpha_\Lambda$ should be considerably smaller.

Another possible cause of false asymmetries is unequal polarization of the Ξ^- and $\overline{\Xi}^+$ hyperons. There are several possible sources of Ξ polarization: misalignment of the target and collimator, polarization of the proton beam or target, and polarized Ξ's from Ω decays. It is known that Ξ^- and $\overline{\Xi}^+$ hyperons are produced polarized in pN interactions at p_t greater than 0.5 GeV. Hyperons produced with zero transverse momentum are constrained by parity conservation in the strong interaction to have no polarization. Hence, the experiment is done by accepting only those Ξ's that are produced at 0° with respect to the incident proton beam. Because of the finite acceptance of the collimator, not all Ξ's are produced with zero transverse momentum and so there is the possibility of a small Ξ polarization for off-axis Ξ's. If the targeting is done symmetrically the average Ξ polarization will be zero. In the unlikely case that we do not target correctly there is a probability of a small residual Ξ polarization. However, its contribution to the measurement of the Λ polarization is significantly reduced by the fact that the Λ polarization is analyzed along the Λ direction in the Ξ rest frame. From Eq. (2) we see that the Λ polarization along its momentum direction is given by the sum of α_Ξ and $P_\Xi \cos\theta$ where θ is the angle between the Ξ polarization and the Λ momentum in the Ξ rest frame. The Λ momentum direction in the Ξ rest frame changes from event to event and due to the uniform Λ acceptance $\cos\theta$ averages to almost zero. Any residual Ξ polarization is thus reduced by about an order of magnitude. Hence we need keep the Ξ polarization to less than 1×10^{-3}.

It is extremely unlikely, but nevertheless possible, that the proton beam or target has a small, but finite polarization which could be transferred to the Ξ. Again, as was discussed above, the effect of such a polarization is greatly reduced by our analysis method.

In any case, we do not intend to only hope for a small Ξ polarization, but to actually measure it. Measuring it to the required 10^{-3} level is possible and would require only a fraction of the total data sample. We expect to find no polarization, but in fact could extract the *CP* asymmetry even in the presence of a polarization greater than 10^{-3}.

There are other potential sources of biases. Secondary production of Ξ's in the collimator could produce biases. Such events are eliminated by requiring that the Ξ's point back to the target. The earth's magnetic field, which won't be flipped, produces slight changes in the acceptance between Ξ^- and $\overline{\Xi}^+$. The effect is small: an added 75 μrad deflection to a 5 GeV/c particle, the lowest momentum accepted by the spectrometer.

To test the level of the systematics we intend to compare the Ξ^- and $\overline{\Xi}^+$ as well as Λ° and $\overline{\Lambda}^\circ$ lifetimes as a function of the hyperon momentum and $\cos\theta$'s in the Ξ and Λ rest frames. They should be identical if CPT is correct.

10 Future Improvements

As we have emphasized, the CP sensitivity of the experiment is not limited by the number of Ξ^- and $\overline{\Xi}^+$ hyperons that can be produced, but by the rates that the wire chambers can handle, the trigger selectivity, and the bandwidth of the data acquisition system (assuming systematic errors can be controlled). New technologies are being developed that are pushing these limits to higher levels. Wire chambers have been built that can take an order of magnitude more flux than we anticipate with no untoward effects [32]. The development of gas microstrip chambers [35] promises an even higher rate capability. Recently an experiment, NA12, has run at high intensities for 100 days with 8 microstrip gas chambers at CERN [36]. The chambers have a rate capability higher than $5 \times 10^7 cm^{-2} s^{-1}$. Vigorous R&D efforts are underway to increase the size and lower the mass of these chambers. If these efforts are successful, fluxes of two orders of magnitude higher than we anticipate in this proposal could be tolerated.

Similar improvements are being made in the data acquisition systems and triggers. Hence we expect in the future that large increases in the yield will be possible and the CP sensitivity of the experiment can be pushed beyond 10^{-4}.

11 Other Physics

Direct CP violation can also show up in charged K decays. The Dalitz plot of $K_{3\pi}$ decay is conventionally parameterized with the form [2]

$$\begin{aligned} |M^2| \;\propto\; & 1 + g\frac{(s_3 - s_0)}{m_\pi^2} + h\frac{(s_3 - s_0)^2}{m_\pi^2} \\ & + j\frac{(s_2 - s_1)}{m_\pi^2} + k\frac{(s_2 - s_1)^2}{m_\pi^2}, \end{aligned} \tag{9}$$

with

$$s_i = (m_K - m_i)^2 - 2m_K T_i, \quad i = 1,2,3, \tag{10}$$

$$s_0 = \frac{1}{3}(m_K{}^2 + m_1{}^2 + m_2{}^2 + m_3{}^2), \tag{11}$$

where m_i and T_i are the mass and the kinetic energy of the i^{th} pion, and the index 3 is used for the opposite sign pion in the decay. The coefficient j is zero if CP is conserved. Furthermore, if any of the slope parameters, g, h, and k for $K^+ \to \pi^+\pi^+\pi^-$ is not the same as that for $K^- \to \pi^-\pi^-\pi^+$ decay, then CP symmetry is again violated.

Experimentally, the values of h and k are found to be very small [2]. As with the observables B or B' in hyperon decays, it is very difficult to search for CP-odd effect by determining the difference in either h or k between $K^+ \to 3\pi$ and $K^- \to 3\pi$ decays. Interest in searching for direct CP violation in $K_{3\pi}$ decay is focused on the charge asymmetry of the slope parameter g defined by

$$\Delta g = \frac{g(K^+) - g(K^-)}{g(K^+) + g(K^-)}. \tag{12}$$

Theoretical predictions of Δg vary from 1.4×10^{-3} to the order of 10^{-6} [37][38]. The best measurement of Δg is from a BNL experiment done in the late 60's. With about 3.2 million $K^\pm \to 3\pi$ decays, Δg was determined to be -0.0070 ± 0.0053 [39].

In our experiment, on the average 2.2% of the $K^\pm$'s will decay in the decay region with the π's inside the spectrometer active area. About 50% of the $K_{3\pi}$ events can be reconstructed and pass all selection cuts. From the yield calculation, it is very likely that in one Fermilab fixed target run we can collect 2×10^9 $K^+ \to \pi^+\pi^+\pi^-$ and 1×10^9 $K^- \to \pi^-\pi^-\pi^+$ decays, along with the Ξ^- and $\overline{\Xi}^+$ events. This implies a sensitivity for CP violation of about 1×10^{-4}, comparable to what can be achieved with a ϕ factory [40].

12 Rough Cost Estimate

While many aspects of the experiment are yet to be determined we can make a rough estimate of the costs.

Beam line equipment and set costs	$ 200K
Hyperon magnet	200K
Hyperon channel	50K
Evacuated decay pipe	10K
Installation of analysis magnet	10K
Portacamp facility	50K
Mechanical and Electrical support	50K
Readout Electronics from PREP	200K
Terminals and network hookups required for online and offline computing	20K
Wire chamber fabrication and testing	200K
Cables for chamber readout	100K
Chamber readout electronics	1,000K
Scintillators and associated electronics	30K
8mm tapes	100K
Offline computers and peripherals	100K
Total cost	2,320K

Appendix 1: What do we Actually Measure?

The angular distribution of the proton in the decay chain: $\Xi^- \to \Lambda^\circ \pi^-$, $\Lambda^\circ \to p\,\pi^-$, where the Ξ^- is produced unpolarized, is given by:

$$\frac{dP}{d\cos\theta} = \frac{1}{2}(1 + a\cos\theta), \tag{1}$$

where $a = \alpha_\Lambda \alpha_\Xi$ and θ is the polar angle of the proton relative to the Λ direction in the Ξ rest frame. Similarly, the angular distribution of the antiproton in the antiprocess: $\overline{\Xi}^+ \to \overline{\Lambda}^\circ \pi^+$, $\overline{\Lambda}^\circ \to \overline{p}\,\pi^+$, where the $\overline{\Xi}^+$ is produced unpolarized, is given by:

$$\frac{dP}{d\cos\theta} = \frac{1}{2}(1 + \overline{a}\cos\theta), \tag{2}$$

where $\overline{a} = \alpha_{\overline{\Lambda}}\alpha_{\overline{\Xi}}$. We write the expression for the alpha parameter of the antiparticles as:

$$\begin{aligned} \alpha_{\overline{\Lambda}} &= -\alpha_\Lambda + \Delta\alpha_\Lambda, \\ \alpha_{\overline{\Xi}} &= -\alpha_\Xi + \Delta\alpha_\Xi. \end{aligned}$$

It is $\Delta\alpha_\Lambda$ and $\Delta\alpha_\Xi$ that we wish to measure: if CP is violated they must be nonzero. Measuring the angular distributions of Eq. (1) and Eq. (2) gives:

$$\begin{aligned} a &= \alpha_\Lambda\alpha_\Xi, \\ \overline{a} &= (-\alpha_\Lambda + \Delta\alpha_\Lambda)(-\alpha_\Xi + \Delta\alpha_\Xi). \end{aligned}$$

The difference between the two asymmetries is:

$$\begin{aligned} \mathcal{A} = \frac{a - \overline{a}}{a + \overline{a}} &= \frac{\alpha_\Lambda\alpha_\Xi - (-\alpha_\Lambda + \Delta\alpha_\Lambda)(-\alpha_\Xi + \Delta\alpha_\Xi)}{\alpha_\Lambda\alpha_\Xi + (-\alpha_\Lambda + \Delta\alpha_\Lambda)(-\alpha_\Xi + \Delta\alpha_\Xi)}, \\ &= \frac{+\alpha_\Lambda\Delta\alpha_\Xi + \alpha_\Xi\Delta\alpha_\Lambda - \Delta\alpha_\Lambda\Delta\alpha_\Xi}{2\alpha_\Lambda\alpha_\Xi - \alpha_\Lambda\Delta\alpha_\Xi - \alpha_\Xi\Delta\alpha_\Lambda + \Delta\alpha_\Lambda\Delta\alpha_\Xi}. \end{aligned}$$

Leaving out terms which are second order in $\Delta\alpha_\Lambda$ and $\Delta\alpha_\Xi$ in the numerator and first order in the denominator gives:

$$\begin{aligned} \mathcal{A} &\cong \frac{\alpha_\Lambda\Delta\alpha_\Xi + \alpha_\Xi\Delta\alpha_\Lambda}{2\alpha_\Lambda\alpha_\Xi}, \\ &\cong \frac{\Delta\alpha_\Xi + \Delta\alpha_\Lambda(\alpha_\Xi/\alpha_\Lambda)}{2\alpha_\Lambda\alpha_\Xi}. \end{aligned}$$

We wish to relate this to the individual asymmetries in the Ξ and Λ alpha parameters:

$$A_\Lambda = \frac{\alpha_\Lambda+\alpha_{\overline{\Lambda}}}{\alpha_\Lambda-\alpha_{\overline{\Lambda}}} = \frac{\Delta\alpha_\Lambda}{2\alpha_\Lambda},$$

$$A_\Xi = \frac{\alpha_\Xi+\alpha_{\overline{\Xi}}}{\alpha_\Xi-\alpha_{\overline{\Xi}}} = \frac{\Delta\alpha_\Xi}{2\alpha_\Xi}.$$

Plugging these in gives:

$$\frac{a-\overline{a}}{a+\overline{a}} = A_\Xi + A_\Lambda. \tag{3}$$

We have gone through this simple derivation in some detail in order to emphasize that what we are sensitive to is the *CP* asymmetry in both the Ξ and the Λ alpha parameters. In fact there is no way the two alpha parameters can be deconvoluted if one measures the Λ polarization through its self-analyzing weak decay. Although in theory $\Delta\alpha_\Lambda$ and $\Delta\alpha_\Xi$ could be equal and opposite in sign, the chances of such a conspiracy are remote: most calculations predict that A_Λ and A_Ξ have equal sign, and in fact the standard model prediction of [12] shows them to be roughly equal in magnitude as well, doubling the size of the measured asymmetry.

Appendix 2: Error in the Asymmetry Measurement

We wish to measure the difference between the the product of the Λ° and Ξ^- alpha parameters and the $\overline{\Lambda}^\circ$ and $\overline{\Xi}^+$ alpha parameters:

$$\mathcal{A} = \frac{\alpha_\Lambda \alpha_\Xi - \alpha_{\overline{\Lambda}} \alpha_{\overline{\Xi}}}{\alpha_\Lambda \alpha_\Xi + \alpha_{\overline{\Lambda}} \alpha_{\overline{\Xi}}} = \frac{a - \overline{a}}{a + \overline{a}} = A_\Lambda + A_\Xi. \tag{1}$$

The error in this measurement is given by:

$$\begin{aligned} \delta\mathcal{A} &= \sqrt{\left(\frac{d\mathcal{A}}{da}\Delta a\right)^2 + \left(\frac{d\mathcal{A}}{d\overline{a}}\Delta\overline{a}\right)^2}, \\ &= \frac{2}{(a+\overline{a})^2}\sqrt{(\overline{a}\Delta a)^2 + (a\Delta\overline{a})^2}, \\ &= \frac{1}{2a}\sqrt{\Delta a^2 + \Delta\overline{a}^2}, \end{aligned}$$

where we have set $a = \overline{a}$. The product of the two alpha parameters is measured by measuring the asymmetry a in the proton (antiproton) decay distribution:

$$\frac{dP}{d\cos\theta} = \frac{1}{2}(1 + a\cos\theta).$$

The error in a is estimated using [41]:

$$\begin{aligned} \Delta a &= \frac{1}{\sqrt{N}}\sqrt{2a^3/(\log(1+a) - \log(1-a) - 2a)}, \\ &\cong \sqrt{\frac{3}{N}}, \end{aligned}$$

where the expression strictly applies only when the acceptance is uniform. We find:

$$\delta\mathcal{A} = \frac{1}{a}\sqrt{\frac{3}{2N}}.$$

The number of events needed to measure $\mathcal{A}$ to $\delta\mathcal{A}$ precision is:

$$\begin{aligned} N &= \frac{3}{2a^2}\frac{1}{(\delta\mathcal{A})^2}, \\ &= \frac{17.5}{(\delta\mathcal{A})^2}, \end{aligned}$$

where we have substituted $a = \alpha_\Lambda \alpha_\Xi = (-0.456)(0.642) = -0.293$. To measure an asymmetry with an error of $\delta\mathcal{A} = 1 \times 10^{-4}$ requires 1.8×10^9 Ξ^- events and the same number of $\overline{\Xi}^+$ events.

References

[1] J.H. Christenson, J.W. Cronin, V.L. Fitch and R. Turlay, Phys. Rev. Lett. **13** (1964) 138.

[2] Review of Particle Properties, Phys. Rev. **D45** 1992) 1.

[3] L. Wolfenstein, Phys. Rev. Lett. **13** (1964) 562.

[4] L.K. Gibbons et al. (E731), Phys. Rev. Lett. **70** (1993) 1203.

[5] H. Burkhardt et al. (NA31), Phys. Lett **B206** (1988) 169.

[6] A. Pais, Phys. Rev. Lett. **3** (1959) 242.
O.E. Overseth and S. Pakvasa, Phys. Rev. **184**, (1969) 1663.

[7] P.M. Ho et al., Phys. Rev. **D44** (1991) 3402.

[8] T.D. Lee and C.N. Yang, Phys. Rev. **108** (1957) 1645.

[9] Tim Brown, S.F. Tuan and Sandip Pakvasa, Phys. Rev. Lett. **51** (1983) 1823.

[10] Ling-Lie Chau and Hai-Yang Cheng, Phys. Lett. **B131** (1983) 202.

[11] John F. Donoghue and Sandip Pakvasa, Phys. Rev. Lett. **55** (1985) 162.

[12] John F. Donoghue, Xiao-Gang He and Sandip Pakvasa, Phys. Rev. **D34** (1986) 833.

[13] John F. Donoghue, Barry R. Holstein and German Valencia, Phys. Lett. **B178** (1986) 319.

[14] John F. Donoghue, Third Conf. on the Intersections between Particle and Nuclear Physics, Rockport ME, 14–19 May, 1988.

[15] M.J. Iqbal and G.A. Miller, Phys. Rev. **D41** (1990) 2817.

[16] X.G. He, H. Steger and G. Valencia, Phys. Lett. **B272** (1991) 411.

[17] S. Weinberg, Phys. Rev. Lett. **37** (1976) 657.
T.D. Lee, Phys. Rev. **D8** (1973) 1226; Phys. Rep. **96** (1974) 143.

[18] M. Kobayashi and T. Maskawa, Prog. Theor. Phys. **49** (1973) 652.

[19] M. Shifman, A. Vainshtein, and V. Zakharov, Nucl. Phys. **B120** (1977) 316.
F. Gilman and M. Wise, Phys. Lett. **B93** (1980) 129.

[20] G. Buchalla, A. Buras and M. Harlander, Nucl. Phys. **B337** (1990) 313.
E.A. Paschos and Y.L. Wu, Mod. Phys. Lett. **A6** (1991) 93.

[21] P. Chauvat et al., Phys. Lett. **163B** (1985) 273.

[22] M.H. Tixier et al., Phys. Lett. **B212** (1988) 523.

[23] P.D. Barnes et al., Phys. Lett. **B199** (1987) 147.

[24] N. Hamann et al., CERN/SPSLC 92–19, 30 March 1992.

[25] S.Y. Hsueh, "Search for direct *CP* violation in $\bar{p}+p \to \bar{\Lambda}+\Lambda \to \bar{p}\pi^+ + p\pi^-$", Proposal to Fermilab, January 2, 1992.

[26] E.M. Gonzalez, Proceedings of the Meeting on the Tau-charm Factory Detector and Machine, University of Seville, Andalucia, Spain, 29 April – 2 May 1991, Ed. by J. Kirkby and J.M. Quesada.

[27] T.R.Cardello et al., Phys. Rev. **D32** (1985) 1.

[28] A.J. Malensek, Fermilab note FN-341 (1981), unpublished.

[29] A. Beretvas et al., Phys. Rev. **D34** (1986) 53.

[30] M. Bourquin et al., Z. Phys. **C5** (1980) 275.

[31] Y.W. Wah, private communication.

[32] J. Fischer, A. Hrisoho, V. Radeka and P. Rehak, Nucl. Instr. and Meth. **A238** (1985) 249.

[33] S. Amato et al., Nucl. Instr. and Meth. **A324** (1993) 535.

[34] Y.B. Hsiung et al., Nucl. Instr. Meth. **A245** (1986) 338.

[35] A. Oed, Nucl. Instr. and Meth. **A263** (1988) 351.
F. Angelini et al., Nucl. Instr. and Meth. **A283** (1989) 755.

[36] F. Angelini et al., Nucl. Instr. and Meth. **A315** (1992) 21.

[37] A.A. Bel'kov et al., Phys. Lett. **B300** (1993) 283.

[38] Hai–Yang Cheng Phys. Rev. **D44** (1991) 919.

[39] W.T. Ford et al., Phys. Rev. Lett. **25** (1970) 1370.

[40] P. Franzini, INFN preprint LNF-92/024 (P) (1992).

[41] A.G. Frodesen, O. Skjeggestad and H. Tofte, "Probability and Statistics in Particle Physics" (Universitetsforlaget, Oslo, 1979) p. 219.

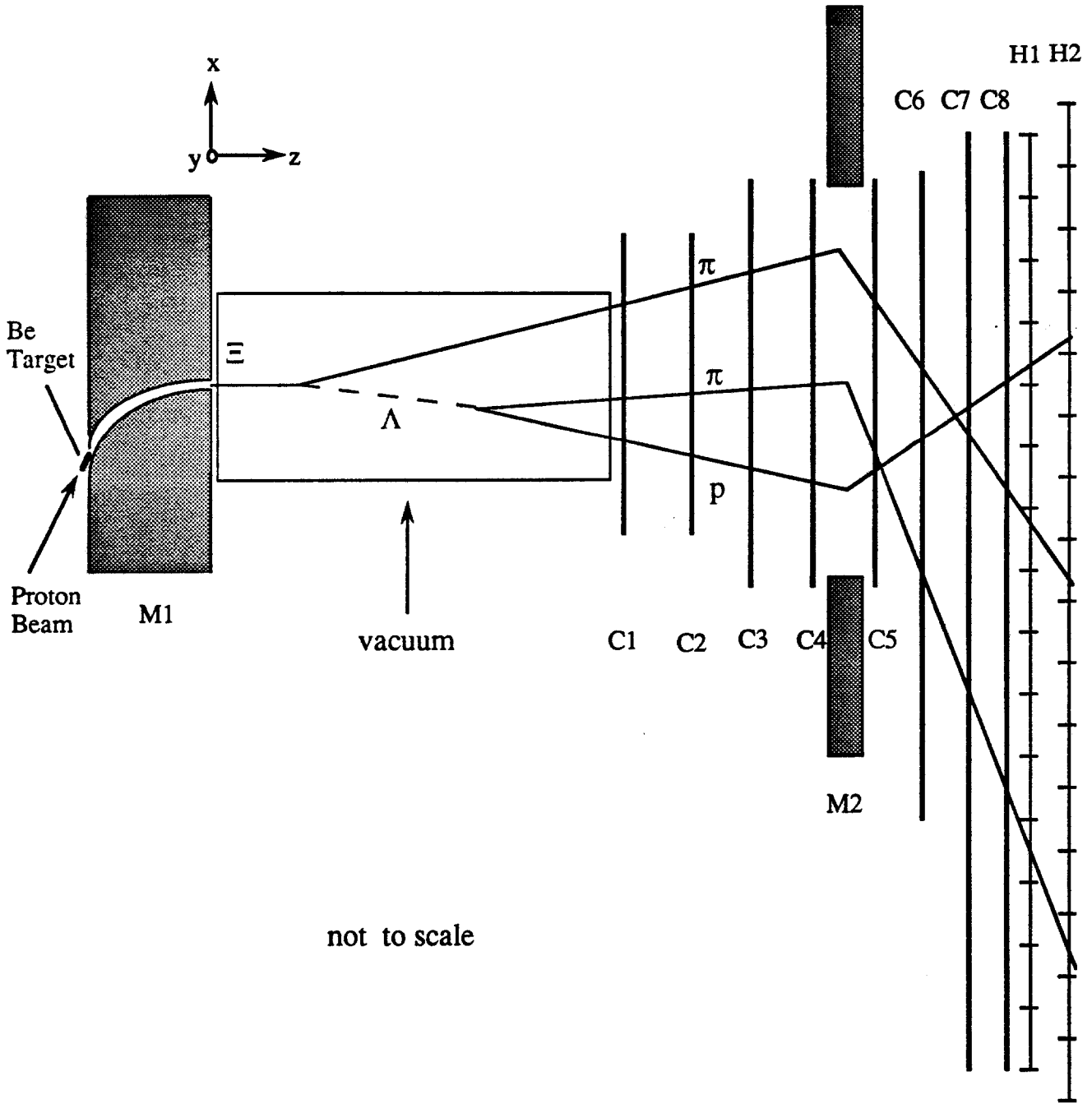

Figure 1: Plan view of spectrometer.

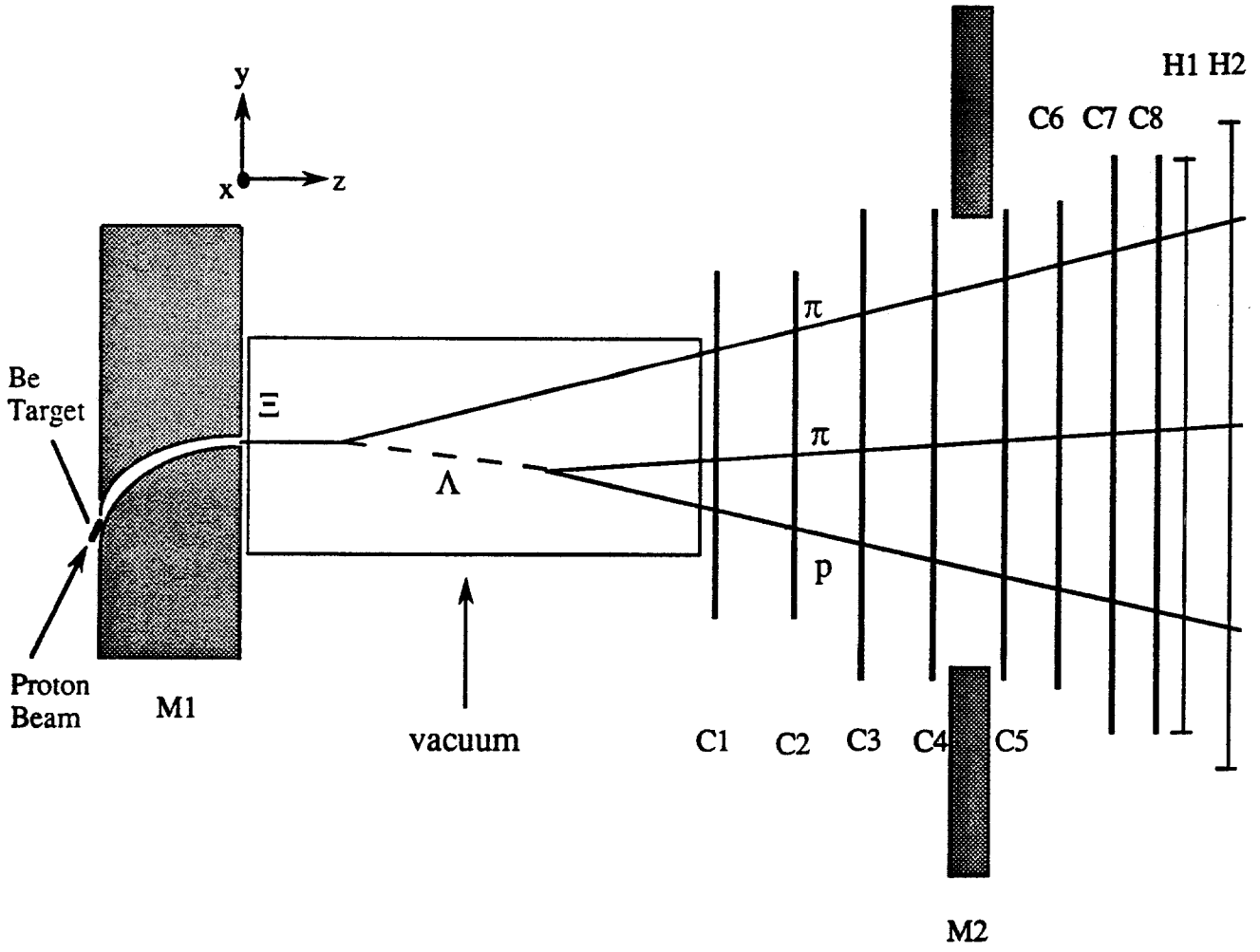

not to scale

Figure 2: Elevation view of spectrometer.

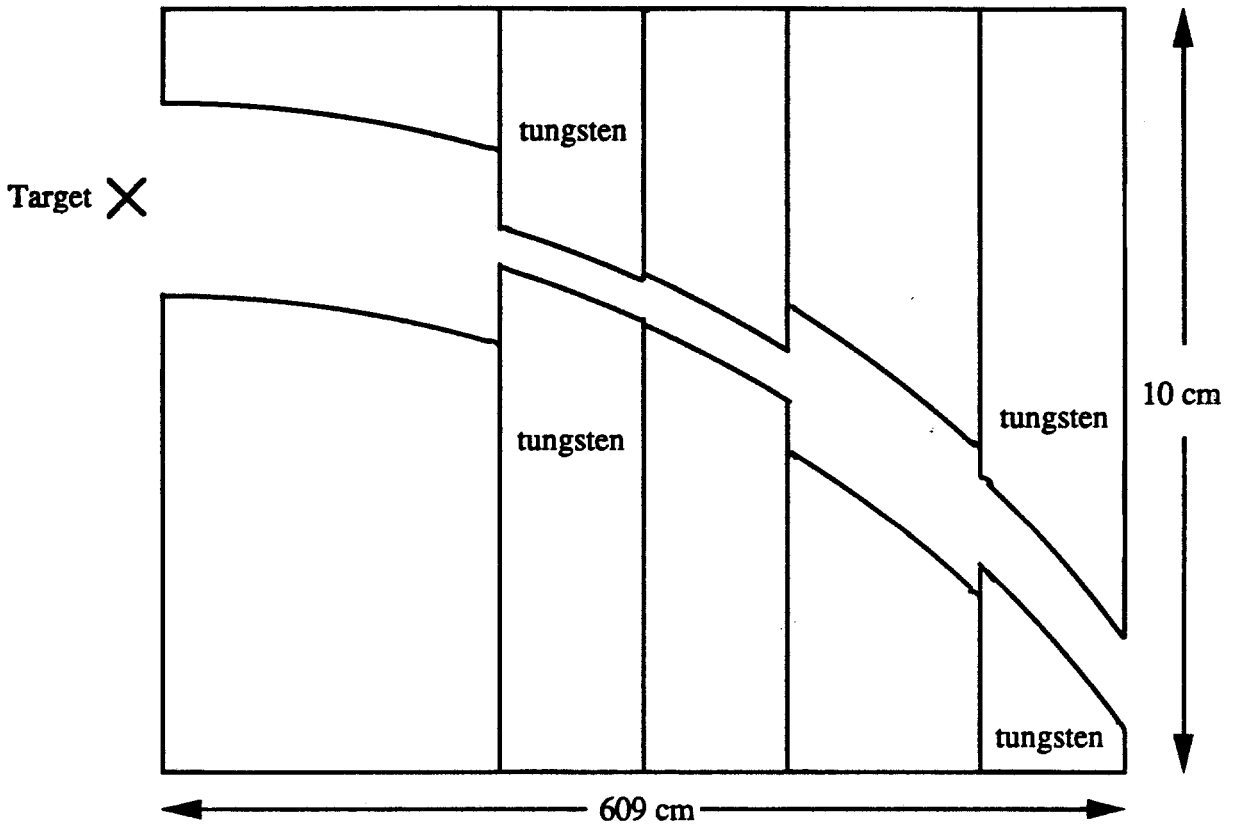

(a) Bend view

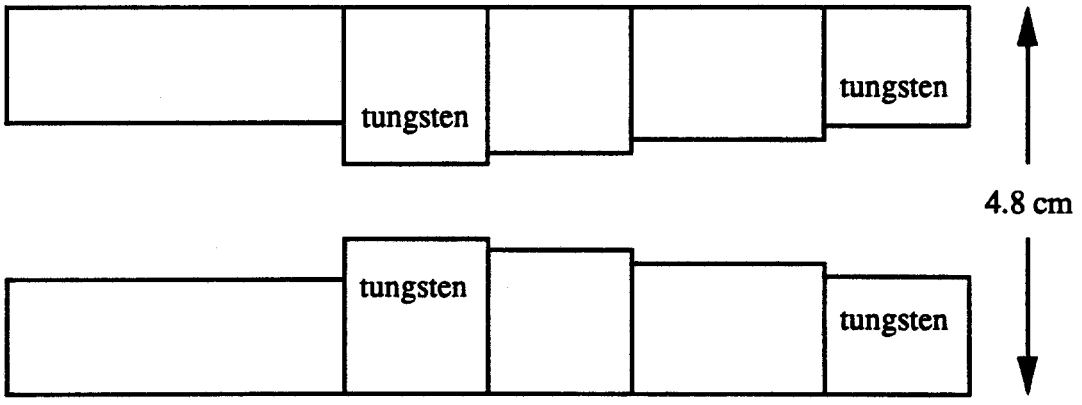

(b) Non-bend view

Figure 3: Hyperon channel.

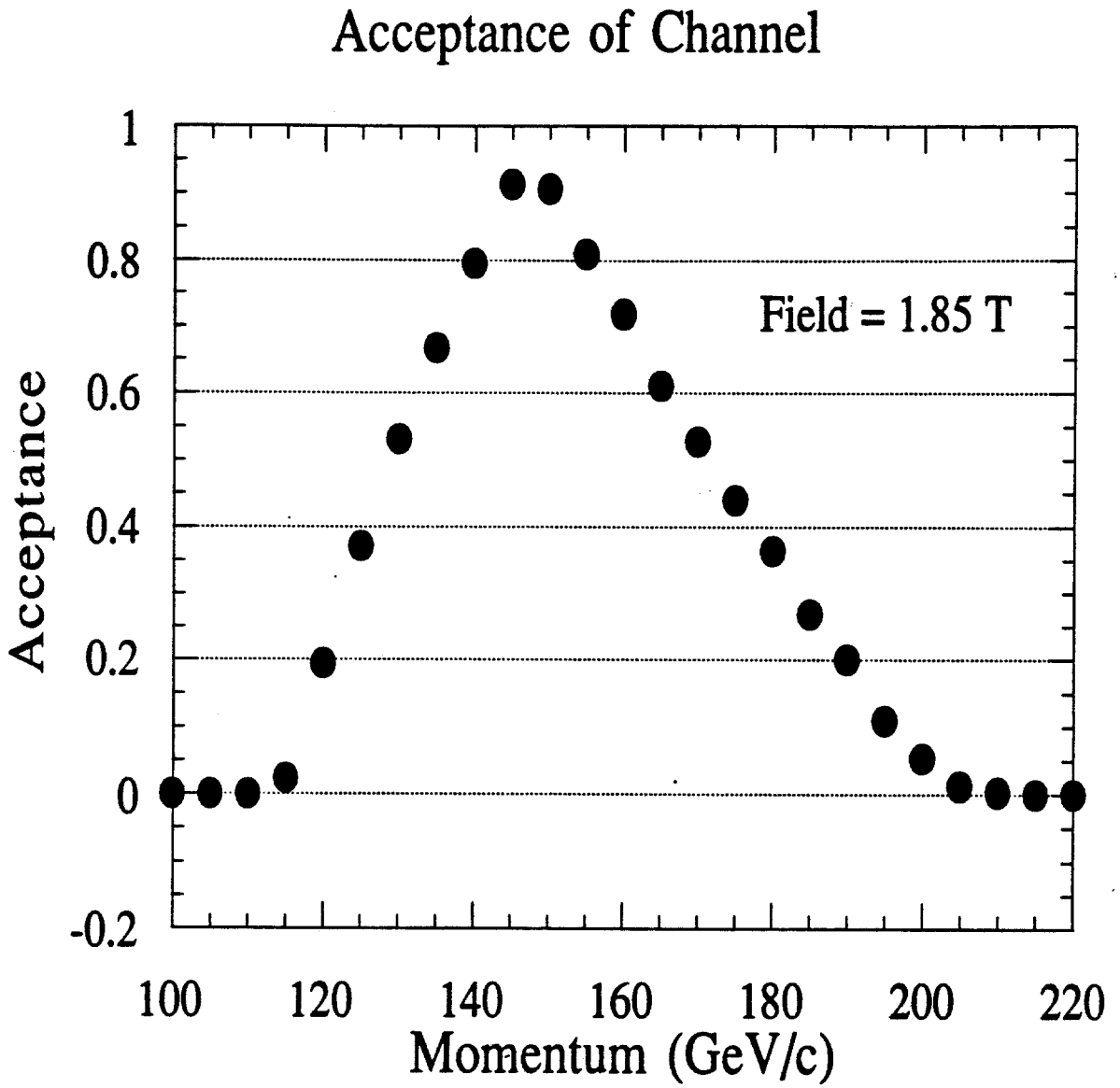

Figure 4: Hyperon channel acceptance.

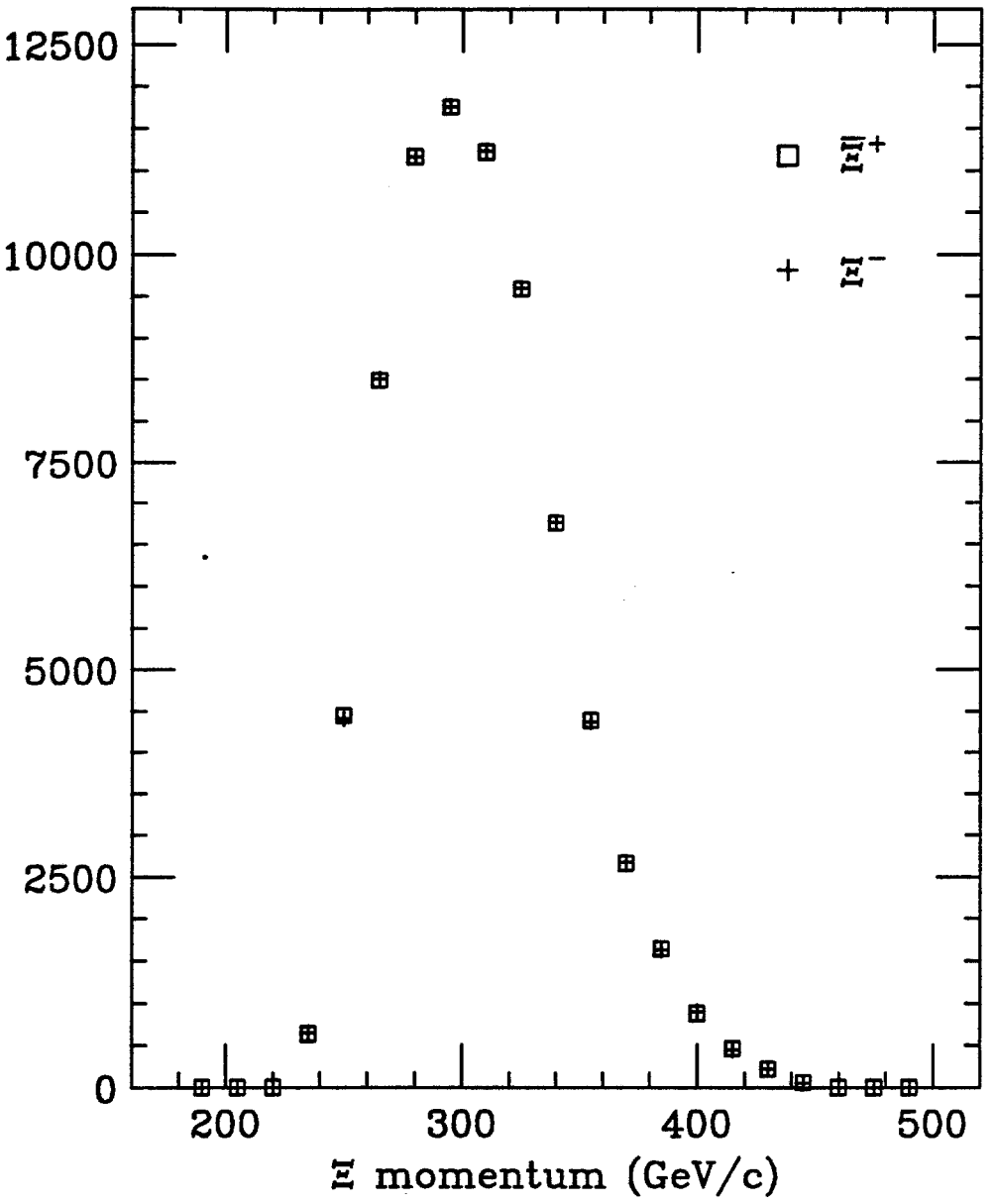

Figure 5: Comparison between the Ξ^- and $\overline{\Xi}^+$ momenta from E756.

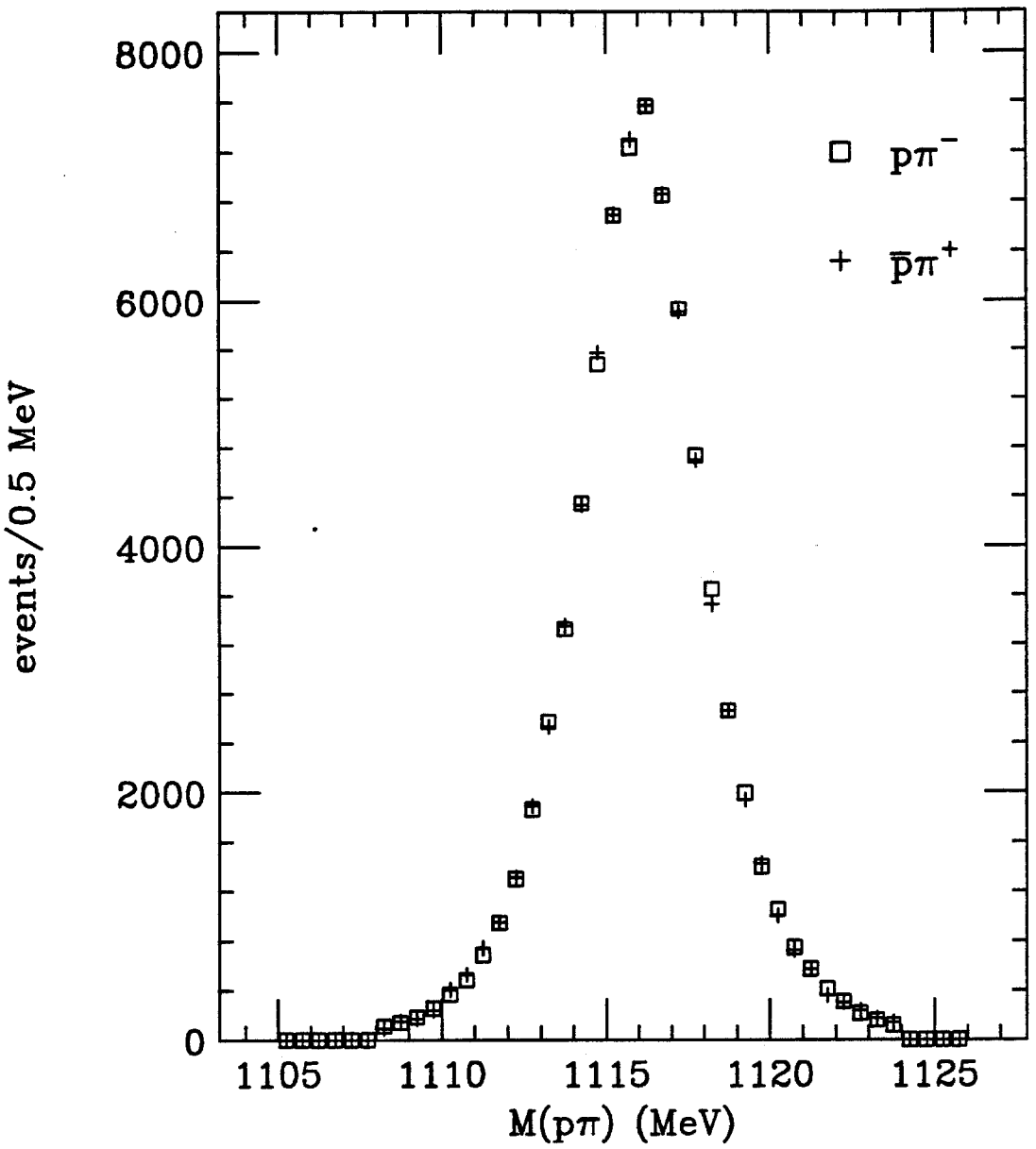

Figure 6: Comparison between the $p\pi^-$ and $\bar{p}\pi^+$ invariant masses from E756.

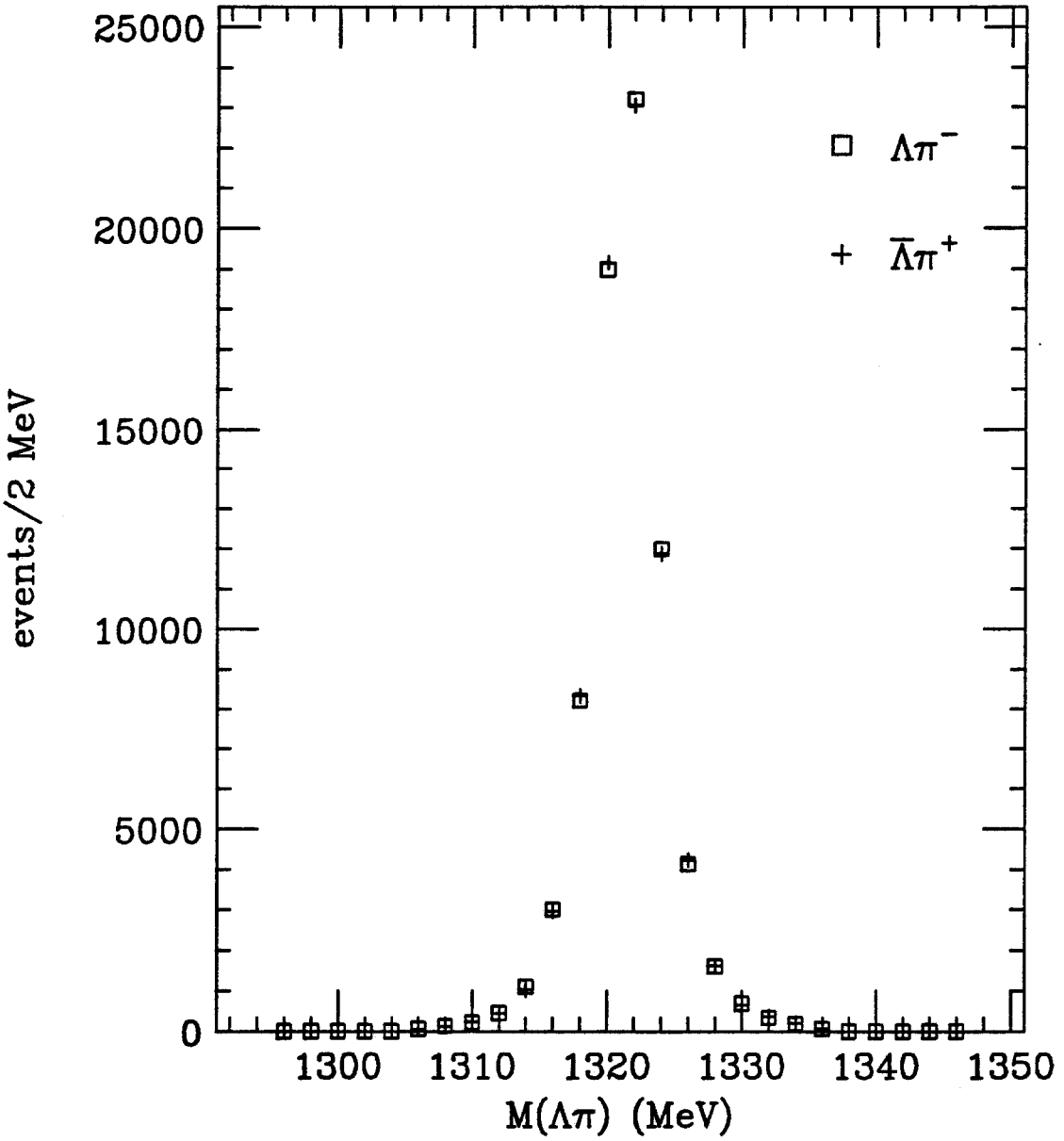

Figure 7: Comparison between the $\Lambda^{\circ}\pi^{-}$ and $\overline{\Lambda}^{\circ}\pi^{+}$ invariant masses from E756.

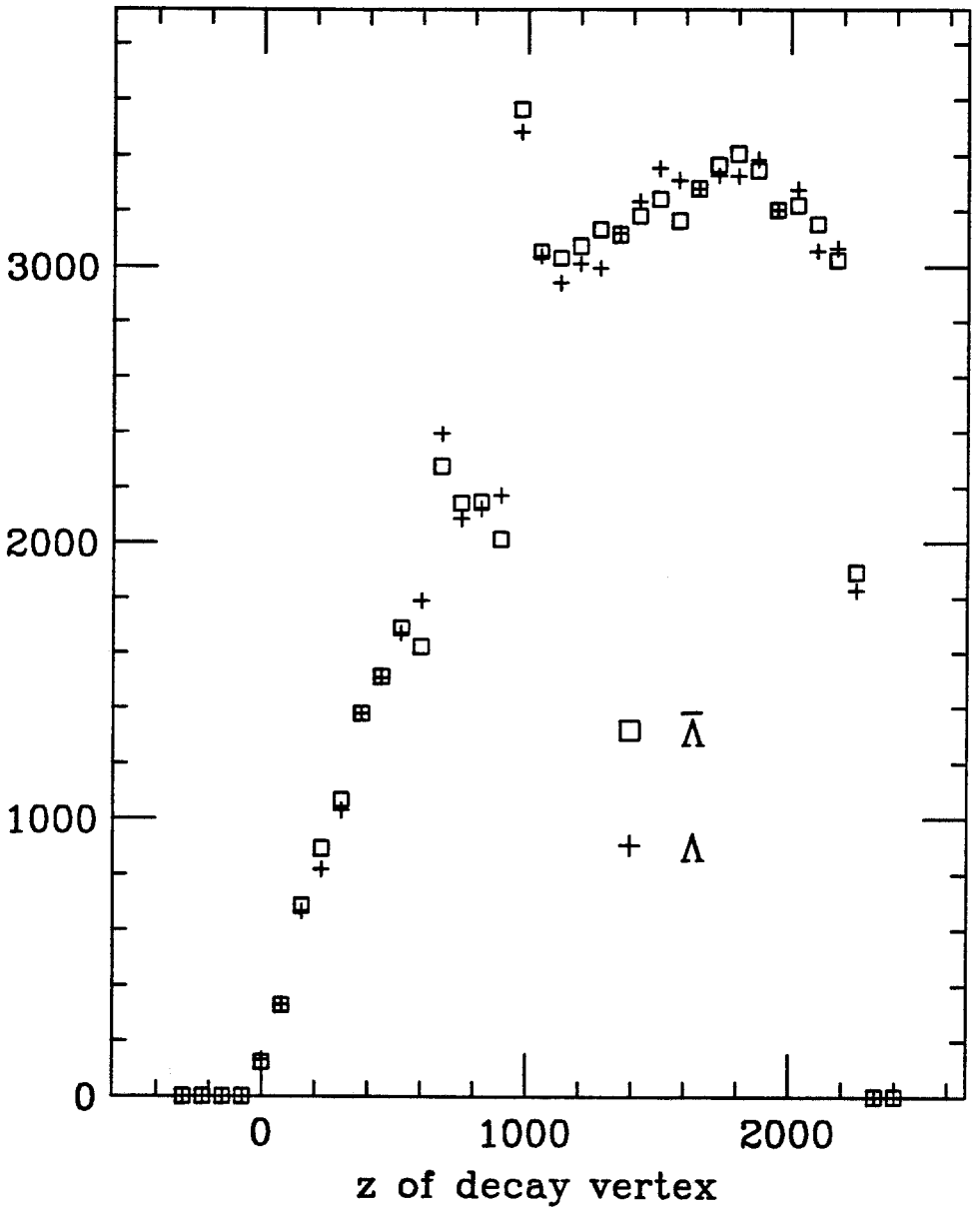

Figure 8: Comparison between the Λ° and $\overline{\Lambda}^\circ$ z decay vertices from E756.

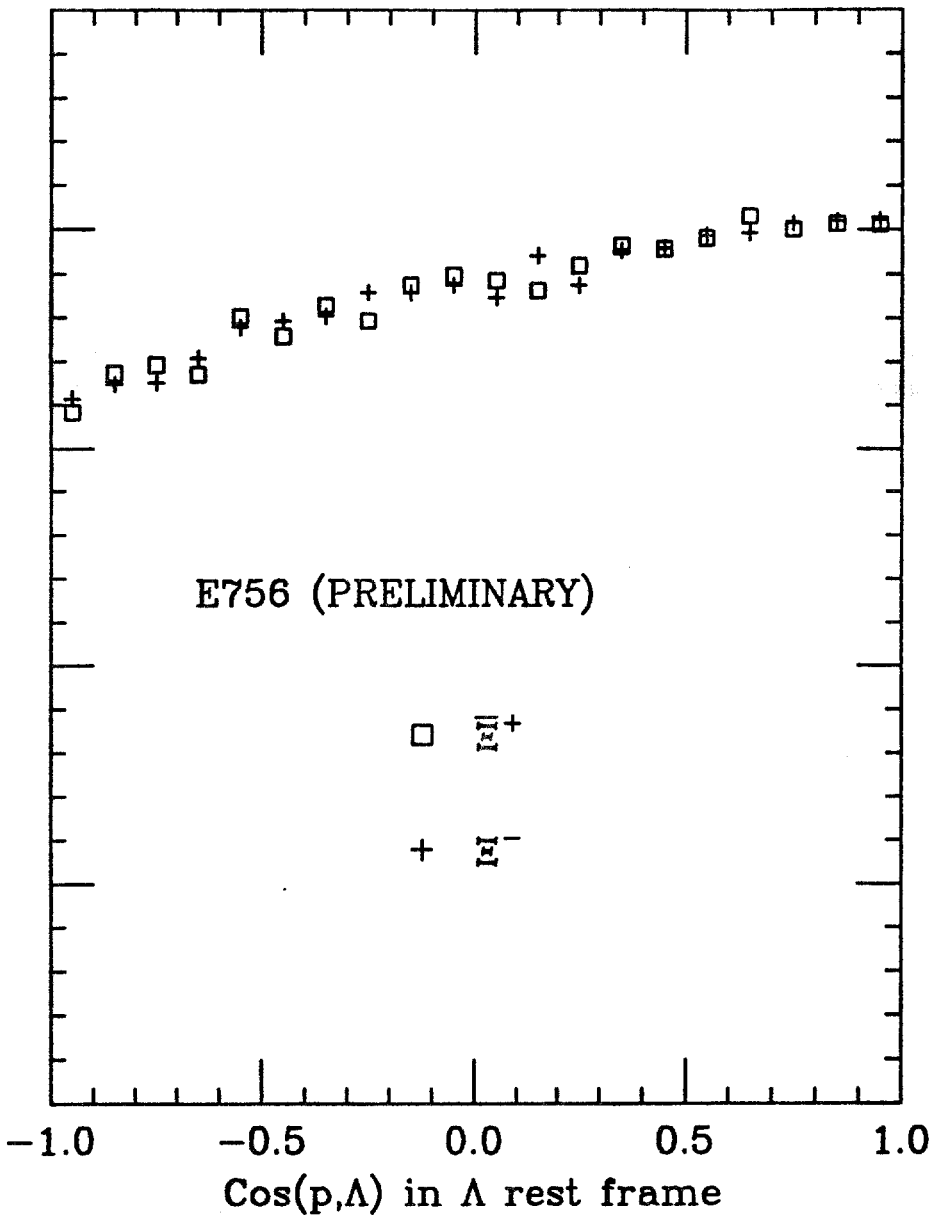

Figure 10: The Comparison between the cosine of the proton and antiproton polar angles in the Λ° and $\overline{\Lambda}^\circ$ rest frames. (The sign of the cosine has been reversed.) No significant difference is evident.

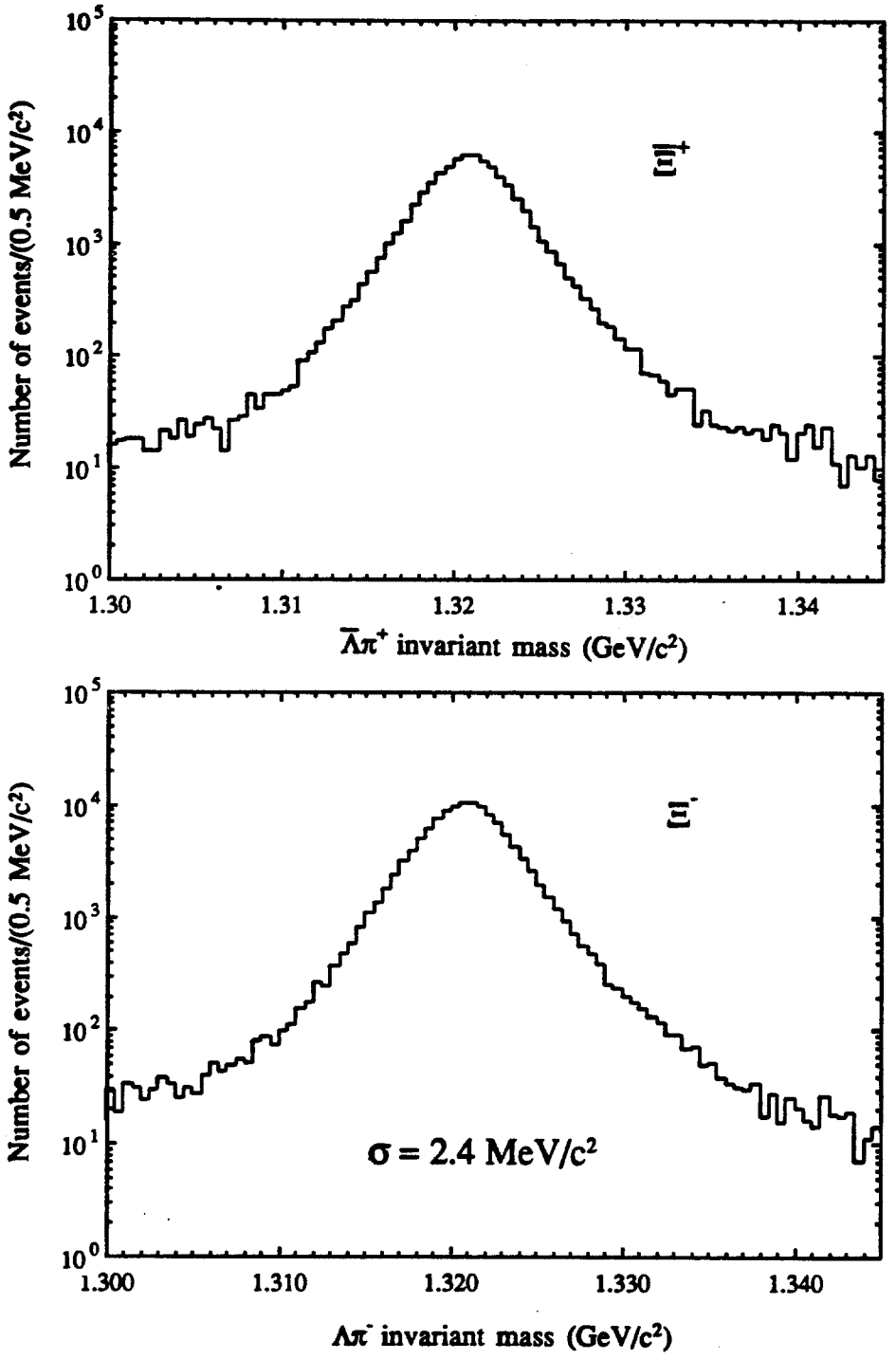

Figure 11: The $\Lambda^\circ\pi^-$ and $\overline{\Lambda}^\circ\pi^+$ invariant masses from E756. Note the excellent mass resolution and small background.